# APPENDIX A

## REPORTS

## CONTENTS

A.1 Investigation of Nondestructive Inspection Methods to Measure Silicon Carbide Coatings on Reinforced Carbon Composites

A.2 Evaluation of the Coating Crazing Phenomena

A.3 Design Evaluation Test Plan, Oxidation Inhibited Reinforced Pyrolyzed Plastic Leading Edge Assemblies, Space Shuttle Wing

1.8

X74-10175

VOUGHT AERONAUTICS

QUALITY ASSURANCE
NDT LABORATORY

**NonDestructive Testing**
RESEARCH AND DEVELOPMENT REPORT

# INVESTIGATION OF NONDESTRUCTIVE INSPECTION METHODS FOR MEASURING SILICON-CARBIDE COATINGS ON REINFORCED CARBON COMPOSITES


**ABSTRACT:**

A program was conducted to determine the best nondestructive method for measuring the thickness of a diffused silicon-carbide coating in a carbon-carbon substrate. Specimens were fabricated in accordance with existing production methods and represented thin, average, and thick coatings.

Three nondestructive inspection methods were evaluated and three laboratories participated: (1) LTV Nondestructive Testing Laboratory - eddy current and ultrasonic, (2) Los Alamos Scientific Laboratory - beta-backscatter, and (3) Oak Ridge National Laboratory - eddy current.

Regression analysis shows the eddy current method at 5 MagaHertz to be superior to beta backscatter, ultrasonics, and eddy current at 1.6 MegaHertz.



| REPARED BY | APPROVED BY | APPROVED BY | REPORT NO: |
|---|---|---|---|
| J. D. Fenton | B. G. Miller | H. E. Abbey | 2-42000/3QCR-02 |
| J. D. Fenton | B. G. Miller | H. E. Abbey | |
| ATE: 2/2/73 | DATE: 2/2/73 | DATE: 2/2/73 | DATE: 2 February 1973 |

# FORWARD

This report was prepared by LTV Aerospace Corporation under NASA Contract NAS9-12763. The study reported was Task 8 of a program to design and fabricate space shuttle leading edge heat shield material from coated reinforced pyrolyzed plastic (RPP). Task 8 was addressed to determine a method for measuring the coating thickness in both production and field applications. The results reported herein were completed between 11 June 1972 and 31 December 1972. The program was conducted under the cognizance of Mr. Frank Coe, NASA/MSC Program Manager.

Mr. B. A. Forcht was LTV Program Manager, Mr. B. G. Miller was Quality Program Coordinator, and Mr. J. D. Fenton was principal investigator. The author of this report, Mr. J. D. Fenton, is indebted to the following individuals: Mr. K. C. Stewart who made all optical thickness measurements, Mr. W. D. Kumpe who compiled the LTV Eddy Current Data, Mr. L. N. Hooker who performed all radiographic inspections, Task 8 consultant Mr. R. W. McClung of the Oak Ridge National Labs, Dr. C. V. Dodd also of the Oak Ridge National Laboratory who made Eddy Current measurements with the Phase Master, and Mr. Jack Fullbright of the Los Alamos Scientific Laboratory who made Beta Backscatter measurements.

TABLE OF CONTENTS


| SECTION | | PAGE |
|---|---|---|
| I | INTRODUCTION | |
| | 1.1 Background | 4 |
| | 1.2 Program Objectives | 5 |
| II | SUMMARY | 6 |
| III | TECHNICAL DISCUSSION | |
| | 3.1 Program Plan | 7 |
| | 3.2 Specimen Manufacturing and Coating of Test Specimens | 7 |
| | 3.3 General Inspection Methods - NDI | 7 |
| | 3.3.1 Radiographic Techniques | 8 |
| | 3.3.2 Ultrasonic Techniques | 9 |
| | 3.4 Method and Laboratory Selection | 10 |
| | 3.5 Specimen Evaluation Schedule | 11 |
| | 3.6 Coating Thickness Measurement Technique | 12 |
| | 3.6.1 Eddy Current Method | 12 |
| | 3.6.2 Beta Backscatter | 15 |
| | 3.6.3 Ultrasonic Pulse Echo | 15 |
| | 3.7 Optical Thickness Measurement | 16 |
| IV | ANALYSIS OF DATA | |
| | 4.1 Data Analysis | 17 |
| | 4.2 Eddy Current Statistical Model (LTV Data) | 17 |
| | 4.3 Eddy Current Statistical Model (Oak Ridge Data) | 18 |
| | 4.4 Beta Backscatter Statistical Model (Los Alamos Data) | 19 |
| | 4.5 Sample Correlation | 19 |
| | 4.5.1 Analysis of LTV Eddy Current Data | 20 |
| | 4.5.2 Analysis of Oak Ridge Eddy Current Data | 20 |
| | 4.5.3 Analysis of Los Alamos Beta Backscatter Data | 20 |
| V | CONCLUSIONS | 22 |
| VI | RECOMMENDATIONS | 23 |
| APPENDIX 1 | STATISTICAL EQUATIONS USED IN DATA ANALYSIS | 60 |

LIST OF FIGURES


| NUMBER | | PAGE |
|---|---|---|
| I | Specimens for Coating Thickness Requirements | 24 |
| II | Photograph of Finished Specimens | 25 |
| III | Machining Requirements for Dash 4 Specimens | 26 |
| IV | Radiograph of Panel No. 8 | 27 |
| V | Ragiographs Showing Variations in Coating Thickness | 28 |
| VI | Radiographs Showing Variations in Coating Thickness | 29 |
| VII | Photograph of Specimen No. 8-4 after Machining | 30 |
| VIII | Ultrasonic Through Transmission Setup | 31 |
| IX | Ultrasonic "C" Scan Recording of Panel No. 8 | 32 |
| X | Photograph Showing Sectioned Dash 2 Specimen | 33 |
| XI | Form for Recording Data from Rectangular Specimens | 34 |
| XII | Form for Recording Data from Round Specimens | 35 |
| XIII | Plastic Template for taking Data from Rectangular Specimens | 36 |
| XIV | Plastic Template for taking Data from Round Specimens | 37 |
| XV | Photograph Showing Template, Specimen, Probe Relationship | 38 |
| XVI | Typical Eddy Current Data Plots | 39 |
| XVII | Eddy Current Lift-Off Characteristics | 40 |
| XVIII | Lift-Off Data Using Plastic Shims | 41 |
| XIX | Basic Beta Backscatter Setup | 42 |
| XX | Oscilloscope Presentation of Ultrasonic Signals - Coating Thickness Measurement | 43 |
| XXI | Microscope used to make Optical Thickness Measurements | 44 |
| XXII | Photograph of Cross-section of Specimens Showing Scribe Lines | 44 |
| XXIII | Photographs of Coating Cross Section | 45 |
| XXIV | Reactance on Resistance Plot of LTV Eddy Current Data Used to Develop Statistical Model | 46 |
| XXV | Eddy Current Statistical Model (LTV Data) | 47 |
| XXVI | Calculated Thickness on Calculated Meter Reading for Plastic Lift-Off and Coated Specimens | 48 |
| XXVII | Eddy Current Statistical Model (Oak Ridge Data) | 49 |
| XXVIII | Beta Backscatter Statistical Model (Los Alamos Data) | 50 |

## LIST OF TABLES


| NUMBER | TITLE | PAGE |
|---|---|---|
| 1 | Schedule of Coating Thickness Requirements | 51 |
| 2 | Schedule of Specimen Shipments | 52 |
| 3 | Lift-Off Data for Machined and Uncoated RPP | 53 |
| 4 | LTV Eddy Current Statistical Model Data | 54 |
| 5 | Oak Ridge National Laboratory Eddy Current Statistical Model Data | 56 |
| 6 | Los Alamos Scientific Laboratory Beta Back-Scatter Statistical Model Data | 58 |

## SECTION I

## INTRODUCTION

1.1 Background - Reinforced Pyrolyzed Plastic (RPP) parts are fabricated by building-up layers of phenolic resin impregnated graphite cloth on a mold until the laminate conforms to specified thickness and configuration requirements. The parts are then autoclave cured and subjected to the first of four pyrolysis cycles. Following the last pyrolysis, the RPP parts are coated to the desired coating thickness.

The purpose of the pyrolysis cycles is to convert the phenolic resin to carbon leaving the graphite cloth in a carbon matrix. Between the first and second, the second and third, and the third and fourth pyrolysis cycles, the parts are impregnated with a high carbon yielding resin. Four pyrolysis cycles are required to build up sufficient carbon matrix to give the laminate the required mechanical properties. The carbon-carbon material is in the cured condition after auto-clave cure, RPP-0 after the first pyrolysis cycle, through RPP-3 after the fourth pyrolysis cycle. The bare RPP-3 surface is coated to withstand oxidation and ablation when exposed to re-entry type temperatures. Coating is by impregnation, by vapor diffusion, with Silicon-Carbide to develop a highly abrasive and oxidation resistance surface.

Task 8 was designed to develop and refine a method for measuring the coating thickness. However, by necessity, NDI techniques had to be refined as much as possible, staying within the scope of the task, so that the specimens could be interrogated as thoroughly as possible prior to and after coating. Therefore, there were two areas of consideration in Task 8: (1) to develop a method and technique to measure the depth of penetration of the silicon-carbide coating, and (2) refine general NDI techniques to inspect for defects and other anomalies during the manufacturing process that would influence the NDI techniques being evaluated.

Some of the conditions that can occur during the manufacturing process that could have adverse effects on the coating thickness measuring method include delaminations, severe porosity, inclusions of foreign material, and insufficient or excessive coating thickness. Therefore, the parts were inspected by visual and Nondestructive Inspection (NDI) methods periodically during the manufacturing process.

The NDI methods employed for evaluating the substrate were radiography and ultrasonics. Radiography of the uncoated RPP was supplemented with carbon-tetrachloride in order to develop radiographic opaqueness differences between porous, or void, areas and the less porous areas. The parts were soaked in the carbon tet for a required period of time and then allowed to surface dry, prior to being x-rayed. The porous areas soak up more carbon tet than the less porous areas and, therefore, became more radiographically opaque than the adjacent less porous areas. This contrast permits the detection of highly porous and delaminated areas. Ultrasonic inspection of the uncoated and coated RPP utilized an immersed two transducer technique that depends on the

sound passing through the part. Ultrasonic energy generated by one transducer, passes through the part, and is detected by the other transducer. For all practical purposes, ultrasonic energy of the frequencies used will not pass through air. Therefore, a section containing an excessive amount of porosity or a delamination can be easily detected.

Task 8 proposed that three methods be investigated as possible techniques for measuring the coating thickness. They are: (1) eddy current, (2) beta backscatter, and (3) ultrasonics. The Phase Master, developed by the Oak Ridge National Labs., and the Nortec NDT-8 were used in evaluating the eddy current method. An instrument designed and built by the Los Alamos Scientific Labs was utilized to evaluate the beta-backscatter method. Short pulsed ultrasonic equipment developed by LTV was utilized to evaluate the ultrasonic method.

1.2 Program Objectives for Task 8 were to (1) determine the best method for measuring coating thickness, (2) determine the accuracy of the method and (3) make firm recommendations for coating thickness measurements for: (a) production control, (b) final acceptance, and (c) post-flight inspections.

## SECTION II

## SUMMARY

The objectives of Task 8, conducted under NASA contract NAS 9-12763, were to (1) determine the best method for measuring coating thickness, (2) determine the initial accuracy of the method using existing equipment, (3) set forth problems related to production, preflight, and postflight inspections using existing equipment, and (4) recommend the solutions to these problems.

The results of the investigation show that the eddy current method can be used to accurately measure coating thickness. Eddy current frequencies of 5 MHz or higher should be used for optimum results. Light weight, battery operated equipment adaptable to both production and field inspections will measure to within 0.0052 inch of the optically measured thickness with 95% reliability. The thickness range over which this accuracy was obtained is 0.010 to 0.060 inch.

Ultrasonic and beta backscatter are not acceptable methods to measure this coating thickness because of the surface and interface roughness, the non-uniform density of the substrate, and the high attenuation properties of the coating.

Additional work is required to develop instrumentation to operate at frequencies above 5 MHz, to develop reference standards, and to determine electrical conductivity differences in specimens layed up at different times.

## SECTION III

## TECHNICAL DISCUSSION

3.1 Program Plan - Test specimens were manufactured and coated in accordance with existing production methods and procedures. All specimens were inspected radiographically and ultrasonically in the RPP-2, RPP-3, and the coated condition. Three NDI methods of measuring coating thickness were evaluated: (1) eddy current, (2) beta-backscatter and (3) ultrasonics. Three rounds of data measurement were conducted utilizing three NDT labs and the above three methods. Following the first round of data gathering, a statistical model was developed from the data furnished by each laboratory and from the optical coating thickness measurements (actuals) from one section (Fig. x, Row D) of each of the nine dash two (-2) specimens (Figure I). The accuracy of the methods and techniques being evaluated was determined from this model. The balance of the data was then taken, a sample of the specimens was sectioned, and the coating thickness was optically measured. A statistical sample of the total data was then compared to the model.

3.2 Manufacturing and Coating of the test specimens were performed in accordance with the existing manufacturing methods and procedures so that the specimens would represent, as nearly as possible, production components. Nine panels, 20 plies in thickness, were layed-up and processed through the fourth pyrolysis cycle (RPP-3). Each of the nine panels were identified and sectioned per Figure I to make five 4.0 x 6.0 inch specimens and two 3.0 inch diameter discs for a total of 63 test specimens. Fifty-four specimens, six from each panel (Figure II), were coated to three nonimal coating thicknesses (Table 1): (1) minimum expected - 0.010 inch, (2) mid-range - 0.030 inch, and (3) maximum expected - 0.050 inch.

The dash one (-1) specimen from each of the nine panels was not coated. The coating from each of the dash four (-4) specimens was removed by machining in accordance with Figure III. These specimens were needed for two purposes: (1) to serve as a bare material reference for eddy current and beta-backscatter, and (2) to determine whether or not any changes in the properties or characteristics of the substrate occurred during the coating process. The dash three "a" and "b" (-3a and -3b) specimens from each of the nine panels were subjected to a simulated re-entry environment utilizing the plasma facility at NASA/MSC. The dash six (-6) specimen from each of the nine panels was heat treated at LTV in order to determine if further exposure to heat cycles would cause additional changes in the substrate that would affect the coating thickness measurements.

3.3 General Inspection Methods (NDI) utilizing radiographic and ultrasonic inspection techniques were used to inspect the panels and to obtain and evaluate as much historical data as possible. The inspections were conducted at four stages during manufacture: (1) after autoclave

cure, (2) after the third pyrolysis cycle (RPP-2), (3) after the fourth pyrolysis cycle (RPP-3), and (4) after coating. It was found that following the first and second pyrolysis cycle, the material uniformly absorbs carbon tet and water because of the general porousness of the material and meaningful results cannot be obtained from radiography or ultrasonics.

3.3.1 Radiographic Techniques were used to evaluate the uncoated specimens for inclusions (foreign material) and highly porous areas. Two basic radiographic techniques were used in evaluating all specimens.

(1) Standard low energy techniques using a fine grain film after the part had been soaked in carbon-tetrachloride.
(2) Standard low energy techniques using a fine grain film without any special processing of the specimen.

The first technique was used to evaluate the specimens after the third and fourth pyrolysis cycles. The second technique was used to evaluate the specimens after autoclave cure.

The carbon-carbon material has very low x-ray absorption properties. These low absorption properties cause low subject contrast and, therefore, reduce the sensitivity when inspecting for delamination, voids, or porosity. In order to develop greater subject contrast, the carbon-carbon material is soaked in carbon-tetrachloride. The carbon tet serves as an attenuator to develop high subject contrast between the areas that are porous and retain the carbon tet, and the less porous areas that have absorbed less of the attenuator.

The soaking operation was conducted at atmospheric pressures, and each specimen was allowed to soak for a period of 30 minutes. Following the soak period, the specimens were allowed to surface dry and were radiographed immediately. Radiography was performed with a Norelco MG 150 x-ray unit, using a 150 KV beryllium window tube and Eastman Kodak Type M film. The film target distance was 36 inches and the exposure was 25 KV at 6 milliampere minutes. The film was processed in a Kodak Model "B" X-Omat using recommended temperatures and solution concentrations.

When radiographed in the RPP-1 and the RPP-2 condition, the panels exhibited a generally uniform condition. This was probably due to the high degree of porousness of the panels that permitted sufficient carbon tet to be soaked up to mask non-uniform porous conditions. In the RPP-3 condition, the material had sufficient density that the less porous areas did not readily soak up the carbon tet and adequate subject contrast was developed for radiographic inspection. Figure IV illustrates the subject contrast that can be developed with the carbon tet attenuator. The light areas on the radiograph represent porous areas in the part that have soaked up the carbon tet and attenuated the x-rays more than in adjacent less porous areas. Radiographs of this panel, when x-rayed without carbon tet, have a uniform density. When the specimens were coated, the coating thickness was greater in the more porous areas than in the less porous areas.

This condition is illustrated in Figures V, VI and VII. The light areas in the Figure V and VI radiographs represent the thicker coating and the dark areas the thinner coating. This condition is further illustrated in the Figure VII photograph. When this specimen was machined, it did not completely clean up; the light areas of Figure V readily correlate with the areas of Figure VII where all of the coating was not removed in the machined area. Radiographically, the degree of this condition cannot be observed for the individual surfaces. The condition observed in Figures IV, V, and VI is for the combination of both surfaces and represents the total depth that the carbon tet has penetrated each surface. Therefore, the radiographic image cannot be used to represent a specific area of one side, or for the center of the panel. However, radiography could be developed as an indicator for the uniformity of the porousness of the surfaces and possible relationships to the uniformity of the depth of penetration of the coating.

3.3.2 Ultrasonic Through Transmission Techniques were used to evaluate the parts for delaminations, gross porous conditions and other anomalies that would affect sound transmission characteristics. The basic ultrasonic through transmission set-up illustrated in Figure VIII was used to evaluate all specimens. The ultrasonic unit used in the evaluation of all Task 8 specimens is a Magnaflux PS 902 with a Broad Band Receiver (RP 1008), a Shade Recorder Adapter (SRA 1000), and Dry "C" Scan Recorder. Both the transmitting and the receiving transducer were 3/4-inch in diameter, short focus, with lithium sulphate elements. The frequency of the transmitting transducer was 5.0 MHz (MegaHertz). The receiving transducer was 2.25 MHz. The ultrasonic "C" scan recording for Panel No. 8 is shown in Figure IX. This recording does not reveal the porous conditions shown in radiography (Figure IV) since the water absorbed by porous surface is not an ultrasonic attenuator.

For general inspection techniques, frequency spectrum analysis revealed that the transmitted frequency ranges from 0.5 to 1.5 MHz, with a central frequency of 1.0 MHz. This relationship held regardless of the frequency content of the wave packet when traversing water only.

The frequency content of the pulse packet was severly altered and attenuated by the carbon-carbon material. However, material thickness changes from 1/4-inch to 5/8-inch further attenuated but did not further distort the wave packet to any appreciable degree. The 5.0/2.25 MHz transducer combination would not penetrate coated specimens. Subsequently, 1.0 MHz, 3/4-inch in diameter, medium focus transducers with the Automation Industries "J" series elements were used on coated specimens and on bare specimens that could not be inspected with the 5.0/2.25

combination. Generally, sensitivity was better with the 5.0/2.25, or in some instances with a 5.0/5.0 combination, than with the 1.0/1.0 combination. However, for very highly attenuating materials, the 5.0 MHz transducers are less sensitive than the 1.0 MHz transducers because of the extreme gain settings required at the higher frequencies.

The nonuniformity of the panel as shown by ultrasonics is confined to the area between the surfaces that have not absorbed water. The high attenuation properties of this material will not permit settings sensitive enough to show the coating thickness differences illustrated in Figures V and VI. The ultrasonic techniques that were employed will detect changes in attenuation properties as a function of the total thickness, but will not distinguish between coating or substrate. The depth of penetration of the coating appears to be associated with porousness of a specific area of the surface or the area immediately under the surface. This method, therefore, could not be used to predict the uniformity of the depth of the coating.

3.4 Method and Laboratory Selection was based upon information obtained from a literature search, discussions with several knowledgeable individuals, and preliminary studies that were conducted by each of the laboratories selected. The laboratories selected and methods to be investigated were: (1) Los Alamos Scientific Labs - Beta-Backscatter, (2) Oak Ridge National Labs - Eddy Current, and (3) LTV Nondestructive Testing Research and Development Lab - Eddy Current and Ultrasonic.

The Eddy Current method was selected because the RPP-3 is electrically conductive, approximately 0.03 to 0.05 IACS (International Annealed Copper Standard), and the coating is less conductive, less than 0.005 IACS. Calculations indicated that the optimum frequency was in the 5 to 15 MHz range. However, since the eddy current method appeared to be the most likely candidate and it appeared from preliminary evaluation that good sensitivity could be obtained at 1.6 MHz (maximum operating frequency of in-house equipment), the decision was made to conduct parallel eddy current tests with one series to be conducted at LTV with a frequency of 1.6 MHz and the other series to be conducted by an outside laboratory with equipment that could operate in the optimum frequency range. The laboratory selected was the Oak Ridge National Lab, Oak Ridge, Tennessee, with Dr. C. V. Dodd conducting the evaluations. The Phase Master (an eddy current instrument developed by Dr. Dodd) was used. Both phase and amplitude measurements were made at 5 MHz (the optimum frequency selected by computer analysis at Oak Ridge). There were two other major reasons for selecting Oak Ridge: (1) past experience in measuring similar coating thickness at high frequencies, and (2) to determine if there would be an advantage in using phase sensitive equipment.

The beta-backscatter method was selected following (1) preliminary evaluations conducted at Superior Circuits, Dallas, Texas, using a Twin City Model NS4-EON Beta-Backscatter Instrument, (2) on the recommendation of Mr. R. W. McClung of the Oak Ridge National Labs who had been secured as consultant for the Task 8 program, (3) following

discussions with Mr. Jack Fullbright of Los Alamos Scientific Labs, and (4) after samples of coated and uncoated RPP-3 had been evaluated by Mr. Jack Fullbright at Los Alamos. The Los Alamos Labs were selected to conduct these tests for two major reasons: (1) several years experience in measuring diffused coating thicknesses on graphite and carbon-carbon substrate, and (2) facilities were available at their lab to encapsulate radioactive sources of the required size and energy level.

The ultrasonic pulse echo method was selected primarily as a back-up technique in case unforeseen problems eliminated either or both eddy current and beta-backscatter. After preliminary investigations by two labs, it was concluded that standard equipment was not available (not presently being manufactured) that would produce and process a signal with consistent and meaningful results. A short pulse ultrasonic instrument was currently being developed by the Vought Aeronautics Company (VAC) NDT Research and Development Lab and preliminary investigation indicated that the signal generation and processing techniques used in this instrument might produce favorable results. The decision was made to conduct ultrasonic evaluations at VAC using this prototype instrument.

3.5 A Specimen Evaluation Schedule was set-up, Table 2, in such a manner that each testing laboratory would receive specimens from each of the three nominal coating thicknesses in each of three rounds of testing. All specimens were evaluated in the first round; one-third by each laboratory. Following the first round, specimens 3a and 3b from each panel were exposed to re-entry conditions at NASA/MSC; specimen 6 from each panel was heat treated by LTV, and specimen 2 from each panel was sectioned at row D, see Figure X. Specimens 1, 2, 4 and 5 were forwarded to the appropriate labs for the Round 2 measurements, while specimens 3a, 3b and 6 were being processed and optical thickness measurements were being made on the dash 2, row D sections. In Round 3, the third set of specimens 1, 2, 4 and 5, and the original set of specimens 3a, 3b and 6 were forwarded to the appropriate lab. All data was recorded on forms furnished to each lab, Figures XI and XII. The forms set-up specific points at which data was to be taken.

Each specimen was divided into four rows and seven columns and thickness measurements were made on each surface at the junction of the rows and columns. Specific points of measurement were necessitated because of the general nonuniformity of the coating thickness as illustrated in Figures V-VI. To assure that optical and NDI thickness measurements were made at the same location, plexiglass templates were fabricated; Figure XIII and XIV. The templates were used as illustrated in Figure XV. The above arrangement permitted the following data points per nominal coating thickness:

467 points on 12 coated specimens
168 points on 3 bare (uncoated) specimens
63 points on 3 bare (machined) specimens
96 points on 3 coated specimens after exposure and heat treat

Following the completion of the third round, all dash 2, 3a and 6 specimens were sectioned and optical thickness measurements were made to determine coating thickness. Specimens 1, 3b, and 5 were retained should further processing technique refinement, or technique verification be required.

3.6 Coating Thickness Measurement Methods were evaluated primarily for four features: (1) accuracy of measurement, (2) repeatability of measurement, (3) portability for both shop and field use, and (4) simplicity of operation. Small battery operated eddy current equipment rated a strong first for items three and four above. However, conductivity differences of as much as 20 percent in an uncoated specimen and variations in readings on coated specimens of equal magnitude indicated possible problems with eddy currents. Since beta-backscatter is being used successfully in several similar applications, this method was considered a good backup candidate. Also, for beta-backscatter, a couplant is not required, however, it does involve the use of a radioactive source. Short pulse, high frequency ultrasonic techniques were considered a second backup if eddy current and beta-backscatter failed.

3.6.1 Eddy current Method - A coil-carrying an alternating current has associated with it a varying magnetic field. When a conductor is placed in the magnetic field of the coil, eddy currents are induced in the conductor. The magnetic fields of the eddy currents (the reaction field) opposes the field of the coil. The original field of the coil is then modified by this reaction field. The modification of the field of the coil has exactly the same effect as would be obtained if the impedance characteristics of the test coil itself had been changed. The test coil has two impedance characteristics:

Inductive reactance $x = 2\pi fL = \omega L$

and

Ohmic resistance $R = R$

The total impedance, Z, of the coil is the sum of these two characteristics and is expressed in rectangular form by:

$$Z = R + jX = R + j2\pi fL = R + j\omega L \qquad (1)$$

Where: L = Self inductance of the coil, $\omega$ = angular frequency, f = frequency, and, $j = \sqrt{-1}$

The total impedance can also be expressed in polar or Steinmetz form by:

$$Z = r\angle\theta \qquad (2)$$

Where: r = Amplitude, and $\theta$ = Phase angle

Equations (1) and (2) are related by:

$$r = \sqrt{R^2 + X^2} \qquad \text{And,} \qquad (3)$$

$$\theta = \text{Arctan}\,\frac{X}{R} \qquad (4)$$

Current across the coil terminals is expressed by ohms law:

$$I = \frac{V}{Z} \qquad (5)$$

The influence of the test object can be described by variations in test coil characteristics. The resistive components, R and r, are associated with the energy dissipated per cycle and the reactive components, X and $\theta$ are associated with the energy stored per cycle. The field produced by the eddy currents causes a reduction in stored energy and an energy loss in the conductor in which the eddy currents are flowing. The influence that materials of different conductivities have on the coil can be studied by plotting the resistive (real) component as the abscissa and the reactive (imaginary) component as the ordinate. The components can be plotted in several relative units: resistance, reactance, phase angle, voltages or energies depending on instrumentation and/or calculated values. Two types of eddy current instruments and methods of data presentation were used on this program. They are (1) an impedance system using a single coil probe (Nortec Model NDT-8), and (2) a phase sensitive system using a three coil probe (Phase Master, Oak Ridge National Labs). Each system and the results that were obtained are discussed in the following paragraphs.

When an eddy current instrument and coil, such as the NDT-8, is excited at a specific frequency and the reactive and resistive components of several materials of different conductivities are measured the data will produce a curve similar to that illustrated in Figure XVI A. Frequency changes will produce a family of curves with the same basic shape, but extend outward for lower frequencies and inward for higher frequencies; for instance, curve 2 would be produced by increasing the frequency. Also, on curve 1, there is less separation of the lower conductive materials and greater separation of the higher conductive materials. The opposite is true for curve 2. When making eddy current measurements, the instrument, the exciting frequency, and the coil characteristics must be selected to obtain optimum results.

If the coil is gradually lifted off the conductor and the resistive and reactive components are plotted with respect to spacing between the coil and conductor, results similar to those illustrated in Figure XVII will be obtained. As the distance from the probe to the conductor increases, the eddy current field is reduced and therefore has less influence on the field of the coil, and the lift-off curve approaches the air balance point. The lift-off curve will not retrace the conductivity curve as illustrated. Since the lift-off curve does not retrace the conductivity curve, it is possible, in most cases, to establish a relationship between coating thickness (lift-off) and impedance changes in the coil. These changes are normally measured as current changes according to equation 4. Lift-off characteristics in RPP are illustrated in Figure XVIII. The expanded section of the conductivity curve is a least squares best fit line connecting air balance, bare uncoated RPP, and bare machined RPP that has been coated and the coating machined off to expose the carbon-carbon substrate. This data was taken from the machined portions of the dash 4 specimens and is recorded in Table 3. Plastic shims placed between the specimen and the probe were used to measure the lift-off distance. These three curves resemble those in Figure XVII.

From this information it can be concluded that eddy currents can be used to measure coating thickness if other factors, such as, nonuniformity of the substrate, are not overshadowing factors. Two approaches were considered when evaluating the LTV Data:

(1) Optically measured coating thickness as the dependent variable and resistance as the independent variable.
(2) Optically measured coating thickness as the dependent variable and vector length (V) as the independent variable

$$V = \sqrt{(R_1 - R_2)^2 + (X_1 - X_2)^2} \qquad (6)$$

Where: $R_1$, $X_1$ is a point selected to maximize the influence of the characteristic being evaluated and minimize all others. This point is called the operating point.

A comparison of columns T(CAL) in Table 3 for both T(ACT)/V and T(ACT)/R reveals that the two regression lines are almost superimposed. For both regression curves:

| | | |
|---|---|---|
| Standard Deviation of Thickness | = | 0.0212 |
| Standard Deviation and V | = | 24.005 |
| Covariance of Thickness/R or V | = | 0.00086 |
| Coefficient of Correlation | = | 0.998 |

From this data it was concluded that either approach would produce almost identical results.

The Phase Master was developed by Dr. C. V. Dodd, at Oak Ridge National Laboratory. It is a phase sensitive instrument that measures both current and the phase angle of the reactive component. In this instrument two coils are mounted co-axially with, inside of, and at each end of, a third coil. The two inner coils are connected in series and oppose each other so that the voltage induced by the third coil is zero when the field of the exciting coils is in the air. When a conductor is placed in the field of the exciting coil, eddy currents are induced in the conductor. The magnetic field of the eddy currents opposes the field of one of the two coils. The other coil is far enough from the conductor that it is not influenced by the eddy current field. This reaction field changes the apparent impedance of the closest coil and causes a voltage to flow across the terminals of the two inner coils. The phase angle between the exciting voltage and the voltage in the two small coils and the magnitude of the voltage across the two small coils is read on instrument meters. Phase and voltage magnitude can be plotted as illustrated in Figure XVIB. Frequency changes cause the same general changes in curve shape that have been previously discussed. Basically, the magnitude can be related to the resistive component and phase can be related to the reactive component of the complex impedance. Either magnitude or phase can be plotted as the ordinate and thickness can be plotted as the abscissa. Also, it is sometimes possible to bias either reading with the other. Test parameters can be selected so that maximum change in phase angle or magnitude is realized for specific lift-off ranges, while the other is suppressed.

3.6.2 Beta-Backscatter techniques are used extensively to measure the cladding on printed circuits, nuclear fuel elements, and other clad and coated material where sufficient beta absorption differences exist between the coat or clad material, and the substrate. A basic set-up is illustrated in Figure XIX(A). When a source that emits beta paricles is positioned near a specimen, some of the particles are absorbed and some are reflected or scattered. A Geiger-Muller Counter Tube appropriately positioned counts the number of scattered particles that strike it. The strikes are registered on a digital counter. The duration of the count is precisely timed by a timer that starts and stops the digital counter. If a thin layer of material is placed between the source and the specimen, and the thickness of the thin layer is varied, the number of particles being absorbed and scattered will vary in a log/log relationship. If the particle count on bare material is subtracted from count obtained when different thicknesses are inserted and the thin layer thickness is plotted against particle count on a log/log scale, a line connecting the points will be straight. For homogeneous materials with smooth surfaces, two points will establish the relationship between counts per unit time and coating thickness. This relationship is illustrated in Figure XIX(B). The counts are normally made on a bare specimen and on one or two specimens of known coating thickness. However, because of the nonhomogeneousness of the coating, the substrate, the roughness of the surface, and the roughness of the coating/substrate interface, sufficient data points were measured on coated RPP to establish statistical accuracy.

3.6.3 Ultrasonic pulse echo techniques were evaluated because of the uncertainty of satisfactory accuracy that would be obtainable with eddy currents and beta-backscatter. Frequencies of 15, 20 and 25 MHz were used. Transducers and instrumentation were used that generated and displayed a maximum pulse length of one and one-half wave length. The high frequency and short pulse was necessary to adequately separate the signals reflected from the front and back surface of the coating. A plastic standoff was used between the transducers and the surface of the material. The signal from the plastic/air surface (front surface signal) is illustrated in Figure XX(A). The upper signal is an expansion of a section of the lower signal and as shown is approximately $1\frac{1}{2}$ cycles long at a frequency of 20 MHz. Figure XX(B) shows the back surface multiples from a 0.012 inch thick titanium specimen. The front surface signal is inverted since the sound is traveling from a less dense to a more dense medium. The downward pointing points are signals from the back surface of the titanium. The clear separation of the back surface multiples illustrates equipment capability. The signal illustrated in Figure XX(C) is from the plastic/coated RPP interface.

3.7 Optical Thickness Measurements were conducted on all dash 2, 3a, and 6 specimens along row A, B, C and D, just off-center from the center line of the effective probe positions. After the specimens were sectioned, the cut surface was scribed at the junction of the rows and columns 1 thru 7 to locate the center line of the probe position with respect to the seven columns, reference Figures XIII, XIV and XXII.

All measurements were made with an American Optical Stereo-Microscope at 60X magnefication using a reticle graduated in 0.001 inch per division. Positioning of the specimen was accomplished with a micrometer adjustable stage graduated in 0.001 inch per division.

Measurements were made on all dash 2 row D measurement points in the "as cut" condition and the metallographically mounted and polished condition. No appreciable difference was observed in the two sets of measurements. Based on these results all subsequent measurements were made in the "as cut" condition. Two measurements were made on all dash 2 specimens at row D:(1) to determine the coating thickness, and (2) to determine surface roughness. The technique for measuring coating thickness was as follows:

(1) Position the reticle reference line, zero inch, parallel to the surface and tangent to the peaks,
(2) Position the reticle center line 0.012 inch on one side of the scribe line,
(3) Measure the distance from the zero line to the interface of the coating and the substrate and record,
(4) Reposition the reticle center line 0.025 inch from the point just measured and in a direction away from the scribe line and repeat steps 1 thru 3 for five measurements
(5) Repeat steps 1 thru 4 on the opposite side of the scribe mark, and
(6) Average the ten measurements.

The technique for measuring surface roughness was as follows:

(1) Position the reticle reference line, zero inch, parallel to the surface and tangent to the peaks,
(2) Position the reticle center line at the center of a valley,
(3) Measure the distance from the peak to the valley,
(4) Make two measurements per surface at each scribe mark and average the measurements for each surface.

The above technique for coating thickness measurements, recommended by Mr. R. W. McClung, permitted all measurements to be made within the $\frac{1}{4}$-inch effective measurement area for all three NDT methods and was used for all coating thickness measurements.

Surface roughness measurements averaged 0.007 inch for the bag side and 0.004 for the mold side of all nine (9) specimens. Figure XXIII illustrates this condition. Also illustrated in Figure XXIII is the roughness of the interface between the coating and the substrate.

## SECTION IV

## ANALYSIS OF DATA

4.1 Data Analysis was accomplished by developing statistical models and comparing a percentage of the total data to the respective model. Statistical methods used in developing the models and in analyzing the samples are shown in Appendix 1. Following the first round of evaluations, all dash 2 specimens were sectioned at Row D and the thicknesses optically measured. This data along with measurements made on areas of zero coating thickness (machined areas of the dash 4 specimens) was used to develop the statistical models. A total of 56 data points were used to set up each model, 14 points for each of the nominal thicknesses (0, 0.020, 0.030 and 0.050).

4.2 Eddy Current Statistical Model for LTV Data was developed from the X and R values, and the actual coating thickness measurements listed in Table 4. A plot, Figure XXIV, of the X and R values for each of the 56 data points in this table shows that they follow the same basic pattern and have generally the same values as the plastic lift-off data plotted in Figure XVIII. Therefore, Figure XVIII was used to select the X and R values of an operating point. The selection was made so that the vector from the operating point to the lift-off curve is relatively perpendicular to the conductivity lines (dashed lines). This selection minimized conductivity differences. The operating point (X=480, R-670) was used to calculate vectors (v) from the operating point to each pair of X and R values. These vectors are listed in Table 4 and were calculated in accordance with Equation 6. If the X and R points on the instrument (Figure XV) were locked at the operating point values, the vector length would represent the meter reading. Therefore, a plot of the optically measured thickness on vector length can actually be considered a plot of coating thickness on meter reading as shown in Figure XXV.

A least squares regression line was calculated for the coating thickness on meter reading plot. A quadratic equation was used since the data formed a slightly curved pattern, Reference Appendix 1. Correlation analysis for Table 4 data shows that:

| | | |
|---|---|---|
| Standard Deviation of Thickness | = | 0.0177 inches |
| Standard Deviation of Vector Length | = | 24.748 |
| Standard Error of Estimate | = | 0.00265 |
| Coefficient of Correlation | = | 0.989 |

(1) The data correlates good with the regression line as indicated by the correlation coefficient, and

(2) Assuming that a given point on the regression line is the mean of a normal probability distribution and that the standard deviation is 0.00265 inches, then

(a) 68% of the measurements will be within ±0.00265 inch of the point on the regression line,

(b) 80% of the measurements will be within ±0.00339 inch of the point on the regression line,

(c) 90% of the measurements will be within ±0.00436 inch of the point on the regression line,
(d) 95% of the measurements will be within ±0.00519 inch of the point on the regression line.

Points of a Y (calculated) ±1.96 times the standard deviation band were calculated and are listed in Table 4. Also, these limits are plotted on Figure XXV.

The operating vector for the plastic lift-off data is listed in Table 3, Column V. This vector length and the lift-off distance (plastic shim thickness) were used to calculate the regression line plotted on Figure XXVI. Also, plotted on Figure XXVI, is the Figure XXVI coating thickness on meter reading regression line. The two lines are separated by an average of 0.00214 inch. The range of the separation is 0.00184 to 0.00225 for the six data points plotted. The calculated plastic thickness is greater than the calculated coating thickness. This almost constant 0.002 inch bias could be caused by one or a combination of several factors, three of which are (1) the influence of the slight conductivity of the coating layer compared to the zero conductivity of the plastic shim, (2) the substrate material on the probe side of the interface, and (3) averaging method for optical thickness measurements.

Regression analysis of the thickness/resistance data in Table 4 produced the following results:

| | | |
|---|---|---|
| Standard Deviation of Thickness | = | 0.0177 inch |
| Standard Deviation of Resistance | = | 24.137 |
| Standard Error of Estimate | = | 0.00245 |
| Coefficient of Correlation | = | 0.990 |

These results show slightly less scatter and better correlation than the thickness/vector data but the thickness/resistance regression line diverged from the plastic lift-off line and this approach is valid only as long as the lift-off line is basically parallel to R. Since the thickness/vector relationship indicated the possibility of using machined RPP and plastic shims as calibration standards, this data was selected for presentation and further analysis.

4.3 <u>The Eddy Current Statistical Model for Oak Ridge Data</u> was developed from amplitude and optically measured thickness values as listed in Table 5. The regression line developed from these values is plotted on Figure XXVII.

Correlation analysis shows that:

| | | |
|---|---|---|
| Standard Deviation of Thickness | = | 0.01494 inch |
| Standard Deviation of Amplitude | = | 1.050 |
| Standard Error of Estimate | = | 0.00191 |
| Coefficient of Correlation | = | 0.993 |

From this information it can be concluded that:

(1) There is good correlation between the data and the regression line as indicated by the correlation coefficient, and
(2) Assuming that a given point on the regression line is the mean of a normal probability distribution and that the standard deviation is 0.00265 inches, then
   (a) 68% of the measurements will be within ±0.0019 inch of the point on the regression line,
   (b) 80% of the measurements will be within ±0.00244 inch of the point on the regression line,
   (c) 90% of the measurements will be within ±0.00314 inch of the point on the regression line,
   (d) 95% of the measurements will be within ±0.00374 inch of the point on the regression line.

Points of a Y (calculated) ±1.96 times the standard deviation band were calculated and are listed in Table 5. Also, these limits are plotted on Figure XVIII. Plastic lift-off data for the Phase Master is not available, however, the fit should be equally as good as the data plotted in Figure XXVI.

4.4 Beta Backscatter Statistical Model for Los Alamos Data was developed from the optically measured coating thicknesses and particle counts listed in Table 6. The data is plotted in Figure XXVIII. The same regression analysis approach that was used for eddy current was used for this data. A base material particle count of 225 was subtracted for each reading prior to analysis. This produces a near zero count for zero coating thickness and increases the sensitivity. Regression data for thickness/particle count is as follows:

| | | |
|---|---|---|
| Standard Deviation for Thickness | = | 0.0126 inch |
| Standard Deviation for Count | = | 199.587 |
| Standard Error of Estimate | = | 0.00331 |
| Coefficient of Correlation | = | 0.965 |

From this information it can be concluded that:

(1) There is good correlation between the data and the regression line as indicated by the correlation coefficient, and
(2) Assuming that a given point on the regression line is the mean of a normal probability distribution and that the standard deviation is 0.00265 inches, then
   (a) 68% of the measurements will be within ±0.00331 inch of the point on the regression line,
   (b) 80% of the measurements will be within ±0.00424 inch of the point on the regression line,
   (c) 90% of the measurements will be within ±0.00514 inch of the point on the regression line,
   (d) 95% of the measurements will be within ±0.00649 inch of the point on the regression line.

Points of a Y (calculated) ±1.96 times the standard deviation band were calculated and are listed in Table 6. Also, these limits are plotted on Figure XXVIII. Inspection of Figure XVIII reveals that a particle count range from 396 to 464 was obtained for a thickness range of 0.020 inches to 0.023 inch. This particle count range also represented a thickness

range of 0.020 inch to 0.035 inch. This high degree of variance is reflected in the value for the standard deviation for particle count.

4.5 Sample correlation was made by randomly selecting 12 rows and observing if the values were within the prediction bands of the respective model. Comparison of the eddy current models shows that the Oak Ridge data exhibits less scatter than the LTV data. Higher operating frequency would reduce the scatter: LTV data was taken at 1.6 MHz and Oak Ridge data at 5.0 MHz. Scatter in all measurements may be reduced by revised optical thickness measurement techniques, and compensation for conductivity differences in the substrate.

4.5.1 Analysis of LTV Eddy Current Data shows that for the 152 points selected, 143 were within the prediction band of the LTV Statistical model. Reanalysis of the data was not conducted since 94.1% of the 152 points were within expected prediction band of the model. It is concluded that the statistical model represents the total data population and that coating thickness can be measured within the accuracy of this model.

The following points were selected for analysis:

| Specimen | Row | Specimen | Row | Specimen | Row |
|---|---|---|---|---|---|
| 1-2 | C | 3-2 | A | 7-2 | C |
| 2-2 | B | 4-2 | B | 8-3a | B |
| 2-3a | C | 5-3a | A | 8-6 | A |
| 2-6 | D | 6-2 | C | 9-2 | C |

4.5.2 Analysis of Oak Ridge Eddy Current Data shows that for the 146 points selected, 113 were within the prediction band of the Oak Ridge Statistical Model. Eleven of the 33 points were less than 0.001 inch outside of the prediction bands. Six of the remaining 22 points have optically measured thicknesses completely out of line with the other thickness values for that row and column. Ten of the remaining points are above 0.045 inch and appear to be data points that should have been included within the prediction band.

The remaining six points are within the normal percentage that were expected to fall outside of the prediction band.

The following points were selected:

| Specimen | Row | Specimen | Row | Specimen | Row |
|---|---|---|---|---|---|
| 1-2 | A | 4-3a | C | 7-3a | B |
| 1-6 | A | 4-6 | D | 7-6 | B |
| 2-2 | C | 5-2 | B | 8-2 | C |
| 3-2 | B | 6-2 | C | 9-2 | A |

4.5.3 Analysis of Los Alamos Beta Backscatter Data shows that for the 148 points selected, 100 were within the prediction bands of the Los Alamos Statistical Model. Since 32.4% of the sample was outside of confidence bands of the model, the model did not represent the total data population. However, since further analysis reveals that, within the 148 data points, a particle count range of 455 to 464 (9 counts) represents a thickness range of 0.0164 inch to 0.0519 inch and the thickness range of 0.020 to 0.025 is represented by a particle count range of 392 to 513 (121 counts), no further analysis was conducted.

The following points were selected:

| Specimen | Row | Specimen | Row | Specimen | Row |
|---|---|---|---|---|---|
| 1-2 | B | 4-2 | C | 7-2 | C |
| 2-2 | A | 5-2 | A | 8-2 | A |
| 3-3a | B | 6-3a | D | 9-3a | A |
| 3-6 | D | 6-6 | B | 9-6 | C |

## SECTION V

## CONCLUSIONS

5.1 From the foregoing data and analysis the following conclusions are drawn.

1. Test Method Selection - The Eddy Current Method will measure coating thickness. The nonhomogeneousness and surface and interface roughness prevent the use of Beta Backscatter. Ultrasonics can not be used because of the surface and interface roughness and the high attenuation properties of the material.

2. Eddy current Technique refinement will be required to reduce the scatter and to optimize this thickness measurement technique.

3. All data was taken from specimens processed at the same time and under basically the same conditions. Substrate conductivity could vary between specimens layed up at different times and under slightly different conditions that would invalidate the foregoing data.

4. Reference standards will be necessary to make production or field use of eddy current coating thickness measurement techniques.

5. No change was observed as a result of plasma arc exposure or from heat treatment.

6. Light weight, battery operated equipment, adaptable to both production and field inspections can be used to measure coating thickness.

## SECTION VI

## RECOMMENDATIONS

6.1 The following recommendations are made, based on the data presented, anticipated use of the material, present status of eddy current techniques used, and availability of equipment.

1. High frequency instrumentation in the 5-15 MHz should be developed to reduce scatter of the data, to furnish a readout in inches of coating thickness, and to make provisions for compensation for possible substrate conductivity differences.

2. Additional work should be accomplished to determine if there are conductivity differences in the substrate of a single specimen of sufficient magnitude to require compensation.

3. Develop reference standards for production and field use.

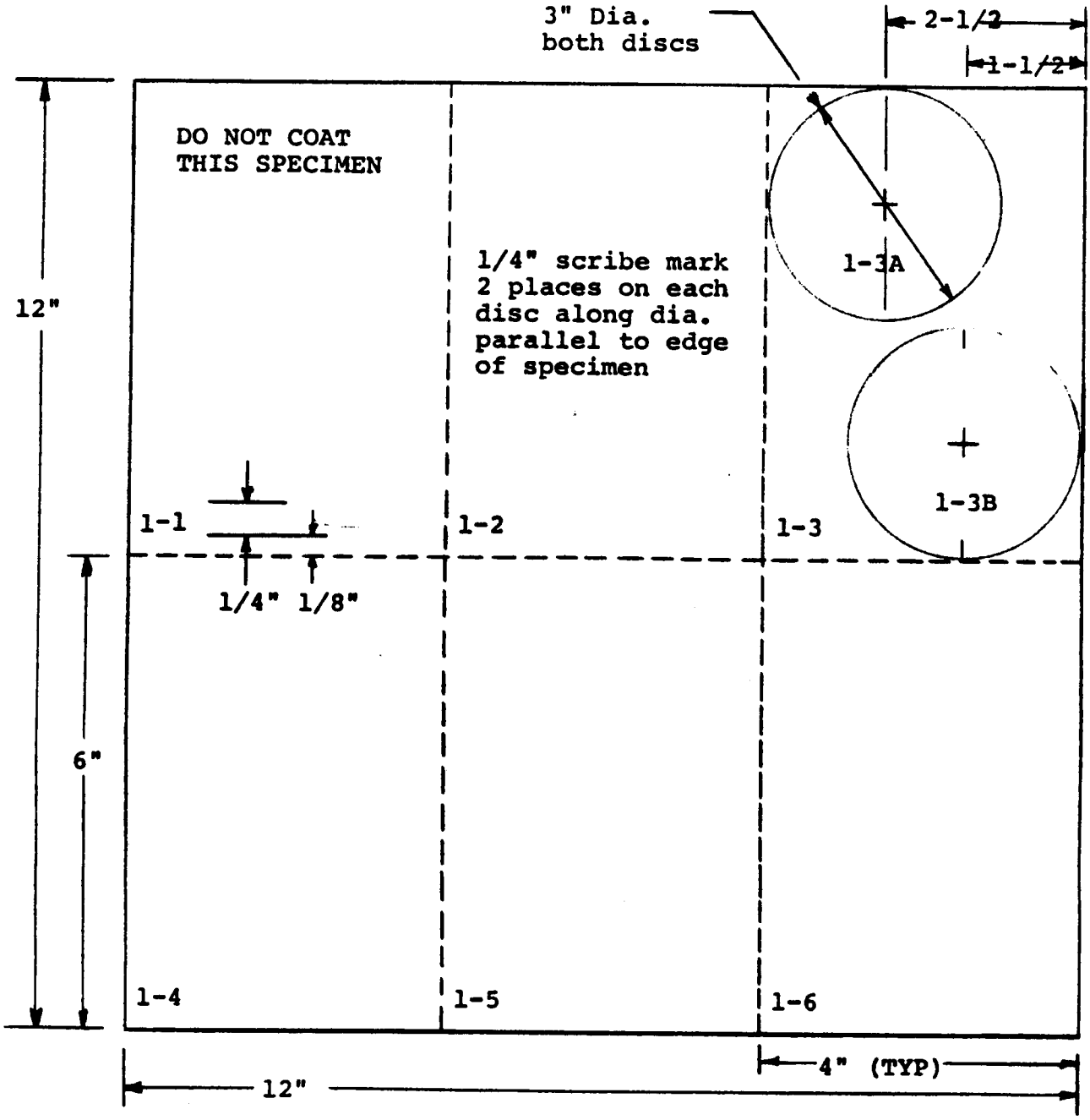


NUMBERING SYSTEM: 1 - 1

Number of the panel sectioned 1 - 9

Section number of the panel 1 - 6 except for No. 3 which will be identified as illustrated.

SPECIMENS FOR COATING THICKNESS MEASUREMENTS

FIGURE I

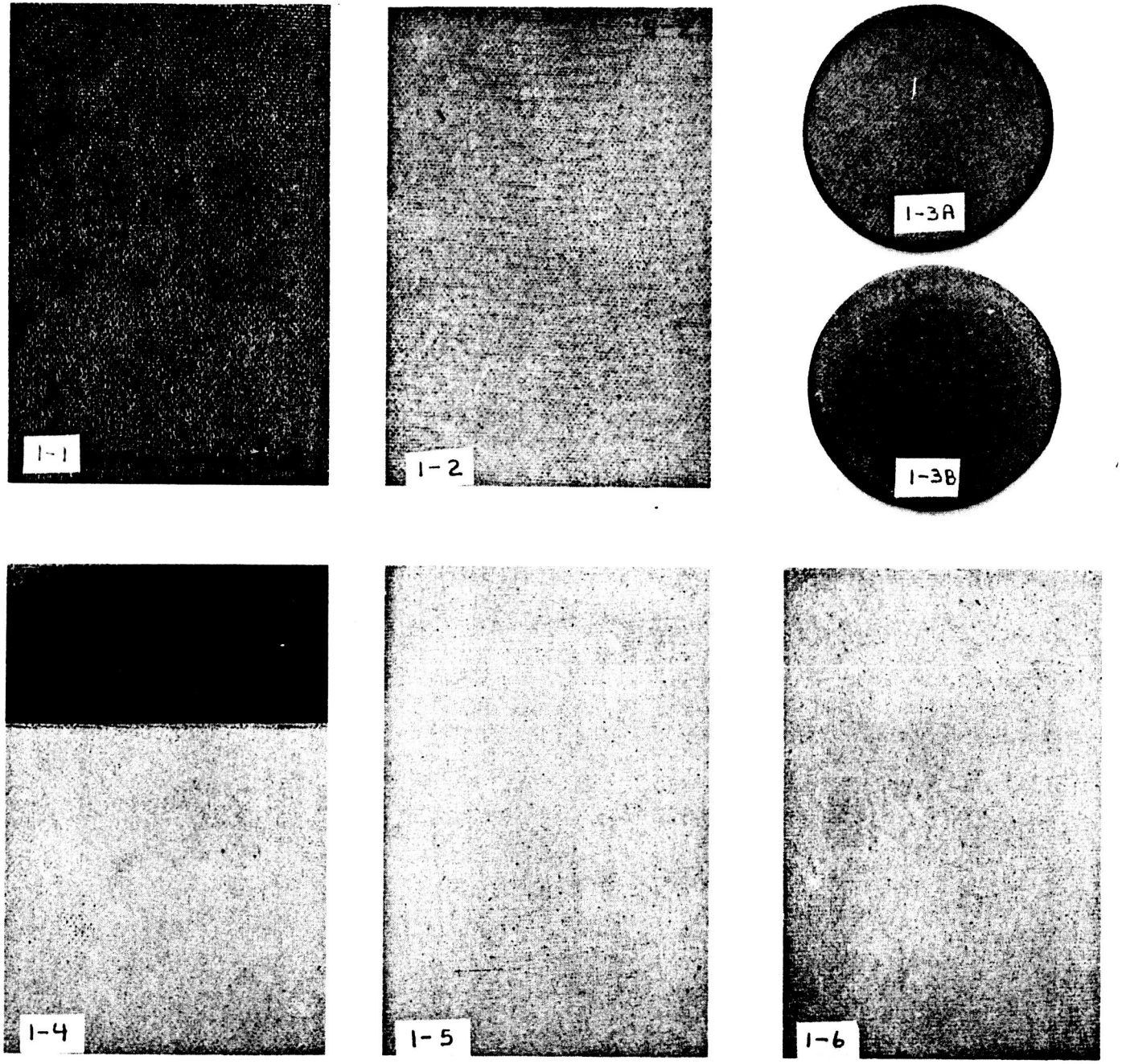


FIGURE II

PHOTOGRAPH OF FINISHED SPECIMENS

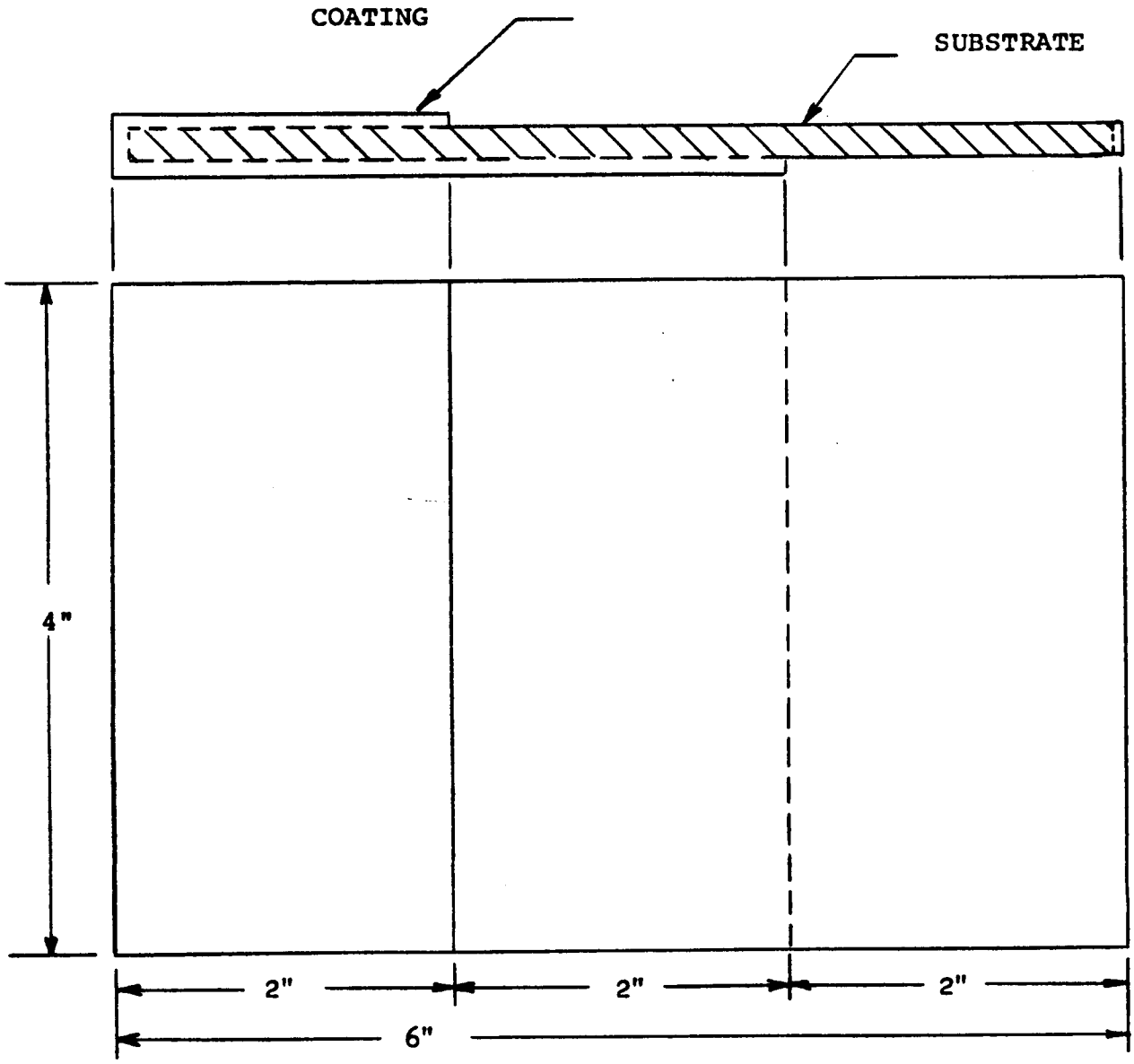


MACHINING REQUIREMENTS FOR THE DASH 4 SPECIMENS

FIGURE III

FIGURE IV

RADIOGRAPH OF PANEL NO. 8

SPECIMEN 6-4

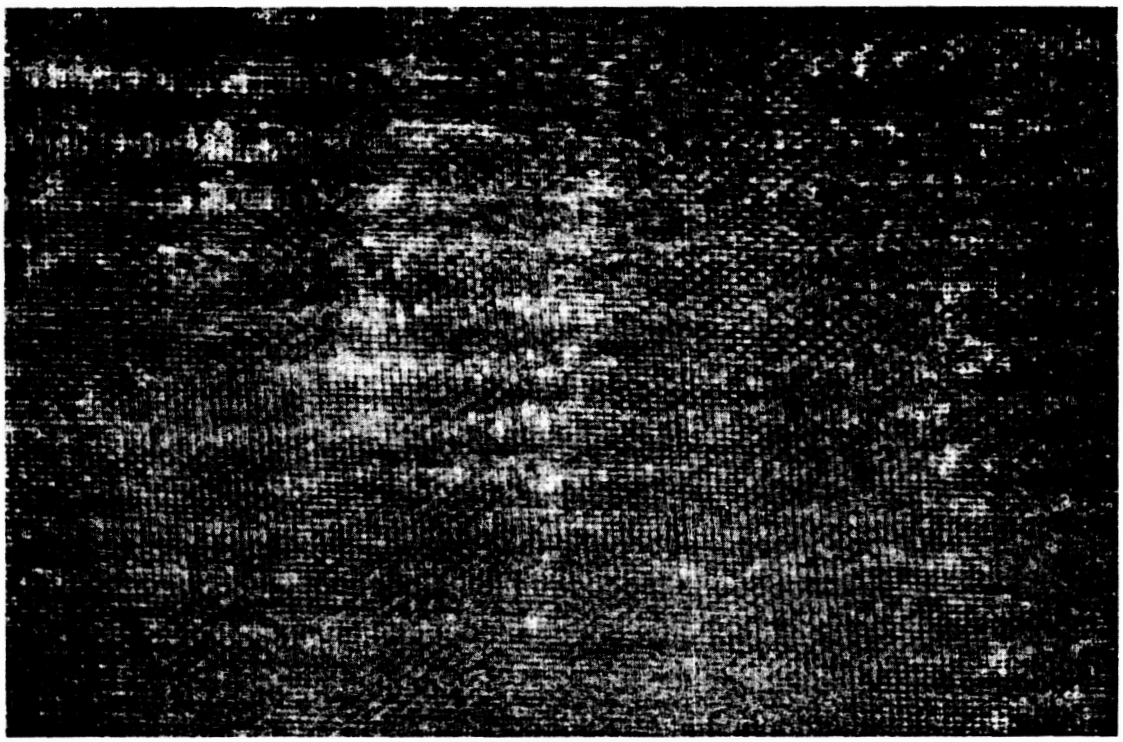

FIGURE V
RADIOGRAPHS SHOWING VARIATIONS
IN COATING THICKNESS

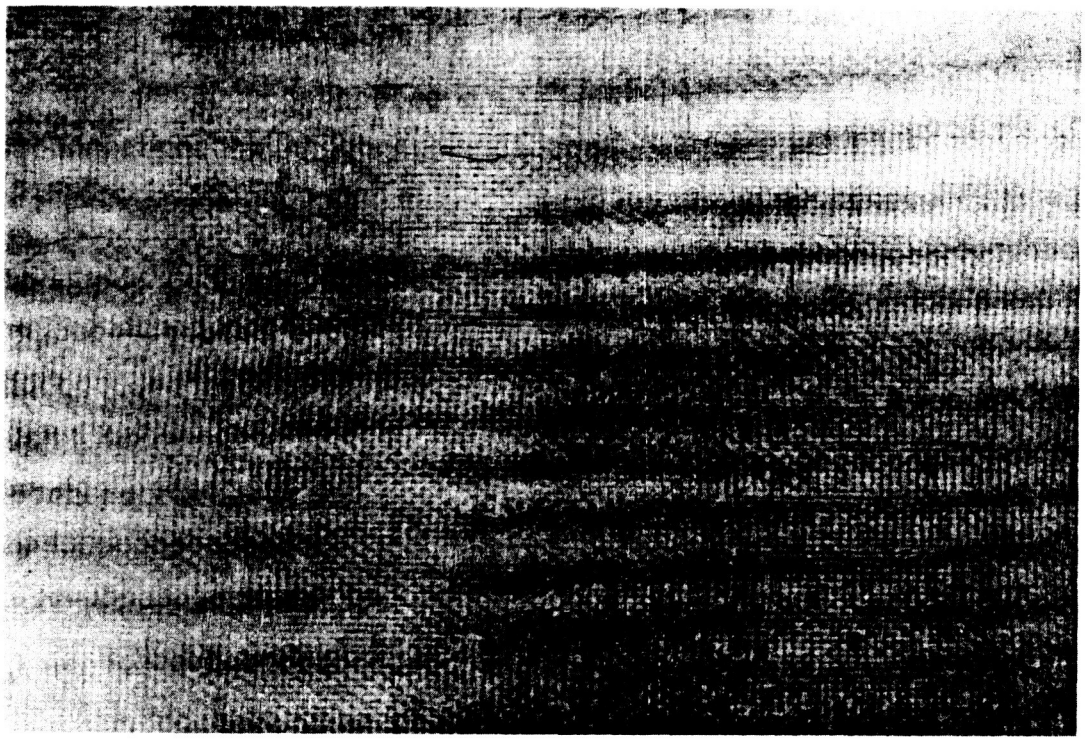

SPECIMEN 8-4

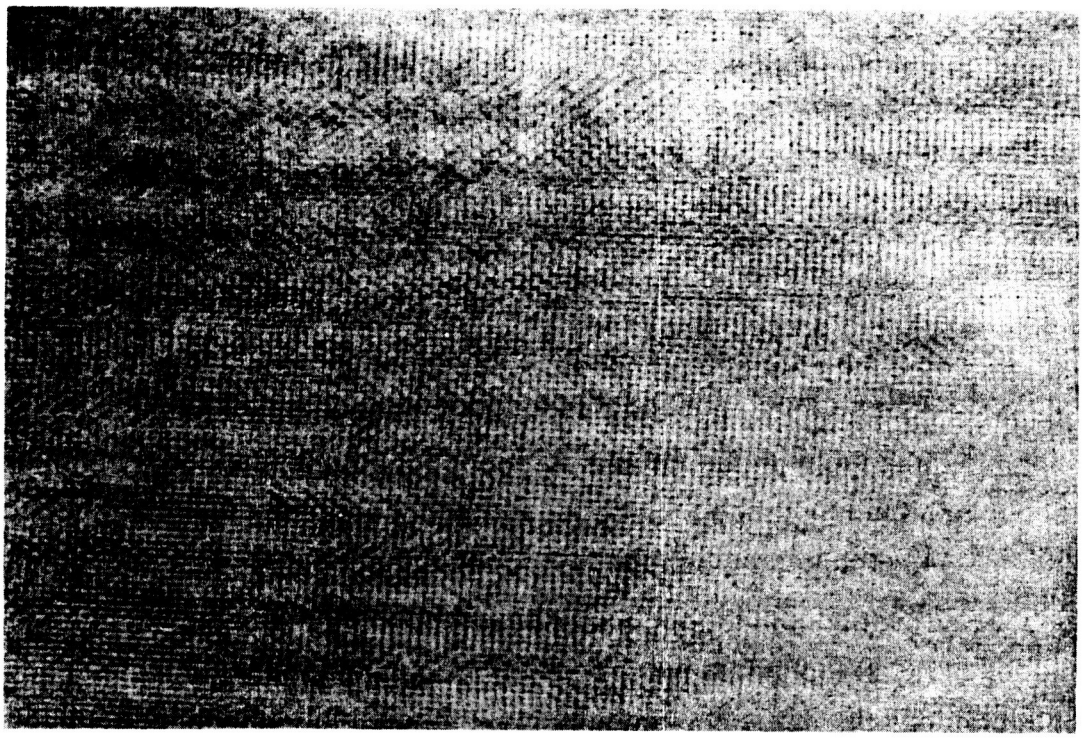

SPECIMEN 9-6

FIGURE VI

RADIOGRAPHS SHOWING VARIATIONS
IN COATING THICKNESS

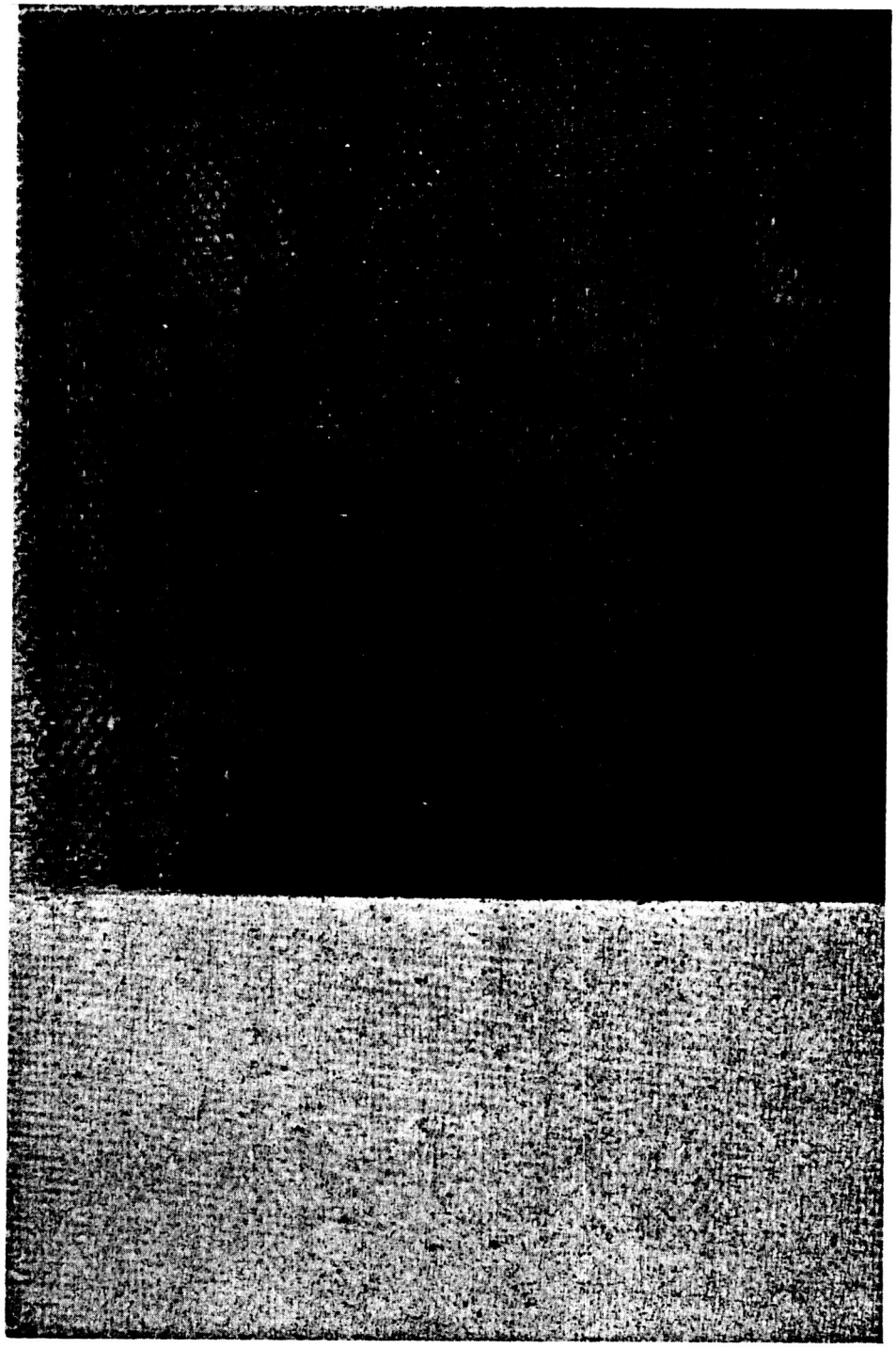

FIGURE VII

PHOTOGRAPH OF SPECIMEN 8-4 AFTER MACHINING

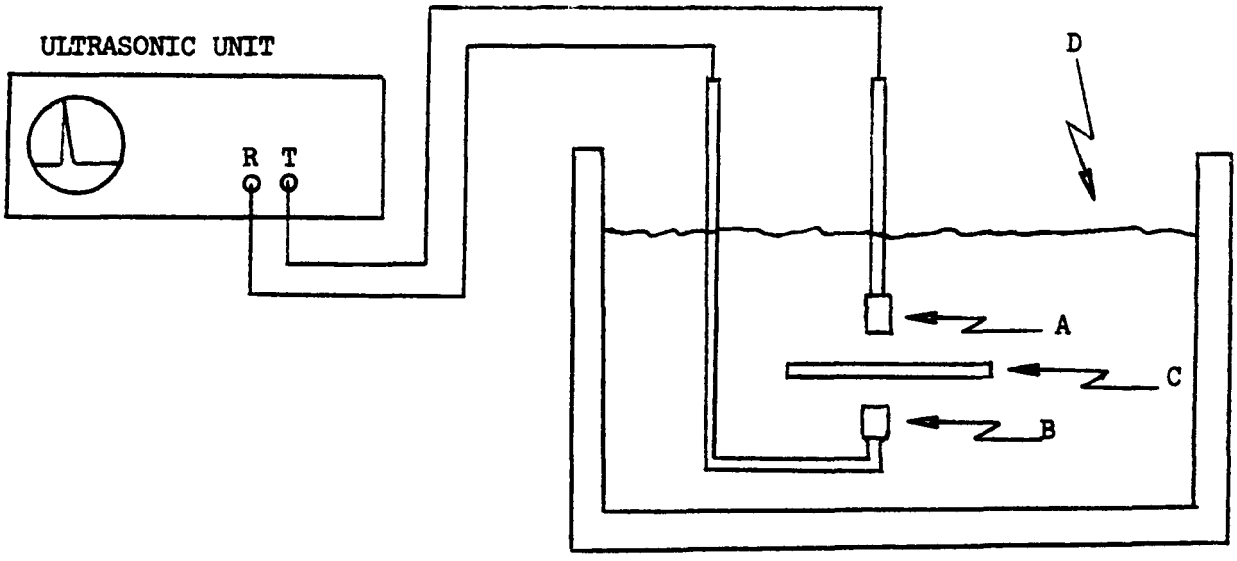


A - Transmitting Transducer

B - Receiving Transducer

C - Specimen Being Evaluated

D - Water Level in Tank

FIGURE VIII

ULTRASONIC THROUGH TRANSMISSION SETUP

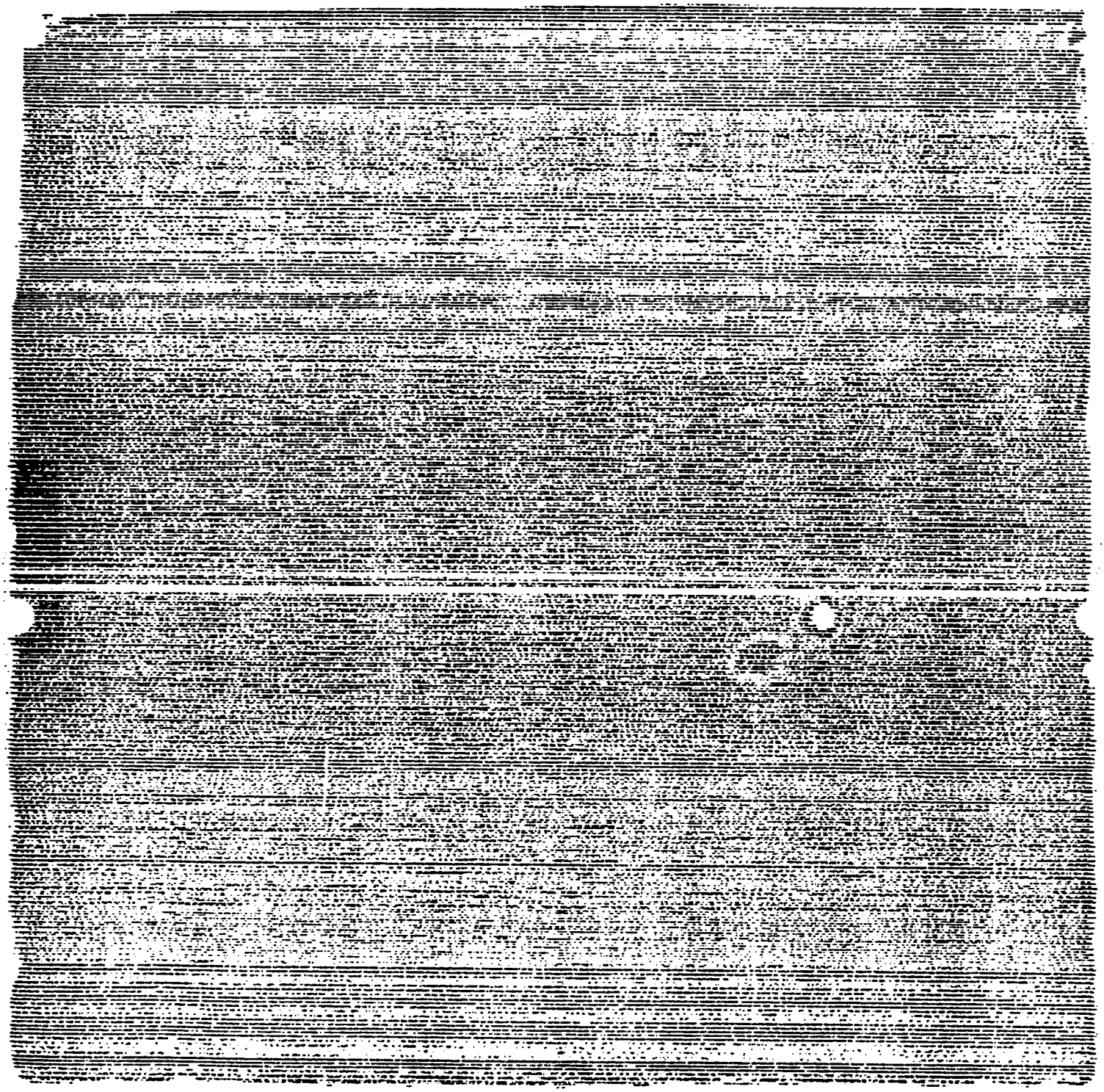

FIGURE IX

ULTRASONIC "C" SCAN RECORDING OF PANEL NO. 8

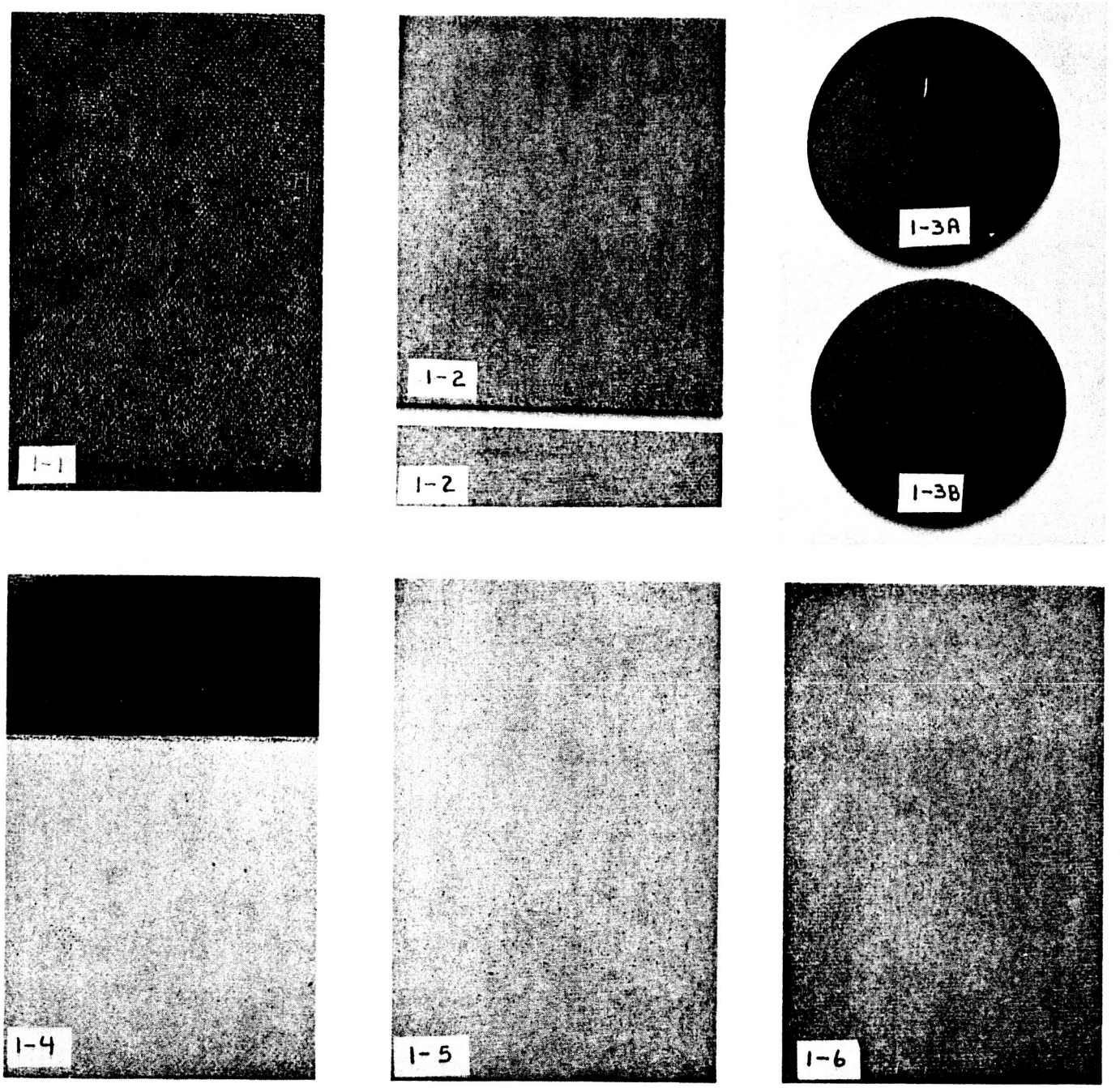


FIGURE X

PHOTOGRAPH SHOWING DASH 2 SPECIMEN SECTIONED AT ROW D

SPECIMEN NO. _____

LABORATORY _____

METHOD _____

EFFECTIVE AREA OVER WHICH READING WAS MADE _____

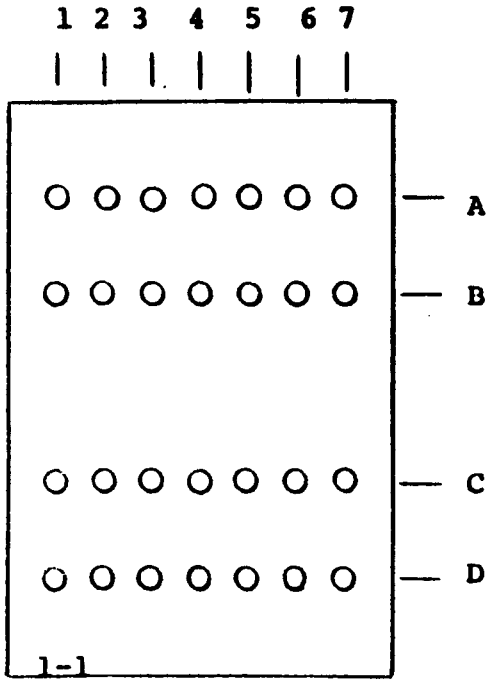


| ROW | SIDE 1 | | | | | | |
|---|---|---|---|---|---|---|---|
| | COLUMN / READING | | | | | | |
| | 1 | 2 | 3 | 4 | 5 | 6 | 7 |
| A | | | | | | | |
| B | | | | | | | |
| C | | | | | | | |
| D | | | | | | | |

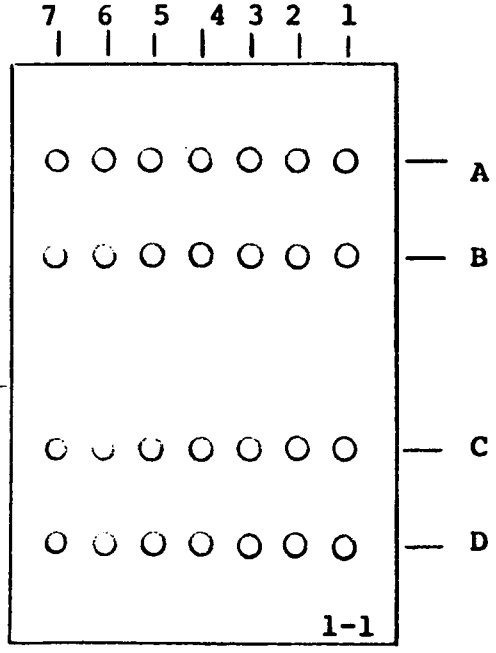


| ROW | SIDE 2 | | | | | | |
|---|---|---|---|---|---|---|---|
| | COLUMN / READING | | | | | | |
| | 1 | 2 | 3 | 4 | 5 | 6 | 7 |
| A | | | | | | | |
| B | | | | | | | |
| C | | | | | | | |
| D | | | | | | | |

FIGURES XI

RECORD OF READINGS FOR THICKNESS DETERMINATION

SPECIMEN NO.

LABORATORY

METHOD

EFFECTIVE AREA OVER WHICH READING WAS MADE

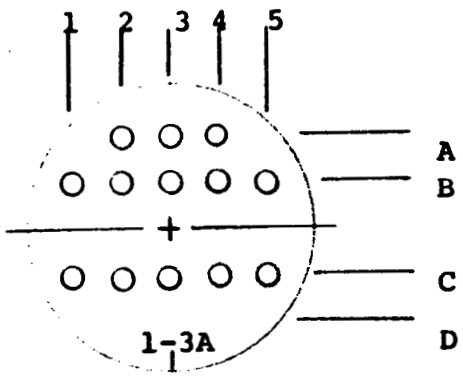


| ROW | SIDE 1 | | | | | | |
|---|---|---|---|---|---|---|---|
| | COLUMN / READINGS | | | | | | |
| | 1 | 2 | 3 | 4 | 5 | | |
| A | — | | | | — | | |
| B | | | | | | | |
| C | | | | | | | |
| D | — | — | — | — | — | | |

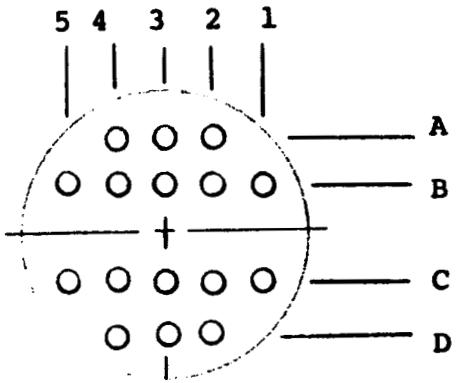


| ROW | SIDE 2 | | | | | | |
|---|---|---|---|---|---|---|---|
| | COLUMN / READINGS | | | | | | |
| | 1 | 2 | 3 | 4 | 5 | | |
| A | | | | | | | |
| B | | | | | | | |
| C | | | | | | | |
| D | | | | | | | |

FIGURE XII

RECORD OF READINGS FOR THICKNESS DETERMINATION

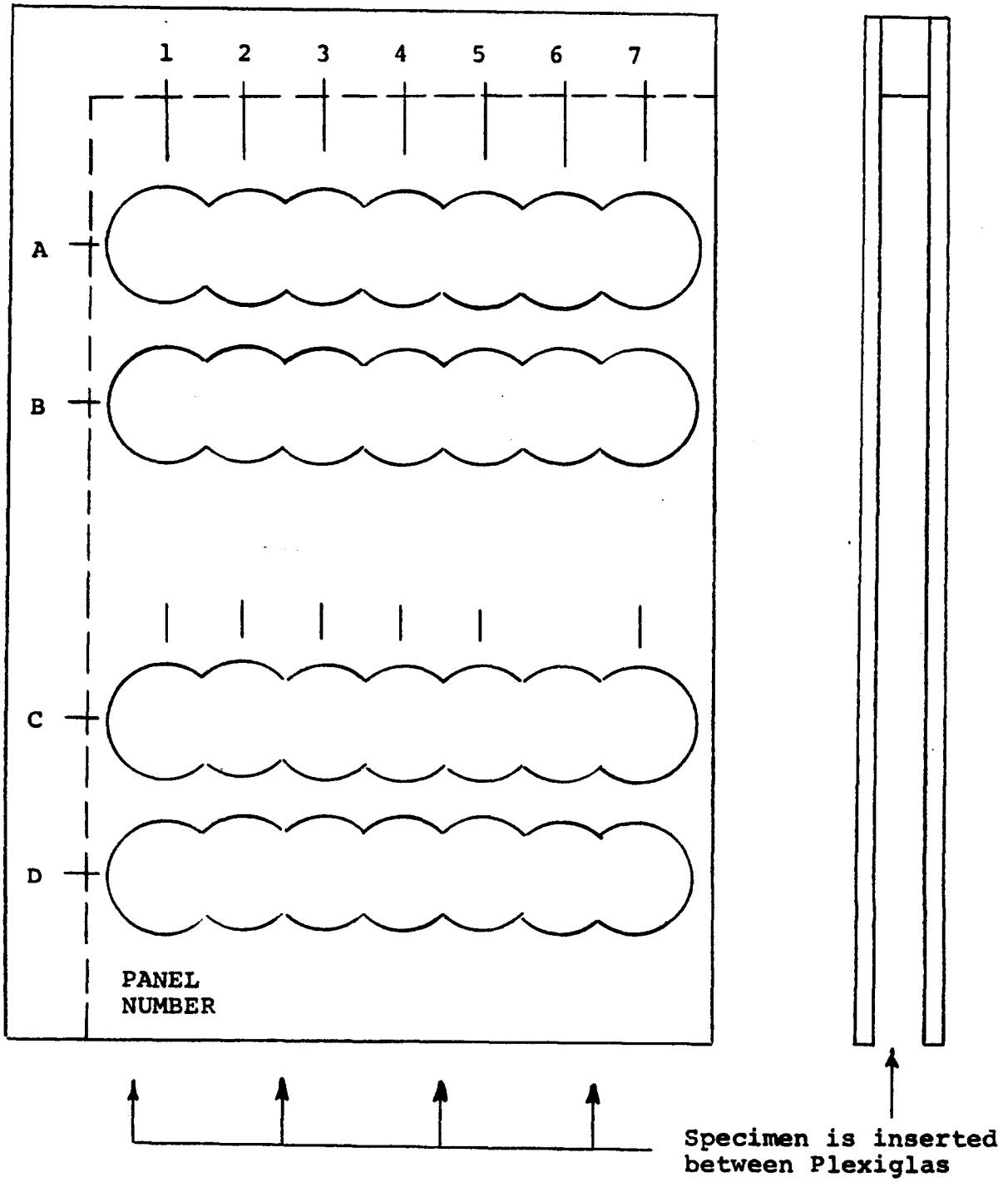


FIGURE XIII

READING TEMPLATE FOR 4.0 X 6.0 INCH SPECIMENS

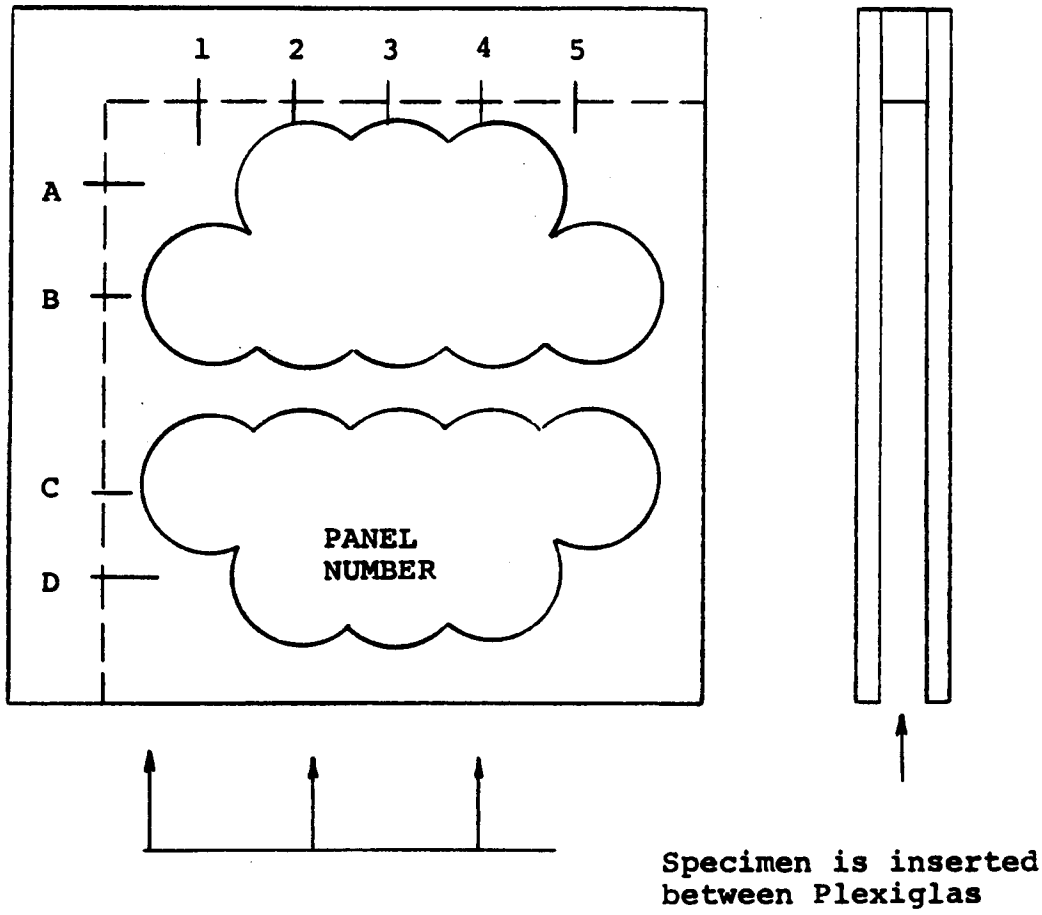


FIGURE XIV

READING TEMPLATE FOR 3.0 INCH
DIAMETER DISCS

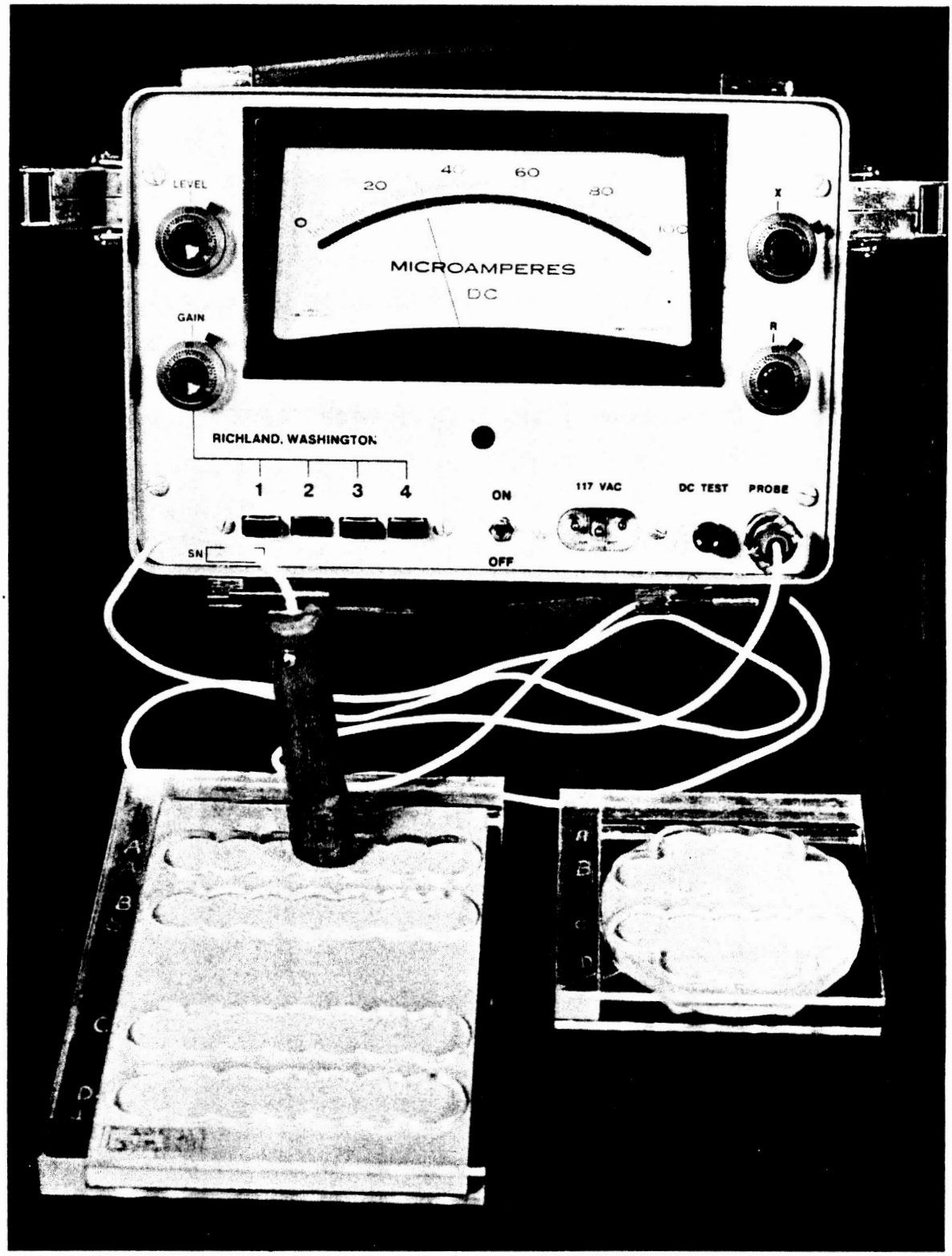


FIGURE XV

PHOTOGRAPH SHOWING TEMPLATE, PROBE, AND SPECIMEN RELATIONSHIP

KEUFFEL & ESSER CO.

FIGURE XVI

TYPICAL EDDY CURRENT DATA PLOTS

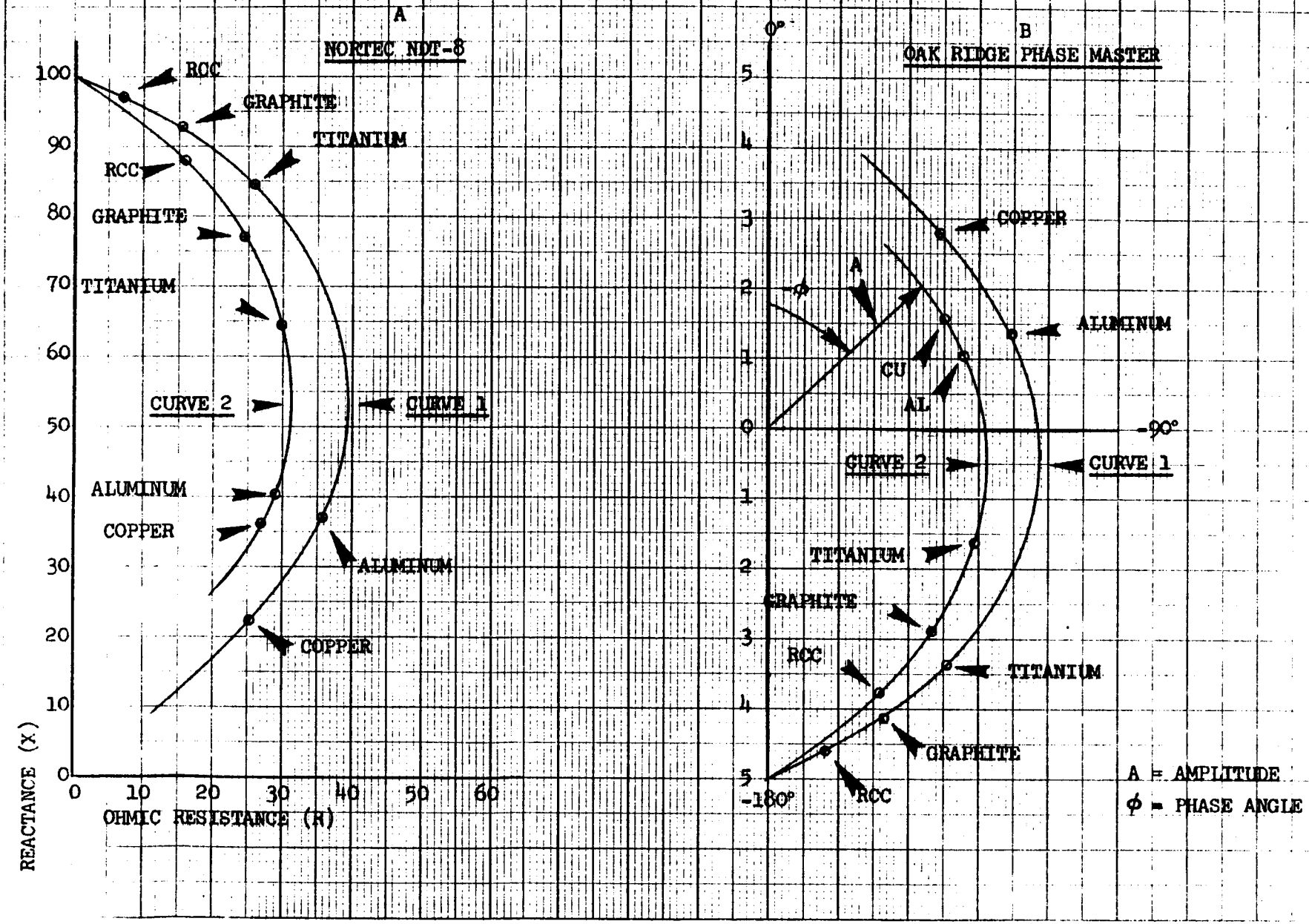

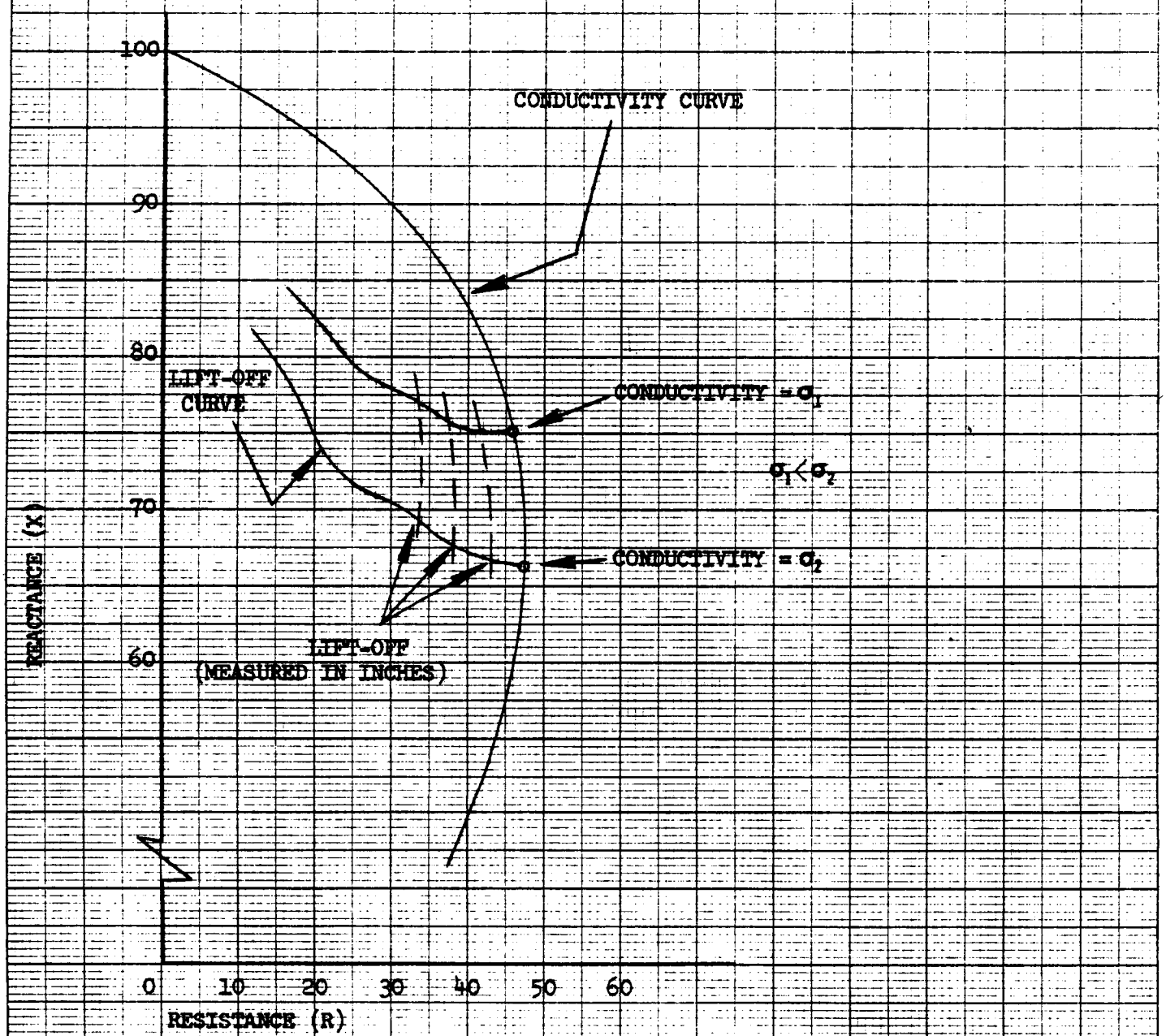


FIGURE XVII

LIFT-OFF CHARACTERISTICS

KEUFFEL & ESSER CO.

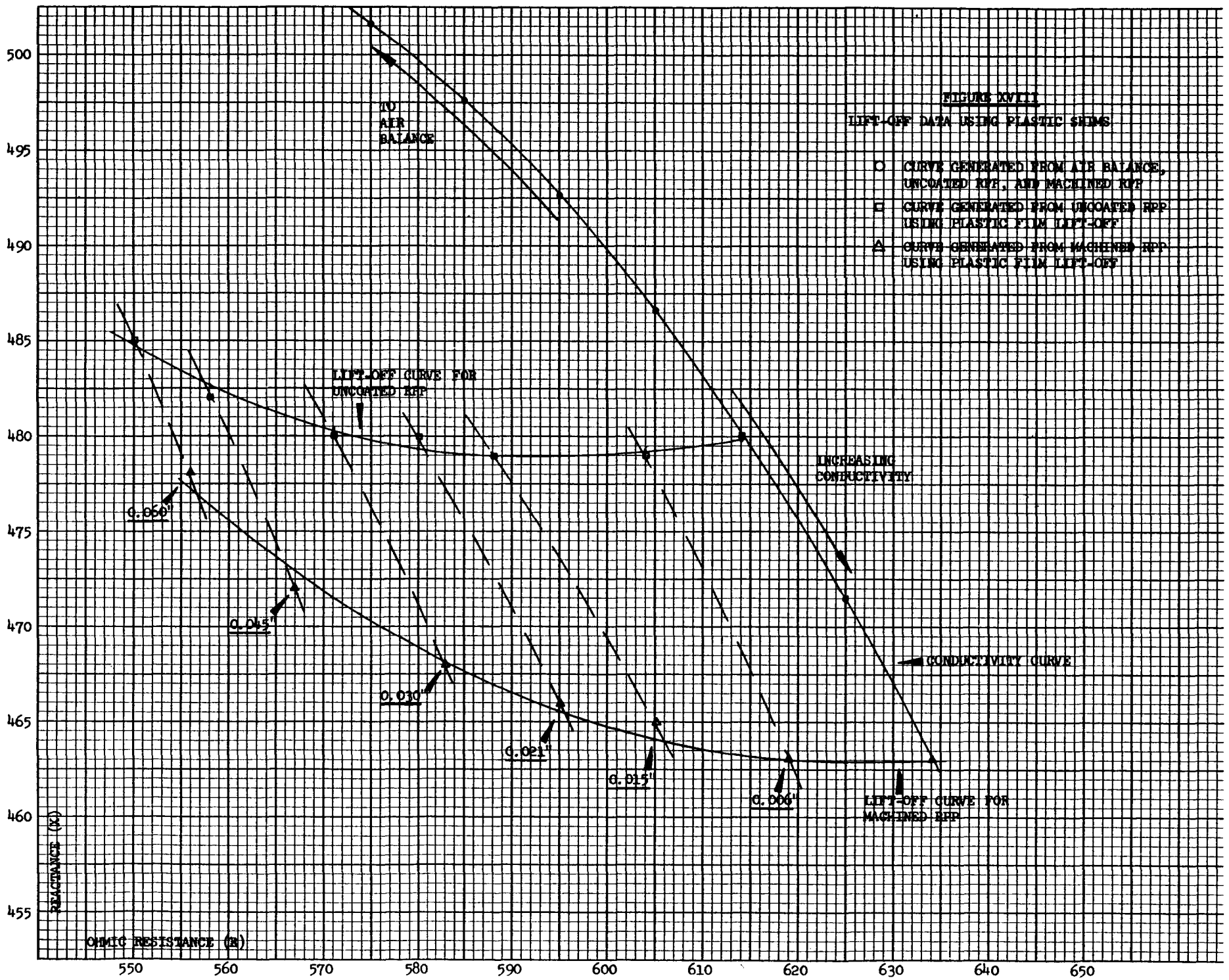


FIGURE XVIII

LIFT-OFF DATA USING PLASTIC SHIMS

○ CURVE GENERATED FROM AIR BALANCE, UNCOATED RPP, AND MACHINED RPP

□ CURVE GENERATED FROM UNCOATED RPP USING PLASTIC FILM LIFT-OFF

△ CURVE GENERATED FROM MACHINED RPP USING PLASTIC FILM LIFT-OFF

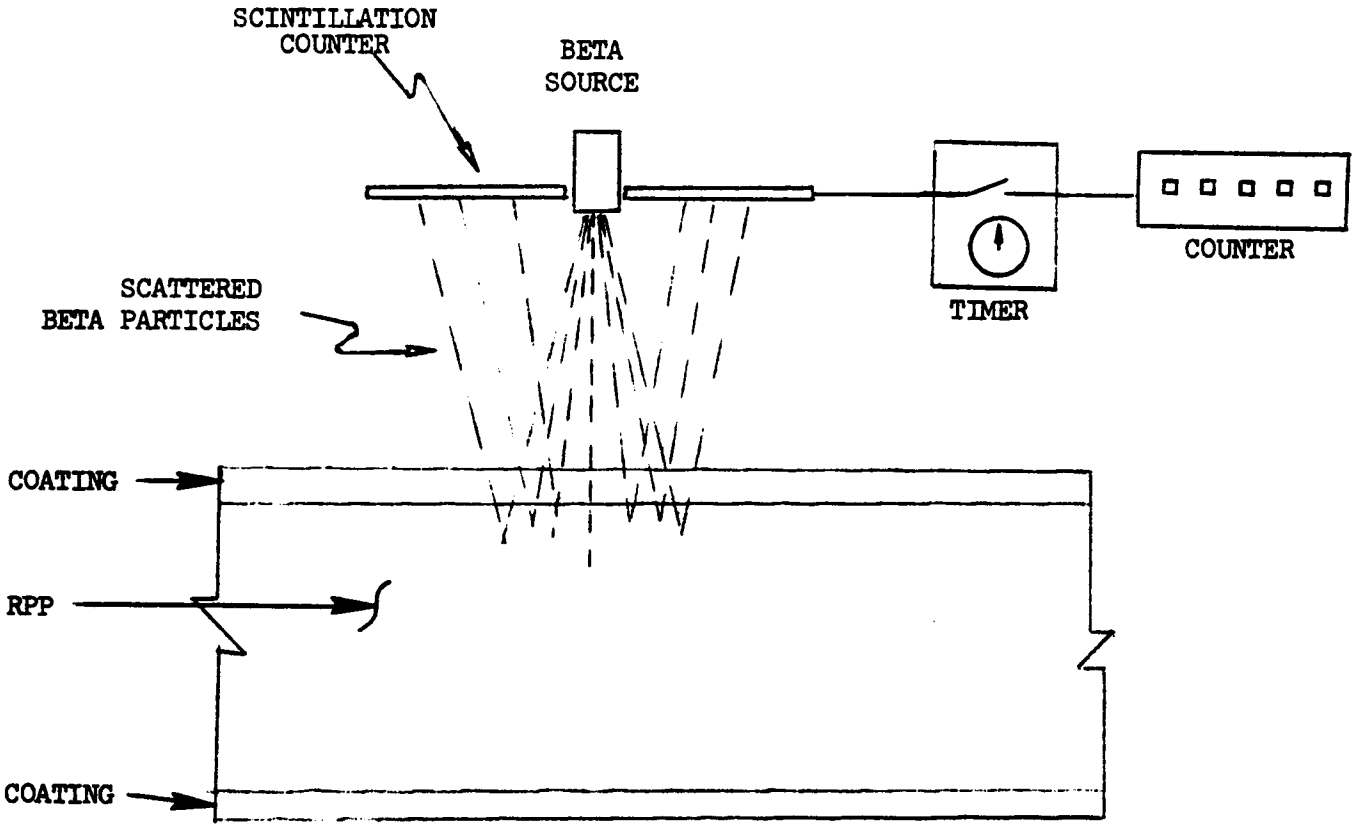


A

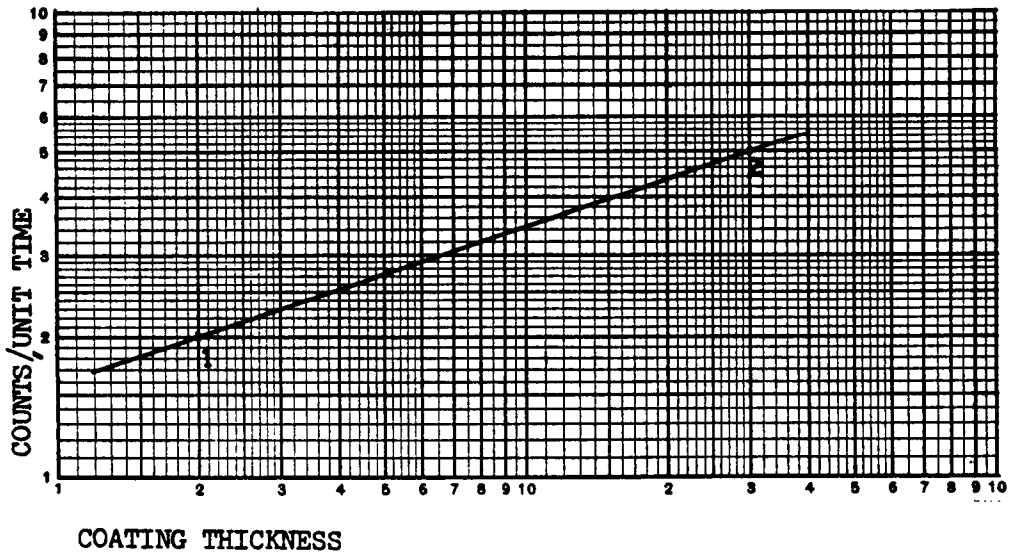


B

FIGURE XIX

BASIC BETA BACKSCATTER SETUP

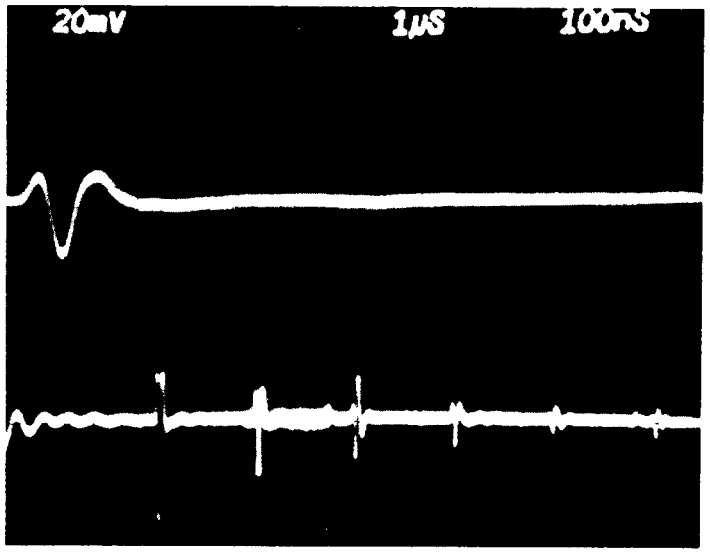


A

PLASTIC STANDOFF
TO
AIR SURFACE

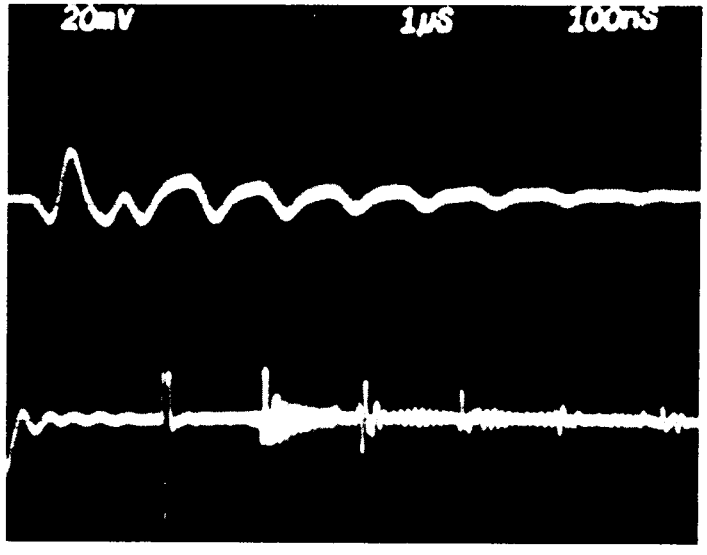


B

PLASTIC STANDOFF
TO
TITANIUM (0.012 INCH)

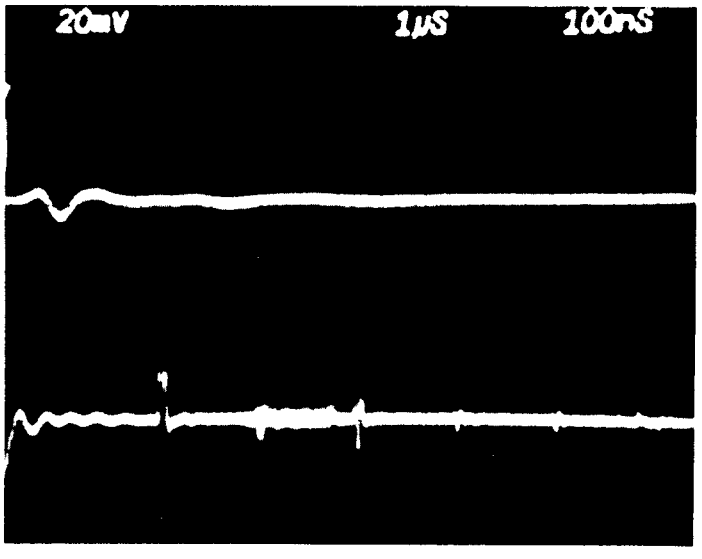


C

PLASTIC STANDOFF
TO
COATED RPP

FIGURE XX

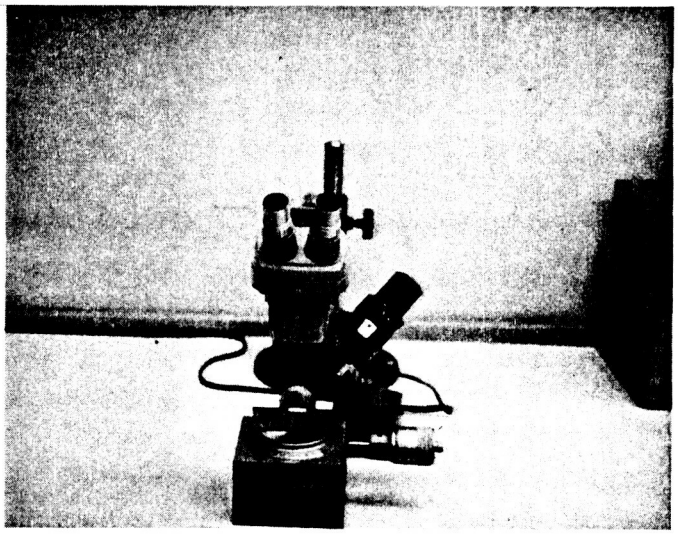

FIGURE XXI

STEREO-MICROSCOPE USED TO MAKE
OPTICAL MEASUREMENTS

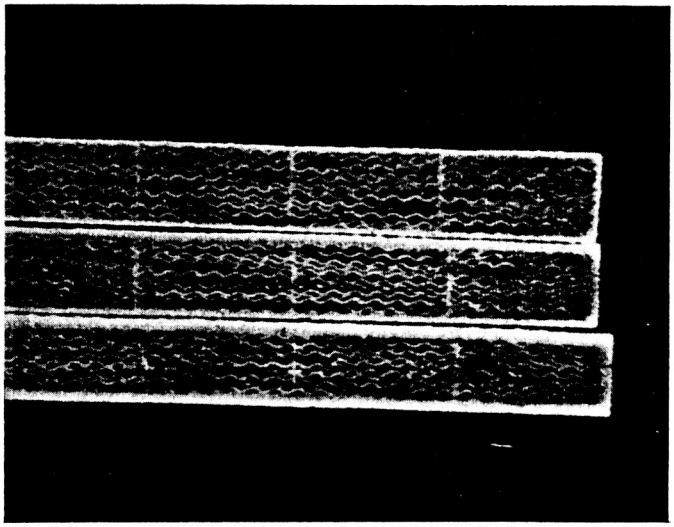

FIGURE XXII

SCRIBE LINES USED TO LOCATE THE
EXACT COLUMN POSITION

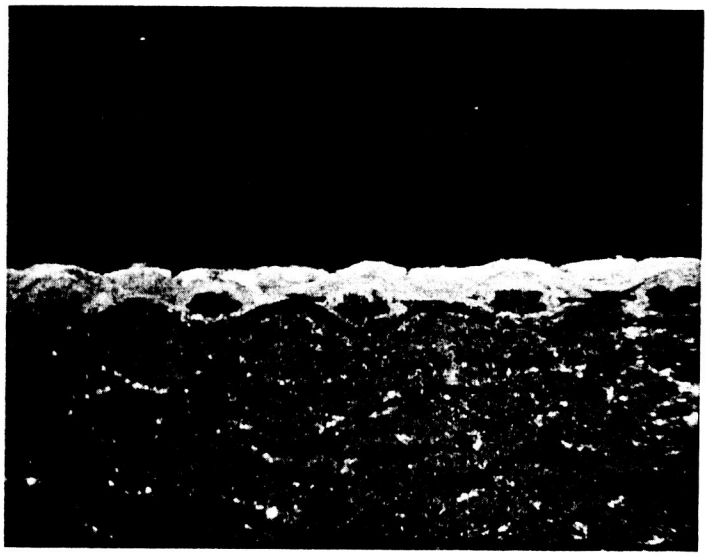

PHOTOGRAPH SHOWING SURFACE AND
INTERFACE ROUGHNESS
(10X)

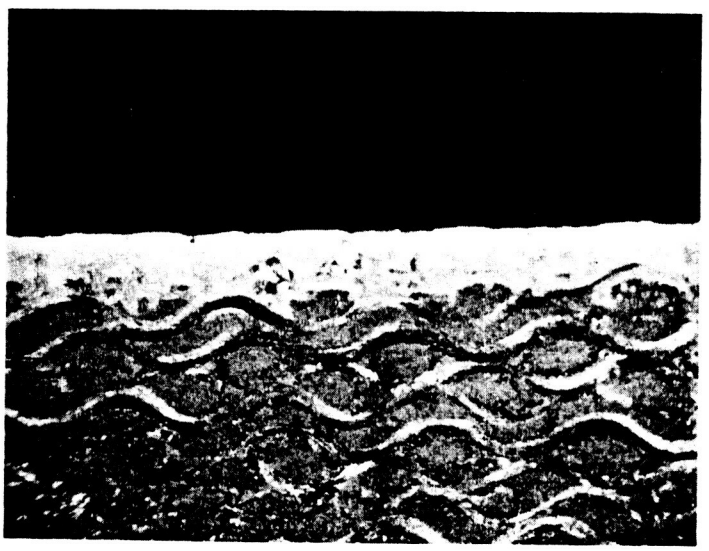

FIGURE XXIII

PHOTOGRAPHS SHOWING COATING CROSS-SECTION

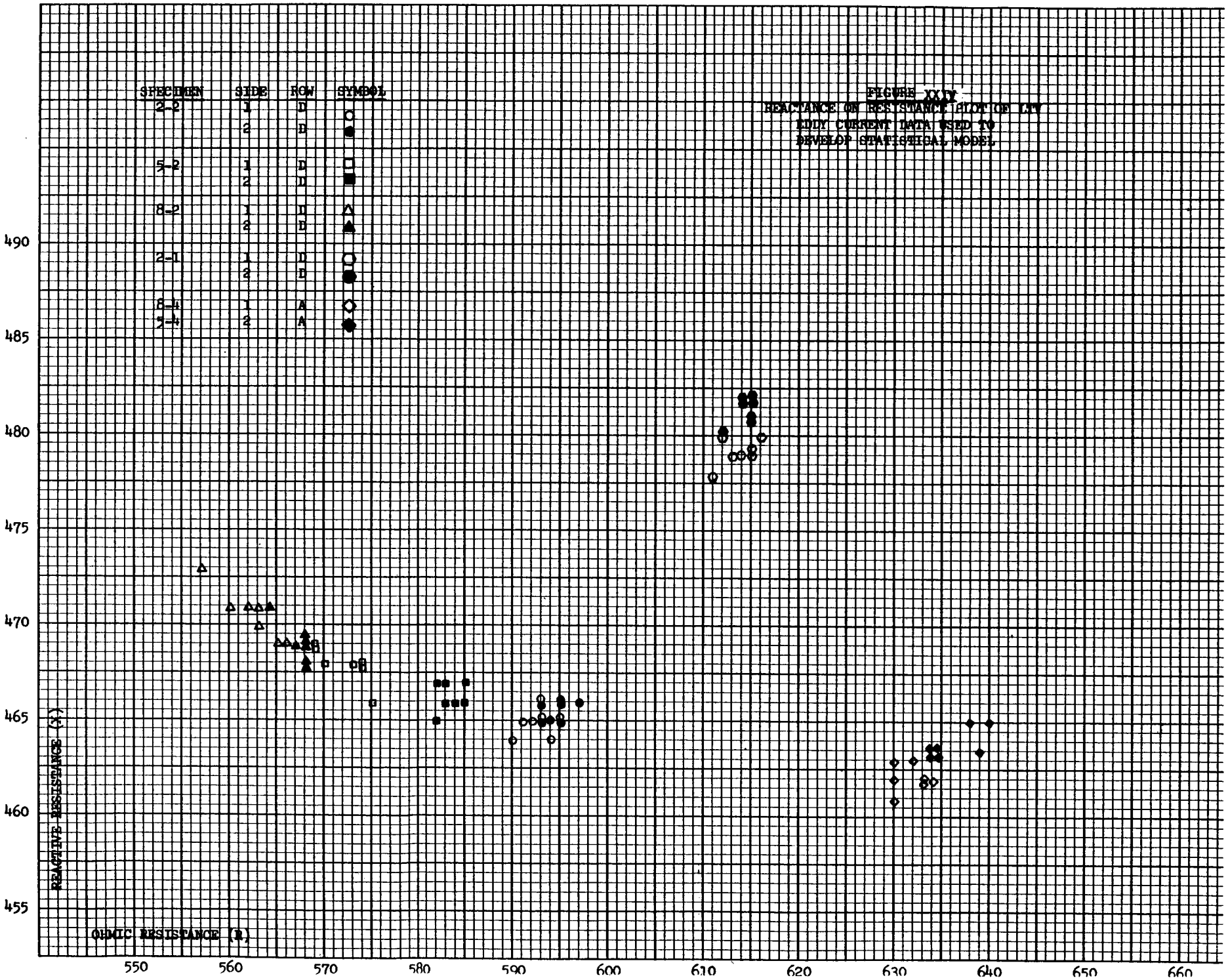


FIGURE XXIV
REACTANCE ON RESISTANCE PLOT OF EDDY CURRENT DATA USED TO DEVELOP STATISTICAL MODEL

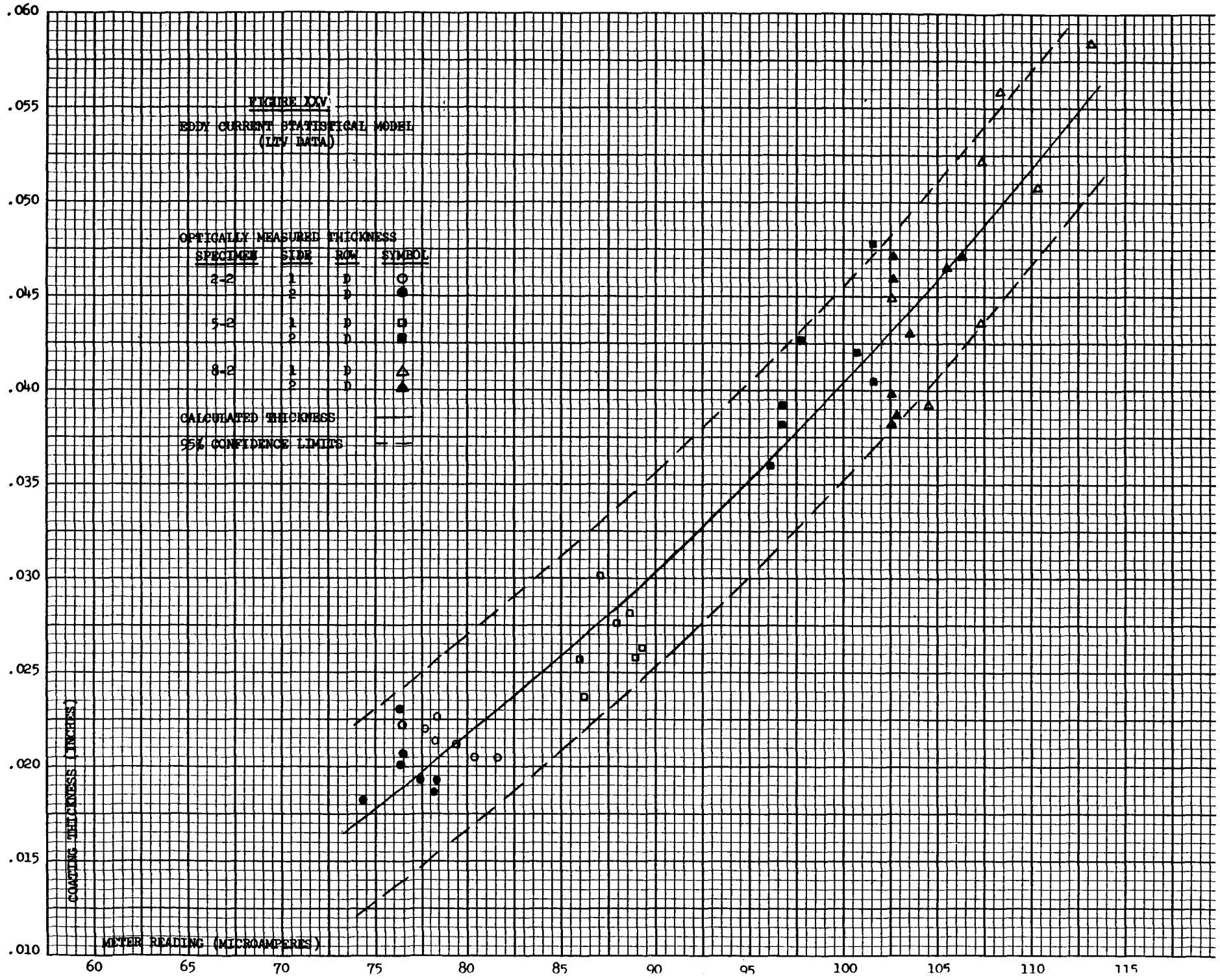
FIGURE XXV
EDDY CURRENT STATISTICAL MODEL
(LTV DATA)
OPTICALLY MEASURED THICKNESS
SPECIMEN SIDE ROW SYMBOL
2-2 1 D
2 D
5-2 1 D
2 D
8-2 1 D
2 D
CALCULATED THICKNESS
95% CONFIDENCE LIMITS
COATING THICKNESS (INCHES)
METER READING (MICROAMPERES)
.060
.055
.050
.045
.040
.035
.030
.025
.020
.015
.010
60
65
70
75
80
85
90
95
100
105
110
115

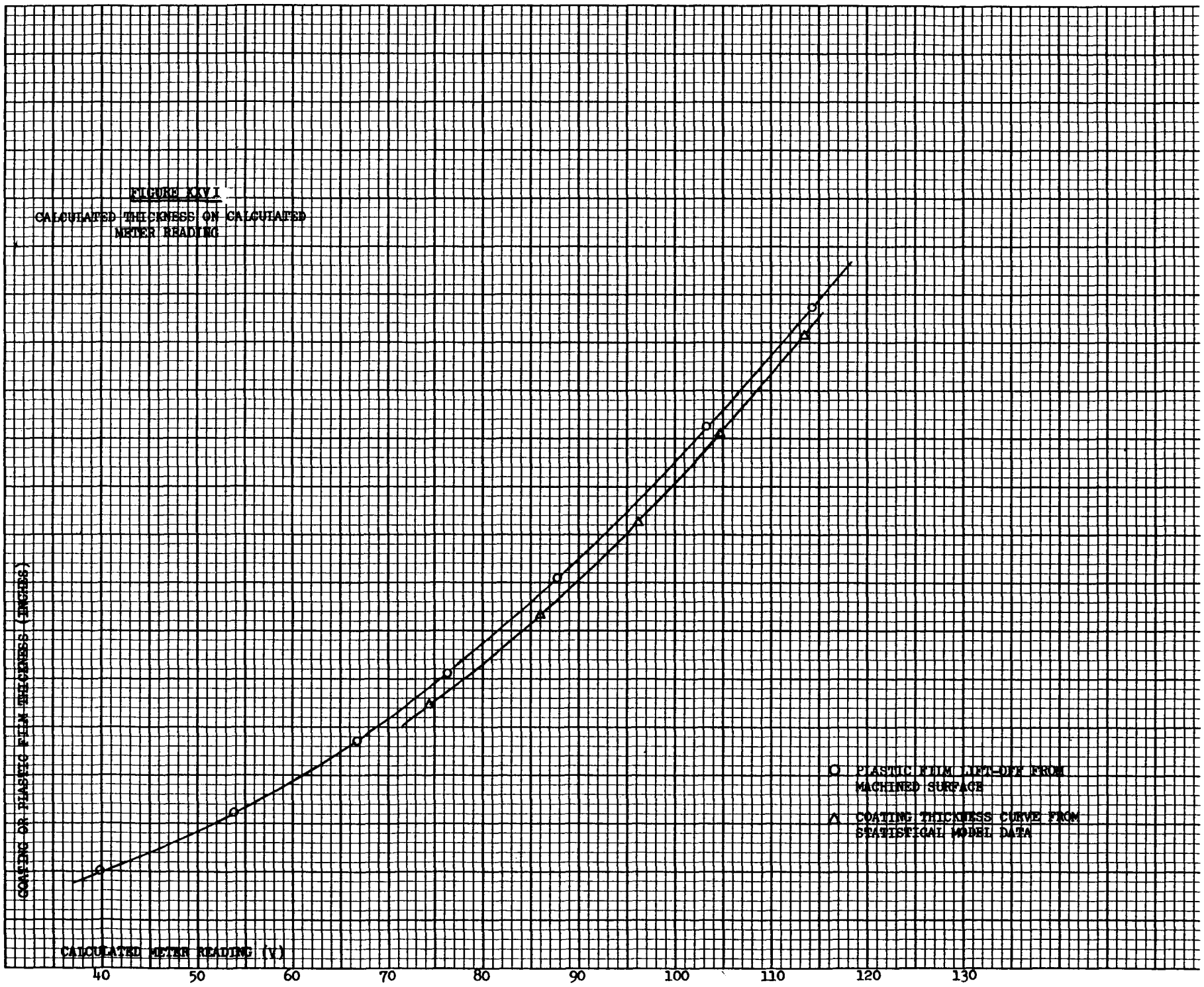
FIGURE XXVI
CALCULATED THICKNESS ON CALCULATED METER READING
COATING OR PLASTIC FILM THICKNESS (INCHES)
.065
.060
.055
.050
.045
.040
.035
.030
.025
.020
.015
.010
.005
.000
CALCULATED METER READING (V)
40
50
60
70
80
90
100
110
120
130
PLASTIC FILM LIFT-OFF FROM MACHINED SURFACE
COATING THICKNESS CURVE FROM STATISTICAL MODEL DATA

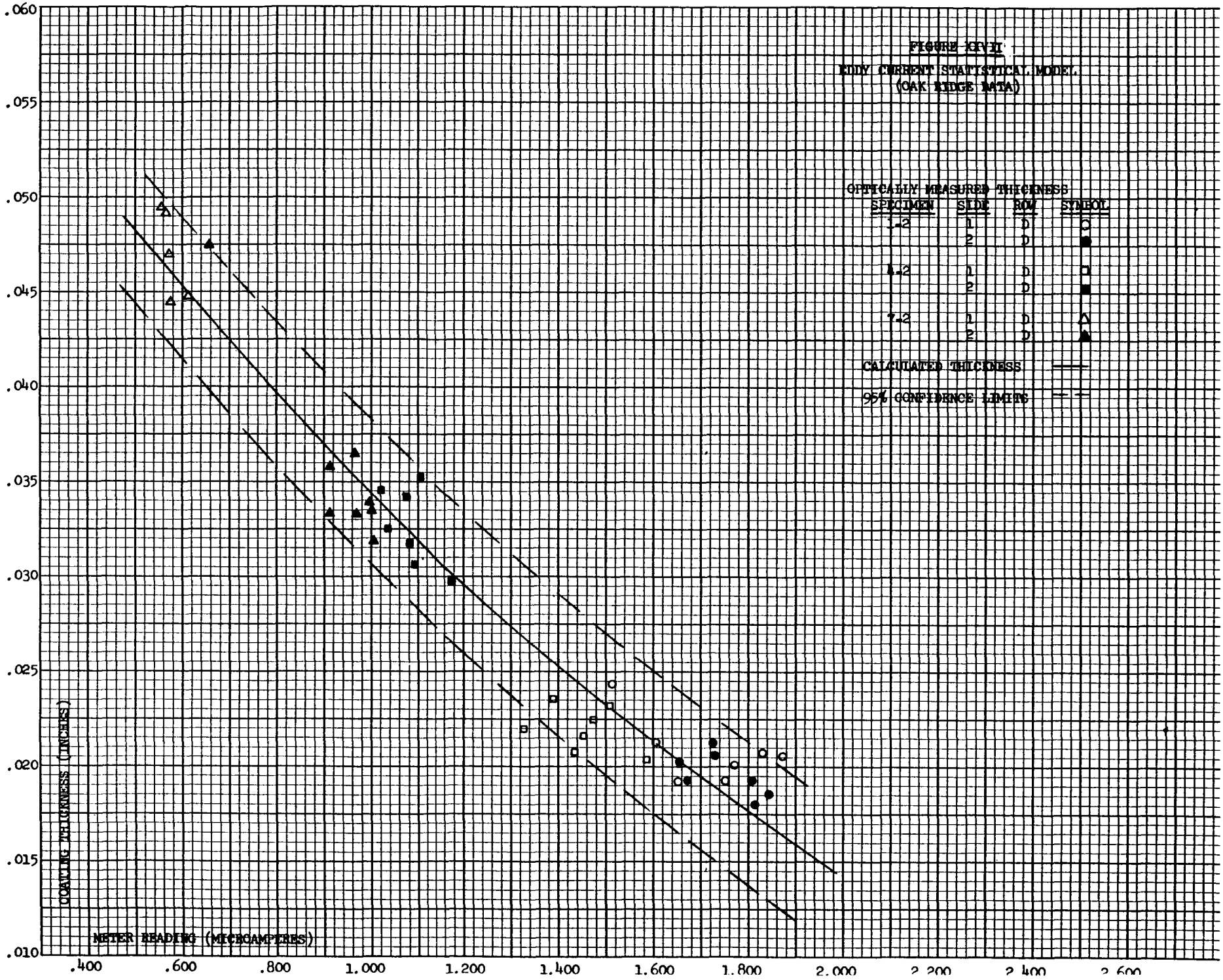
FIGURE XXVII
EDDY CURRENT STATISTICAL MODEL
(OAK RIDGE DATA)
OPTICALLY MEASURED THICKNESS
SPECIMEN SIDE ROW SYMBOL
1-2 1 D
2 D
4-2 1 D
2 D
7-2 1 D
2 D
CALCULATED THICKNESS
95% CONFIDENCE LIMITS
COATING THICKNESS (INCHES)
METER READING (MICROAMPERES)
.060
.055
.050
.045
.040
.035
.030
.025
.020
.015
.010
.400
.600
.800
1.000
1.200
1.400
1.600
1.800
2.000
2.200
2.400
2.600

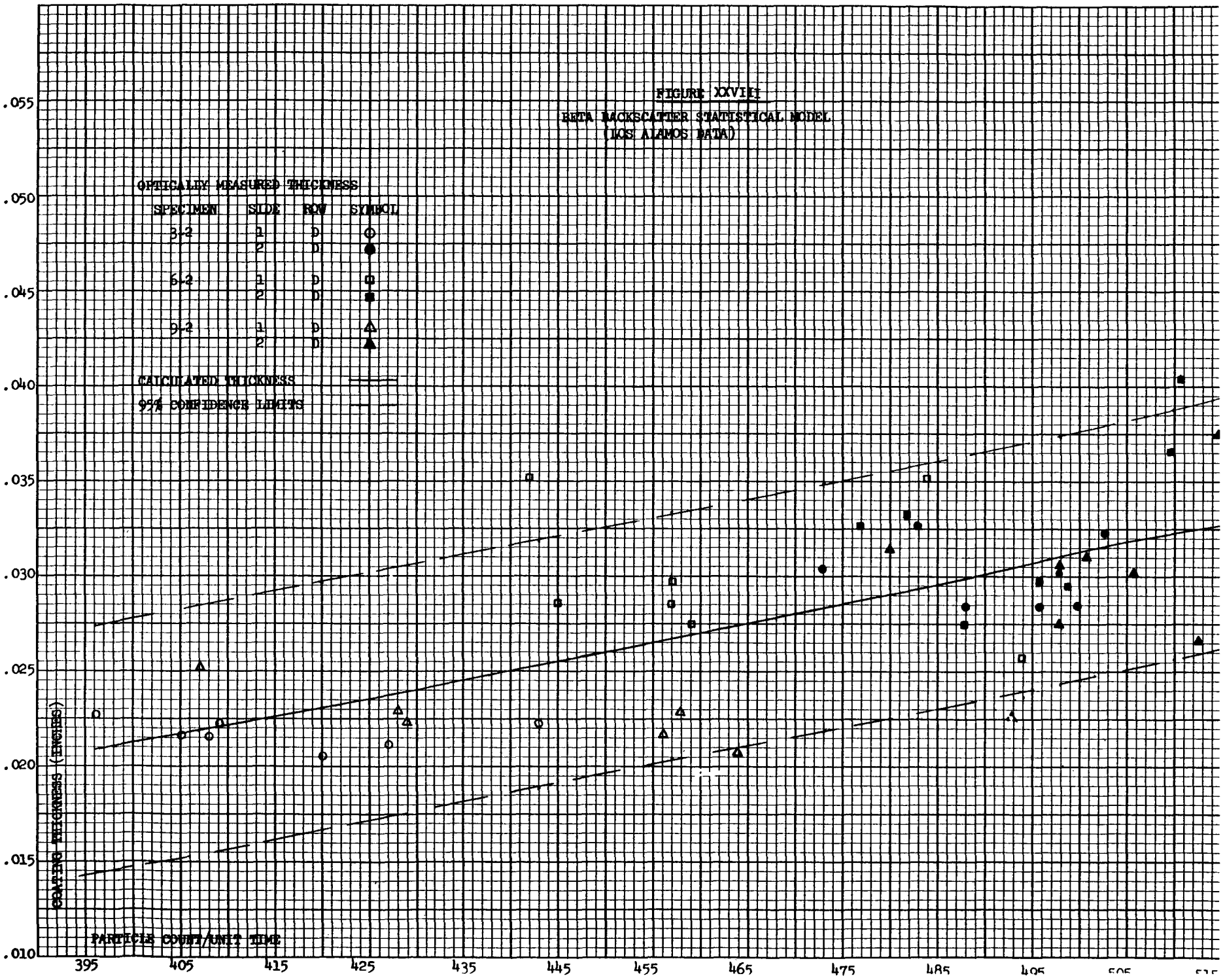


FIGURE XXVIII

BETA BACKSCATTER STATISTICAL MODEL
(LOS ALAMOS DATA)

TABLE I

SCHEDULE OF COATING THICKNESS REQUIREMENTS

| Panel No. | Dash No. | Coating Thickness | Panel No. | Dash No. | Coating Thickness |
|---|---|---|---|---|---|
| 1 | 1 | Do not coat | 6 | 1 | Do not coat |
| | 2 | 0.010 | | 2 | 0.030 |
| | 3 | 0.010 | | 3 | 0.030 |
| | 4 | 0.010 (1) | | 4 | 0.030 (1) |
| | 5 | 0.010 | | 5 | 0.030 |
| | 6 | 0.010 | | 6 | 0.030 |
| | 7 | 0.010 | | 7 | 0.030 |
| 2 | 1 | Do not coat | 7 | 1 | Do not coat |
| | 2 | 0.010 | | 2 | 0.050 |
| | 3 | 0.010 | | 3 | 0.050 |
| | 4 | 0.010 (1) | | 4 | 0.050 (1) |
| | 5 | 0.010 | | 5 | 0.050 |
| | 6 | 0.010 | | 6 | 0.050 |
| | 7 | 0.010 | | 7 | 0.050 |
| 3 | 1 | Do not coat | 8 | 1 | Do not coat |
| | 2 | 0.010 | | 2 | 0.050 |
| | 3 | 0.010 | | 3 | 0.050 |
| | 4 | 0.010 (1) | | 4 | 0.050 (1) |
| | 5 | 0.010 | | 5 | 0.050 |
| | 6 | 0.010 | | 6 | 0.050 |
| | 7 | 0.010 | | 7 | 0.050 |
| 4 | 1 | Do not coat | 9 | 1 | Do not coat |
| | 2 | 0.030 | | 2 | 0.050 |
| | 3 | 0.030 | | 3 | 0.050 |
| | 4 | 0.030 (1) | | 4 | 0.050 (1) |
| | 5 | 0.030 | | 5 | 0.050 |
| | 6 | 0.030 | | 6 | 0.050 |
| | 7 | 0.030 | | 7 | 0.050 |
| 5 | 1 | Do not coat | | | |
| | 2 | 0.030 | | | |
| | 3 | 0.030 | | | |
| | 4 | 0.030 (1) | | | |
| | 5 | 0.030 | | | |
| | 6 | 0.030 | | | |
| | 7 | 0.030 | | | |

(1) Requires machining after coating.

TABLE 2

SCHEDULE OF SPECIMEN SHIPMENT

| PANEL NO. | ROUND/SPECIMEN/LAB | | | | | | | | | | | | | | | | | | | | | |
|---|---|---|---|---|---|---|---|---|---|---|---|---|---|---|---|---|---|---|---|---|---|---|
| | ROUND 1 - 1 SEPT. 1972 | | | | | | | EXPOSURE (1) 18 SEPT. 1972 | | | | ROUND 2 29 SEPT. 1972 | | | | ROUND 3 - 20 OCT 1972 | | | | | | |
| | 1 | 2 | 3a | 3b | 4 | 5 | 6 | 3a | 3b | 6 | 2 | 1 | 2 | 4 | 5 | 1 | 2 | 3a | 3b | 4 | 5 | 6 |
| 1 | O | O | O | O | O | O | O | N | N | M | M | L | L | L | L | V | V | O | O | V | V | O |
| 2 | V | V | V | V | V | V | V | N | N | M | M | O | O | O | O | L | L | V | V | L | L | V |
| 3 | L | L | L | L | L | L | L | N | N | M | M | V | V | V | V | O | O | L | L | O | O | L |
| 4 | O | O | O | O | O | O | O | N | N | M | M | L | L | L | L | V | V | O | O | V | V | O |
| 5 | V | V | V | V | V | V | V | N | N | M | M | O | O | O | O | L | L | V | V | L | L | V |
| 6 | L | L | L | L | L | L | L | N | N | M | M | V | V | V | V | O | O | L | L | O | O | L |
| 7 | O | O | O | O | O | O | O | N | N | M | M | L | L | L | L | V | V | O | O | V | V | O |
| 8 | V | V | V | V | V | V | V | N | N | M | M | O | O | O | O | L | L | V | V | L | L | V |
| 9 | L | L | L | L | L | L | L | N | N | M | M | V | V | V | V | O | O | L | L | O | O | L |

O = Oak Ridge
L = Los Alamos
V = VAC

M = VMSC for Heat Treat and Sectioning at Row "D".
N = NASA for Re-entry Exposure

1. The "exposure" round was set up to show availability of specimens for exposure by NASA and heat treat by VMSC and sectioning of row "D" on all -2 specimens for first optical thickness measurement.

TABLE 3
LIFT-OFF DATA FOR MACHINED AND UNCOATED RPP

| X(1) | R | V | T(ACT) | T(ACT) / V | | | | T(ACT) / R | | | |
|---|---|---|---|---|---|---|---|---|---|---|---|
| | | | | T(CAL) | ΔVT | PREDICTION BANDS UPPER | PREDICTION BANDS LOWER | T(CAL) | ΔRT | PREDICTION BANDS UPPER | PREDICTION BANDS LOWER |
| MACHINED | | | | | | | | | | | |
| 463 | 634 | 39.81 | 0(2) | 0.00111 | -0.00011 | 0.00279 | -0.00058 | 0.00115 | -0.00015 | 0.00283 | -0.00054 |
| 463 | 619 | 53.76 | 0.006 | 0.00655 | 0.01386 | 0.00823 | 0.00486 | 0.00644 | -0.00043 | 0.00812 | 0.00475 |
| 465 | 605 | 66.71 | 0.015 | 0.01386 | 0.00114 | 0.01555 | 0.01217 | 0.01389 | 0.00111 | 0.01557 | 0.01220 |
| 466 | 595 | 76.30 | 0.021 | 0.02068 | 0.00032 | 0.02236 | 0.01899 | 0.02070 | 0.00031 | 0.02238 | 0.01900 |
| 468 | 583 | 87.82 | 0.030 | 0.03040 | -0.00044 | 0.03213 | 0.02876 | 0.03049 | -0.00049 | 0.03217 | 0.02880 |
| 472 | 567 | 103.31 | 0.045 | 0.04629 | -0.00129 | 0.04798 | 0.04461 | 0.04632 | -0.0131 | 0.04800 | 0.04463 |
| 478 | 556 | 114.02 | 0.060 | 0.05908 | 0.00092 | 0.06076 | 0.05739 | 0.05904 | 0.00096 | 0.06070 | 0.05735 |
| UNCOATED | | | | | | | | | | | |
| 480 | 614 | 56.0 | 0 (2) | 0.00266 | -0.00166 | 0.00539 | -0.00002 | 0.00267 | -0.00167 | 0.00539 | -0.00005 |
| 479 | 608 | 62.0 | 0.006 | 0.00408 | 0.00192 | 0.00676 | 0.00140 | 0.00407 | 0.00193 | 0.00680 | 0.00135 |
| 479 | 588 | 82.0 | 0.015 | 0.01451 | 0.00049 | 0.01720 | 0.01183 | 0.01450 | 0.00050 | 0.01722 | 0.01177 |
| 480 | 580 | 90.0 | 0.021 | 0.02115 | -0.00015 | 0.02383 | 0.01846 | 0.02114 | -0.00014 | 0.02386 | 0.01841 |
| 480 | 571 | 99.00 | 0.030 | 0.03028 | -0.00028 | 0.03297 | 0.02760 | 0.03030 | -0.00029 | 0.03302 | 0.02758 |
| 482 | 558 | 112.02 | 0.045 | 0.04665 | -0.00165 | 0.04933 | 0.04369 | 0.04699 | -0.00169 | 0.04941 | 0.04397 |
| 485 | 550 | 120.10 | 0.060 | 0.05867 | 0.00133 | 0.06136 | 0.05599 | 0.05863 | 0.00137 | 0.06136 | 0.05591 |
| AIR BALANCE | | | | | | | | | | | |
| 504 | 523 | | | | | | | | | | |

(1) The following abbreviations are used in this and the following tables:
X - Reactance R - Resistance
V - Vector length from operating point to X,R point
T(ACT) - Thickness of plastic shim used for lift-off measurement
ΔVT - Difference between T(ACT) and calculated thickness using vector length as the independent variable
ΔRT - Difference between T(ACT) and calculated thickness using resistance as the independent variable

(2) For calculation purposes 0.001 inch rather than 0 was used for zero coating thickness

TABLE 4

LTV EDDY CURRENT STATISTICAL MODEL DATA

| Panel No. | Side Row | Col. | X | R | V | Actual Thick. | Cal. Thick. | Δ Thick. | PREDICTION BANDS Upper | Lower |
|---|---|---|---|---|---|---|---|---|---|---|
| 8-4 | 1A | 1 | 462 | 630 | 43.86 | 6(1) | | | | |
| | | 2 | 462 | 633 | 41.15 | 0 | | | | |
| | | 3 | 463 | 632 | 41.63 | 0 | | | | |
| | | 4 | 462 | 633 | 41.15 | 0 | | | | |
| | | 5 | 462 | 634 | 40.25 | 0 | | | | |
| | | 6 | 463 | 630 | 43.46 | 0 | | | | |
| | | 7 | 461 | 630 | 44.28 | 0 | | | | |
| 5-4 | 2A | 1 | 465 | 638 | 35.34 | 0 | | | | |
| | | 2 | 465 | 640 | 33.54 | 0 | | | | |
| | | 3 | 463 | 634 | 39.81 | 0 | | | | |
| | | 4 | 463 | 634 | 39.81 | 0 | | | | |
| | | 5 | 463 | 634 | 39.81 | 0 | | | | |
| | | 6 | 463 | 634 | 39.81 | 0 | | | | |
| | | 7 | 463 | 638 | 36.23 | 0 | | | | |
| 2-2 | 1D | 1 | 465 | 595 | 76.48 | 0.0225 | 0.0191 | 0.0034 | 0.0242 | 0.0139 |
| | | 2 | 464 | 594 | 77.67 | 0.0220 | 0.0200 | 0.0020 | 0.0251 | 0.0148 |
| | | 3 | 464 | 590 | 81.58 | 0.0205 | 0.0231 | -0.0026 | 0.0282 | 0.0179 |
| | | 4 | 465 | 592 | 79.43 | 0.0212 | 0.0213 | -0.0001 | 0.0265 | 0.0162 |
| | | 5 | 465 | 591 | 80.41 | 0.0205 | 0.0221 | -0.0016 | 0.0272 | 0.0170 |
| | | 6 | 465 | 593 | 78.45 | 0.0227 | 0.0206 | 0.00214 | 0.0257 | 0.0154 |
| | | 7 | 466 | 593 | 78.26 | 0.0213 | 0.0204 | 0.0009 | 0.0255 | 0.0153 |
| | 2D | 1 | 465 | 595 | 76.48 | 0.0207 | 0.0191 | 0.0016 | 0.0242 | 0.0139 |
| | | 2 | 466 | 597 | 74.33 | 0.0182 | 0.0175 | 0.0008 | 0.0226 | 0.0124 |
| | | 3 | 465 | 593 | 78.45 | 0.0193 | 0.0206 | -0.0013 | 0.0257 | 0.0154 |
| | | 4 | 465 | 594 | 77.47 | 0.0193 | 0.0198 | -0.0005 | 0.0249 | 0.0147 |
| | | 5 | 466 | 595 | 76.30 | 0.0201 | 0.0189 | 0.0012 | 0.0241 | 0.0138 |
| | | 6 | 466 | 595 | 76.30 | 0.0231 | 0.0189 | 0.0042 | 0.0241 | 0.0138 |
| | | 7 | 466 | 593 | 78.26 | 0.0187 | 0.0204 | -0.0017 | 0.0255 | 0.0153 |
| 5-2 | 1D | 1 | 466 | 578 | 96.03 | 0.0361 | 0.0363 | 0.0002 | 0.0414 | 0.0312 |
| | | 2 | 468 | 577 | 96.75 | 0.0393 | 0.0371 | 0.0022 | 0.0422 | 0.0319 |
| | | 3 | 468 | 577 | 96.75 | 0.0283 | 0.0371 | 0.0011 | 0.0422 | 0.0319 |
| | | 4 | 468 | 573 | 100.72 | 0.0421 | 0.0413 | 0.0009 | 0.0464 | 0.0361 |
| | | 5 | 468 | 576 | 97.74 | 0.0428 | 0.0381 | 0.0047 | 0.0432 | 0.0330 |
| | | 6 | 469 | 572 | 101.60 | 0.0406 | 0.0422 | -0.0016 | 0.0473 | 0.0371 |
| | | 7 | 469 | 572 | 101.60 | 0.0479 | 0.0422 | 0.0057 | 0.0473 | 0.0371 |
| | 2D | 1 | 465 | 584 | 89.27 | 0.0264 | 0.0298 | -0.0034 | 0.0349 | 0.0246 |
| | | 2 | 467 | 584 | 88.96 | 0.0258 | 0.0295 | -0.0037 | 0.0346 | 0.0243 |
| | | 3 | 466 | 585 | 88.12 | 0.0281 | 0.0287 | -0.0006 | 0.0338 | 0.0236 |
| | | 4 | 466 | 586 | 87.13 | 0.0303 | 0.0281 | 0.0025 | 0.0329 | 0.0227 |
| | | 5 | 467 | 587 | 85.99 | 0.0262 | 0.0268 | -0.0006 | 0.0319 | 0.0217 |
| | | 6 | 466 | 587 | 86.15 | 0.0237 | 0.0269 | -0.0032 | 0.0321 | 0.0218 |
| | | 7 | 467 | 586 | 87.97 | 0.0276 | 0.0286 | -0.0010 | 0.0337 | 0.0234 |
| 8-2 | 1D | 1 | 469 | 566 | 104.58 | 0.0392 | 0.0455 | -0.0063 | 0.0507 | 0.0404 |
| | | 2 | 469 | 565 | 105.57 | 0.0465 | 0.0467 | -0.0002 | 0.0518 | 0.0415 |
| | | 3 | 471 | 563 | 107.38 | 0.0436 | 0.0488 | -0.0052 | 0.0539 | 0.0437 |
| | | 4 | 470 | 563 | 107.47 | 0.0521 | 0.0489 | 0.00322 | 0.0540 | 0.0438 |
| | | 5 | 471 | 560 | 110.37 | 0.0519 | 0.0524 | -0.0005 | 0.0575 | 0.0472 |
| | | 6 | 471 | 562 | 108.37 | 0.0559 | 0.0500 | 0.00590 | 0.0551 | 0.0448 |
| | | 7 | 473 | 557 | 113.22 | 0.0585 | 0.0559 | 0.0026 | 0.0610 | 0.0508 |

TABLE 4(CONT)

LTV EDDY CURRENT STATISTICAL MODEL DATA

| Panel No. | Side Row | Col. | X | R | V | Actual Thick. | Cal. Thick. | Δ Thick. | PREDICTION BANDS Upper | Lower |
|---|---|---|---|---|---|---|---|---|---|---|
| | 2D | 1 | 468 | 568 | 102.70 | 0.0383 | 0.0434 | -0.0051 | 0.0486 | 0.0383 |
| | | 2 | 469 | 568 | 102.59 | 0.0460 | 0.0433 | 0.0027 | 0.0484 | 0.0382 |
| | | 3 | 469 | 568 | 102.59 | 0.0398 | 0.0433 | -0.0035 | 0.0484 | 0.0382 |
| | | 4 | 468 | 568 | 102.70 | 0.0387 | 0.0434 | -0.0047 | 0.0486 | 0.0383 |
| | | 5 | 469 | 567 | 103.59 | 0.0430 | 0.0444 | -0.0014 | 0.0495 | 0.0393 |
| | | 6 | 469 | 568 | 102.59 | 0.0471 | 0.0433 | 0.0038 | 0.0482 | 0.0382 |
| | | 7 | 471 | 564 | 106.38 | 0.0471 | 0.0476 | -0.0005 | 0.0527 | 0.0425 |

TABLE 5
OAD RIDGE EDDY CURRENT STATISTICAL MODEL DATA

| Panel No. | Side Row | Col. | Phase Angle (Neg) | Ampl. | Actual Thick. | Cal. Thick. | Δ Thick. | PREDICTION BANDS Upper | Lower |
|---|---|---|---|---|---|---|---|---|---|
| 7-4 | 1A | 1 | 131.60 | 2.473 | 0 | | | | |
| | | 2 | 137.22 | 3.475 | 0 | | | | |
| | | 3 | 137.53 | 3.606 | 0 | | | | |
| | | 4 | 138.14 | 3.725 | 0 | | | | |
| | | 5 | 137.77 | 3.485 | 0 | | | | |
| | | 6 | 138.00 | 3.458 | 0 | | | | |
| | | 7 | 138.02 | 3.483 | 0 | | | | |
| 4-4 | 2A | 1 | 137.61 | 3.281 | 0 | | | | |
| | | 2 | 137.88 | 3.586 | 0 | | | | |
| | | 3 | 138.22 | 3.664 | 0 | | | | |
| | | 4 | 138.49 | 3.625 | 0 | | | | |
| | | 5 | 138.09 | 3.529 | 0 | | | | |
| | | 6 | 138.14 | 3.634 | 0 | | | | |
| | | 7 | 137.80 | 3.690 | 0 | | | | |
| 1-2 | 1D | 1 | 124.30 | 1.770 | 0.0205 | 0.01670 | 0.00370 | 0.02034 | 0.01326 |
| | | 2 | 123.52 | 1.752 | 0.0177 | 0.01714 | 0.00056 | 0.02068 | 0.01360 |
| | | 3 | 125.46 | 1.870 | 0.0171 | 0.01499 | 0.00212 | 0.01853 | 0.01145 |
| | | 4 | 124.72 | 1.834 | 0.0176 | 0.01563 | 0.00198 | 0.01917 | 0.01209 |
| | | 5 | 122.17 | 1.658 | 0.0182 | 0.01896 | -0.00076 | 0.02250 | 0.01542 |
| | | 6 | 121.14 | 1.604 | 0.0193 | 0.0201 | -0.00075 | 0.02359 | 0.01651 |
| | | 7 | 120.13 | 0.515 | 0.0224 | 0.02191 | 0.00049 | 0.02546 | 0.01837 |
| 1-2 | 2D | 1 | 133.91 | 1.735 | 0.0190 | 0.01746 | 0.00154 | 0.02100 | 0.01392 |
| | | 2 | 125.05 | 1.818 | 0.0172 | 0.01591 | 0.00129 | 0.01946 | 0.01237 |
| | | 3 | 125.45 | 1.842 | 0.0175 | 0.01548 | 0.00202 | 0.01902 | 0.01194 |
| | | 4 | 124.02 | 1.732 | 0.0170 | 0.01752 | -0.00052 | 0.02106 | 0.01398 |
| | | 5 | 123.11 | 1.667 | 0.0171 | 0.01878 | -0.00168 | 0.02232 | 0.01524 |
| | | 6 | 122.40 | 1.644 | 0.0199 | 0.01924 | 0.00066 | 0.02278 | 0.01570 |
| | | 7 | 124.90 | 1.807 | 0.0188 | 0.01612 | 0.00269 | 0.01966 | 0.01257 |
| 4-2 | 1D | 1 | 116.75 | 1.328 | 0.0220 | 0.02612 | -0.00412 | 0.02966 | 0.02258 |
| | | 2 | 118.70 | 1.433 | 0.0208 | 0.02371 | -0.00291 | 0.02725 | 0.02017 |
| | | 3 | 118.80 | 1.453 | 0.0217 | 0.02327 | -0.00157 | 0.02681 | 0.01973 |
| | | 4 | 121.11 | 1.582 | 0.0204 | 0.02050 | -0.00010 | 0.07404 | 0.01696 |
| | | 5 | 119.26 | 1.507 | 0.0232 | 0.02209 | 0.00111 | 0.02563 | 0.01855 |
| | | 6 | 118.04 | 1.471 | 0.0225 | 0.02287 | -0.00037 | 0.02641 | 0.01933 |
| | | 7 | 116.34 | 1.390 | 0.0237 | 0.02468 | -0.0010 | 0.02822 | 0.02114 |
| 4-2 | 2D | 1 | 109.69 | 1.178 | 0.0297 | 0.02977 | -0.00007 | 0.03331 | 0.02623 |
| | | 2 | 106.67 | 1.0 | 0.0308 | 0.03194 | -0.00114 | 0.03548 | 0.02840 |
| | | 3 | 107.62 | 1.105 | 0.0353 | 0.03163 | 0.00367 | 0.03517 | 0.02809 |
| | | 4 | 106.18 | 1.072 | 0.0343 | 0.03249 | 0.00181 | 0.03603 | 0.02895 |
| | | 5 | 106.81 | 1.080 | 0.0319 | 0.03228 | -0.00038 | 0.03582 | 0.02874 |
| | | 6 | 103.69 | 1.021 | 0.0346 | 0.03385 | 0.00075 | 0.03739 | 0.08031 |
| | | 7 | 104.65 | 1.038 | 0.0326 | 0.03339 | -0.00079 | 0.03693 | 0.02985 |

TABLE 5 (CONT)
OAK RIDGE EDDY CURRENT STATISTICAL MODEL DATA

| Panel No. | Side Row | Col. | Phase Angle (Neg) | Ampl. | Actual Thick. | Cal. Thick. | Δ Thick. | PREDICTION BANDS Upper | Lower |
|---|---|---|---|---|---|---|---|---|---|
| 7-2 | 1D | 1 | 45.42 | 0.568 | 0.0492 | 0.0471 | 0.00207 | 0.05068 | 0.04359 |
| | | 2 | 62.60 | 0.613 | 0.0448 | 0.04572 | -0.00092 | 0.04926 | 0.04217 |
| | | 3 | 48.38 | 0.573 | 0.0471 | 0.04698 | 0.000124 | 0.05052 | 0.04344 |
| | | 4 | 38.05 | 0.560 | 0.0496 | 0.04739 | 0.00221 | 0.05093 | 0.04385 |
| | | 5 | - | - | 0.0517 | - | - | | |
| | | 6 | 51.40 | 0.576 | 0.0445 | 0.04688 | -0.00238 | 0.05042 | 0.04334 |
| | | 7 | - | - | 0.0470 | - | - | | |
| 7-2 | 2D | 1 | 100.64 | 0.972 | 0.0365 | 0.03518 | 0.00132 | 0.03872 | 0.03164 |
| | | 2 | 101.02 | 0.976 | 0.0330 | 0.03507 | -0.00207 | 0.03861 | 0.03153 |
| | | 3 | 102.06 | 0.998 | 0.0340 | 0.03467 | -0.00047 | 0.03801 | 0.03093 |
| | | 4 | 102.14 | 1.004 | 0.0336 | 0.03431 | -0.00071 | 0.03785 | 0.03077 |
| | | 5 | 102.16 | 1.005 | 0.0318 | 0.03428 | -0.00248 | 0.03782 | 0.03074 |
| | | 6 | 96.87 | 0.915 | 0.0333 | 0.03676 | -0.00346 | 0.04030 | 0.03322 |
| | | 7 | 71.76 | 0.660 | 0.0476 | 0.04426 | 0.00335 | 0.04780 | 0.04071 |

TABLE 6
LOS ALAMOS BETA BACKSCATTER STATISTICAL MODEL DATA

| Panel No. | Side Row | Col. | Part. Count | Count | Actual Thick. | Cal. Thick. | Δ Thick. | PREDICTION BANDS Upper | Lower |
|---|---|---|---|---|---|---|---|---|---|
| 9-4 | 1A | 1 | 254 | 29 | 0 | | | | |
| | | 2 | 238 | 13 | 0 | | | | |
| | | 3 | 242 | 17 | 0 | | | | |
| | | 4 | 244 | 19 | 0 | | | | |
| | | 5 | 247 | 22 | 0 | | | | |
| | | 6 | 242 | 17 | 0 | | | | |
| | | 7 | 247 | 22 | 0 | | | | |
| 3-4 | 2A | 1 | 254 | 29 | 0 | | | | |
| | | 2 | 244 | 19 | 0 | | | | |
| | | 3 | 243 | 18 | 0 | | | | |
| | | 4 | 238 | 13 | 0 | | | | |
| | | 5 | 237 | 12 | 0 | | | | |
| | | 6 | 236 | 11 | 0 | | | | |
| | | 7 | 229 | 4 | 0 | | | | |
| 3-2 | 1D | 1 | 621 | 396 | 0.0227 | 0.02094 | 0.00176 | 0.02744 | 0.01445 |
| | | 2 | 630 | 405 | 0.0192 | 0.02175 | -0.00255 | 0.02824 | 0.01576 |
| | | 3 | 645 | 420 | 0.0206 | 0.02313 | -0.00253 | 0.02962 | 0.01663 |
| | | 4 | 633 | 408 | 0.0216 | 0.02202 | -0.00042 | 0.02851 | 0.01553 |
| | | 5 | 634 | 409 | 0.0223 | 0.02211 | 0.00019 | 0.02860 | 0.01562 |
| | | 6 | 652 | 427 | 0.0212 | 0.02378 | -0.00258 | 0.03027 | 0.01729 |
| | | 8 | 668 | 443 | 0.0223 | 0.02532 | -0.00302 | 0.03181 | 0.01883 |
| 3-2 | 2D | 1 | 721 | 496 | 0.0285 | 0.03075 | 0.00225 | 0.03725 | 0.02426 |
| | | 2 | 713 | 488 | 0.0285 | 0.02990 | -0.00140 | 0.03639 | 0.02341 |
| | | 3 | 723 | 498 | 0.0302 | 0.03097 | -0.00077 | 0.03746 | 0.02448 |
| | | 4 | 698 | 473 | 0.0305 | 0.02833 | 0.00217 | 0.03482 | 0.02184 |
| | | 5 | 725 | 500 | 0.0285 | 0.03119 | -0.00269 | 0.03768 | 0.02469 |
| | | 6 | 728 | 503 | 0.0324 | 0.03151 | 0.00089 | 0.03800 | 0.02502 |
| | | 7 | 708 | 483 | 0.0328 | 0.02937 | 0.00343 | 0.03586 | 0.02288 |
| 6-2 | 1D | 1 | 719 | 494 | 0.0258 | 0.03054 | -0.00474 | 0.03703 | 0.02405 |
| | | 2 | 670 | 445 | 0.0286 | 0.02551 | 0.00309 | 0.03201 | 0.01902 |
| | | 3 | 684 | 459 | 0.0275 | 0.02690 | 0.00060 | 0.03339 | 0.02041 |
| | | 4 | 682 | 457 | 0.0286 | 0.02670 | 0.00190 | 0.03319 | 0.02021 |
| | | 5 | 682 | 457 | 0.0299 | 0.02670 | 0.00320 | 0.03319 | 0.02021 |
| | | 6 | 709 | 484 | 0.0352 | 0.02948 | 0.00572 | 0.03597 | 0.02299 |
| | | 7 | 667 | 442 | 0.0352 | 0.02522 | 0.01000 | 0.03171 | 0.01873 |
| 6-2 | 2D | 1 | 724 | 499 | 0.0296 | 0.03108 | -0.00148 | 0.03757 | 0.02459 |
| | | 2 | 702 | 477 | 0.0329 | 0.02874 | 0.00416 | 0.03524 | 0.02225 |
| | | 3 | 721 | 496 | 0.0298 | 0.03075 | -0.00095 | 0.03725 | 0.02426 |
| | | 4 | 713 | 488 | 0.0276 | 0.03000 | -0.00230 | 0.03639 | 0.02341 |
| | | 5 | 707 | 482 | 0.0334 | 0.02930 | 0.00413 | 0.03576 | 0.02278 |
| | | 6 | 735 | 510 | 0.0367 | 0.03228 | 0.00442 | 0.03877 | 0.02579 |
| | | 7 | 736 | 511 | 0.0406 | 0.03239 | 0.00821 | 0.03888 | 0.03590 |

Count = Actual Count - 225.

TABLE 6 (CONT)
LOS ALAMOS BETA BACKSCATTER STATISTICAL MODEL DATA

| Panel No. | Side Row | Col. | Part. Count | Count | Actual Thick. | Cal. Thick. | Δ Thick. | PREDICTION BANDS Upper | Lower |
|---|---|---|---|---|---|---|---|---|---|
| 9-2 | 1D | 1 | 689 | 464 | 0.0209 | 0.02741 | -0.00651 | 0.03390 | 0.02092 |
| | | 2 | 653 | 428 | 0.0230 | 0.02388 | -0.00088 | 0.03037 | 0.01739 |
| | | 3 | 654 | 429 | 0.0224 | 0.02397 | -0.00157 | 0.03046 | 0.01748 |
| | | 4 | 683 | 458 | 0.0230 | 0.02680 | -0.00380 | 0.03329 | 0.02031 |
| | | 5 | 632 | 407 | 0.0252 | 0.02193 | 0.00327 | 0.02842 | 0.01544 |
| | | 6 | 681 | 456 | 0.0218 | 0.02660 | -0.00480 | 0.03309 | 0.02011 |
| | | 7 | 718 | 493 | 0.0227 | 0.03043 | -0.00773 | 0.03692 | 0.02394 |
| 9-2 | 2D | 1 | 738 | 513 | 0.0267 | 0.03261 | -0.00591 | 0.03910 | 0.02612 |
| | | 2 | 726 | 501 | 0.0311 | 0.03129 | -0.00019 | 0.03779 | 0.02480 |
| | | 3 | 723 | 489 | 0.0306 | 0.03097 | -0.00037 | 0.03746 | 0.02448 |
| | | 4 | 731 | 506 | 0.0304 | 0.03184 | -0.00144 | 0.03833 | 0.02535 |
| | | 5 | 705 | 480 | 0.0315 | 0.02906 | 0.00244 | 0.03555 | 0.02257 |
| | | 6 | 723 | 498 | 0.0276 | 0.03097 | -0.00337 | 0.03746 | 0.02448 |
| | | 7 | 740 | 515 | 0.0376 | 0.03283 | 0.00477 | 0.03932 | 0.02634 |

## APPENDIX I

## STATISTICAL EQUATIONS USED IN DATA ANALYSIS

The following statistical relationships were used when analyzing the data in this report.

All curve fitting was to the quadratic equation:

$$Y = a_o + a_1 x + a_2 x^2 \tag{1}$$

The standard deviation for both variables was calculated by the relationship

$$S = \sqrt{\frac{1}{N(N-1)} \left[ N\Sigma X^2 - (\Sigma X)^2 \right]} \tag{2}$$

The coefficient of correlation was taken as the square root of the coefficient of determination which was calculated by the relationship

$$r^2 = \frac{a_1\left[\Sigma XY - \frac{(\Sigma X)(\Sigma Y)}{N}\right] + a_2\left[\Sigma X^2 Y - \frac{(\Sigma X^2)(\Sigma Y)}{N}\right]}{\Sigma Y^2 - \frac{(\Sigma Y)^2}{N}} \tag{3}$$

The standard error of estimate was calculated by the relationship

$$S_{x.y} = S_Y \sqrt{1-r^2} \tag{4}$$

### DEFINITIONS

Regression Analysis - Analysis of data by regressing the data, by averaging methods, to a line that best represents the data distribution, and analyzing the variations in the actual data, the means, and the calculated values. The averaging method used in this report was the least squares method.

Standard Deviation - A measure of dispersion of the numerical data of the variable being evaluated about an average value.

Coefficient of Correlation - The ratio of explained variation to total variation. The range of the ratio is from -1 to +1. Zero correlation indicates no relationship between the data and curve to which the data is being fit. Correlation of ±1 indicates perfect fit between the data and the curve to which the data is being fit. The correlation coefficient is a measure of how good the data fits the curve, it is not a measure or an indication of the indirect or direct dependence of the variables.

Standard Error of Estimate - The standard deviation of the error of estimating the variables.

2

"EVALUATION OF THE COATING CRAZING PHENOMENA"

FINAL REPORT FOR

TASK 9 OF NASA CONTRACT NAS9-12763

VSD REPORT NO. T143-5R-30005

20 February 1973


| Prepared By | Approved By | Approved By |
|---|---|---|
| D.C. Rogers | J.W. Seeger | D.M. While |

Vought Systems Division
LTV Aerospace Corporation
P.O. Box 6267
Dallas, Texas 75222


A-2i

## FOREWORD

This report was prepared by the Vought Systems Division of LTV Aerospace Corporation and is the final report for the Task 9 effort of the program, "Development of a "Fail-Safe" Design Oxidation Resistant Reinforced Carbon Thermal Protection System for the Wing Leading Edge of a Space Shuttle Vehicle", under Contract No. NASA/MSC NAS9-12763. The program was administered under the direction of Mr. Frank Coe of NASA-MSC, Houston as the Technical Monitor. Mr. B.A. Forcht was VSD Program Manager.

This program was under the technical management of Mr. D.M. While; Mr. D.C. Rogers was the Technical Project Engineer.

Technical direction for the work and able editorial assistance was provided by Mr. J.W. Seeger.

## TABLE OF CONTENTS


| | Page |
|---|---|
| INTRODUCTION | 1 |
| SUMMARY | 4 |
| DISCUSSION | 9 |
| PROCESS HISTORY | 9 |
| TECHNICAL DISCUSSIONS | 9 |
| EXPERIMENTAL MATERIALS | 12 |
| MISCELLANEOUS STUDIES | 13 |
| EMPIRICAL STUDIES | 22 |
| SUBSTRATE MODIFICATION | 42 |
| COATING MODIFICATIONS | 45 |
| PROCESS MODIFICATION INFLUENCE | 47 |
| CONCLUSIONS | 50 |
| RECOMMENDATIONS | 51 |
| BIBLIOGRAPHY | 52 |
| APPENDIX | 53 |
| DIFFUSION COATING RUNS (TABLE 18) | 54 |

## LIST OF TABLES


| Table No. | Title | Page |
|---|---|---|
| 1 | Crazing Evaluation Program Task Flow Table | 2 |
| 2 | Degree of Crazing Improvement | 6 |
| 3 | Performance Data for Specimens Coated Using the Crazing Improvement Techniques | 7 |
| 4 | Process History Data | 10 |
| 5 | Packed Powder Tightness | 14 |
| 6 | Thermal Expansion Coefficients Room Temperature to 3000°F | 18 |
| 7 | Expansion Anisotrophy at 3000°F RCC-3 Bare, Coated RCC-3 and Coating | 19 |
| 8 | Differential Expansion Ratio at 3000°F Bare RCC-3 and Coating | 19 |
| 9 | Chemical Analyses Results Metallic Elements (PPM) | 23 |
| 9a | Chemical Analyses Results Metallic Elements, Upper Limits Only | 24 |
| 10 | Chemical Analyses Results (%) Elemental Silicon, $H_2O$ and Non-Metallic Elements | 25 |
| 11 | X-ray Diffraction Analyses of Individual Materials | 30 |
| 12 | X-ray Diffraction Analyses of Fired Mixtures | 31-32 |
| 13 | Concentration (X $10^4$) of Gas Species Observed by Time-of-Flight (TOF) Mass Spectroscopy of Knudsen Cell Products | 34 |
| 14 | X-ray Diffraction Analysis of Production Retort Affluent Collected as Deposits From Furnace After Coating Run | 34 |
| 15 | Possible Reactions Involved in Coating Process | 36-37 |
| 16 | Calculated Equilibrium Reaction Product Gas Pressure (3100°F) | 39 |
| 17 | Bulk Density and Pore Data | 40 |
| 18 | Data - Diffusion Coating Runs | 53 - 69 |

## LIST OF FIGURES


| Figure No. | Title | Page |
|---|---|---|
| 1 | Coating Temperature Curves Step Heating Versus Standard Run | 5 |
| 2 | Thermal Expansion, Silicon Coating, Bare RCC-3 and Siliconized RCC-3 | 16 |
| 3 | Craze Pattern Display - Coated RCC-3 Specimens | 21 |
| 4 | Thermocouple Data to Detect Possible Exothermic Reactions in Pack During Coating Run M-126 | 39 |

## ABSTRACT

An investigation into the crazing phenomena of the VSD siliconized coating for RCC-3 was undertaken. A basic study was made to understand the high temperature reactions and reaction products occurring between the 10% $Al_2O_3$ - 60 % SiC - 30% Si pack mix constituents and the RCC-3 substrate. The thermal expansion characteristics of bare RCC-3, siliconized RCC-3, and siliconized coating were studied up to 3500°F. Experiments were conducted to determine the influence on the crazing phenomena of modifying the siliconized coating chemically, adjusting the physical properties of the RCC-3 substrate, and varying the furnace firing cycle. Tests on siliconized RCC-3 specimens were made to determine the performance of the most promising modifications for strength and oxidation resistance. Test results indicated a significant reduction for crazing visibility when furnace cycle ramp hold times and pack additives were employed in the coating process.

## 1.0 INTRODUCTION

The Vought Systems Division (VSD) has developed a siliconized carbon-carbon composite that has satisfied the requirements for use as the leading edge material of the Space Shuttle Orbiter Vehicle. The basic composite is a laminated structure, made from a phenolic prepregged woven graphite cloth fabric, which is pyrolyzed to the carbon state. The pyrolyzed substrate is subjected to three furfuryl alcohol impregnations, each followed by pyrolysis to improve the density and strength properties. After the third furfuryl impregnation and pyrolysis the substrate is designated RCC-3. The siliconizing of the outer fibers of the RCC-3 to provide the needed oxidation resistance is conducted in a fairly typical pack cementation process. The RCC-3 substrate is placed in a graphite retort entirely surrounded by a powder mix composed of 10 $Al_2O_3$ - 60 SiC - 30 Si. After drying at 400°F for 16 hours the packed retort is fired at 3100°F for 2-3/4 hours under an inert gas blanket. Specimens are recovered easily and cleaned by brushing and light air flush. The uniqueness of the process is that dimensional changes to the RCC-3 do not occur. Net trim can be made on the RCC-3 prior to coating because thickness does not change due to coating application. The coating is a result of a diffusion mechanism which carries the reactive silicon species into the RCC-3 where it reacts to form silicon carbide. This diffusion reaction process can be varied by adjusting the time at temperature to gain a thicker or thinner coating layer as desired.

The finished coating has a generally green-grey appearance which shows clearly the converted cloth structure on all surfaces. The natural pores of the fiber/resin surface are well filled and closed. Critical pore sizes have not been found although drilled holes .050" in diameter 1/4" deep to 3/4" diameter through holes have been coated. Of some concern was a craze pattern in the coating which was visible at 1X magnification but found to be innocuous to the performance of the siliconized system. Because of the level of visible crazing it was decided an investigation was to be performed to determine the cause and/or means to minimize or eliminate it.

The extent of the effort on this program is shown in the flow diagram of Table 1 . A basic study was performed to gain insight to the possible reaction mechanisms and reaction products occurring during the coating

TABLE 1

CRAZING EVALUATION PROGRAM TASK FLOW TABLE

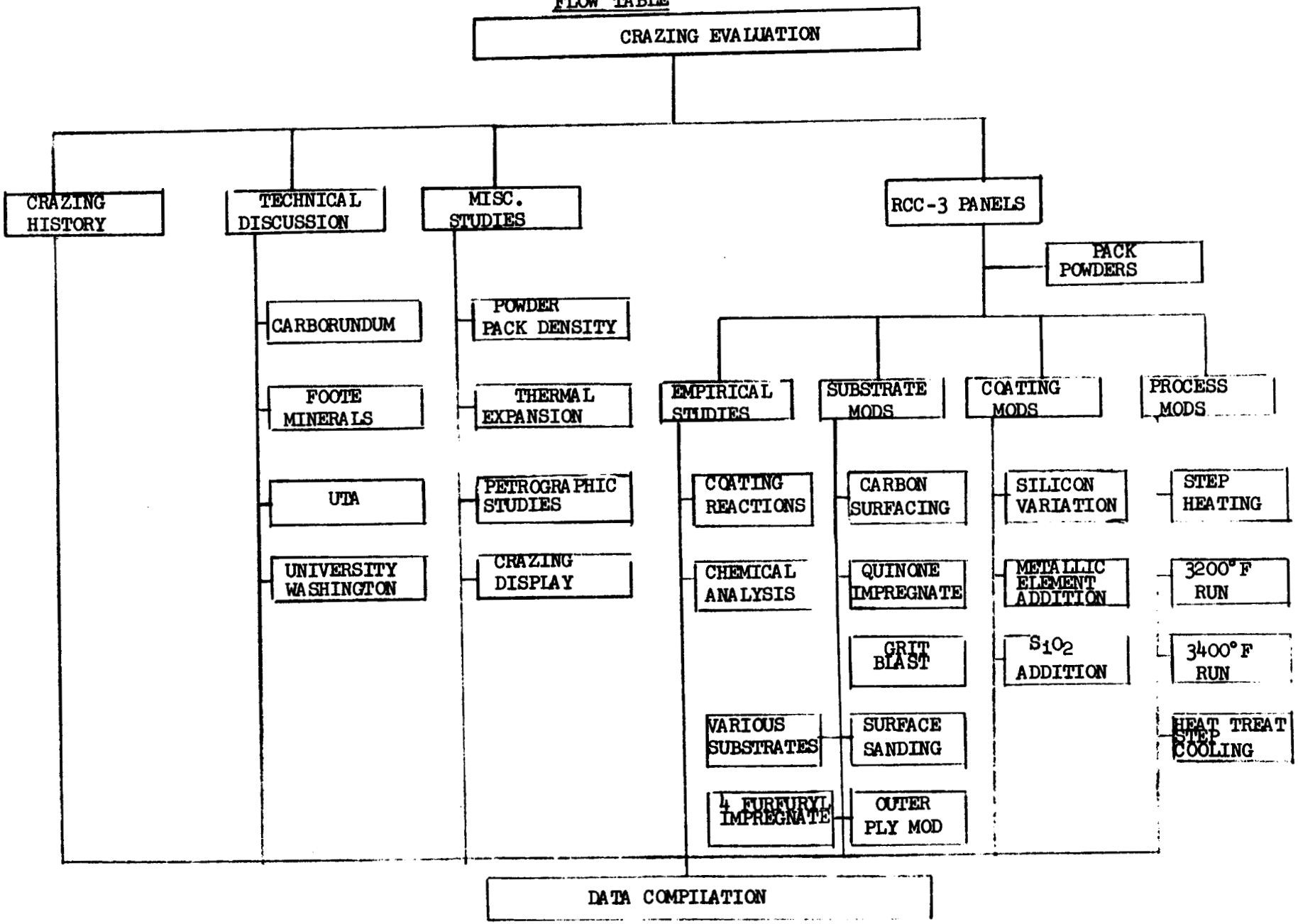

process. This information was to lead to the design of experiments where the controlling coating mechanisms could possibly be varied to favor formation of a craze free coating. A thermal expansion study of bare RCC-3, coated RCC-3, and the RCC-3 coating was made to determine the boundaries of a coating/substrate mismatch. Experimental modifications were made to the RCC-3 substrate, siliconized coating, and coating process to determine their influence on the coating crazing. Technical discussions were held with personnel with expertise in the field of high temperature chemistry and coatings for graphite. Preliminary strength and oxidation resistance performance was determined on specimens of the coated systems which had improved, reduced, or eliminated craze patterns. The basic study for determination of reaction mechanisms was done at the University of Washington. Chemical analysis to characterize the starting materials was conducted at Coors Spectrochemical Laboratory. All other investigations were performed by VSD.

## 2.0 SUMMARY

The investigation into the crazing phenomena of the VSD siliconized coating for RCC-3 is summarized in this section. Theoretical studies based on the concentrations of the gas species evolved from pack material combinations and observed by mass spectroscopy of Knudsen cell products has shown a reactive role possibly for the aluminum oxide. Aluminum gas phase species, i.e., Al, $Al_2O$, $Al_2$, were detected in sufficient quantities to suggest direct interaction between pack components and RCC-3 substrate to provide a continuing SiO concentration for vapor phase transport of silicon, and substrate carbon removal by CO. This chemical interchange is suggested to explain a material balance phenomena between the silicon carbide coating layer and RCC-3 substrate to account for the lack of dimensional change due to the coating pick-up and penetration. The thermal expansion study indicates that a mismatch between the substrate does exist which could contribute to the crazing phenomena. Experimentally, this mismatch was reduced significantly by a heat-up hold in the coating cycle for one hour at 2500°F, and silicon dioxide additions to the pack material. Boron additions appear to have the capability of eliminating crazing, at least as can be detected by optical examinations of 60X magnifications.

### 2.1 CRAZING REDUCTION IMPROVEMENT

The degree to which coating crazing was improved or eliminated by this effort is presented in the Table 2 below. Comparison is made to the crazing on a coating from a standard coating run. Step heating, or hesitation, in the ramp time at 2500°F for one hour produced coated specimens that were visibly uncrazed through optical examination at 10X magnification, or an improvement equivalent to an order of magnitude. The furnace cycle curves for step-heating run M203 and standard run M205 are shown in Figure 1. The precise reason for this improvement is not known but hypothesized to be due to a more strain free coating, reduction of temperature gradients just prior to entering the coating temperature or an expansion gradient zone at the coating/substrate interface. Verification runs have been made and in each case the coating crazing condition has been reduced. The improvement from $SiO_2$ additions to the pack material are most effective in concentration between 1/2 to 1% when fired at a 3250°F temperature indicating the chemical incorporation of the $SiO_2$ into the coating. A $SiO_2$ additive run fired at

FIGURE 1

CORING TEMPERATURE CURVES STEP-HEATING

VERSUS STANDARD RUN

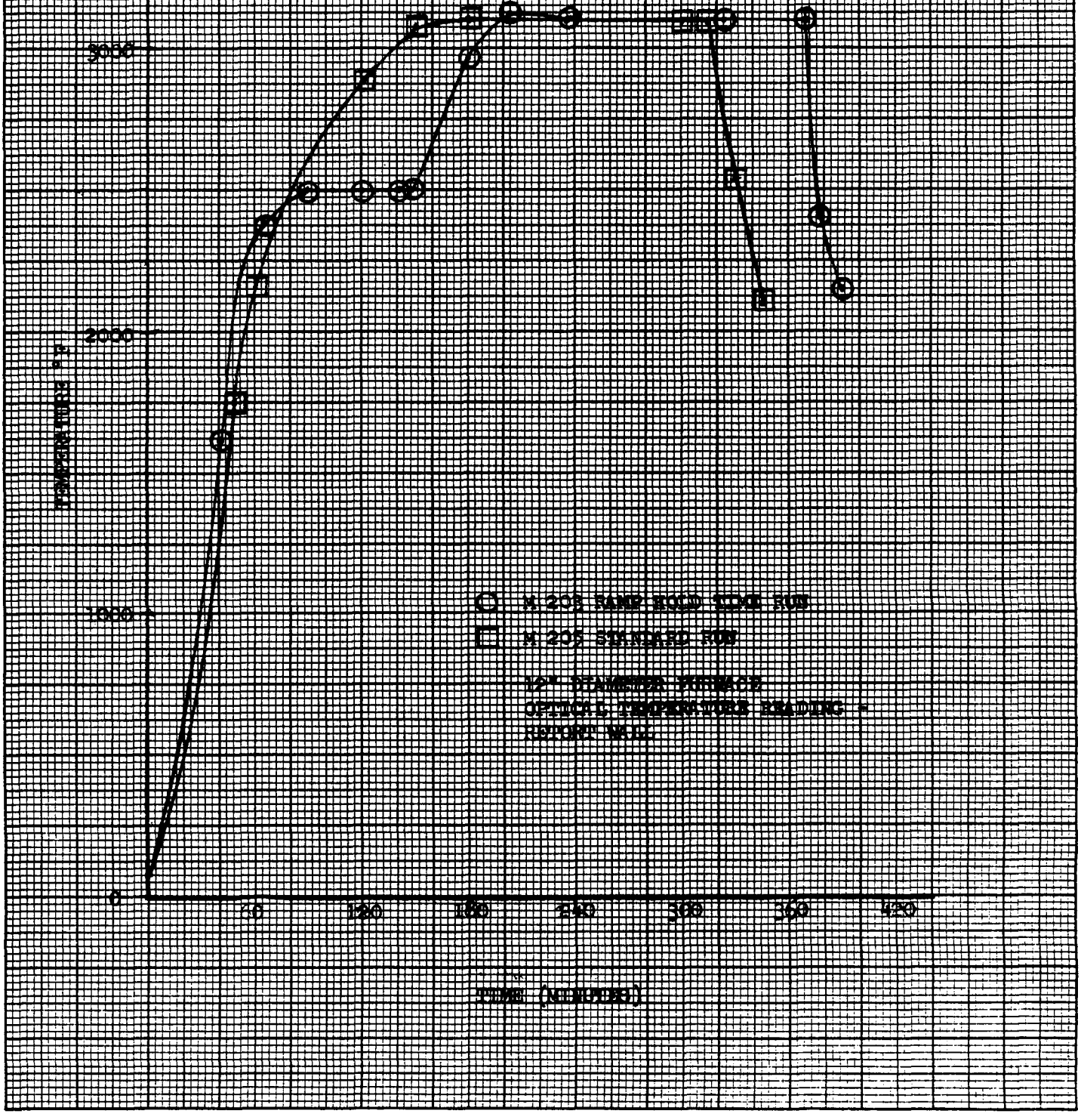


A-2-5

3100°F did not materially reduce the crazing phenomena. The most noticeable effect on the coating crazing phenomena was the run that contained 0.5% boron content which apparently smoothed out the substrate/coating mismatch to a point where crazing was not visible when the coated specimens were examined under 60X magnification. A gradient zone of boron carbide located between the coating and substrate could provide this expansion mismatch relief.

Table 2

Degree of Crazing Improvement

| System | Crazing Visibility Level | | | |
|---|---|---|---|---|
| | 1X (1) | 10X (1) | 30X(1) | 60X (1) |
| Standard Coating | slightly crazed | --- | --- | --- |
| Step heating | not crazed | not crazed | crazed | --- |
| $SiO_2$ additions | not crazed | not crazed | crazed | --- |
| Boron additions | not crazed | not crazed | not crazed | not crazed |

(1) X = Optical Magnification

## 2.2 PERFORMANCE LEVEL

The performance level of specimens coated using the best of the crazing improvement techniques from this effort is shown in Table 3. Data was generated on as-fabricated specimens to provide a common base for comparison of results. Coated specimens were not heat treated. The data indicates that each crazing improvement technique imposes somewhat more-or-less of an effect on the system. Overall, the step-heating technique imposes the least amount of noticeable effect and produces specimens with essentially the same performance as the standard specimens. This was evident even from the data as a result of specimens coated in the W19 verification run. A lower plasma capability was found for the specimens coated by $SiO_2$ additives technique. These tests were run under the same conditions as the tests made on the specimens from standard (M215) and step heated (M19, M203) runs. However, the strength was found to be 8910 to 11,240 psi which is a decrease over the standard and step heated specimens. The lower plasma performance could be due to the non-optimum coating temperature or time at temperature, which deposited but did not react to completion all the low temperature performers such as boron and

Table 3

Performance Data for Specimens Coated Using the Crazing Improvement Techniques

| SYSTEM | RUN NO. | FLEX STRENGTH(2) ROOM TEMP. (PSI) | PERENY DATA(1) | | PLASMA ARC(3) RATIO RELATIVE TO STANDARD RUN M215 |
|---|---|---|---|---|---|
| | | | ΔWT % | FLEX STRENGTH (PSI)(2) | |
| Standard | M215 | 12580 | -0.1 | 14080 | 1 |
| Step Heating | M203 | 20260 | +0.01 | 18930 | 1 |
| Step Heating (Verification) | W19 | 16800 | -1.03 | 14210 | 1 |
| Boron Mod. | M212 | 17590 | -2.8 | 11080 | 0.80 |
| $SiO_2$ 1/2% Mod. | M211 | 8910 | +1.4 | 6370 | 0.72 |
| $SiO_2$ 10% Mod. | M211 | 11240 | +0.9 | 7950 | 0.64 |
| 3400°F | M216 | 14170 | -1.07 | 9152 | 1.24 |

(1) Air Glo Bar furnace preset at 2300°F into and from which specimens are placed and withdrawn directly for five (5) cycles.

(2) Four point flexure test 4.2" span - 1.7" load span 0.05 in/min load rate room temperature test

(3) Three identical 5 min. exposures heating rate 130 BTU/ft$^2$sec enthalpy 8300 BTU/lb specimens were tested as-fabricated, not heat treated.

$SiO_2$. These low melting ingredients would have been lost early from the surface of the specimens during heat up in the low pressure experienced in the plasma test. This effect would impose a high mass loss on specimens that would otherwise have a better plasma performance. The results of the studies at 2300°F in the Pereny furnace indicate the low temperature oxidation resistance capability for all the systems.

## 3.0 DISCUSSION

### 3.1 PROCESS HISTORY

In order to establish the extent of the coating crazing an examination of specimens from prior coating runs was made. The runs represented a cross-section of the work done in previous phases of shuttle leading edge work. Specimens coated in both the 24" diameter horizontal furnace and 12" diameter vertical furnace were examined. Retort sizes were evaluated for size effect on the craze pattern. Packing methods were examined to relate apparent pack density and specimen density to the craze pattern. The magnification level at which crazing became noticeable was determined.

Table 4 shows the results of a set of compilations involving 10 coating runs and 19 specimens. The pack composition in all but one case was 10% $Al_2O_3$ -60% SiC - 30% Si. Two of the runs contained spent pack material from 10% $Al_2O_3$ - 60% SiC - 30% Si runs. The data shown was from specimens coated in that area of the pack. The different silicon metal powder lots and silicon carbide powder lots used are shown. Also, the black or green color designation for the silicon carbide powder is indicated. Crazing was not a function of either the black or green silicon carbide. The aluminum oxide powder was from one lot. Of particular interest is that the furnace coating time and temperature for coating weight gain was found to be directly related. Since all runs shown were tightly packed, a discrimination cannot be made between different packing techniques. Retort size variations do not appear to affect crazing. Thin graphite walls of 3/4 inch or less apparently do not affect heat flow sufficiently to influence crazing; however, there must be some thickness that would show an effect either to increase or decrease stress induced crazing.

### 3.2 TECHNICAL DISCUSSIONS

Trips were made to discuss the technical aspects of the VSD coating process with persons knowledgeable in the field of high temperature chemistry or with expertise in the area of coatings for carbonaceous materials. Experience in the high temperature field was fairly wide spread. With this abundance of experience to choose from the job became one of screening to decide who had the most experience applicable to the effort at hand, which of course, was to study the crazing phenomena. From a carefully compiled list of possible candidates a few were chosen who had previously expressed an inclination and interest in oxidation resistance coatings for carbon-carbon composites. Fortunately, two

TABLE 4 - PROCESS HISTORY DATA

| RUN NO. | SPECIMEN IDENTIFICATION | PACK COMPOSITION | SILICON POWDER | SILICON CARBIDE POWDER | FURNACE TYPE | FURNACE TEMP. °F | COATING TIME HRS. | COATING WT. GAIN % | APPEARANCE OF COATED SPECIMENS: COLOR | CRAZED CONDITION 1X(2) | 10X(2) | 30X(2) | 60X(2) | PACKING HISTORY (3) | RETORT SIZE | REMARKS |
|---|---|---|---|---|---|---|---|---|---|---|---|---|---|---|---|---|
| M101 | -1 Flex Bar(1)<br>-5 3/4" Dia. Disk | 10 60 30<br>$Al_2O_3$ SiC Si | Lot No. 721 | Lot No. 822992 Green | 12" Dia. | 3200 | 6 | 32.2<br>42.0 | Greenish | None | Crazed | - | - | Tight | 6" Dia. x 5" L<br>1/2" wall thick. | |
| M168 | -12 Flex Bar<br>-15 Flex Bar | 10 60 30<br>$Al_2O_3$ SiC Si | Lot No. 1471 | Lot No. A6220 Green | 12" Dia. | 3100 | 2-3/4 | 51.6<br>52.6 | Greenish | None | None | None | - | Tight | 12" Dia. x 11" L<br>3/8" wall thick. | -15 Heat Treated 3200°F Run M 170 |
| M161 | -15 Flex Bar | Spent Pack<br>10 60 30<br>$Al_2O_3$ SiC Si | - | - | 12" Dia. | 3100 | 2-3/4 | 28.4 | Light Green | None | Crazed | - | - | Tight | 12" Dia. x 3" L<br>3/8" wall thick. | -15 Heat Treated 3200°F Run M162 |
| M180 | C1-4 Flex Bar<br>C3-4 Flex Bar | 10 60 30<br>$Al_2O_3$ SiC Si | Lot No. 1471 | Lot No. A6220 Green | 12" Dia. | 3100 | 2-3/4 | - | Light Green | None | Crazed | - | - | Tight | 12" Dia x 3" L<br>3/8" wall thick. | |
| M171 | -9 Flex Bar<br>-8 Flex Bar | | Lot No. 1471 | Lot No. A6220 Green | 12" Dia. | 3100 | 2-3/4 | 21.1<br>23.5 | Green One Side | None | Crazed | - | - | Tight | 12" Dia. x 3" L<br>3/8" wall thick. | |
| M115 | -5B 3/4" Dia. Disk<br>-6B 3/4" Dia. Disk | | Lot No. 468 | Lot No. 822992 Green | 12" Dia. | 3100 | 4 | 61.0<br>53.0 | Light Green | Crazed | One | Side | - | Tight | 12" Dia. x 3" L<br>3/8" wall thick. | |
| M129 | -11B 3/4" Dia. Disk<br>-15B 3/4" Dia. Disk | 10 60 30<br>$Al_2O_3$ SiC Si | Lot No. 468 | Lot No. 113 Black<br>Lot No. 822992 Green | 12" Dia. | 3170 | 2-1/2 | 39.2<br>32.0 | Light Green | Crazed | - | - | - | Tight | 12" Dia. x 3" L<br>3/8" wall thick. | |
| S-2 | -5 Flex Bar<br>-8 Flex Bar | Spent Pack<br>10 60 30<br>$Al_2O_3$ SiC Si | - | - | 24" Dia. | 3100 | 2-3/4 | 19.7<br>26.6 | Bluish Green | Crazed | - | - | - | Tight | 18" x 30" x 16"<br>3/4" wall thick. | Leading Edge Retort |
| W-8 | -5 Flex Bar<br>-6 Flex Bar | 10 60 30<br>$Al_2O_3$ SiC Si | Silicon Mixture | Lot No. 00776 Green | 24" Dia. | 3050 | 2-1/2 | 20.6<br>20.9 | Green | None | Crazed | - | - | Tight | 24" x 20" x 6"<br>3/4" wall thick. | Belly Panel Retort |
| M133 | -7 Flex Bar<br>-19 Flex Bar | 33 33 33<br>$Al_2O_3$ Sic Si | 532 | Lot No. 00774 Black | 12" Dia. | 2900 | 6 | 23.8<br>26.7 | Bluish Green | None | None | -7 Crazed | - | Tight | 12" Dia. x 3" L<br>3/8" wall thick. | -7 Heat Treated in M135 |

(1) All Flex Bars Nominally 3/4" W x 5" L in Size and 13 Plies Thick
(2) Magnification employed for visual examination
(3) All packing per Table 5 this report

FOLDOUT FRAME



FOLDOUT FRAME

of these candidates were employees of companies that supplied powders for the VSD coating process. A synopsis of these discussions is presented.

3.2.1 Carborundum

By far the most knowledgeable people encountered, regarding the production of silicon carbide, were employees of the Carborundum Company. Their added interest in the area of carbon-carbon composites and bulk graphite certainly placed them high on the list of qualified personnel. Of particular assistance was Dr. P. Shaffer of the Carborundum Research Department who was most helpful in discussions dealing with the chemistry of silicon carbide and the effects of small concentrations of impurities during its formation. He was able to illustrate a rather pure silicon carbide and show that it was near white in color with a milk-glass cast. This same silicon carbide with a nitrogen content was green. A boron content produced a silicon carbide that was brown in color. A sample with aluminum contamination discolored the silicon carbide to a dark black ebony hue. Each of these elemental contaminations are combined tenaciously within the silicon carbide cell structure either substitutionally or interstitially. The possibility of purifying silicon carbide once it becomes contaminated is very remote and not at all commercially practical at present. It was stated that contamination levels are best controlled during the initial fabrication to form the silicon carbide by proper selection of raw materials and processing. The possibility of elemental diluents for silicon carbide which might influence its thermal expansion properties was discussed and it was concluded that small doping quantities would not be terribly effective, if at all. Larger injected amounts would probably alter the refractoriness of the silicon carbide, changing its high temperature performance capability. The chance for a thermal expansion mismatch between the substrate and a silicon carbide coating was considered to be a real possibility which could give rise to a crazing condition within the coating. This condition would not necessarily be harmful, as this type of crazing crack tends to close up during heating.

3.2.2 Foote Mineral Co.

Mr. John Warnach, Plant Manager of Foote Mineral Company's silicon metal powder plant at Wennatchee, Washington was briefed on the use of Foote silicon in the VSD coating process. Samples of bare and coated RCC-3 were viewed and discussed. Very little was gained regarding the coating crazing phenomena except the way in which silicon could be a contributing factor.

It was suggested that the purity level factor might be influential if diffusion coefficients or silicon vapor pressure were controlled by contaminant level concentrations. This is probably not valid as many different lots of silicon powder have been used and crazing is noticeable when standard processing is employed.

### 3.2.3 University of Texas in Arlington (UTA)

Dr. Burke Burkart of the Geology Department at UTA was introduced to the VSD coating process and coated specimens were examined. Aside from discussions regarding a possible thermal mismatch between the RCC-3 substrate and coating layer another possibility for the crazing phenomena was offered. It was mentioned that a possible stress was set up within the coating layer if the silicon carbide grains had competed for nucleation sites and growing room was limited sufficiently to cause crystal growth misalignment. Petrographic examinations of thin coating sections, however, showed a rather uniform crystal structure which would indicate less strain than what was initially anticipated to cause the typically observed craze pattern. Dr. Burkart's preliminary study is presented in the petrographic studies section of this report.

### 3.2.4 University of Washington

The discussions with Dr. J. Mueller of the University of Washington revealed that an understanding of the reactions and reaction products occurring during the standard process using characterized starting materials might give insight to process variables that could be controlled to influence the crazing phenomena. Further work was conducted along this line and is reported in the section under University of Washington studies.

## 3.3 EXPERIMENTAL MATERIALS

### 3.3.1 RCC Substrate

Thirteen-ply panels from two standard processing runs were fabricated as the substrate material for experimental use. Four 10" x 12" panels were fabricated from which flexure bars 3/4" x 5" and 3/4" diameter disks were obtained. The flexure bars were cut from the panel in the warp direction. Two 5" x 10" specialty panels were constructed where the two outer plies were altered by substituting for the WCA graphite fabric a cloth with a different weave. Specimens cut from the four standard panels were selected at random

for coating experiments since the panels represented the standard fabrication process which has produced variations that have been fairly well characterized. All specimens would have properties that fell within the expected variations. In both strength and appearance the panels were acceptable. Ultrasonic and radiographic evaluations indicated that the panels were sound. Gross defects were not noticed and delamination and ply separation was not visibly evident. Weight gains for furfuryl impregnations were standard or adjusted to meet the density norm. A review of the processing record did not show variations of concern. To conserve material for experimentation a detail characterization of the panels was not performed. A semi-quantitative analysis was performed on the RCC-3 substrate and on the various substrate components at the Coors Spectrographic Laboratory.(See the Coors section of this report).

3.3.2 Pack Powders

The coating powders used for the experiments in this task were the characterized powders remaining from previous leading edge program efforts. RCC-3 specimens coated in packs composed of these powders were tested at VSD and offsite at NASA-MSC, Southern Research and Battelle. To further characterize the powders a semi-quantitative analysis was performed at the Coors Spectrographic Laboratory. A brief description of the powder lots is as follows.

Silicon Carbide - The silicon carbide powder was a green variety from the Carborundum Co. Grit size was designated RA 1200 which is too fine for mechanical screen classification but reported by Carborundum to be between 3 to 12 microns. Lot 6220 was used for the bulk of the experimental work and Lot 9949 was used when the 6220 lot quantity was depleted. Crystal structure of the 6220 lot was alpha, a hexagonal silicon carbide.

Silicon Metal Powder - One lot of silicon metal powder from the Foote Mineral Co. was used. This lot was 1471 with a grit size of minus 200. Crystal structure was cubic.

Aluminum Oxide Powder - A single lot of $Al_2O_3$ powder from Aluminum Company of America with a grit size of minus 325 was used. Crystal structure was hexagonal. Lot number was Phase 2 type.

3.4 MISCELLANEOUS STUDIES

3.4.1 Pack Powder Density (Tightness) of Packed and Fired Retort

The density to which the 10 $Al_2O_3$ -60 SiC - 30 Si powders are packed around the RCC-3 parts during packing has proved to be a controllable operational step. A preliminary penetration value for a typically "tight" packed retort has

been measured. Values between .75 to 1.2 ton/ft$^2$ were measured for the tight pack condition. This value increases to nearly 20 ton/ft$^2$ after firing in a standard coating cycle at 3100°F for 2-3/4 hours. The tool used to measure pack tightness to provide a knowledge of the powder density is a simple "Soiltest" device which consists of a calibrated spring, contact plunger of known diameter, and readout scale. This tool is hand-held and is about the size of a standard screw driver. It is highly mobile and no doubt will become a part of the "retort packers" tool kit. Its low cost and ease-of-use make a most attractive combination.

The following table illustrates the values initially measured for Run M217.

Table 5

Packed Powder Tightness

| POSITION | PACK HEIGHT FROM BOTTOM OF RETORT | TIGHTNESS VALUE (TONS/FT$^2$) AS-PACKED | AFTER FIRE |
|---|---|---|---|
| 1 | 1/2 inch | 1.0 | 14 |
| 2 | (Fresh Pack Materials) | .75 - 1.0 | 20 |
| 3 | | .75 - 1.0 | 20 |
| 4 | | .75 - 1.0 | 20 |
| 5 | | .75 | 20 |
| 6 | 1 inch | .75 | 18 |
| 7 | (Fresh Pack Materials) | .75 - 1.0 | 20 |
| 8 | | .75 - 1.0 | 18 |
| 9 | | .75 - 1.0 | 18 |
| 10 | | .75 - 1.0 | 18 |
| 11 | 1-1/2 inch | 1.0 | 10.4 - 11.0 |
| 12 | (Spent Pack Materials) | 1.0 - 1.2 | 10.0 |
| 13 | | 1.0 | 12-13 |
| 14 | | 1.0 | 7-8 |
| 15 | | 1.0 | 17-18 |
| 16 | | 1.0 | 7-8 |
| 17 | | 1.0 | 17 |
| 18 | | 1.0 | 9-10 |
| 19 | | 1.0 | 9-10 |

The as-packed tightness values increase from .75 to 1.0 ton/ft$^2$ at the 1/2 to 1 inch pack height to a 1.0 to 1.2 tons/ft$^2$ at the 1-1/2 inch pack height. This is probably a density increase due to the bridging effect which has been noticed mainly when deeper retorts are loaded, and is a natural phenomena of dry powders. Now that packing density can be measured readily, a close control of powder bridging can be employed. Also the top layer was composed of spent pack material which probably packs differently from the fresh pack. The increase in tightness due to sintering or the after-fire condition of the fresh pack materials from nearly 1.0 ton per foot square to nearly 20 tons per foot square is a result of the exposure to furnace coating conditions. The increase for the spent pack material of near 10 tons/ft$^2$ illustrates the presintered condition due to the previous firing and is about 1/2 that experienced by the fresh pack.

The increase is not excessive and in part is a driving force for the good diffusion of the coating into the RCC-3 substrate. The controlled density (tightness) increase accompanied by pack shrinkage maintains a constant intimate contact between the pack and RCC-3 parts. The specimens from Run M217 were removed easily and cleaned up nicely by brushing and light air flushing. This mode of packing for tight packs was maintained for the experiments of this entire effort.

### 3.4.2 Thermal Expansion

Thermal expansion measurements were made and evaluated to determine the relative mismatch between the siliconized coating and RCC-3 substrate. Measurements were made over the temperature range room temperature to 3500°F. Data that was available from previous expansion tests conducted at VSD and Battelle Memorial Institute were utilized. All expansion data on RCC-3, both bare and siliconized, available at the time was evaluated. Coating depth effect on expansion properties was compared with data for bare RCC-3 and against the data for a hot pressed silicon carbide material. The results of this evaluation are presented in graph form in Figure 2, which gives the data plotted in percent expansion through the 3500°F test temperature and shows the variance that was determined between uncoated RCC-3, coated RCC-3, and the RCC-3 coating. The RCC-3 coating specimens were made by coating a standard RCC-3 thirteen ply laminate totally throughout to the apparent complete consumption of the carbonaceous substrate content. Generally, the bare RCC-3 and RCC-3

FIGURE 2 - THERMAL EXPANSION

SILICON COATING, BARE RCC-3 AND SILICONIZED RCC-3

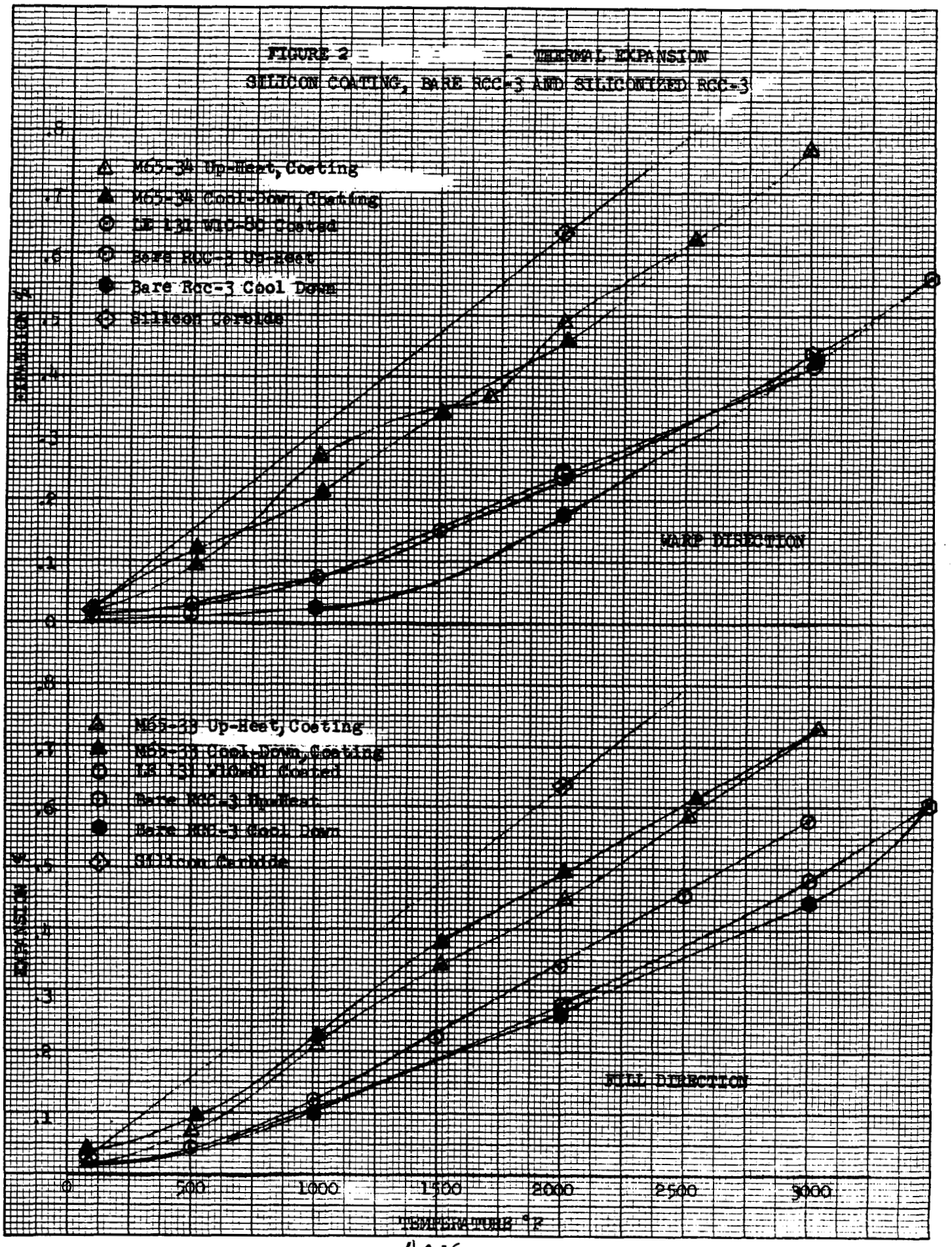

coated in a standard fashion have very similar curves showing the influence of the RCC-3 substrate fraction over the coating layer. The curves of the totally coated specimens or coating shows a vastly different situation and indicates the true expansion difference between the RCC-3 substrate and coating where thermal expansion is much higher throughout the temperature test range. The curves for the hot pressed silicon carbide indicate that the coating data should fall somewhat higher than the curves for the coated RCC-3 as the coating has been determined to be essentially a chemically modified silicon carbide species.

The data given in Table 6 is presented to show the expansion percent and a calculated coefficient of thermal expansion for the tested samples. The real differences between the warp and fill, coated and bare substrate is vividly seen at the 3000°F temperature level. The analysis of this data is given in Tables 7 and 8 where the isotropy ratio and differential expansion ratio are shown in relation to warp and fill direction at 3000°F.

Table 7 indicates that the warp and fill directions for the bare RCC-3 substrate is in a ratio of 1:1.06 or of near 7%. This is understandable as the actual warp and fill yarn count for the starting WCA fiber cloth is 28 to 22 and a higher carbon char influence would be noticed in the fill direction. The carbon char expansion is apparently higher than the equivalent quantity of graphite fibers. The ratio increase for the standard coated system of 1:1.36, warp to fill direction, indicates that the coating penetration is greatest through the carbon char. More coating in the fill direction would account for the increased expansion ratio. The almost equal expansion ratio for the totally coated samples in the warp and fill direction shows the predictable influence of the silicon carbide coating on the substrate.

There is a noticeable expansion difference between the RCC-3 substrate and siliconized coating applied in the VSD coating process, as shown in Table 8. The true magnitude of this difference is not known but it could be the cause of the coating crazing. It is shown by experiments discussed in this report that modifications to reduce the craze pattern can be made with simple adjustment to the processing cycle and additions to the pack materials.

### 3.4.3 Petrographic Studies

Petrographic studies involved Geology Department personnel at the University of Texas at Arlington, under direction of Dr. Burke Burkart. A preliminary

TABLE 6

THERMAL EXPANSION COEFFICIENTS
ROOM TEMPERATURE TO 3000°F

| Specimen | Test Direction | % Expansion | Coefficients ($x10^{-6}$ in/in/°F) |
|---|---|---|---|
| RCC-3 Bare | Warp | .43 | 1.472 |
| Coated RCC-3 Standard (W10-80) | Warp | .42 | 1.438 |
| Coated RCC-3 Totally Coated (M65-34) | Warp | .77 | 2.634 |
| RCC-3 Bare | Fill | .46 | 1.575 |
| Coated RCC-3 Standard (W10-81) | Fill | .58 | 1.986 |
| Coated RCC-3 Totally Coated (M65-33) | Fill | .72 | 2.465 |
| Silicon Carbide Hot Pressed | — | .92 | 3.493 |

TABLE 7

EXPANSION ANISOTROPHY AT 3000°F RCC-3 BARE, COATED RCC-3 AND COATING

| Specimen | Thermal Expansion Coefficients Direction | | Anisotrophy Ratio |
|---|---|---|---|
| | Warp | Fill | |
| Bare RCC-3 | 1.472 | 1.575 | 1:1.06 |
| Coated RCC-3 | 1.438 | 1.986 | 1:1.36 |
| Coating | 2.634 | 2.465 | 1:0.97 |

TABLE 8

DIFFERENTIAL EXPANSION RATIO AT 3000°F BARE RCC-3 AND COATING

| Direction | Condition | | Ratio |
|---|---|---|---|
| | Bare | Coating | |
| Warp | 1.472 | 2.634 | 1: 1.84 |
| Fill | 1.575 | 2.465 | 1: 1.57 |

examination was performed on 30 microns thick sections of coating to determine the texture, homogenity, crystal phases, crazing patterns and other defects. Basically the results showed that the silicon carbide fraction of the coating consists mainly of beta phase and only a slight amount of alpha phase. That is, only one index of refraction was predominant which is typical of a cubic crystal such as beta silicon carbide. A bi-refringence or double refraction index was barely detected. Isotropic minerals or compounds show no color change when the minerals are rotated in polarized light while an anisotropic mineral does show a color change. A slight color change in a mixture would indicate the presence of a small fraction of anisotropic mineral which, in the case of the silicon carbide coating, could be hexagonal alpha phase. In no case was a concentration of any crystal phase found oriented in such a manner as to give rise to an explanation for the crazing phenomena.

3.4.4 Crazing Display

At the beginning of the Task 9 effort the only method for study of crazing and crazing patterns was by use of optical microscope or radiographic negative and light box. These techniques were fine but confined the examination to the metallurgical and x-ray laboratories. Another method to reveal specimen surface conditions was needed. Several techniques were examined. Zyglo techniques using oil and water base impregnants followed by drying and black-light inspection were tried. The surface patterns produced were altogether too shaded by the impregnant weeping from the rough surface areas from which it had been washed clean. The craze pattern was not sharp in detail. Direct photographs of the specimen surface were made but the resultant pictures did not readily expose the craze patterns. Photomicrography produced good pictures but the total craze area reproduced on any one image was not sufficient to warrant this technique. The best method developed was a procedure for photographic reproduction of the crazing pattern in radiographs of coated RCC-3. In fact, two methods were developed which work quite well. Method A was: a radiograph negative of the crazed specimen was taped onto a glass surface and illuminated from behind by a diffuse light source. The radiograph was photographed so that a one-to-one or larger reproduction of the area of interest was obtained. Enlargements are made from the resulting negative in which the tones correspond to those of the original radiograph, i.e., the coating will be light while the crazing pattern will be dark. Method B was simply to make an enlarged positive of the radiograph negative of the specimen area of interest. Prints made in this manner will show a tone reversal from the original radiograph.

FIGURE 3

CRAZE PATTERN DISPLAY - COATED RCC-3
SPECIMENS

Mag - 8X

Photoradiograph of coated specimen, flex bar, showing craze pattern, standard processing techniques.

Mag -8X

Photoradiograph of coated specimen flex bar, showing diminished craze pattern due to results of step heating process work of Task 9 effort.

Examples of the photo-radiograph of sections of flexure bars are shown in the following prints. Illustrated are two specimens (1) one showing quite a bit of crazing and (2) a specimen that was processed as a result of the work of Task 9, which shows a greatly diminished craze pattern, reference Figure 3.

## 3.5 EMPIRICAL STUDIES

### 3.5.1 Chemical Analysis

The results of chemical analysis conducted by Coors Spectrographic Laboratory on shuttle leading edge materials are presented in Tables 9, 9a and 10 of this section. The materials analyzed were:

| Material | Identification | Supplier |
|---|---|---|
| $Al_2O_3$ | Phase 2 Type | Alcoa |
| Silicon | Lot 1471 | Foote Minerals |
| Silicon | Lot 44474 | Union Carbide |
| Silicon Carbide | Lot 6220 | Carborundum |
| Carbon Char | Phenolic | Coast Mfg.(1) |
| Carbon Char | Furfuryl | Quaker Oats(2) |
| Graphite Fibers | WCA | Union Carbide |
| RCC-3 Substrate | Panel (3) | VSD |
| Siliconized RCC-3 | (4) | VSD |
| Heat Treated Siliconized RCC-3 | (5) | VSD |

(1) (2) These resins were cured and pyrolyzed to char at VSD, utilizing standard procedures for fabrication of RCC-3 substrate.

(3) Standard RCC-3 panel.

(4) Siliconized coating from standard coating run; 3100°F for 2-3/4 hours.

(5) Standard coating heat treated to 3200°F for 3/4 hour.

Of the 38 metallic elements sought, 13 were detected in sufficient amounts to quantitize. Two of these thirteen, Al and Si, are in the system from the alumina and silicon metal powder fractions of the 10% alumina, 60% silicon carbide, 30% silicon pack. Four (Ca, Fe, Mg, B) appear to concentrate in the coating, becoming part of the coating system. These concentrations of contaminants in the coating have not proved detrimental to the performance of the coating. The heat treatment tends to reduce the contaminant amount in the

TABLE 9

CHEMICAL ANALYSES RESULTS
METALLIC ELEMENTS (PPM) *

| ELEMENT | DETECTION LIMIT (PPM) | SAMPLES ANALYZED | | | | | | | | | |
|---|---|---|---|---|---|---|---|---|---|---|---|
| | | $Al_2O_3$ PHASE 2 | Si LOT 1471 | Si LOT 44474 | SiC 6220 | PHENOLIC CHAR | FURFURYL CHAR | WCA FIBERS | RCC-3 | COATED RCC-3 | COATED RCC-3 HEAT TREATED |
| Al | 1 | Major | 0.5% | .1% | 500 | 150 | 60 | 20 | 100 | 0.5% | 0.5% |
| B | 10 | 20 | 20 | - | - | - | - | - | - | 60 | 50 |
| Ca | 100 | 200 | 300 | 100 | 100 | - | 50 | - | 100 | 500 | 200 |
| Cr | 10 | - | 50 | 0.1% | - | 50 | - | - | 20 | - | - |
| Cu | 1 | 2 | 600 | 100 | 30 | 60 | 20 | 20 | 20 | 10 | 2 |
| Fe | 4 | 200 | 1.5%<br>1.0% | 0.5 | 150 | 100 | 200 | - | 50 | 450 | 100 |
| Ga | 10 | 500 | - | - | - | - | - | - | - | - | - |
| Mg | 1 | 0.12% | 500 | 30 | 50 | 10 | 20 | 10 | 10 | 800 | 350 |
| Mn | 1 | 20 | 600 | 0.1% | - | - | - | 10 | - | - | - |
| Ni | 10 | - | 800 | - | 30 | 30 | 50 | - | - | - | 30 |
| Si | 1 | 0.15% | Major | Major | Major | 0.1% | 500 | 10 | 750<br>200 | Major | Major |
| Ti | 10 | 20 | 300 | 200 | 300 | - | - | - | - | 15 | 50 |
| V | 10 | - | 500 | 100 | 50 | - | 20 | - | - | - | 20 |

(-) Not found

* Accurate to ±50% of amount reported.

TABLE 9a

CHEMICAL ANALYSES RESULTS METALLIC ELEMENTS, UPPER LIMITS ONLY

| ELEMENT | DETECTION LIMIT (PPM) | SAMPLES ANALYZED | | | | | | | | | |
|---|---|---|---|---|---|---|---|---|---|---|---|
| | | $Al_2O_3$ PHASE 2 | LOT 1471 | LOT 44474 | SiC LOT 6220 | PHENOLIC CHAR | FURFURYL CHAR | WCA FIBERS | RCC-3 | COATED RCC-3 | COATED RCC-3 HEAT TREATED |
| As | 50 | | | | | | | | | | |
| Ba | 100 | | | | | | | | | | |
| Be | 1 | | | | | | | | | | |
| Bi | 10 | | | | | | | | | | |
| Cd | 50 | | | | | | | | | | |
| Co | 100 | | | | | | | | | | |
| Ge | 10 | | | | | | | | | | |
| Hg | 25 | | | | | | | | | | |
| In | 25 | | | | | | | | | | |
| K | 500 | | | | | | | | | | |
| Li | 500 | | | | | | | | | | |
| Mo | 10 | | | | | | | | | | |
| Na | 100 | | | | | | | | | | |
| Nb | 25 | | | | | | | | | | |
| P | 100 | | | | | | | | | | |
| Pb | 10 | | | | | | | | | | |
| Rb | 500 | | | | | | | | | | |
| Sb | 10 | | | | | | | | | | |
| Sn | 10 | | | | | | | | | | |
| Sr | 100 | | | | | | | | | | |
| Tl | 75 | | | | | | | | | | |
| W | 75 | | | | | | | | | | |
| Zn | 25 | | | | | | | | | | |
| Zr | 25 | | | | | | | | | | |

The elements in this table were not detected in any of the samples analyzed; however, it can be stated that their concentrations are below a certain level. This level is called an upper limit derived from the detection limits of the analytical technique employed and subject to the same tolerances.

TABLE 10

CHEMICAL ANALYSES RESULTS (%) ELEMENTAL SILICON, $H_2O$ AND NON-METALLIC ELEMENTS

| SAMPLE | $O_2$ | $H_2$ | $N_2$ | S | Si FREE | Si TOTAL | F | TOTAL HALIDES | $H_2O$ CONTENT |
|---|---|---|---|---|---|---|---|---|---|
| $Al_2O_3$ | - | - | - | .002 | - | 0.15 | < 5PPM | < 10 PPM | <1 |
| Silicon Lot 1471 | .0443 | .0059 | .0178 | .003 | 97.20 | 97.70 | < 5 PPM | < 10 PPM | <1 |
| Silicon Carbide | .169 | .0089<br>.0099<br>.0093 | .00231 | - | 0.20 | 69.67 | < 5 PPM | <10 PPM | <1 |
| RCC-3 | 3.30 | .4490<br>.4416 | .3525<br>.3477 | <.001 | - | - | - | - | - |
| Coated RCC-3 | .381 | .0235 | .0537 | <.001 | - | - | - | - | - |
| Coated RCC-3 Heat Treated | .182 | .0112 | .0637 | <.001 | - | - | - | - | - |

(-) Not determined

A.2-25

coating. Seven (Cr, Cu, Mn, Ni, Ti, V, Ga) apparently remain in the pack material. The major source of contaminants is the silicon metal powder and constitutes the one site for improvement if contamination proves to be a problem. Most metallic elements are tied up in complex intermetallic arrangements, some more stable than others, which could make purification difficult.

Five non-metallic elements were sought. Oxygen was found in all specimens. The 3.3% found in the RCC-3 substrate indicates the gettering capability and tight chemical affinity that carbon has for oxygen. This is a sorption phenomena not easily explained. Oxygen carried into the pack by the RCC-3 substrate is expected to be appreciable. Its role in the process is oxidative in nature and could provide a cleaning action during the coating process or raise the oxidation state of silicon and silicon carbide to a stable oxide level. Oxygen in the silicon and silicon carbide is probably in the form of an oxide, not necessarily that of silicon, but significant to the process.

The hydrogen content is small in the powders and coating systems, but rather significant in the RCC-3 substrate. Nitrogen concentration follows essentially the same trend as hydrogen, being high in the RCC-3. The overall high concentration of oxygen, nitrogen, and hydrogen could mean that thermal decomposition products of incomplete resin charring still remain in the RCC-3 substrate or alternately the carbon sorption of these gases. In either case these gases would be detected by chemical analysis. Sulfur determinations indicate that small amounts are to be found in the alumina and silicon metal powder pack materials which do not show up in the coating. Fluorine determinations show that fluoride transport of silicon can be ruled out as a prime working mechanism during coating process. The $H_2O$ content of pack powders as received was less than 1%.

Oxygen tied up as oxide of silicon, reported to be near 1% in the silicon carbide and in an unknown but probably small quantity in the silicon metal powder could, along with the available residual oxygen and any thermally or chemically stripped from the $Al_2O_3$ or moisture, be a prime method for silicon transport within the pack during coating.

### 3.5.2 University of Washington

The University of Washington was placed under contract to analytically evaluate the RCC-3 coating process to determine what aspects of the high temperature chemistry, if any, could best be varied to control the crazing phenomena. In order to accomplish this task a two phase approach was established to determine the possible reactions and define the reaction products.

This involved sample preparation followed by analytical determination for reaction products formed under known process conditions and using characterized starting materials. A series of fired and unfired samples were examined. Combinations of starting materials and small size one-sample graphite retorts were prepared and heat treated in standard, high fire, and low fire temperature coating cycles. These samples were utilized to study the interaction between the graphite retort, RCC-3 substrate and pack materials. A Knudsen cell mass spectroscopy study was provided by the NASA-Lewis Research Center to determine the prevalent gas species produced during the high temperature coating cycles. A judgement regarding the possible thermal expansion mismatch between the coating and substrate and its effect on crazing was made.

The salient portion of the work accomplished at the University of Washington is given in this report. A more detailed account is being published in a separate report from the university.

Literature Review - A broad literature review was conducted to provide background for the analytical work to be done during this task. Of the many available publications in the high temperature field of chemistry only a few were closely akin to the work at hand but even these were in many instances fragmentary in nature. However, enough informative data was obtained to provide the necessary insight to outline an approach to the overall problems of applying the known principles of Si-O-C chemistry to the siliconized RCC-3 coating and process.

Packing Materials - The packing materials used in the process and in the investigation are noted in the following table:

| Material | Grade | Purity | Lot No. | Manufacturer | Grain Size |
|---|---|---|---|---|---|
| $Al_2O_3$ Tabular | T-61 Commercial | 99.0 | Phase 2 Type | Alcoa | -325 mesh |
| SiC | RA 1200 Commercial Green | 99.0 | 6220 | Carborundum | 1200 grit |
| Silicon | Commercial | 98.5 | 1471 | Foote Mineral | -200 mesh |

These materials were selected for use due to the acceptable performance level attained by the coating system produced for RCC-3 when these materials were used. Other materials did not produce good performing coatings. The

retorts were fabricated from ATL graphite and prefired before use. The characterization of these powders by chemical analysis by Coors Spectrographic Laboratory is shown in the chemical analyses section of this report.

Test and Analytical Procedures - Phase I - This study included the characterization of the raw materials and the investigation of their interactions when heated. All batching, mixing and firing was accomplished at VSD using standard equipment, materials and process conditions. See Table 18 for fabrication history. Samples were placed in prefired carbon crucibles and fired in a 12" diameter carbon resistance furnace with an argon atmosphere. These samples were examined visually and a portion of each was ground to minus 200 mesh in a Diamonite mortar. Analytical methods included scanning electron microscopy (SEM), fluorescent x-ray spectrometry (XRS), and x-ray diffractometry (XRD). When the initial XRD data resulted in unexplained peaks, another pattern was obtained of that sample using a lower scale factor to intensify the small peaks for better resolution. XRS on these specimens was performed to assist in the identification of compounds present. Preparation for SEM study included sprinkling of a small amount of the as-received powder on "double stick" Scotch tape, lightly blowing off the excess and vacuum depositing a gold-palladium coating of the specimen.

Dr. F.J. Kohl, NASA-Lewis Research Center, performed mass spectrometry analysis of the gas species on firing of two samples. A 10-60-30*packing mix and a mixture of 50% 10-60-30 and 50% fiber plus chars were heated in a graphite lined, Tungsten Knudsen cell on predetermined schedules, the gaseous reaction products were analyzed in a time-of-flight mass spectrometer.

Test and Analytical Procedures - Phase II - This study was to analyze the results of process firing on various combinations of composites and packings. All batching, mixing and firing was done at VSD. The sample to be coated was placed in a 2-1/4" diameter x 2-1/4" carbon crucible and surrounded with the experimental packing material. A layer of SiC was placed on top of the packing and a machined carbon cover placed on the crucible. After normal firing and cooling, the crucibles were impregnated with a Marset epoxy resin under vacuum. The purpose of the latter treatment was to keep all the post-processed materials insitu. The potted crucibles were cut through the center, on the diameter, with a diamond saw. No lubricant was utilized so that none of the powders would be leached or reacted. Thin slices were cut axially and

* 10% $Al_2O_3$, 60 % SiC, 30% Si abbreviation

radially from one of the halves for subsequent analyse. Electron microprobe (EMP) traces and XRD patterns were obtained on these slices starting from the center of the composite and moving to the crucible wall.

Bulk density determinations of the coating were made to assist in material balance calculations. Normal coated samples were selected and the outer surface of the coating was lightly ground on a diamond lap until it was flat and smooth. The coating was then removed by cutting parallel to the surface with a diamond bladed slicing saw. The bars were mounted with a thermal wax, coating side down, on a precision ground tile. The carbon backing was then diamond ground until only the coating remained. When the wax was dissolved, the mechanically thinned coating broke into small rectangular pieces. The pieces were thoroughly cleaned, dried then tested in an Aminco 15,000 psi Mercury Porosimeter. Bulk densities were then calculated using the porosimetry data. Standard methods of bulk density determinations were also made by measuring the bulk volume and the weight of sample.

Phase I - Results - As stated previously, the purpose of Phase I study was to characterize as-received materials and observe the results of possible high temperature reactions taking place in the individual materials and combinations of these.

The results of XRD analyses of the individual materials are given in Table 11. Most of the reaction products were as anticipated but it is significant that the $Al_2O_3$ does not act as an inert filler. When the pure oxide (G-2) was fired in a carbon crucible, traces of aluminum metal, and aluminum carbides and oxycarbides were identified. As will be noted later, analysis of any fired sample having $Al_2O_3$ as a starting material should be similar to that obtained for G-2. The increase of the iron content and the relatively high calcium content in the fired furfuryl char (C-2) as evidenced by spectral analyses cannot be explained. Studies were made of the calcium contents of all materials involved with no success.

Mixtures of various combinations of the beginning materials were fired and analyzed. The results are shown in Table 12. In most instances, it will be noted that raw silicon disappears upon firing leaving only trace amounts. It probably reacts with the carbon crucible forming SiC but it may also react with $SiO_2$ layer on the SiC forming SiO gas or, by mass action, reducing the

TABLE 11

X-RAY DIFFRACTION ANALYSES OF INDIVIDUAL MATERIALS

| Code | Sample | Treatment | Phases Identified | Remarks |
|---|---|---|---|---|
| A-1 | Graphite Fibers (WCA) | As Received | Carbon | Poorly Graphitized |
| A-2 | Graphite Fibers (WCA) | Fired | Carbon | Poorly Graphitized |
| B-1 | Phenolic Char | As Received | Carbon | Very Poorly Graphitized |
| B-2 | Phenolic Char | Fired | Carbon | Improved Graphitized |
| C-1 | Furfuryl Char | As Received | Carbon | Poorly Graphitized (better than A-1) |
| C-2 | Furfuryl Char | Fired | Carbon | Improved Graphitization Possible $Al_4C_3$ |
| D-1 | Naphthaquinone Char | As Received | Carbon | Poorly Graphitized |
| D-2 | Naphthaquinone Char | Fired | Carbon | Best Graphitization Observed |
| E-1 | Silicon | As Received | Silicon | |
| E-1 | Silicon | (Not Fired) | | |
| F-1 | SiC | As Received | SiC II<br>SiC III<br>SiC | Possible SiC I |
| F-2 | SiC | Fired | SiC I<br>SiC II<br>SiC III<br>SiC | Unmatched Peak at d = 3.37 |
| G-1 | $Al_2O_3$ | As Received | $Al_2O_3$ | Unmatched peaks at d = 2.25, 1.57, 1.31 |
| G-2 | $Al_2O_3$ | Fired | $Al_2O_3$ | Traces of Al, $Al(OH)_3$ $Al_2OC$, $Al_4O_4C$, $Al_4C_3$ |

A.2-30

TABLE 12

X-RAY DIFFRACTION ANALYSES OF FIRED MIXTURES

| Code | Sample | Phase Identified | Remarks |
|---|---|---|---|
| H | Si + SiC | SiC I, II, III and SiC | No Si detected |
| J | Si + $Al_2O_3$ | SiC II, III and SiC $Al_2O_3$ | Traces of $Al_4C_3$ and Al Possible $Al_2OC$ and $SiO_2$ |
| K | 60-30-10 | SiC II, III and SiC $Al_2O_3$ | Possible SiC I and mullite. SiC intensities greater than observed in unfired mix. |
| L | 68-30-2 | SiC II, III and SiC | Possible SiC I and IV, Al, $Al_4O_4C$ |
| R | $Al_2O_3$ & SiC | $Al_2O_3$, SiC II, III and SiC | Possible SiC I, $SiO_2$, mullite, $Al_4O_4C$, $Al_4C_3$, $Al_2OC$, $Al_4SiC_4$ |
| M-A | Fiber + Si | SiC, trace Si | Possible SiC III, FeC |
| M-B | Phen. Char + Si | SiC, Carbon | Many VWUL* |
| M-C | Furfuryl Char + Si | SiC, Carbon, Trace of SiC | Possible Mullite SVWUL** |
| N-A | Fiber + SiC | Carbon, SiC I, II, III and and SiC | SVWUL |
| N-B | Phen. Char + SiC | Carbon, Sic II, III and and SiC | SVWUL |

* VWUL - Very Weak Unmatched Lines
** SVWUL - Several very weak unmatched lines

A.2-31

TABLE 12
(Continued)

| Code | Sample | Phase Identified | Remarks |
|---|---|---|---|
| N-C | Furfuryl Char + SiC | Carbon, SiC I, II, III and SiC | SVWUL |
| P-A | Fiber + $Al_2O_3$ | $Al_2O_3$, Carbon, $Al_2OC$ | Possible SiC, Al, $Al_4SiC_4$ SVWUL |
| P-B | Phen. Char + $Al_2O_3$ | $Al_2O_3$, Carbon, $Al_2OC$ | Trace $Al_4C_3$, Al Possible $Al_4SiC_4$ - SVWUL |
| P-C | Furfuryl Char + $Al_2O_3$ | $Al_2O_3$, Carbon, $Al_2OC$ $Al_4O_4C$ | Possible Al, $Al_4SiC_4$ |
| Q-A | 60-30-10 + Fiber | SiC II, III and SiC, $Al_2O_3$, $Al_2OC$ | Trace mullite-possible Al SVWUL |
| Q-B | 60-30-10 + Phen. Char | SiC II, III and SiC, $Al_2O_3$ Carbon | Possible mullite, $Al_4C_3$, $Al_4O_4C$ - SVWUL |
| Q-C | 60-30-10 + Furfuryl | SiC II, III and SiC, $Al_2O_3$ Carbon | Possible SiC I, mullite, Al, $Al_4O_4C$ - SWUL |

$Al_2O_3$. The cubic or $\beta$ SiC was the predominate crystal species found. Small amounts of hexagonal or $\alpha$ SiC types I, II, and III were found in some of the samples and subsequently in the coatings.

Trace amounts of mullite were found in the fired 10-60-30 (sample K) and in mixtures of 10-60-30 with the different carbons (Q-A, B, C). However, no mullite was found on any composite specimens. The latter were analyzed by mounting the specimen in place of the sample holder in the diffractometer. Assuming the mullite was most concentrated in the outer layer of the coating, an XRD pattern of just this material should indicate the presence of mullite. A small disk was cut in half with a diamond saw and the coated surfaces rubbed together. This small amount of powder was packed into a glass capillary tube and placed in a Debye-Scherrer camera. Analysis of the film indicated that $\beta$ SiC was the major constituent, $\alpha$ SiC I as the minor. Trace amounts of Al and Si were noted. No extraneous lines were detected on the film even after overexposing the pattern, indicating that no mullite was present.

Fluorescent x-ray analyses were performed on specimens that gave unexplained diffraction lines. Iron was detected in most of the samples. The as-received silicon contains 1% Fe according to Coor's analysis so iron might be present in the furnace system. Another source could be the blades of the Waring Blender used to pulverize the carbon samples. As stated, the source of the calcium is questionable but the silicon did contain 600 ppm of this element, see Coors Data Section.

Sample S4-4 was checked directly by x-ray spectrometry which indicated traces of aluminum, calcium and iron in the coating. A distinctive odor was noted when the specimen was diamond ground with water. This may have been due to the formation of acetylene gas from $CaC_2$. While calcium carbide was never specifically verified by XRD, several samples gave diffraction patterns indicating some possible form of calcium and/or iron carbide.

In order to obtain information on the vapor species present during thermal reactions, handbook values of vapor pressures of various materials were obtained and reviewed. Dr. Fred J. Kohl, NASA-Lewis Research Center, performed Knudsen cell mass spectrometry on 10-60-30 material and on a mixture of 10-60-30 plus the various carbons. These experiments were performed up to 1650°C and the results are presented in Table 13. Aluminum vapor is noted to be the most dominant gas species followed by $CO_2$, CO, Si, SiO and various SiC species. While the complete reduction of alumina may have been

TABLE 13

Relative Concentration ($x10^4$) of Gas Species Observed By Time-of-Flight (TOF) Mass Spectroscopy of Knudsen Cell Products

| Temperature (°F) | 2800 | | | | 3000 |
|---|---|---|---|---|---|
| Time (hours) | 1-1/2 | 2 | 3-1/2 | 4-1/2 | 1/2 |
| Gas Species | | | | | |
| $Al_2O$ | 38 | 5.8 | | .06 | .13 |
| $Si_2C$ | | .81 | | .69 | 1.8 |
| $SiC_2$ | | .03 | | .011 | .017 |
| $CO_2$ | | 42 | | 25 | 20 |
| SiO | | 5.4 | | 1.1 | .06 |
| $Si_2$ | .82 | .3 | .039 | | |
| Al Si | | .92 | | .16 | .038 |
| $Al_2O$; $Al_2$ | | .045 | | | |
| SiC | | 1.8 | | 2.3 | .039 |
| CO | | 14 | | 14 | 31 |
| Si | 6.8 | 8.8 | 15 | | |
| Al | | 160 | 150 | 110 | 90 |

TABLE 14

X-ray Diffraction Analysis of Production Retort Affluent Collected as Deposits from Furnace After Coating Run

| Sample Designation | Approximate Temperature (°F) | Phases Ident. | Remarks |
|---|---|---|---|
| Lid Scrapings | 3200 | β SiC | Trace α SiC I, Al, mullite possible $Al_4C_3$, $SiO_2$ |
| Hi-Temp. Deposit | 3400 | β SiC | |
| Intermediate Temp. | 3000 | β SiC, Si | |
| Low Temp. | 1000 | β SiC | Trace α SiC possible Al, mullite, $Al_4O_4C$, $Al_2OC$ |
| Brown Deposit | Less Than 1000 | Si, $Al_2O_3$ | Possible $Al_4C_3$, $Al_2OC$ |

accelerated by the graphite surfaces in the cell, the presence of Al(g) is highly significant and verifies the XRD detection of Al(s) in some of the specimens. The Al(g) would be the most likely species to vaporize from the coated composite upon further heat treatment. Silicon is definitely vapor transported but SiO is also present in approximately the same concentration. Finally SiC, $Si_2C$ all have finite vapor pressures and might add to the transport. This mass spectrometer data seems to verify that the coating reactions may be rate controlled by vapor transport of silicon.

XRD studies were made of certain discolorations observed on the outside of the production retorts and of deposits which appeared to be condensed vapor phases or reaction products found in various parts of the furnace. The results of these analyses are shown in Table 14.

Phase II - Results - The second phase of this study examined fired samples which were vacuum impregnated with epoxy in the crucible. Typical electron microprobe traces clearly delineated the coating thickness by an even silicon concentration with the aluminum concentration decreasing as the beam moved into the coated composite. An "unreacted" zone usually about 4 mm wide, appeared in the packing between the composite and the crucible. Light reflections from large agglomerated silicon particles were readily visible to the naked eye. A semi-quantitative XRD analysis was performed on pack material and it was determined that the $Al_2O_3$, as well as Si, concentration is reduced in the visibly depleted zone. This reduction in $Al_2O_3$ content would support the assumption that this fraction of the pack mix enters into the high temperature chemical reactions.

Discussion of Possible Reactions - A list of possible reactions involved in the coating process, together with the calculated values of free energy ($\Delta F^\circ$) and enthalpy ($\Delta H^\circ$), are given in Table 15. The $\Delta F^\circ$ and $\Delta H^\circ$ values were calculated from thermodynamic data with temperature at 3100°F. The mass spectrometry results indicate high emissions of Al, Al Si, $Al_2O$ and SiO during the initial measurements at 2800°F and a reduction of these specie with time. This is accompanied by an increase in $Si^+$ ion emission during the same time period. These data support the previously discussed concept that the aluminum oxide is the source of oxygen for transport of CO(g) from the coating area of the composite to account for the necessary carbon loss. The actual reactions would have to satisfy (1) the gas specie reaction products and (2) the thermodynamic requirements of low free energy. It should be noted that

TABLE 1)

Possible Reactions Involved in Coating Process

| No. | Task 9 data Reactions | $\Delta F°$ | $\Delta H°$ |
|---|---|---|---|
| 1 | $Al_2O_3 + 2\ Si(l) \rightarrow Al_2O + 2\ SiO$ | 131.6 | 276.1 |
| 2 | $Al_2O_3 + 2\ Si(l) \rightarrow 2\ Al(l) + SiO(g) + SiO_2(s)$ | 65.2 | 145.1 |
| 3 | $Al_2O_3 + 2\ Si(l) \rightarrow 2\ Al(g) + SiO(g) + SiO_2(s)$ | 93.4 | 256.1 |
| 4 | $Al_2O_3 + 3\ Si(l) \rightarrow 2\ Al(g) + 3SiO(g)$ | 35.6 | 430.1 |
| 5 | $Al_2O_3 + SiC \rightarrow 2\ Al(\ ) + SiO(g) + CO_2$ | 104.9 | 284.3 |
| 6 | $Al_2O_3 + SiC \rightarrow 2\ Al(g) + SiO(g) + CO_2$ | 143.1 | 395.3 |
| 7 | $Al_2O_3 + SiC \rightarrow Al_2O(g) + SiO + CO$ | 46.5 | 312 |
| 8 | $2\ Al_2O_3 + 3SiC \rightarrow 4Al(g) + SiO + 3CO$ | 13.1 | 968.5 |
| 9 | $Al_2O_3 + 3C \rightarrow 2\ Al(g) + 3CO$ | 82.5 | 460.2 |
| 10 | $Al_2O_3 + 2C \rightarrow 2Al(l) + CO + CO_2$ | 84.2 | 286.2 |
| 11 | $Al_2O_3 + 2C \rightarrow 2\ Al(g) + CO + CO_2$ | 122.4 | 397.2 |
| 12 | $Al_2O_3 + C \rightarrow Al_2O + CO_2$ | 81.2 | 258.5 |
| 13 | $2\ Al_2O_3 + 9C \rightarrow Al_4C_3 + 6CO$ | 70.4 | 697.1 |
| 14 | $2\ Al_2O_3 + 5C \rightarrow Al_4C_3 + CO_2 + CO$ | 317.1 | 628.0 |
| 15 | $Al_2O_3 + 2C \rightarrow Al_2OC + CO_2$ | - | - |
| 16 | $2Al_2O_3 + 2C \rightarrow Al_4O_4\ C + CO_2$ | - | - |
| 17 | $2Al_2O_3 + 3C \rightarrow Al_4O_4C + 2CO$ | - | - |
| 18 | $Al_2O_3 + 4Al(g) \rightarrow 3Al_2O(g)$ | -46.8 | -31.8 |
| 19 | $2SiO_2 + SiC \rightarrow 3\ SiO(g) + CO$ | 13.7 | 317.1 |
| 20 | $SiO_2(s) \rightarrow SiO(g) + 1/2\ O_2(g)$ | 66.4 | 178.8 |

A.2-36

TABLE 15 (Cont'd)

| No. | Task 9 data Reactions | $\Delta F°$ | $\Delta H°$ |
|---|---|---|---|
| 21 | $SiO_2 + 2Al(g) \rightarrow Al_2O(g) + SiO(g)$ | -47.0 | -13.7 |
| 22 | $SiO_2 + 2Al(l) \rightarrow Al_2O(g) + SiO(g)$ | -8.8 | +123.7 |
| 23 | $3SiC + 4\ Al(g) \rightarrow Al_4C_3(s) + 3Si(l)$ | -71.6 | -238.1 |
| 24 | $3SiC + 4\ Al(l) \rightarrow Al_4C_3(s) + 3\ Si(l)$ | + 4.6 | +55.0 |
| 25 | $3C + SiO_2 \rightarrow SiC + 2CO$ | -18.8 | 134.0 |
| 26 | $2C + SiO(g) \rightarrow SiC + CO$ | 16.7 | -16.3 |
| 27 | $C + Si(l) \rightarrow SiC$ | -7.6 | -33.55 |
| 28 | $C + Si(g) \rightarrow SiC$ | -31 | -129.2 |
| 29 | $5C + 2\ Al_2O \rightarrow Al_4C_3(s) + 2\ CO$ | -8.4 | 8.86 |
| 30 | $C + CO_2 \rightarrow 2\ CO$ | -41.8 | 37.7 |
| 31 | $3C + 4\ Al(l) \rightarrow Al_4C_3$ | 18.2 | -26.1 |
| 32 | $3C + 4\ Al(g) \rightarrow Al_4C_3$ | -94.6 | -319.2 |
| 33 | $C + Al_2O\ (g) \rightarrow Al(\ ) + CO$ | 5.0 | 19.5 |
| 34 | $C + Al_2O(g) \rightarrow Al(g) + CO$ | 43.2 | 164.1 |
| 35 | $Si\ (s) \rightarrow Si\ (L)$ | | 12.1 |

the latter are to be used only as a guide since no equilibrium conditions are realized in the process and that reactions with positive free energies may proceed if the reaction products are removed as they are formed, e.g., liquids or especially gases. Table 16 shows the result of calculating the equilibrium pressures of reaction product gases for several of the possible reactions. The higher the equilibrium gas pressures, the greater is the probability that the reaction will proceed.

It is also significant to observe the enthalpy values as this will indicate whether the reaction is to be endothermic or exothermic. Examination of temperatures measured during a typical firing cycle (Figure 4) shows evidence that various reactions are taking place inside the retort. It will be noted both TC-3 (top of retort) and TC-1 (middle of retort) follow similar slopes from 1500° to about 2400°F. From 2400° to 3100°F, TC-1 lags behind TC-3, indicating that an endothermic reaction is occurring. Above the 3100° furnace temperature, TC-1 shows retort temperatures as high as 3280°F, indicating that exothermic reactions are proceeding.

Based upon these data and observation, it is suggested that the following are the primary reactions taking place.

<u>In Pack</u>

(35) $Si(s) \rightarrow Si(L)$ $\Delta H° = 12.1$ at 2574°F

(4) $Al_2O_3 + 3\,Si(l) \rightarrow 2\,Al(g) + 3\,SiO(g)$

$\Delta F° + 35.6$ $\Delta H° = 430.1$

(21) $Si_2O + 2\,Al(g) \rightarrow Al_2O(g) + 3\,SiO(g) + SiO(g)$

$\Delta F° = 47.0$ $\Delta H° = -13.7$

(8) $2Al_2O_3 + 3\,SiC \rightarrow 4Al(g) + 3\,SiO(g) + 3\,CO(g)$

$\Delta F° = 13.1$ $\Delta H° = 968.5$

(23) $3\,SiC + Al(g) \rightarrow Al_4C_3\,(s) + Si(l)$

$\Delta F° = -71.6$ $\Delta H° = -238.1$

(19) $2S_iO_2 + SiC \rightarrow 3\,SiO + CO$

$\Delta F° = 13.7$ $\Delta H° = 317.1$

<u>At Carbon Interfaces (composite and retort)</u>

(9) $2Al_2O_3 + 3C \rightarrow 2Al(g) + 3CO(g)$

$\Delta F° = 82.5$ $\Delta H° = 460.2$

(12) $Al_2O_3 + C \rightarrow Al_2O(g) + CO_2(g)$

$\Delta F° = 81.2$ $\Delta H° = 258.5$

(17) $2Al_2O_3 + 3C \rightarrow Al_4O_4C(s) + 2CO(g)$

TABLE 16

Calculated Equilibrium Reaction Product Gas Pressure
(3100°F)

| Reaction No. | Reaction Product | Pressure (atmos) |
|---|---|---|
| 4 | Al | .12 |
| 8 | Al | 1.16 |
| | SiO | .87 |
| | CO | .87 |
| 9 | Al | $1.17 \times 10^{-2}$ |
| | CO | $1.16 \times 10^{-2}$ |
| 19 | SiO | .549 |
| | CO | .183 |

FIGURE 4

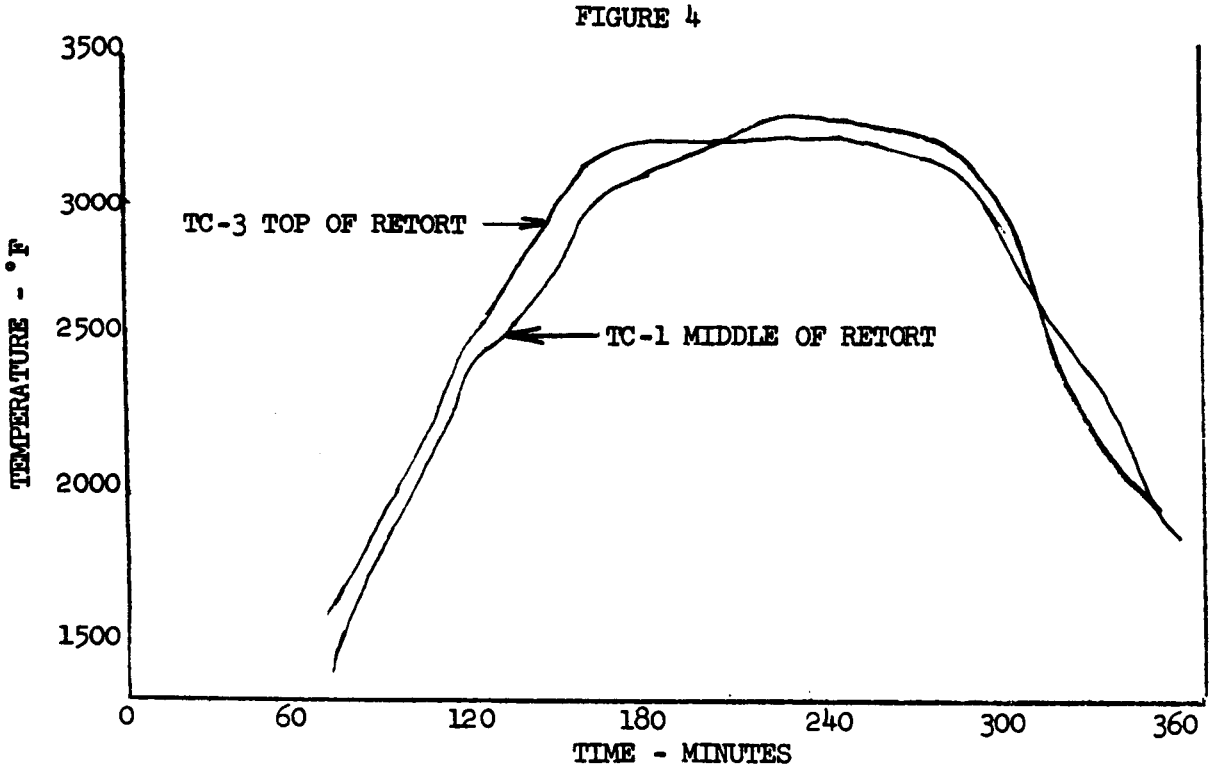


Thermocouple data to detect possible exothermic reactions in pack during coating run M-126.

Coating Reactions

(26) $2C + SiO(g) \rightarrow SiC(s) + CO(g)$

$\Delta F^\circ = 16.7$ $\Delta H^\circ = -16.3$

(27) $C + Si(l) \rightarrow SiC(s)$

$\Delta F^\circ = -7.6$ $\Delta H^\circ = -35.55$

(28) $C + Si(g) \rightarrow SiC(s)$

$\Delta F^\circ = -31$ $\Delta H^\circ = -129.2$

(29) $5C + 2Al_2O \rightarrow Al_4C_3(s) + 2\ CO(g)$

$\Delta F^\circ = -8.4$ $\Delta H^\circ = 8.86$

It will be noted that the endothermic reactions in Figure 4 can be explained by reactions 35, 4, 8, 9, 12 and 19, all of which are necessary in order to account for carbon loss and to develop the gas species required for vapor transport. The exothermic reactions are numbers 26, 27, 28.

Material balance calculations furnished further information for this study. The bulk density of the carbon-carbon fiber composite together with bulk and true densities of the coating were necessary for these. A bulk density of 1.36 g/cc was typical for RCC-3 as determined from the total weight and measured bulk volume of the samples. The true density of the coating was assumed equal to the density of SiC, or 3.20 g/cc. The bulk density as determined by mercury porosimetry together with average pore size and percent porosity are given in Table 17. Direct measurement of the volume and weight gave comparable numbers, so a value 2.23 g/cc for the bulk density of the coating was considered reasonable for this analysis.

Table 17

Bulk Density and Pore Data
(Mercury Porosimeter)

| Measurement | M-143 B-14 | W-2-13 10 | S4-4 18 | RCC-3 |
|---|---|---|---|---|
| Bulk Density $\frac{gm}{cc}$ | 2.26 | 2.19 | 2.26 | 1.357 |
| Porosity (%) | 29.0 | 31.7 | 29.3 | 7.61 |
| Mid Pore Size ($\mu$ m) | 0.13 | 0.35 | 0.33 | 2.6 |

Material balance calculations for specimen M-192 indicated a 50.2% carbon loss in the coated volume. Similar calculations were made on 17 other coated samples which gave carbon loss values between 48 and 51%.

Assuming no loss of carbon and that only silicon was transported into the composite, the density of the coating would be greater than the theoretical density of SiC. This is obviously not possible, but if the 3.20 gm/cc value was approached, the surface would seal and no further coating would occur. It therefore is apparent that a carbon loss is required in order for the coating to proceed to reasonable depths.

Crazing of the SiC Coating

Surface crazing was visible in most of the coated samples. It was observed after diamond polishing the surface in samples where crazing was not visually (10 x mag) apparent. Optical examination at 50 x of sample M-142-2, M-144 HT showed cracks about every 3 mm in the fill direction and 1.5 mm in the warp direction.

It is felt that differential expansion between the coating and RCC-3 substrate is the cause of the crazing. This may be due to firing shrinkage after the coating is formed or thermal expansion mismatch. VSD's experimental determination of the thermal expansion of coated and uncoated RCC-3 specimens together with the curve for SiC show that the carbon-carbon fiber composite has a lower thermal expansion than the SiC in the coating. When the coating is formed on RCC-3 at 3100°F there are probably no stresses, but as the materials cool to room temperature, the SiC shrinks more than the carbon. The coating goes into tension and fractures in stress relief, forming the crazing pattern.

A stress calculation has been made assuming coating thicknesses of 0.020" and 0.010". The theoretical values obtained are shown below:

| Coating Thickness (in) | Calculated Stresses (psi) (SiC) Tension | (c-c) Compression |
|---|---|---|
| 0.010 | 210,000 | 3,100 |
| 0.020 | 560,000 | 6,000 |

The bowing observed when making the initial cut to separate the coating from the composite for the porosimetry and density data determination is experimental evidence of the tensile stresses present in the SiC coating. The handbook ultimate tensile stress of SiC is approximately 5,000 psi and the calculated values exceed this by about two orders of magnitude. Using the ultimate

tensile stress for SiC, the distance between cracks was calculated to be about 1.1 mm. While this does not exactly correspond to the observed values of 1.5 and 3 mm for fill and warp directions, it does tend to indicate that thermal expansion mismatch is the source of crazing.

It is concluded that the crazing is probably caused by thermal expansion mismatch. To eliminate the crazing would require modifications of the carbon-carbon fiber composite to match or exceed the thermal expansion of SiC or modified coating for lower expansion. Additives to the surface may give some cosmetic help but the inherent problem would still exist. However, subsurface additives which influence the coating or coating/substrate interface could have a favorable effect. VSD has shown that $SiO_2$ and boron additives to the pack and ramp hold times in the furnace cycle are effective in reducing the crazing phenomena.

## 3.6 SUBSTRATE MODIFICATION

The experiments to modify the RCC-3 substrate in order to more nearly match the siliconized coating to reduce crazing were selected and conducted to cause the least amount of basic change to the substrate. The basic RCC-3 characteristics of good strength and ease of manufacture were to be maintained. Since the WCA graphite fibers provide the bulk of the properties to the RCC-3 composite they were to be altered as little as possible to avoid possible property degradation. These experiments are discussed in the following text. The details of the coating process for each experiment are presented in the table of diffusion coating runs of the Data section to this report.

### 3.6.1 Carbon Surfacing

Carbon powder was added to the surface of a standard RCC-3 composite in a paste mix with furfuryl alcohol. The 13 ply 5" x 6" substrate was in the RCC-0 condition impregnated with uncured furfuryl at the time the carbon/furfuryl paste was brushed onto the surface and cured. Two further furfuryl alcohol impregnations and subsequent pyrolysis cycles were made to bring the substrate to the RCC-3 level. The carbon surfacing layer adhered well to the substrate through the first impregnation but after the third impregnation was mostly visibly gone. Some carbon powder had penetrated and filled the natural pores of the RCC. Flexure bars and plasma buttons were cut from the panel and coated in a standard coating run, M217. Examination after coating showed that the remaining carbon had only a small effect on the surface crazing which was noticeable at 10X magnification. This result is directly opposite to an identical experiment performed previously where crazing had been eliminated by this technique. However, the

previous experimental panel had retained a large portion of the applied carbon layer. The reason for the loss of the carbon layer on the more recent RCC-3 panel is unknown. It is suspected that too vigorous a cleaning after the second impregnation or a draw-off of the liquid furfuryl alcohol into the substrate during the brush application of the carbon slurry mix may have caused the problem. A loss of furfuryl from the mix by wicking into the substrate prior to curing would have produced a resin starved carbon layer that would have been easily brushed off or may have even flexed off during heating in the cure and/or pyrolysis cycles.

3.6.2 Quinone Impregnation

Specimens which were impregnated with naptha quinone and quinone derivatives were processed in standard coating run M193. Substrates without furfuryl impregnation, (RCC-0) and those impregnated three times with furfuryl (RCC-3) were treated with the quinone impregnation. After coating the specimens were examined and the crazing pattern was found to be entirely different from that normally found on standard coated panels. The crazing pattern was in the form of small Y-shaped configurations instead of the square pattern normally seen which follows the weave of the WCA cloth pattern. Most specimens were delaminated slightly which could be the reason for the lack of a normal craze pattern. A degree of noticeable defoliation of the cloth layers at the edges of most all of the coated specimens was found which caused a thickening at the warp ends. This type of delamination would be most harmful to the strength of the coated laminate. The quinone type impregnations would best be utilized if the resultant resin char could be confined to the outer plies instead of completely saturating through the substrate. This would then provide a coating layer which is highly reactive and readily crystallized in the region of the substrate that needs to be coated. The reactivity of the quinone char was observed and to help explain this phenomena x-ray diffraction studies were made. The char was found to convert from an amorphous carbon structure to a more graphitic structure even at the 3100°F temperature of a standard coating cycle. This is reported in the analytical work conducted by the University of Washington. Other quinone derivatives might not be as easily graphitized since they tend to have a more glassy appearance much like phenolic and furfuryl alcohol resin chars. The interesting aspect of the quinone experiment is that the normal craze pattern was altered significantly by its use. It is felt now that a more judicious application would have produced a coated substrate with a minimum craze pattern and less objectionable side effects.

### 3.6.3 Surface Preparation by Grit Blasting

Previous observations on coated RCC-3 found subtle changes to the craze pattern as it passed from surfaces of rich resin char to surface conditions devoid of resin char. Surfaces of bare RCC-3 were prepared by grit blasting to remove excess resin char without disrupting the outer fiber bundles greatly. A uniform matte type surface was achieved using an 800 grit silicon carbide powder. Coating was conducted in a standard coating run, M193. Examination of the coated specimens showed that the craze pattern was not influenced by the grit blasting procedure. However, it was noticed that a more visibly uniform coated surface was produced.

### 3.6.4 Surface Preparation by Sanding

The surface sanding experiment was conducted to determine the effect of uniform sanding with progressively finer silicon carbide paper to reach a surface finish produced by 400 grit paper. Specimens were coated in the standard M193 coating run. The crazing pattern was essentially unchanged although the coating surface finish was visibly more uniform in appearance.

### 3.6.5 Outer Ply Modification

This experiment was conducted to determine the influence on crazing of exchanging the outer two WCA graphite cloth plies of a standard 13 ply RCC-3 laminate for a coarse weave Kurea KCF-100 fabric and a very fine weave Union Carbide 112 cloth. Fabrication of the two 5" x 10"laminates was done normally except the face cloth plies were prepregged and "B" staged to a desired resin content of near 50% with R120 phenolic resin at VSD. The 9 center plies for the composite were cut from a standard roll of prepregged WCA cloth. The three flexure bars and three 3/4" diameter disks from each panel were coated in diffusion coating run M196. Examination of the coated specimens showed that the outer ply modification was not instrumental in influencing the crazing pattern; however, it was noticed that the weight gain due to coating in both cases was higher than normally expected for standard RCC-3 panel. This indicated that coating penetration was not confined to the two modified outer plies but involved the center section of WCA fibers. To correct this fault the experiment should be rerun in a shorter furnace time cycle to eliminate the excessive coating penetration.

### 3.6.6 Various Substrates Influence

Carbon-carbon composites are fabricated industry wide by many companies. Some varieties are at times available commercially. These are usually flat stock from which to fashion more complex items by machining. As these composites are introduced from time-to-time they are examined and tested at VSD. One test of

the more promising types is to process them through the standard VSD coating process. Runs M192, M193 and M207 contained various carbon-carbon sunstrates and one bulk graphite specimen. In all cases the crazing pattern was more severe than for coated VSD RCC-3. The coating produced on some of the specimens was not up to the standard set for the RCC-3. All information for these runs is presented in Table 18 of this report.

### 3.6.7 Furfuryl Alcohol Influence

The influence on crazing of RCC which was over-impregnated by furfuryl alcohol was tested by impregnating a panel four times. This brought the impregnation level to one more than the accepted standard. Specimens from this panel were coated and examined. The examination showed that furfuryl over-impregnation did not affect the craze pattern after coating.

## 3.7 COATING MODIFICATIONS

Modifications were made to affect only the siliconized RCC-3 coating layer. These experiments involved material additions or silicon modifications to the standard 10%$Al_2O_3$ -60% SiC -30% Si pack. Metallic element additions were made with aluminum, chromium, titanium, boron, and iron. Chemical compound additions were made with silicon dioxide. The additives and silicon modifications were introduced directly into the pack materials and blended in the standard fashion to a uniform powder pack mix. No problems were experienced in the preparation or packing of retorts with these pack material changes. See following for details of these modifications.

### 3.7.1 Pack Silicon Modifications

A standard diffusion furnace run, M205, was made to evaluate the effect of varying the pack silicon metal content on the crazing phenomena. Silicon metal content was varied between 25 to 39 weight percent and at the same time varying the $Al_2O_3$ content between 1 to 15 weight percent. The craze pattern on the coated RCC-3 specimens was not appreciably affected, although the crazing on the specimen coated in the standard 10%$Al_2O_3$ - 60%SiC -30% Si pack was slightly more noticeable at 1X magnification. The results of this experiment might indicate that the 10%$Al_2O_3$ -60% SiC -30% Si pack mix might not be sacred and that slight concentration variations are tolerable as long as all three components are present in sufficient quantity.

### 3.7.2 Metallic Additive Influence

Metallic element additions were made to the standard 10 $Al_2O_3$ - 60 SiC - 30 Si pack and RCC-3 specimens were coated with the resultant pack mix. Iron, chromium, titanium at 1.9%, aluminum 0.8% and boron 0.6% were blended individually into batches of the standard pack mix, packed into one segmented retort and fired

at one time in a standard firing cycle, Run M212. Examination of the coated specimens revealed that the doping quantities of boron, titanium and aluminum did effect the crazing pattern. The aluminum and titanium fractions reduced the craze pattern to a point where it became distinctly visible only under 30X magnification. The iron and chromium additions were ineffective and the pattern was essentially the same as on the standard coated specimen. The pleasant surprise was that the boron specimen was entirely free of crazing when examined under magnification up to 60X. It is felt that the effect imposed on the coating system by the aluminum, titanium and boron to reduce crazing is not basically a chemical union with the SiC coating layer but a modifying influence to the combined diffusion factors which occur naturally in the standard pack and coating cycles. Aluminum melts early and reactive products would become available at a low temperature to initiate a low level reaction system to diffuse toward and into the outer surfaces of the RCC-3 substrate to find compatible nucleation sites from which to grow a more uniform strain-free silicon carbide coating layer. Titanium, although not a low melter, diffuses into and reacts with carbon at very low temperatures in the 1200°F range. Above 1500°F titanium transforms from a hexagonal to a cubic crystal structure which like silicon shows a good affinity for carbon. Titanium in carbide form at the silicon carbide/RCC-3 interface could provide a thermal expansion gradient zone which would smooth out the mismatch between the substrate and coating, hence producing a tendency to reduce crazing. Boron additions probably act in the same fashion as the titanium, and even more so, to produce a gradient zone at the coating/substrate interface. Weight pickup data for the boron addition shows that boron is picked up preferentially by the RCC-3 to the exclusion of the silicon. The 11.5% weight gain is only a third of what would be expected for a similar RCC-3 specimen in a standard run without the small boron addition. Smaller amounts of boron could be employed to provide the needed coating/substrate expansion match to reduce crazing while still maintaining the good performance level indicative of a silicon carbide coating.

### 3.7.3 Silicon Dioxide Additive Influence

Diffusion furnace runs M206 and M211 were made with $SiO_2$ (cabosil M5) additions directly into the standard 10%$Al_2O_3$ -60% SiC - 30%Si pack material. Silicon dioxide additive concentrations ranged from 1/2% to 10% by weight. Run M206 was made at 3100°F for 2-3/4 hours while M211 was exposed to the higher temperature 3250°F for the same length of time.

Examination of the coated specimens from both runs showed that at 1X magnification a no-craze condition existed. At 10X the 3100°F fired specimen and the specimens coated in the high fire run with 10% $SiO_2$ additive showed a craze pattern. The specimens with the 1/2% and 1.0% $SiO_2$ additions fired at 3250°F were uncrazed under 10X magnification. Specimens in the high fire run examined at 30X magnification were crazed. The improvements due to the $SiO_2$ additions indicates strongly that it is incorporated chemically into the coating as opposed to being a silicon carrier and oxygen supplier for the overall reaction kinetics. If it were, the decrease in visual crazing would not have occurred at the higher firing temperature. Indications are that small $SiO_2$ additions of near 1% to the standard pack fired at higher than 3250°F would produce craze free specimens up through examination at 30X magnification and higher. Specimens were recovered easily and cleaned up well by brushing after coating in the $SiO_2$ pack additive experiments. This experiment was the first clear indication that oxides of silicon were important factors in the coating mechanism. What is difficult about the chemistry of $SiO_2$ is that the analytical techniques for its detection are ill defined and not reliable. In most cases the $SiO_2$ is amorphous and not detectable by diffraction techniques. These factors lead to the conclusion that a chemical aspect affecting the coating mechanism might be working in our favor which might not be easily measured.

## 3.8 PROCESS MODIFICATION INFLUENCE

Process modifications were designed and experiments conducted to determine their effect on the crazing pattern. Variations in the coating ramp time, coating temperatures different from the standard cycle, and step cooling after heat treating were tried. Certain distinctly favorable results were obtained. Crazing can apparently be diminished to a more acceptable level by adjustments to provide hesitations in the heat-up portion of the coating cycle. Step cooling after heat treating seems to maintain the craze pattern to a visibly acceptable level. Coating temperatures at 3400°F produce coated specimens that do not need heat treating for good plasma performance.

### 3.8.1 Step Heating Influence

Previous experience suggested that hold times in the heat-up cycle of the coating runs would produce specimens that were essentially craze free. Run M168 produced specimens that were craze free through coating, heating to 3200°F, and 5 cycles to 2300-2500°F in the Pereny furnace. The concern for these specimens were that the long holds in the ramp time caused a deeper penetration

and higher weight gain to the RCC-3 substrate than desired. To control the coating weight gain and penetration, experiments were designed using the standard 10%$Al_2O$ -60% SiC - 30%Si pack where holds in the ramp times were held to a minimum at specific temperatures. The temperatures selected were 2500°F and 2800°F for times of 1 and 2 hours. One below the melting point of silicon (near 2600°F) and the other far above to take advantage of the vapor pressure from a hot solid and a melted silicon. In all cases there appeared to be a reduction in the amount of coating crazing over that normally expected. The best results were obtained when the 1 hour hold time was employed,and the 2500°F and 2800°F appeared to be equally effective. Weight gains of between 24% and 26.5% on flexure bars were comparable to weight picked up in standard coating runs indicating that the hold times were instrumental in crazing reduction. The hypothesis for the hold time effect is several fold, that a more orderly strain free coating is derived from the less rapidly exploited coating nucleation sites, that the temperature gradient is less severe and coating initiation is more uniform over the surface of the RCC-3 from top-to-bottom and end-to-end, and that diffusion of the silicon into the RCC-3 is more pronounced which causes a deeper penetration prior to reaction with carbon to form SiC. A verification run W-19 for the 1 hour hold at 2500°F was made in the 24" diameter furnace using the large 2' x 1 1/2' x 6" retort to contain all the specimens. Thirteen, 20, and 34 ply panels were coated and in all cases the crazing was barely visible under 10X magnification.

3.8.2 3200°F Coating Temperature Influence

A coating run (M215) was made to determine the effect of a slightly higher than normal coating temperature on coating crazing. The furnace cycle used had a slightly longer heat up time to get up to the 3200°F and the time at temperature was cut from 2 3/4 to 2 hours to control coating weight gain to near 30%. Specimen examination did show that this type of cycle was not effective in reducing the crazing normally experienced on specimens from standard runs.

3.8.3 3400°F Coating Temperature Influence

Coating run M216 was made at 3400°F to determine the effect of a high temperature coating run on the coating crazing. A longer heat-up time was employed to get to 3400°F and a 1 1/2 hour time at temperature gave a 31% weight gain on flexure bars due to coating. The specimens were slightly crazed under

10X magnification. What could be important is the good plasma performance of specimen M216-10 which was equal to a 3200°F heat treated specimen coated at 3100°F. A higher coating temperature could conceivably eliminate the heat treatment step and simplify the total process.

3.8.4 Step Cooling After Heat Treating

Two heat runs W-17 and W-20 were made in the 24" diameter furnace on specimens from coating runs W-16 and W-19, respectively. Specimens heat treated in run W-17 were visibly crazed while the specimens from run W-20 were to a large part visibly craze free. One specimen toward the bottom of the retort was crazed. One of the main differences between the two runs was that a step cooling cycle was imposed on the W-20 run. Also, W-20 was better insulated. Specimens from heat treat run W-20 increased very slightly from .07 to .1% in weight after exposure to heat treatment. Specimens from W-17 lost from between .1 to .6 weight percent. Step cooling and proper insulation are the recommended guides for heat treating furnace cycles to minimum weight loss and maintain coating crazing to a minimum.

## 4.0 CONCLUSIONS

The investigation yielded results indicating that the crazing phenomena visible normally on the surface of the VSD siliconized RCC-3 system can be diminished to visibility above 10X magnification by manipulation of the firing cycle ramp time or silicon dioxide additions to the packing material. Boron metal powder additive to the packing material apparently eliminates crazing completely. The ramp time variation of one hour hold at 2500°F is easiest to incorporate into the present coating procedures, while the silicon dioxide and boron additives would need further evaluation prior to incorporation. Verification coating runs were made to show the merit of the ramp time hold technique. The strength and oxidation resistance performance of these siliconized RCC-3 specimens was equal to or better than equivalent specimens coated in a run with no ramp time hold. Because of the good results of this investigation the ramp time hold technique has been integrated into the standard coating firing cycle. Further consideration is warranted for extending the potential of the silicon dioxide and boron additions to eliminate crazing completely.

## 5.0 RECOMMENDATIONS

The results of the Task 9 effort have indicated that certain approaches are successful in reducing the extent of the crazing phenomena. To extend these approaches the following recommendations are made:

1. Continue the evaluation of processing variation, especially in the area of ramp time studies. This will provide one aspect of the needed information applicable to the prediction of heat-up times for retorts which will be used in production to coat the larger complex RCC-3 parts. This effort would examine the effect of controlled cooling after coating and heat treat of coated specimens.

2. Continue the pack $SiO_2$ additives studies and the impact on performance if craze free specimens are fabricated.

3. Continue the boron additives studies which has shown the most promise for a total elimination of the coating crazing phenomena.

4. Initiate an experimental/analytical study to augment the 3400°F coating trial which produced specimens with as-fabricated plasma performance equal to heat treated specimens coated at 3100°F. A coating process which would eliminate the need for the current post coating heat treatment for attainment of plasma performance would be a processing plus and a huge cost savings.

## 6.0 BIBLIOGRAPHY


1. J.E. Campbell & E.M. Sherwood, High Temperature Materials and Technology, John Wiley & Sons, Inc., New York, New York.

2. R.B. Sosman, "The Phases of Silica", Rutgers University Press, New Brunswick, New Jersey.

3. Max Hansen, "Constitution of Binary Alloy", McGraw-Hill Book Company, New York, New York.

4. W.D. Kingery, "Introduction to Ceramics", John Wiley and Sons, New York, New York.

5. H.K. Henisch & R. Roy, "Silicon Carbide", Pergamon Press, New York, New York.

6. E.M. Levin, C.R. Robbins & H.F. McMurdie, "Phase Diagrams for Ceramists", The American Ceramic Society, Columbus, Ohio.

7. E. Rudy, "Compendium of Phase Diagram Data", Air Force Materials Lab, Metals and Ceramics Division, Wright-Patterson Air Force Base, Ohio.

8. D.M. While, VMSC Report No. T143-5R-00044, "Development of a Thermal Protection System for the Wing of a Space Shuttle Vehicle", Phase I Final Report, Dallas, Texas.

9. D.M. While, VMSC Report No. T143-5R-00124, "Development of a Thermal Protection System for the Wing of a Space Shuttle Vehicle", Phase II Final Report, Dallas, Texas.

10. F.P. Kirkhart, et al, "Evaluation of Nonmetallic Thermal Protection Materials for the Manned Space Shuttle, Volume VI, June 1972, Battelle, Columbus, Ohio.

11. P.T.B. Shaffer, "Survey of Literature on Silicon Carbide", Volume I, January 1972, The Carborundum Company, Niagara Falls, New York.

12. D.C. Rogers, "Oxidation Inhibited Carbon-Carbon Composites", VMSC Report No. 00.1243, November 1969.

13. A.F. Rogers, P.F. Kerr, "Optical Mineralogy", 2nd Edition, 1942, McGraw-Hill Book Company, Inc., New York, New York.

APPENDIX - DATA SECTION

TABLE 18

The following pages contain the data for the furnace runs to produce samples for off-site analysis and the experimental coating runs to examine the effects on crazing by modifications made to the RCC substrate, the siliconized coating and coating process.

TABLE 18 DATA-DIFFUSION COATING RUNS

| Run No. | Pack Composition | Pack Powders $Al_2O_3$ | Si | SiC | RCC Substrate | Specimen Ident | Ramp | Run Time(Hr) | Temp(°F) | Wt. Gain (%) | Remarks |
|---|---|---|---|---|---|---|---|---|---|---|---|
| M178 | | | | | | | | 2 3/4 | 3100 | | Samples for determination of reaction products and reaction mechanisms. |
| | WCA Fibers | -- | -- | -- | -- | A-2 | | | | | |
| | Phenolic Char | -- | -- | -- | -- | B-2 | | | | | |
| | Furfuryl Char | -- | -- | -- | -- | C-2 | | | | | |
| | Naptha Quinone Char | -- | -- | -- | -- | D-2 | | | | | |
| | Silicon Carbide | -- | -- | Lot 6220 | -- | F-2 | | | | | |
| | $AL_2O_3$ | Phase 2 | -- | -- | -- | G-2 | | | | | |
| | 50 $AL_2O_3$ 50 SiC | Phase 2 | -- | Lot 6220 | | R | | | | | |
| M179 | | | | | | | | 2 3/4 | 3100 | | Samples for determination of reaction products and reaction mechanisms |
| | 50 Si 50 SiC | -- | Lot 1471 | Lot 6220 | | H | | | | | |
| | 50 Si 50 $AL_2O_3$ | Phase 2 | Lot 1471 | | | J | | | | | |

TABLE 18 DATA-DIFFUSION COATING RUNS

| Run No. | Pack Composition | Pack Powders $Al_2O_3$ | Pack Powders Si | Pack Powders SiC | RCC Substrate | Specimen Ident | Ramp | Run Time(Hr) | Run Temp(°F) | Wt. Gain (%) | Remarks |
|---|---|---|---|---|---|---|---|---|---|---|---|
| M179 (Cont.) | | | | | | | | 2 3/4 | 3100 | | |
| | 10 $AL_2O_3$ 60 SiC 30 Si | Phase 2 | Lot 1471 | Lot 6220 | | K | | | | | |
| | 2 $AL_2O_3$ 68 SiC 30 Si | Phase 2 | Lot 1471 | Lot 6220 | | L | | | | | |
| | 95 Si 5 WCA | -- | Lot 1471 | -- | | M-A | | | | | |
| | 50 Si | | | | | | | | | | |
| | 50 Phenolic Char | -- | Lot 1471 | | | M-B | | | | | |
| | 50 Si | | | | | | | | | | |
| | 50 Furfuryl Char | -- | Lot 1471 | | | M-C | | | | | |
| | 95 SiC | | | | | | | | | | |
| | 5 WCA Fibers | -- | -- | 6220 | -- | N-A | | | | | |

TABLE 18 DATA-DIFFUSION COATING RUNS

| Run No. | Pack Composition | Pack Powders $Al_2O_3$ | Pack Powders Si | SiC | RCC Substrate | Specimen Ident | Ramp | Run Time(Hr) | Run Temp(°F) | Wt. Gain (%) | Remarks |
|---|---|---|---|---|---|---|---|---|---|---|---|
| M179 (Cont.) | 50 Sic | | | | | | | 2 3/4 | 3100 | | |
| | 50 Phenolic Char | -- | -- | 6220 | -- | N-B | | | | | |
| | 50 SiC | | | | | | | | | | |
| | 50 Furfuryl Char | -- | -- | 6220 | -- | N-C | | | | | |
| | 95 $AL_2O_3$ | | | | | | | | | | |
| | 5 WCA Fibers | Phase 2 | -- | -- | -- | P-A | | | | | |
| | 50 $AL_2O_3$ | | | | | | | | | | |
| | 50 Phenolic Char | Phase 2 | -- | -- | -- | P-B | | | | | |
| | 50 $AL_2O_3$ | | | | | | | | | | |
| | 50 Furfuryl Char | Phase 2 | -- | -- | -- | P-C | | | | | |

TABLE 18 DATA-DIFFUSION COATING RUNS

| Run No. | Pack Composition | Pack Powders $Al_2O_3$ | Pack Powders Si | Pack Powders SiC | RCC Substrate | Specimen Ident | Ramp | Run Time(Hr) | Run Temp(°F) | Wt. Gain (%) | Remarks |
|---|---|---|---|---|---|---|---|---|---|---|---|
| M179 (Cont.) | 95 Standard Pack<br>5 WCA Fibers | Phase 2 | Lot 1471 | Lot 6220 | | Q-A | | 2 3/4 | 3100 | | |
| | 50 Standard Pack<br>50 Phenolic Char | Phase 2 | Lot 1471 | Lot 6220 | | Q-B | | | | | |
| | 50 Standard Pack<br>50 Furfuryl Char | | | | | Q-C | | | | | |
| M181 | 10 $AL_2O_3$<br>60 SiC 30 Si | Phase 2 | Lot 1471 | Lot 6220 | | A | | 2 3/4 Unfired | 3100 | | Samples for chemical systemization analysis of coating process |

TABLE 18 DATA-DIFFUSION COATING RUNS

| Run No. | Pack Composition | Pack Powders $Al_2O_3$ | Si | SiC | RCC Substrate | Specimen Ident | Ramp | Run Time(Hr) | Run Temp(°F) | Wt. Gain (%) | Remarks |
|---|---|---|---|---|---|---|---|---|---|---|---|
| M181 (Cont.) | 10 $AL_2O_3$ 60 SiC | | 30 Si | | | B | | 2 3/4 Unfired | 3100 | -- | |
| | 2 $AL_2O_3$ 68 SiC | | 30 Si | | | E | | | | -- | |
| | 15 $AL_2O_3$ 55 SiC | | 30 Si | | | F | | | | -- | |
| | 10 $AL_2O_3$ 60 SiC | | 30 Si | | | G-1 (D-1) | | | | -- | |
| | 10 $AL_2O_3$ 60 SiC | | 30 Si | | | J | | | | -- | |

TABLE 18 DATA-DIFFUSION COATING RUNS

| Run No. | Pack Composition | Pack Powders $Al_2O_3$ | Pack Powders Si | Pack Powders SiC | RCC Substrate | Specimen Ident | Ramp | Run Time(Hr) | Run Temp(°F) | Wt. Gain (%) | Remarks |
|---|---|---|---|---|---|---|---|---|---|---|---|
| M182 | 10 $AL_2O_3$ 60 SiC 30 Si | Phase 2 | Lot 1471 | Lot 6220 | RCC-3 | G | | 2 3/4 | 3300 | -- | Samples for chemical systemization analysis of coating process. |
| M183 | 10 $AL_2O_3$ 60 SiC 30 Si | Phase 2 | Lot 1471 | Lot 6220 | RCC-3 | H | | 2 3/4 | 2900 | -- | Samples for chemical systemization analysis of coating process. |
| M184 | Carbon Felt | | | | | M181-J8 | | 3/4 | 3200 | | Samples for chemical systemization analysis of coating process. |
| M192 | 10 $AL_2O_3$ 60 SiC 30 Si | Phase 2 | Lot 1471 | Lot 6220 | | L-1 | | 2 3/4 | 3100 | 42.2 | |
| | | | | | Super Temp | S/T | | | | 2.9 | |
| | | | | | 3-M | P-505 | | | | 3.3 | |
| | | | | | Fiberite | 3DCVD | | | | 62.5 | |
| | | | | | Fiberite | 3D | | | | 65.4 | |
| | | | | | Carborundum | C100 | | | | 12.2 | |
| | | | | | " | C500 | | | | 16.0 | |
| | | | | | " | C700 | | | | 12.3 | |

TABLE 18 DATA-DIFFUSION COATING RUNS

| Run No. | Pack Composition | Pack Powders $Al_2O_3$ | Pack Powders Si | Pack Powders SiC | RCC Substrate | Specimen Ident | Ramp | Run Time(Hr) | Run Temp(°F) | Wt. Gain (%) | Remarks |
|---|---|---|---|---|---|---|---|---|---|---|---|
| M193 | 10 $Al_2O_3$ 60 SiC 30 Si | Phase 2 | Lot 1471 | Lot 6220 | RCC-3 | | | 2 3/4 | 3100 | | |
| | | | | | Grit Blast Surface | G-1 | | | | 28.5 | |
| | | | | | | G-2 | | | | 29.7 | |
| | | | | | | G-3 | | | | 27.2 | |
| | | | | | | G-1B | | | | 38.6 | |
| | | | | | | G-2B | | | | 42.2 | |
| | | | | | | G-3B | | | | 41.4 | |
| | | | | | Sanded Surface | S-1 | | | | 41.3 | |
| | | | | | | S-2 | | | | 35.6 | |
| | | | | | | S-3 | | | | 32.8 | |
| | | | | | | S-1B | | | | 34.2 | |
| | | | | | | S-2B | | | | 33.4 | |
| | | | | | | S-3B | | | | 37.0 | |
| | | | | | Four Furfuryl Impregnations | R4-1 | | | | 24.8 | |
| | | | | | | R4-2 | | | | 23.8 | |
| | | | | | | R4-3 | | | | 26.7 | |
| | | | | | | R4-1B | | | | 28.0 | |
| | | | | | | R4-2B | | | | 30.4 | |
| | | | | | | R4-3B | | | | 30.8 | |
| | | | | | RCC-O | O | | | | 65.3 | |

TABLE 18 DATA-DIFFUSION COATING RUNS

| Run No. | Pack Composition | Pack Powders $Al_2O_3$ | Pack Powders Si | Pack Powders SiC | RCC Substrate | Specimen Ident | Ramp | Run Time(Hr) | Run Temp(°F) | Wt. Gain (%) | Remarks |
|---|---|---|---|---|---|---|---|---|---|---|---|
| M193 (Cont.) | | | | | RCC-3 and Quinone Impregnation | S-1 | | | | 22.3 | |
| | | | | | | S-2 | | | | 28.2 | |
| | | | | | | S-3 | | | | 30.7 | |
| | | | | | | S-4 | | | | 31.1 | |
| | | | | | RCC-0 and Quinone Impregnations | 1-1 | | | | 47.6 | |
| | | | | | | 1-3 | | | | 24.9 | |
| | | | | | | 1-5 | | | | 21.6 | |
| | | | | | | 2-1 | | | | 45.6 | |
| | | | | | | 2-3 | | | | 22.6 | |
| | | | | | | 2-5 | | | | 14.0 | |
| | | | | | | 3-1 | | | | 42.4 | |
| | | | | | | 3-3 | | | | 22.4 | |
| | | | | | | 3-5 | | | | 19.2 | |
| | | | | | | 4-1 | | | | 52.1 | |
| | | | | | | 4-3 | | | | 33.3 | |
| | | | | | | 4-5 | | | | 24.5 | |
| | | | | | Graphite | RT0029 | | | | 1.6 | |
| M196 | 10 $AL_2O_3$ 60 SiC 30 Si | Phase 2 | Lot 1471 | Lot 6220 | RCC-3 | | | 2 3/4 | 3100 | | |

TABLE 18 DATA-DIFFUSION COATING RUNS

| Run No. | Pack Composition | Pack Powders $Al_2O_3$ | Pack Powders Si | Pack Powders SiC | RCC Substrate | Specimen Ident | Ramp | Run Time(Hr) | Run Temp(°F) | Wt. Gain (%) | Remarks |
|---|---|---|---|---|---|---|---|---|---|---|---|
| M196 (Cont.) | | | | | | | | 2 3/4 | 3100 | | |
| | | | | | Face Cloth | KCF-1B | | | | 55.0 | |
| | | | | | | KCF-2B | | | | 52.4 | |
| | | | | | | KCF-3B | | | | 52.0 | |
| | | | | | | KCF-1 | | | | 47.2 | |
| | | | | | | KCF-2 | | | | 47.6 | |
| | | | | | | KCF-3 | | | | 45.0 | |
| | | | | | | WCL-1B | | | | 42.0 | |
| | | | | | | WCL-2B | | | | 42.4 | |
| | | | | | | WCL-3B | | | | 41.0 | |
| | | | | | | WCL-1 | | | | 35.2 | |
| | | | | | | WCL-2 | | | | 34.2 | |
| | | | | | | WCL-3 | | | | 33.6 | |
| M203 | 10 $AL_2O_3$ 60 SiC 30 Si | Phase 2 | Lot 1471 | Lot 6220 | RCC-3 | | 1 hour hold at 2500°F | 2 3/4 | 3100 | | |
| | | | | | | 1 | | | | 25.2 | |
| | | | | | | 2 | | | | 25.1 | |
| | | | | | | 3 | | | | 24.4 | |
| M204 | 10 $AL_2O_3$ 60 SiC 30 Si | Phase 2 | Lot 1471 | Lot 6220 | RCC-3 | | 1 hour hold at 2800°F | 2 3/4 | 3100 | | |
| | | | | | | 4 | | | | 29.7 | |
| | | | | | | 5 | | | | 29.7 | |
| | | | | | | 6 | | | | 29.4 | |

TABLE 18 DATA-DIFFUSION COATING RUNS

| Run No. | Pack Composition | Pack Powders $Al_2O_3$ | Pack Powders Si | Pack Powders SiC | RCC Substrate | Specimen Ident | Ramp | Run Time(Hr) | Run Temp(°F) | Wt. Gain (%) | Remarks |
|---|---|---|---|---|---|---|---|---|---|---|---|
| M205 | | Phase 2 | Lot 1471 | Lot 6220 | RCC-3 | | | 2 3/4 | 3100 | | |
| | 10 $AL_2O_3$ 60 SiC 30 Si | | | | | 7 | | | | 25.8 | |
| | | | | | | 8 | | | | 25.4 | |
| | 1\ $AL_2O_3$ 60 SiC 39 Si | | | | | 9 | | | | 25.0 | |
| | | | | | | 10 | | | | 25.6 | |
| | 5 $AL_2O_3$ 60 SiC 35 SI | | | | | 11 | | | | 23.7 | |
| | | | | | | 12 | | | | 24.6 | |
| | 15 $AL_2O_3$ 60 SiC 25 Si | | | | | 13 | | | | 24.3 | |
| | | | | | | 14 | | | | 23.5 | |
| | Spent Pack | | | | | 15 | | | | 21.5 | |
| | | | -- | -- | | X | | | | 27.5 | |
| | | -- | -- | 6220 | | XX | | | | 25.5 | |

TABLE 18 DATA-DIFFUSION COATING RUNS

| Run No. | Pack Composition | Pack Powders $Al_2O_3$ | Pack Powders Si | Pack Powders SiC | RCC Substrate | Specimen Ident | Ramp | Run Time(Hr) | Run Temp(°F) | Wt. Gain (%) | Remarks |
|---|---|---|---|---|---|---|---|---|---|---|---|
| M206 | | | | | | | | 2 3/4 | 3100 | | |
| | 10 $AL_2O_3$ 60 SiC 30 Si | Phase 2 | Lot 1471 | Lot 6220 | RCC-3 | 16 | | | | 25.2 | |
| | | | | | | 17 | | | | 27.2 | |
| | 10 $AL_2O_3$ 60 SiC 30 Si 1/2% $SiO_2$ | | | | | 18 | | | | 29.0 | |
| | | | | | | 19 | | | | 29.5 | |
| | 10 $AL_2O_3$ 60 SiC 30 SI 1% $SiO_2$ | | | | | 20 | | | | 29.1 | |
| | | | | | | 21 | | | | 29.5 | |
| | 10 $AL_2O_3$ 60 SiC 30 Si 10% $SiO_2$ | | | | | 22 | | | | 32.5 | |
| | | | | | | 23 | | | | 33.5 | |

TABLE 18 DATA-DIFFUSION COATING RUNS

| Run No. | Pack Composition | Pack Powders $Al_2O_3$ | Pack Powders Si | Pack Powders SiC | RCC Substrate | Specimen Ident | Ramp | Run Time(Hr) | Run Temp(°F) | Wt. Gain (%) | Remarks |
|---|---|---|---|---|---|---|---|---|---|---|---|
| M207 | 10 $AL_2O_3$ 60 SiC 30 Si | Phase 2 | Lot 1471 | Lot 6220 | | | | 2 3/4 | 3100 | | |
| | | | | | Union Carbide | D-52 | | | | 12.3 | |
| | | | | | | D-43 | | | | 14.3 | |
| | | | | | | D-43 | | | | 20.0 | |
| | | | | | | D-53 | | | | 16.4 | |
| | | | | | | D-52 | | | | 19.5 | |
| | | | | | Fiberite | ZR/Si | | | | 16.5 | |
| | | | | | RCC-3 | B | | | | 31.0 | |
| | | | | | RCC-3 | Boron | | | | 19.0 | |
| | | | | | RCC-3 | Titanium | | | | 20.4 | |
| M209 | 10 $AL_2O_3$ 60 SiC 30 SI | Phase 2 | Lot 1471 | Lot 6220 | RCC-3 | | 2 hr hold at 2500°F | 2 3/4 | 3100 | | |
| | | | | | | 1 | | | | 25.3 | |
| | | | | | | 2 | | | | 26.5 | |
| | | | | | | 3 | | | | 24.0 | |
| | | | | | | 1B | | | | 26.5 | |
| | | | | | | 2B | | | | 30.4 | |
| | | | | | | 3B | | | | 26.8 | |

TABLE 18 DATA-DIFFUSION COATING RUNS

| Run No. | Pack Composition | Pack Powders $Al_2O_3$ | Pack Powders Si | Pack Powders SiC | RCC Substrate | Specimen Ident | Ramp | Run Time(Hr) | Run Temp(°F) | Wt. Gain (%) | Remarks |
|---|---|---|---|---|---|---|---|---|---|---|---|
| M210 | 10 $AL_2O_3$ 60 SiC 30 Si | Phase 2 | Lot 1471 | Lot 6220 | RCC-3 | | 2 hr hold at 2800°F | 2 3/4 | 3100 | | |
| | | | | | | 4 | | | | 29.2 | |
| | | | | | | 5 | | | | 29.2 | |
| | | | | | | 6 | | | | 29.1 | |
| | | | | | | 4B | | | | 32.0 | |
| | | | | | | 5B | | | | 32.4 | |
| | | | | | | 6B | | | | 33.7 | |
| M211 | 10 $AL_2O_3$ 60 SiC 30 Si | Phase 2 | Lot 1471 | Lot 6220 | RCC-3 | | | 2 3/4 | 3250 | | |
| | | | | | | 7 | | | | 36.1 | |
| | | | | | | 8 | | | | 40.4 | |
| | | | | | | 7B | | | | 41.9 | |
| | | | | | | 8B | | | | 46.7 | |
| | 10 $AL_2O_3$ 60 SiC 30 Si 1/2% $SiO_2$ | | | | | 9 | | | | 38.8 | |
| | | | | | | 10 | | | | 42.5 | |
| | | | | | | 9B | | | | 37.1 | |
| | | | | | | 10B | | | | 43.2 | |

TABLE 18 DATA-DIFFUSION COATING RUNS

| Run No. | Pack Composition | Pack Powders $Al_2O_3$ | Pack Powders Si | Pack Powders SiC | RCC Substrate | Specimen Ident | Ramp | Run Time(Hr) | Run Temp(°F) | Wt. Gain (%) | Remarks |
|---|---|---|---|---|---|---|---|---|---|---|---|
| M211 (Cont.) | | | | | | | | 2 3/4 | 3250 | | |
| | 10 $AL_2O_3$ 60 SiC 30 Si 1% $SiO_2$ | | | | | 11 | | | | 41.1 | |
| | | | | | | 12 | | | | 42.5 | |
| | | | | | | 11B | | | | 44.5 | |
| | | | | | | 12B | | | | 45.2 | |
| | 10 $AL_2O_3$ 60 SiC 30 Si 10% $SiO_2$ | | | | | 13 | | | | 42.3 | |
| | | | | | | 14 | | | | 39.4 | |
| | | | | | | 13B | | | | 41.5 | |
| | | | | | | 14B | | | | 46.0 | |
| M212 | | Phase 2 | Lot 1471 | Lot 6220 | RCC-3 | | | 2 3/4 | 3100 | | |
| | 10 $AL_2O_3$ 60 SiC 30 Si 1.9% Fe | | | | | 15 | | | | 25.5 | |
| | 10 $AL_2O_3$ 60 SiC 30 Si 1.9% Cr | | | | | 16 | | | | 16.5 | |

TABLE 18 DATA-DIFFUSION COATING RUNS

| Run No. | Pack Composition | Pack Powders $Al_2O_3$ | Si | SiC | RCC Substrate | Specimen Ident | Ramp | Run Time(Hr) | Run Temp(°F) | Wt. Gain (%) | Remarks |
|---|---|---|---|---|---|---|---|---|---|---|---|
| M212 (Cont.) | | | | | | | | 2 3/4 | 3100 | | |
| | 10 $AL_2O_3$ 60 SiC 30 Si 0.5% B | | | | | 17 | | | | 11.5 | |
| | 10 $AL_2O_3$ 60 SiC 30 Si 1.9% Ti | | | | | 18 | | | | 18.2 | |
| | $AL_2O_3$ 60 SiC 30 Si .8% AL | | | | | 19 | | | | 20.3 | |
| | 10 $AL_2O_3$ 60 SiC 30 Si | | | | | C | | | | 23.0 | |

A.2-68

TABLE 18 DATA-DIFFUSION COATING RUNS

| Run No. | Pack Composition | Pack Powders $Al_2O_3$ | Pack Powders Si | Pack Powders SiC | RCC Substrate | Specimen Ident | Ramp | Run Time(Hr) | Run Temp(°F) | Wt. Gain (%) | Remarks |
|---|---|---|---|---|---|---|---|---|---|---|---|
| M215 | | | | | | | | 2 | 3200 | | |
| | 10 $AL_2O_3$ | Phase 2 | Lot 1471 | Lot 9947 | RCC-3 | | | | | | |
| | 60 SiC | 30 Si | | | | | | | | | |
| | | | | | | 8 | | | | 31.4 | |
| | | | | | | 9 | | | | 31.6 | |
| | | | | | | 10 | | | | 31.4 | |
| | | | | | | 8B | | | | 32.8 | |
| | | | | | | 9B | | | | 30.8 | |
| | | | | | | 12B | | | | 31.2 | |
| M216 | 10 $AL_2O_3$ | Phase 2 | Lot 1471 | Lot 9947 | | | | 1 1/2 | 3400 | | |
| | 60 SiC | 30 Si | | | | | | | | | |
| | | | | | | 11 | | | | 33.3 | |
| | | | | | | 12 | | | | 35.5 | |
| | | | | | | 13 | | | | 32.3 | |
| | | | | | | 10B | | | | 39.6 | |
| | | | | | | 11B | | | | 38.3 | |
| | | | | | | 13B | | | | 41.2 | |
| M217 | 10 $AL_2O_3$ | Phase 2 | Lot 1471 | Lot 9947 | RCC-3 | | | 2 3/4 | 3100 | | |
| | 60 SiC | 30 Si | | | | | | | | | |
| | | | | | | C-1 | | | | 24.9 | |
| | | | | | | C-2 | | | | 23.8 | |
| | | | | | | C-3 | | | | 23.3 | |
| | | | | | | C-1B | | | | 30.2 | |
| | | | | | | C-2B | | | | 29.4 | |
| | | | | | | C-3B | | | | 29.3 | |

MSC-06849

# DESIGN EVALUATION TEST PLAN

# OXIDATION INHIBITED

# REINFORCED PYROLYZED PLASTIC

# LEADING EDGE ASSEMBLIES

# SPACE SHUTTLE WING

REPORT No. T143T-5R-30745

D. M. While
Approved

B. A. Forcht
Approved

A. 3. i

TABLE OF CONTENTS


| | | Page |
|---|---|---|
| 1.0 | INTRODUCTION | 1 |
| 2.0 | OBJECTIVE | 3 |
| 3.0 | DESCRIPTION OF TEST ARTICLE | 4 |
| 4.0 | APPROACH | 13 |
| 5.0 | TESTS | 18 |
| | 5.1 Entry Temperature Tests | 18 |
| | 5.2 Boost Pressure Loads Tests | 32 |
| | 5.3 Orbital Vacuum/Temperature Test | 61 |
| | 5.4 Boost Acoustic Noise Test | 64 |
| 6.0 | INSPECTION | 74 |
| 7.0 | ACCEPTANCE/FAILURE CRITERIA | 76 |
| 8.0 | DOCUMENTATION | 82 |
| REFERENCES | | 83 |

## 1.0 INTRODUCTION

Two Reinforced Pyrolyzed Plastic (RPP) leading edge assemblies have been fabricated by VSD* under NASA-MSC contract NAS9-12763 to represent a viable design for the wing leading edge of the Space Shuttle. The leading edge assemblies were designed to withstand 100 high cross range missions through launch, entry and cruise flight without failure. The assemblies consist of the oxidation inhibited leading edge, metal support fittings and support structure, insulation heatshields to protect the metallic structure, a simulated wing front spar, and ground test fittings to hold the assembly to appropriate test fixtures. Two complete assemblies were fabricated, which can be tested singly or together. Each assembly is nominally 15 inches wide and represents one full scale segment of the leading edge.

As part of the total evaluation of the application of RPP to the Shuttle leading edge, these two leading edge assemblies are to be subjected to a series of ground tests simulating multiple Shuttle missions. This report defines the tests to be conducted by NASA-MSC on the two assemblies to evaluate performance in design environments. Only those test conditions that should have the most critical effect on the leading edge assembly performance will be tested. Further, in the interest of economy, plasma arc exposure of the assemblies to simulate entry heating/oxidation conditions has been eliminated in favor of radiant heating. Thermal/oxidation performance of the RPP material

*Vought Systems Division, LTV Aerospace Corporation

system has been demonstrated by element and small component testing in plasma arc test facilities.

Because of a limitation on the availability and cost of RSI insulation materials for the current technology program, a substitute insulation was required. The substitute, while possessing desirable thermal and thermoelastic attributes, lacks acceptable short transverse strength that makes it subject to failure in dynamic loading environments. For this reason early failure of the insulation may occur in the acoustic environment, and may require removal and substitution of equivalent mass for this test only.

In the Phase II portion of this technology program, two full scale leading edges were successfully tested to boost pressure, and entry temperature design conditions to demonstrate structural integrity of RPP leading edges. Those tests were restricted only to the RPP leading edge components, whereas the current test plan covers the leading edge assemblies, including insulation and support structure, produced in the Phase III program.

This test plan describes the tests to be performed on the two Phase III leading edge assemblies, instrumentation required, test procedures, acceptance/failure criteria, precautions to be observed, inspection requirements and documentation of results.

Detail test procedures, based on this test plan, should be reviewed by VSD to ensure compliance with the intent of this test plan. All testing should be witnessed by a VSD representative, and test failures or anomalies shall be brought to the immediate attention of VSD.

## 2.0 OBJECTIVE

The objective of these tests is to prove the feasibility and viability of an RPP leading edge system for the Shuttle application. This will be accomplished by demonstration of the structural integrity of the RPP leading edge and support structure, and the thermal integrity of the insulation components under ground test conditions simulating Shuttle flight environments.

## 3.0 DESCRIPTION OF TEST ARTICLE

The leading edge assemblies are depicted in drawing T143T00019, which illustrates how the two leading edge assemblies are mated to form a two-segment assembly. The top assembly drawing, T143T00017, provides details and requirements for the assemblies. The drawing breakdown, Sheet 1 of drawing T143T00017, shows all of the drawings necessary for individual and two-segment assemblies. Basic geometry data is given on drawing T143E00003.

The RPP leading edge panel (T143T00007) was designed to permit one safe entry to landing in the event the coating was non-existent at the initiation of entry. This resulted in a skin thickness requirement varying from 34 plies (0.44 in.) at the stagnation line to 20 plies at the windward trailing edge and 16 plies at the leeward trailing edge. Integrally formed ribs, 12 plies thick, and trailing edge spars reinforce the skin. The layup technique employed for the ribs and spars produces a thickened (23 ply) region at each support lug. Trailing edge "T" section members are integrally RPP riveted and carbon bonded to the basic leading edge segment to form an overlap seal at the RPP/RSI (simulated) interface. Similarly, a "floating" "T" curved RPP strip is employed between leading edge segments to seal the expansion gap against direct influx of air.

Each leading edge segment is supported by four lug type fittings. Adjacent segments share Inconel 718 attachment bolts. The upper fittings

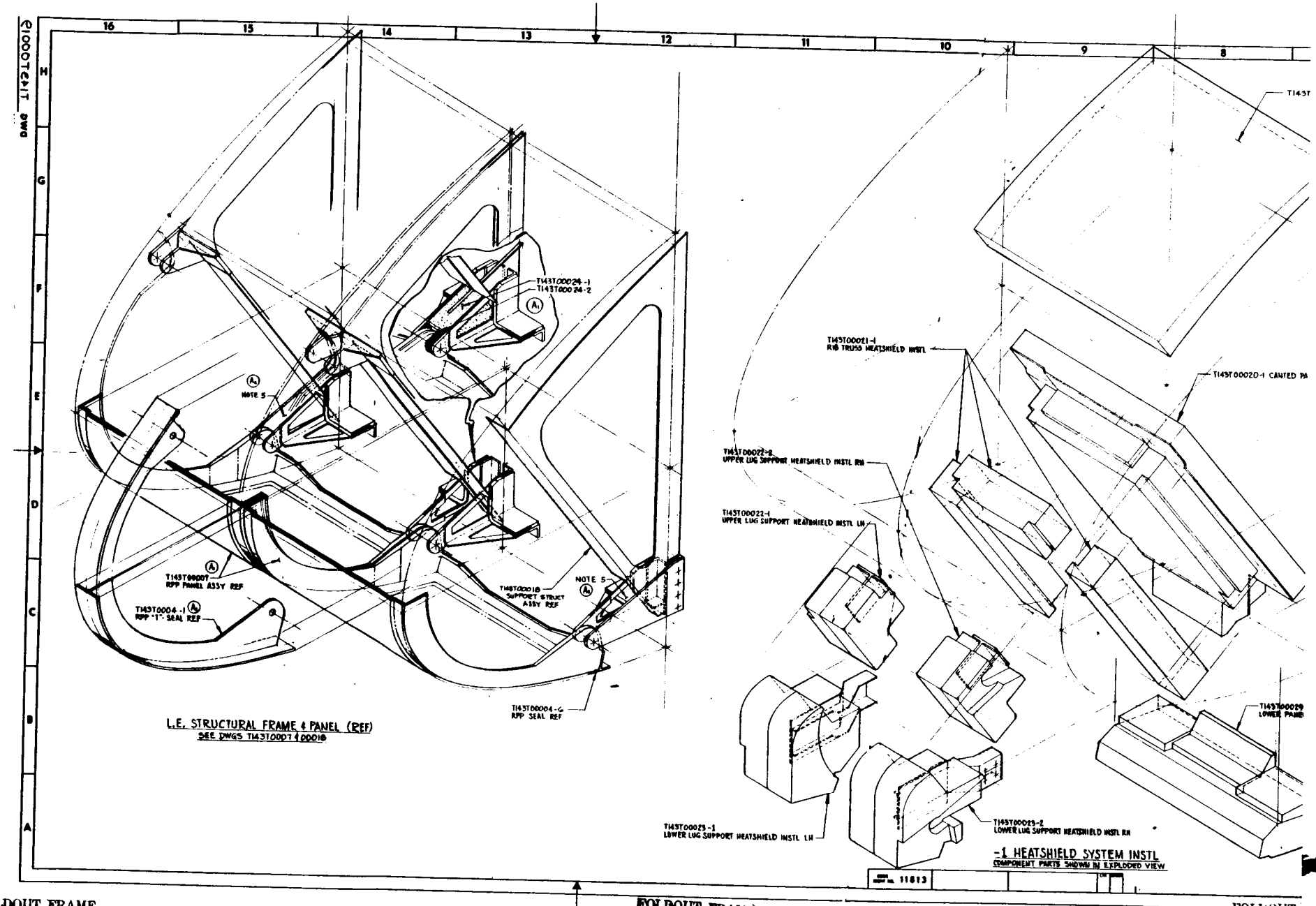


FOLDOUT FRAME 1

FOLDOUT FRAME 2

FOLDOUT FRAME 3

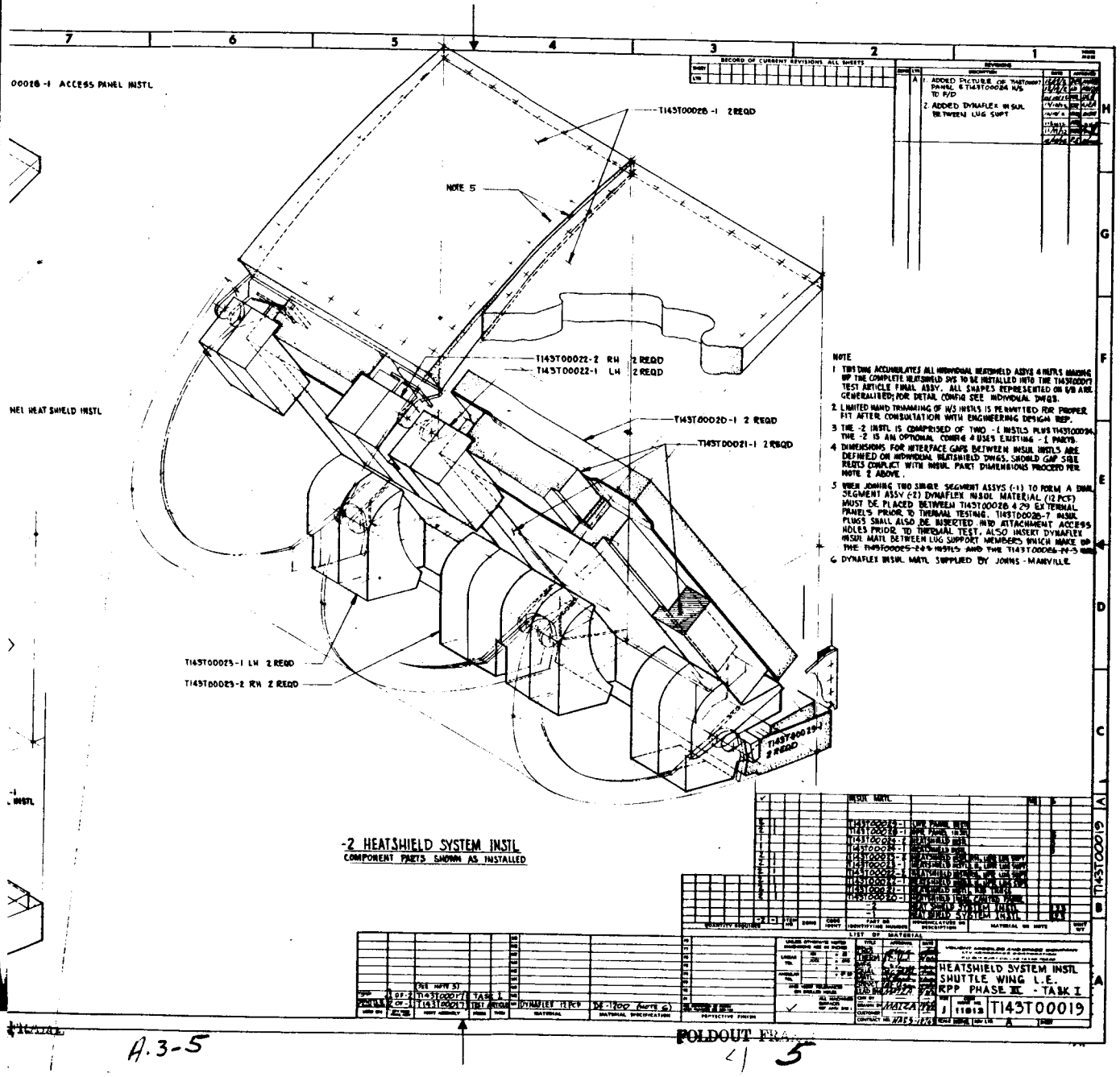
00028-1 ACCESS PANEL INSTL
HEI HEAT SHIELD INSTL
T143T00028-1 2 REQD
NOTE 5
T143T00022-2 RH 2 REQD
T143T00022-1 LH 2 REQD
T143T00020-1 2 REQD
T143T00021-1 2 REQD
T143T00023-1 LH 2 REQD
T143T00023-2 RH 2 REQD
T143T00029-1 2 REQD
-2 HEATSHIELD SYSTEM INSTL
COMPONENT PARTS SHOWN AS INSTALLED
RECORD OF CURRENT REVISIONS ALL SHEETS
REVISIONS
A 1. ADDED PICTURE OF T143T00027 PANEL & T143T00024 W/S TO F/D
2. ADDED DYNAFLEX INSUL BETWEEN LUG SUPT
NOTE
1 THIS DWG ACCUMULATES ALL INDIVIDUAL HEATSHIELD ASSYS & INSTLS MAKING UP THE COMPLETE HEATSHIELD SYS TO BE INSTALLED INTO THE T143T00001 TEST ARTICLE FINAL ASSY. ALL SHAPES REPRESENTED ON F/D ARE GENERALIZED; FOR DETAIL CONFIG SEE INDIVIDUAL DWGS.
2 LIMITED HAND TRIMMING OF W/S INSTLS IS PERMITTED FOR PROPER FIT AFTER CONSULTATION WITH ENGINEERING DESIGN REP.
3 THE -2 INSTL IS COMPRISED OF TWO -1 INSTLS PLUS T143T00034. THE -2 IS AN OPTIONAL CONFIG & USES EXISTING -1 PARTS.
4 DIMENSIONS FOR INTERFACE GAPS BETWEEN INSUL INSTLS ARE DEFINED ON INDIVIDUAL HEATSHIELD DWGS. SHOULD GAP SIZE REQTS CONFLICT WITH INSUL PART DIMENSIONS PROCEED PER NOTE 2 ABOVE.
5 WHEN JOINING TWO SINGLE SEGMENT ASSYS (-1) TO FORM A DBL SEGMENT ASSY (-2) DYNAFLEX INSUL MATERIAL (12 PCF) MUST BE PLACED BETWEEN T143T00028 & 29 EXTERNAL PANELS PRIOR TO THERMAL TESTING. T143T00026-7 INSUL PLUGS SHALL ALSO BE INSERTED INTO ATTACHMENT ACCESS HOLES PRIOR TO THERMAL TEST. ALSO INSERT DYNAFLEX INSUL MATL BETWEEN LUG SUPPORT MEMBERS WHICH MAKE UP THE T143T00025-2 & 4 INSTLS AND THE T143T00026-7 & -3
6 DYNAFLEX INSUL MATL SUPPLIED BY JOHNS-MANVILLE.
LIST OF MATERIAL
HEATSHIELD SYSTEM INSTL
SHUTTLE WING L.E.
RPP PHASE II - TASK I
T143T00019
DYNAFLEX 11PCF
DE-1200 (NOTE 6)
A.3-5
FOLDOUT FRAME 5

| ZONE | LTR | DESCRIPTION | DATE |
|---|---|---|---|
| | A | REVISED SHEET 3 | 1-8-73 |
| | | 1. REVISED DWG BREAKDOWN | 1-8-73 |
| | | 2. ADDED NOTE G | |

NOTE

1. THIS DWG PRESENTS IN ITS DELIVERED CONFIGURATION THE "FAIL SAFE" SHUTTLE WING L.E. TEST ARTICLE FINAL ASSY. THIS DWG ALSO ACCUMULATES ALL SUBORDINATE DESIGN DWGS OF THE TEST ARTICLE CONSTITUENT DETAILS & ASSYS.
2. PARTS WILL BE FAB FOR TWO (2) OF -1 TEST ARTICLE ASSY'S WHICH ARE THE DELIVERABLE END ITEMS. ADDITIONAL PARTS ARE FURNISHED TO FACILITATE CONVERSION OF THE OF THE -1 ASSY'S FROM THE "SINGLE-SECTION CONFIG" TO THE -2 ASSY "DUAL-SECTION CONFIG"
3. THE T143T00004-1 "T" STRIP SEAL IS AN EXISTING PART FROM THE PHASE II PROG.
4. THE T143T00025-1 & T143T00026-1 LUG SUPPORT INSTLS ARE MADE UP OF EXISTING PARTS FROM T143T00025-2 & -3 AND T143T00026-2 & -3. FOR PARTS UTILIZATION INSTRUCTIONS ON THE CONVERSION FROM THE "SINGLE" TO THE "DUAL" SECTION CONFIG SEE DWGS T143T00025 & T143T00026 SUPT INSTL.
5. AN INSPECTION SHALL BE MADE TO ASSURE THAT A MINIMUM GAP OF .060 IS PROVIDED BETWEEN THE T143T00004-1 "T" STRIP SEAL & THE T143T00007-1 PANEL LUGS WHEN JOINING TWO -1 SINGLE-SECTION ASSYS TO FORM THE -2 DUAL-SECTION ASSY
G. GAPS SHALL BE 0.030 MIN, 0.090 MAX AT INTERFACES BETWEEN HEATSHIELD ASSYS & BETWEEN HEAT SHIELDS & ADJACENT STRUCTURAL PARTS

## DRAWING BREAKDOWN

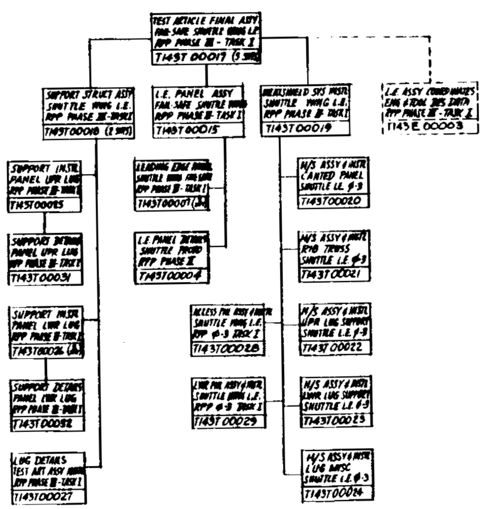


| QTY -2 | QTY -1 | ITEM NO | ZONE | CODE IDENT | PART OR IDENTIFYING NUMBER | NOMENCLATURE OR DESCRIPTION | MATERIAL OR NOTE | UNIT WT |
|---|---|---|---|---|---|---|---|---|
| | | | | | T143T00026-1 | SUPPORT INSTL | 4 | |
| | | | | | T143T00025-1 | SUPPORT INSTL | 4 | |
| | | | | | T143T00019-2 | HEATSHIELD SYSTEM INSTL | | |
| | | | | | T143T00019-1 | HEATSHIELD SYSTEM INSTL | | |
| | | | | | T143T00018-1 | SUPPORT STRUCT ASSY | | |
| | | | | | T143T00015-1 | RPP L.E. PANEL ASSY (FAIL SAFE) | | |
| | | | | | T143T00004-1 | SEAL, "T"-STRIP | 3 | |
| | | | | | -2 | TEST ARTICLE FINAL ASSY | 2,5 | |
| | | | | | -1 | TEST ARTICLE FINAL ASSY | | |

LIST OF MATERIAL

UNLESS OTHERWISE NOTED DIMENSIONS ARE IN INCHES

TEST ARTICLE FINAL ASSY
"FAIL SAFE" SHUTTLE WING L.E.
RPP PHASE III - TASK I

SIZE E | CODE IDENT NO 11813 | T143T00017

SCALE — | REV LTR A | SHEET 1 OF 3

RPP SHUTTLE L.E. | SEE NOTE 2 | TASK I TEST ARTICLE

DWG T143T00017 SH 1 34X44

FOLDOUT FRAME

A.3-6

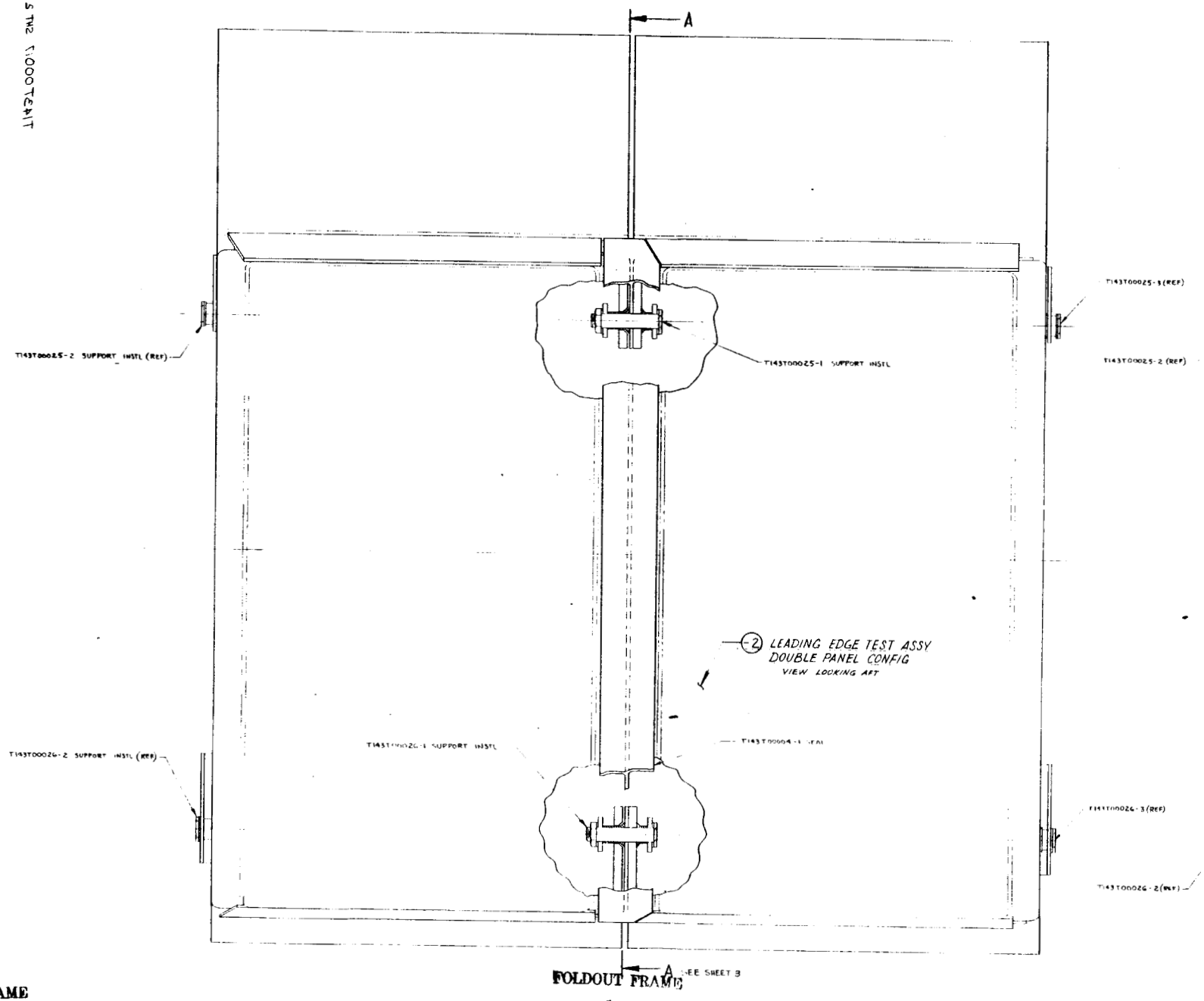


FOLDOUT FRAME

FOLDOUT FRAME

FOLDOUT FRAME

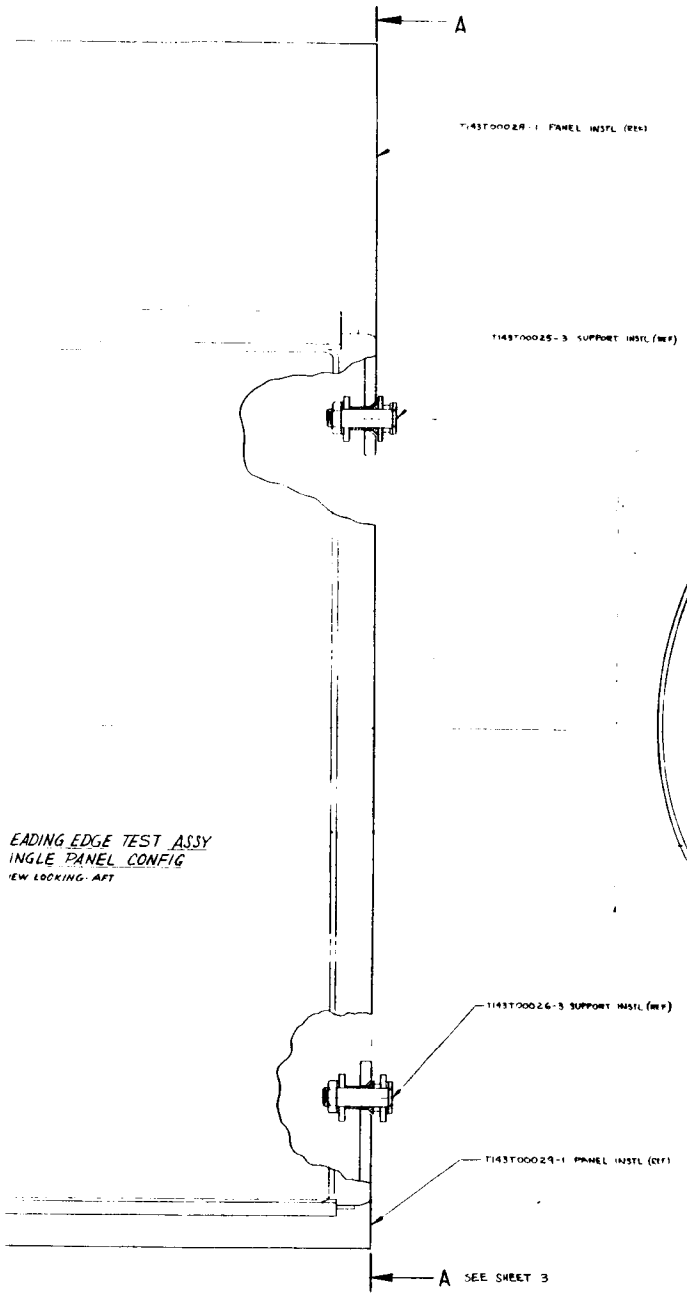


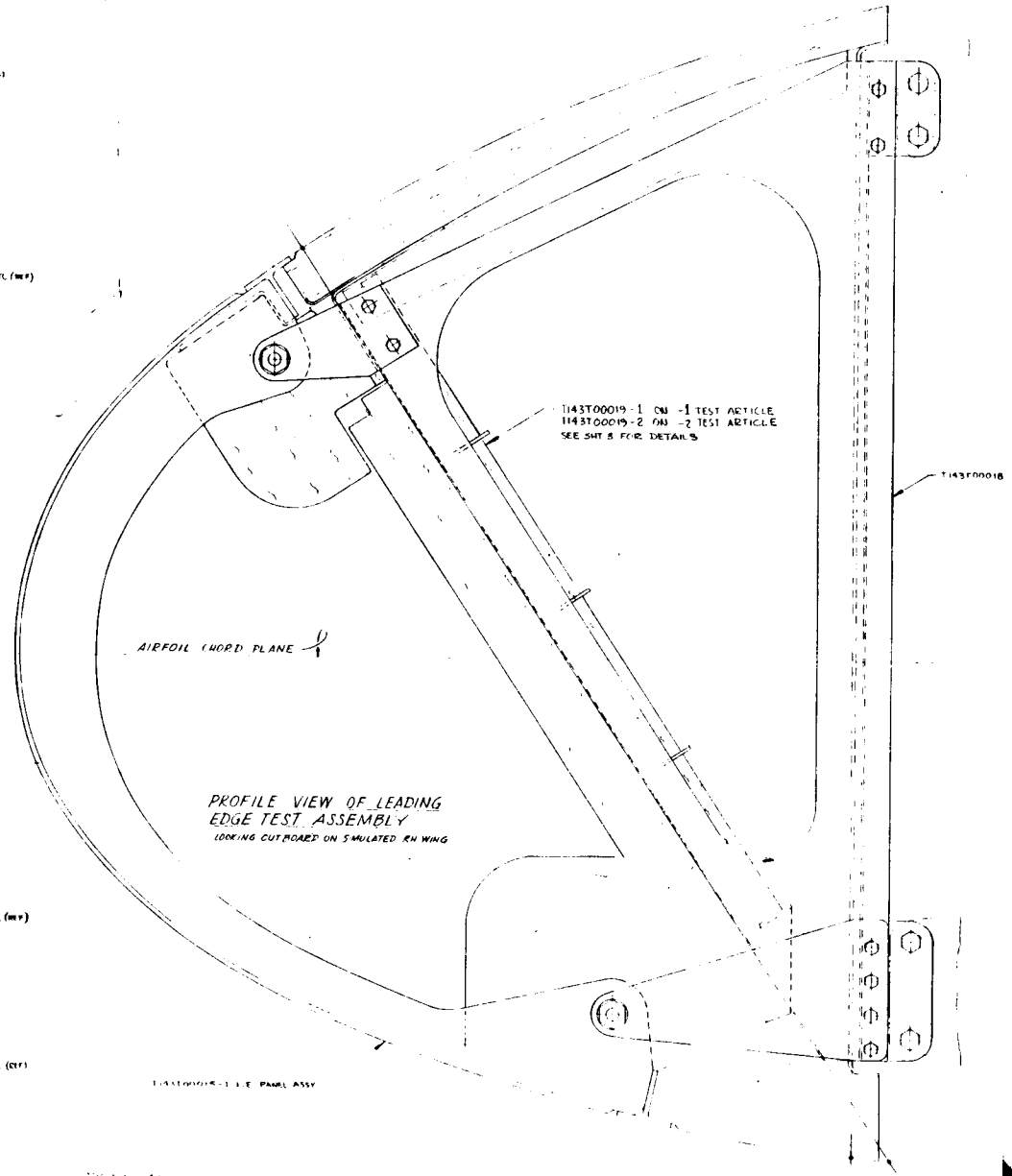


FOLDOUT FRAME

4

FOLDO

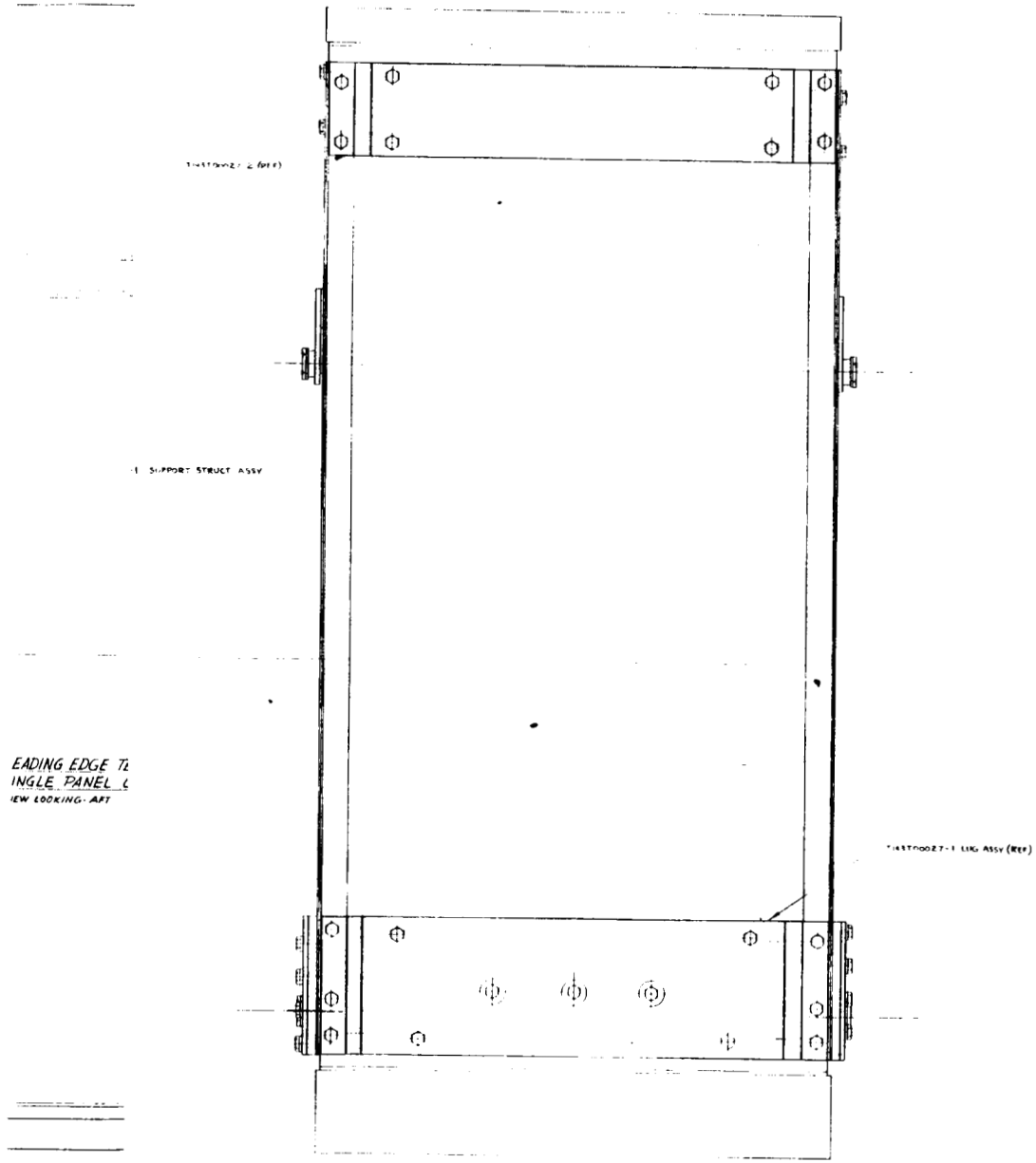


TEST ARTICLE ASSY
SHUTTLE RPP L.E.
PHASE III TASK I
T143T00017

FOLDOUT FRAME 5

FOLDOUT FRAME 6

A-3-7

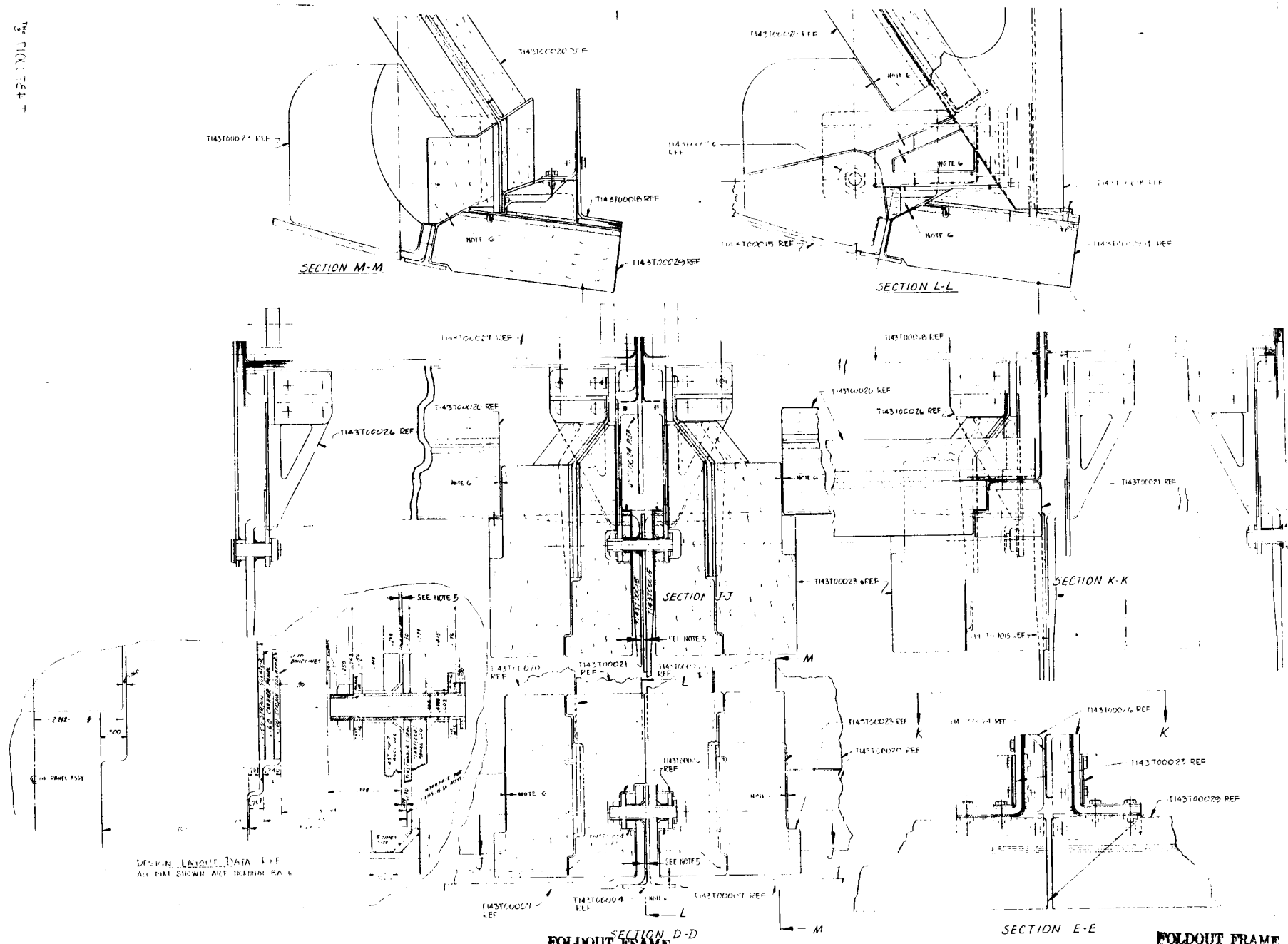


FOLDOUT FRAME 1

FOLDOUT FRAME 2

FOLDOUT FRAME 3

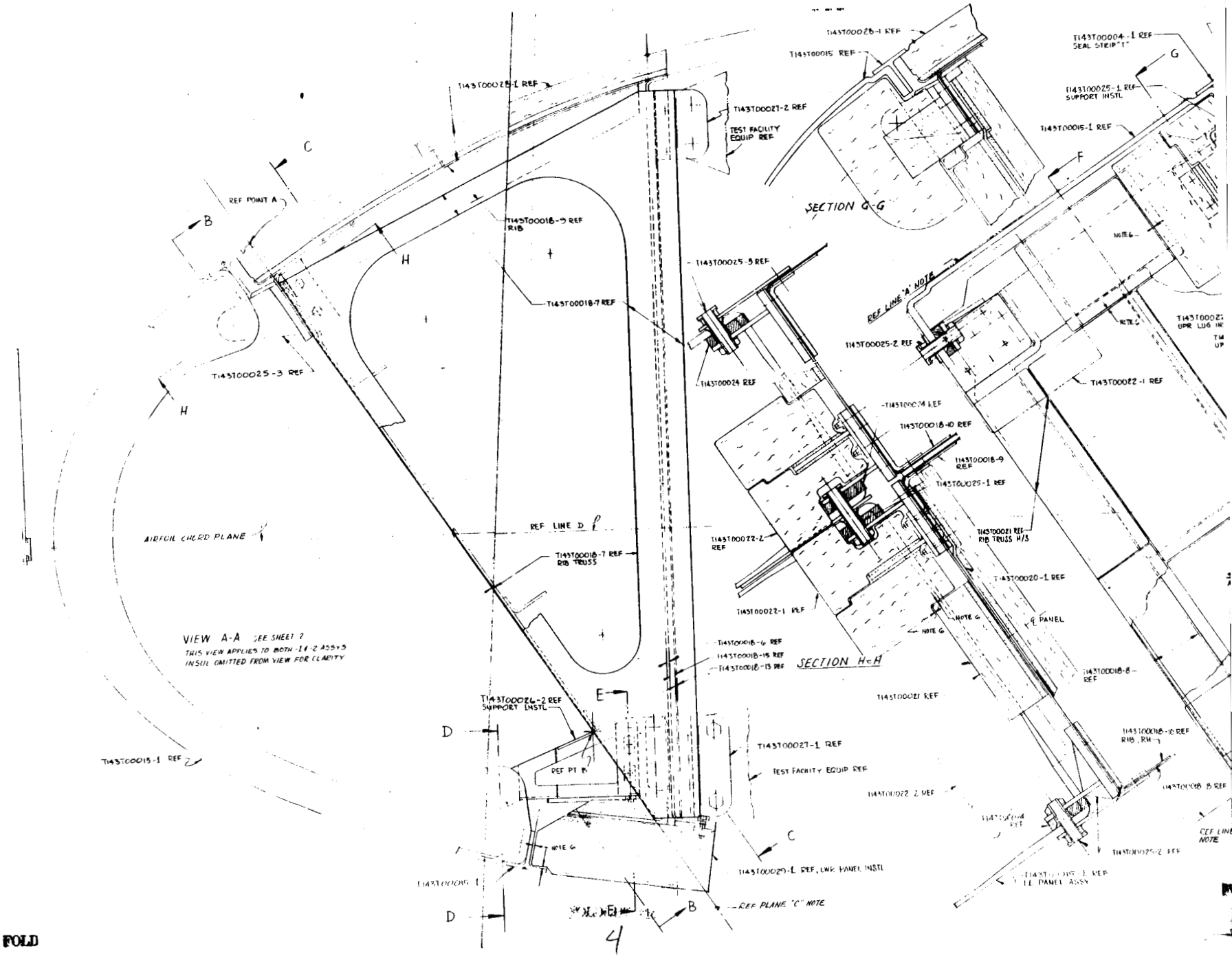

T143T00028-1 REF
T143T00027-2 REF
TEST FACILITY EQUIP REF
REF POINT A
T143T00018-9 REF RIB
T143T00018-7 REF
T143T00025-3 REF
AIRFOIL CHORD PLANE
REF LINE D
T143T00018-7 REF RIB TRUSS
VIEW A-A SEE SHEET 2
THIS VIEW APPLIES TO BOTH -1 & -2 ASSYS
INSUL OMITTED FROM VIEW FOR CLARITY
T143T00026-2 REF SUPPORT INSTL
REF PT B
T143T00015-1 REF
T143T00027-1 REF
TEST FACILITY EQUIP REF
T143T00029-1 REF, LWR PANEL INSTL
REF PLANE "C" NOTE
T143T00015 REF
T143T00004-1 REF SEAL STRIP "T"
T143T00025-1 REF SUPPORT INSTL
T143T00015-1 REF
SECTION G-G
T143T00025-3 REF
T143T00024 REF
REF LINE "A" NOTE
T143T00025-2 REF
T143T00022-1 REF
T143T00018-10 REF
T143T00018-9 REF
T143T00025-1 REF
T143T00021 REF RIB TRUSS H/S
T143T00022-2 REF
T143T00020-1 REF
T143T00022-1 REF
NOTE 6
℄ PANEL
SECTION H-H
T143T00018-6 REF
T143T00018-15 REF
T143T00018-13 REF
T143T00021 REF
T143T00018-8 REF
T143T00018-10 REF RIB, RH
T143T00022 2 REF
T143T00025-2 REF


FOLD

4

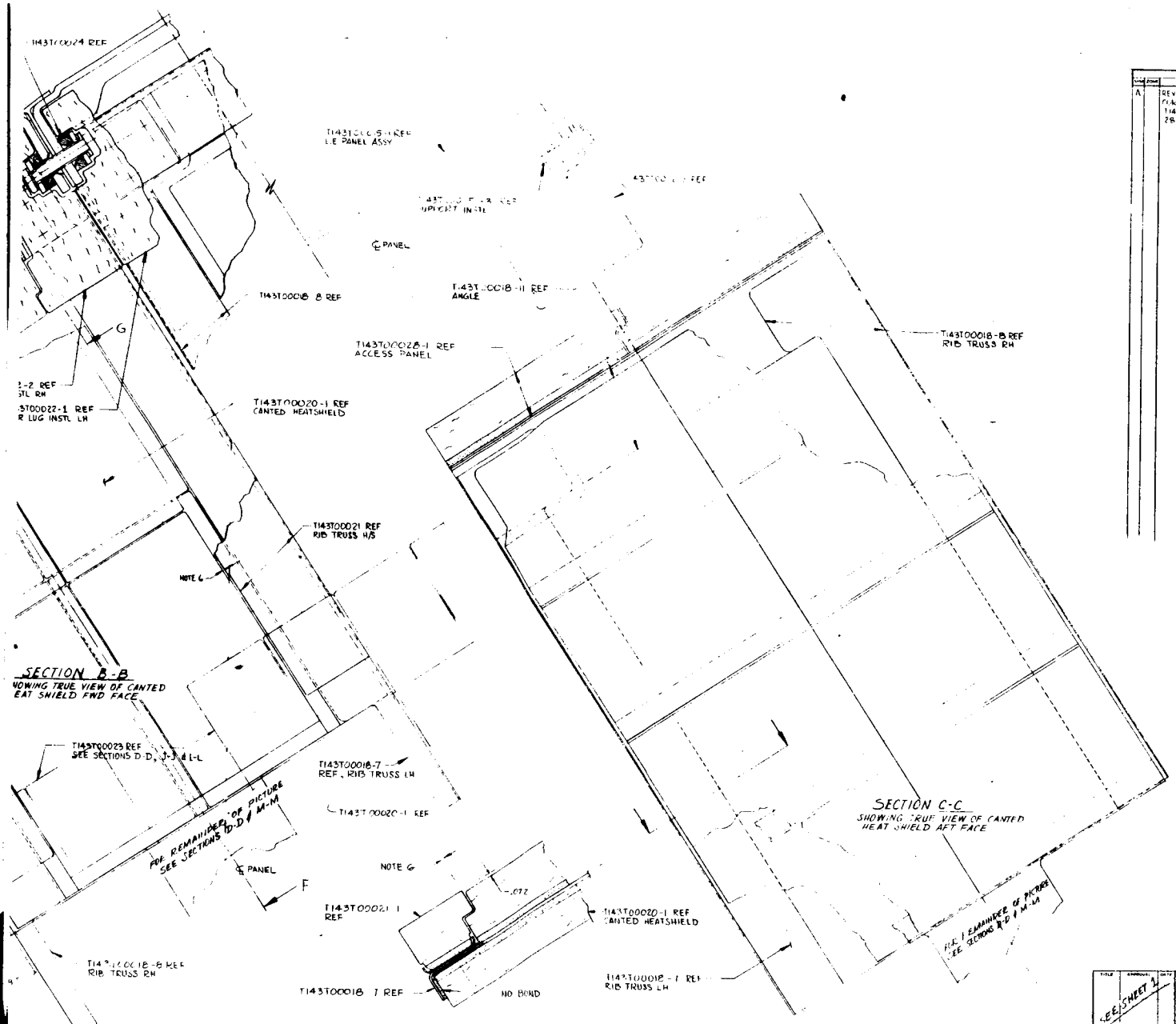
T143T00024 REF
T143T00018 8 REF
T143T00020-1 REF
CANTED HEATSHIELD
T143T00021 REF
RIB TRUSS H/S
NOTE 6
SECTION B-B
SHOWING TRUE VIEW OF CANTED
HEAT SHIELD FWD FACE
T143T00023 REF
SEE SECTIONS D-D, J-J & L-L
T143T00018-7
REF. RIB TRUSS LH
T143T00020-1 REF
FOR REMAINDER OF PICTURE
SEE SECTIONS D-D & M-M
℄ PANEL
F
G
NOTE 6
T143T00021 1
REF
.072
T143T00020-1 REF
CANTED HEATSHIELD
T143T00018 7 REF
NO BOND
T143T00018-7 REF
RIB TRUSS LH
T143T00018-8 REF
RIB TRUSS RH
T143T00018-8 REF
RIB TRUSS RH
SECTION C-C
SHOWING TRUE VIEW OF CANTED
HEAT SHIELD AFT FACE
FOR REMAINDER OF PICTURE
SEE SECTIONS D-D & M-M
T143T00018-11 REF
ANGLE
T143T00028-1 REF
ACCESS PANEL
℄ PANEL
REVISIONS
REVISED ALL VIEWS, TO INCORPORATE CHANGES TO: T143T00020, 21, 22, 23, 24, 28 & 29 HEAT SHIELD DESIGNS
LEE SHEET 2
TEST ARTICLE FINAL ASSY
"FAIL SAFE" SHUTTLE WING L.E.
RPP PHASE III - TASK I
T143T00017
A.3-8

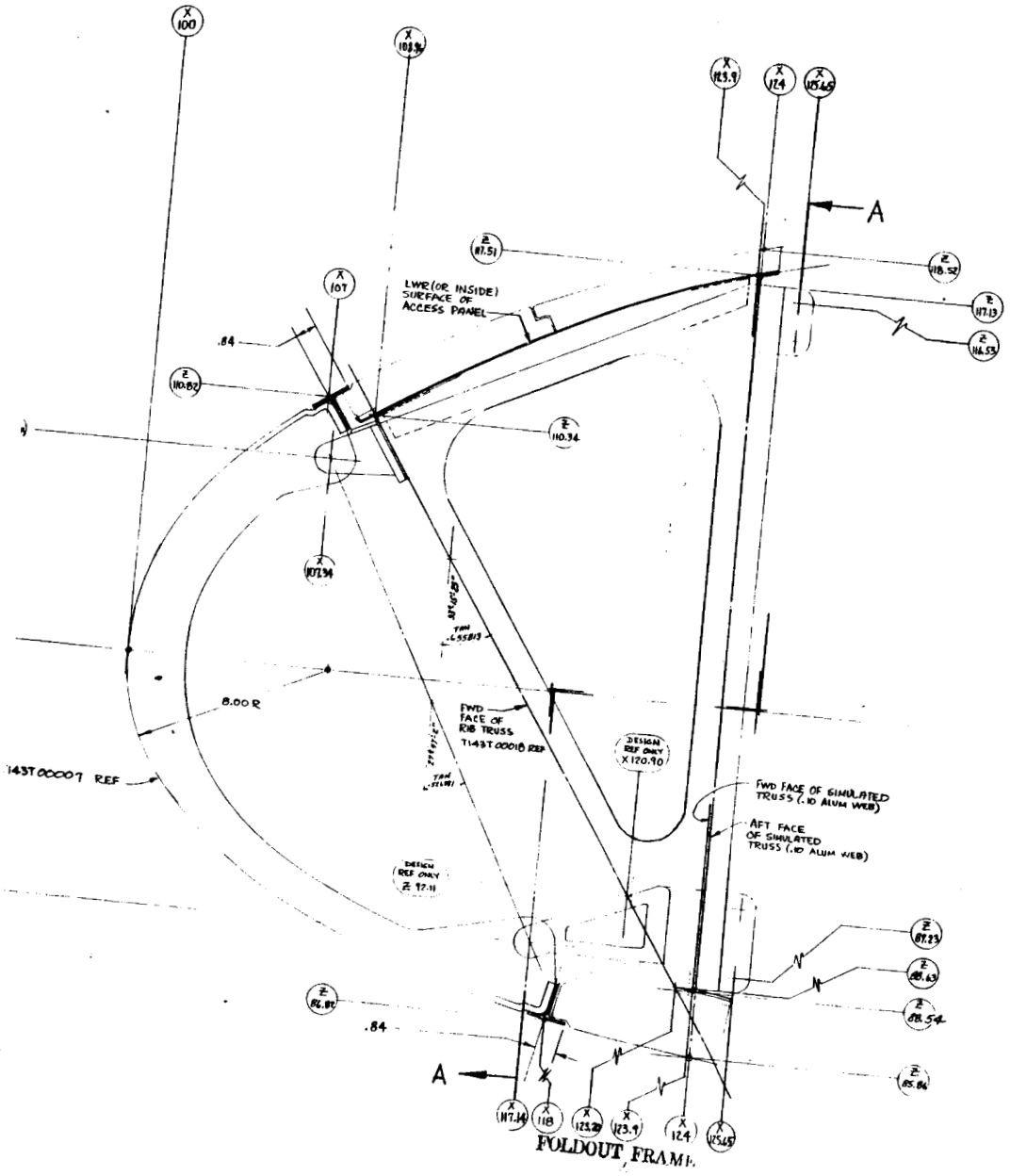


FOLDOUT FRAME

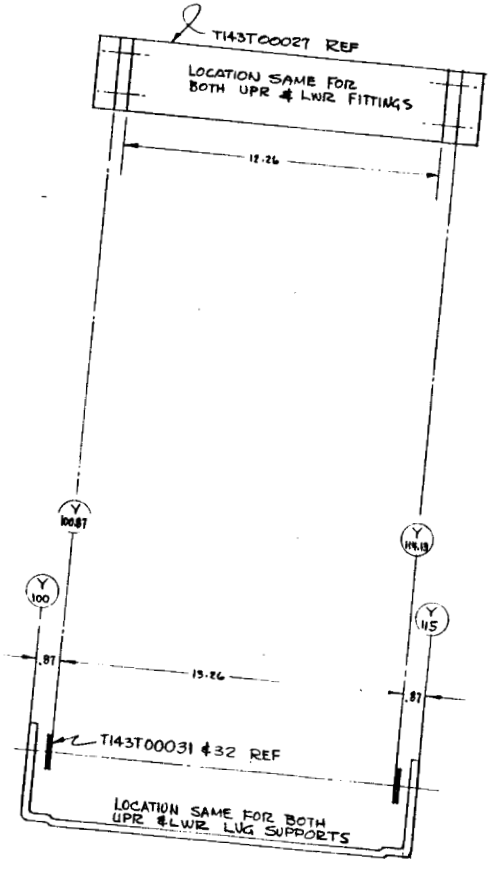


SECTION A-A

NOTE

1 THE COORDINATES DEFINED ON THIS DWG MAY BE USED FOR ENGINEERING DESIGN BASIC DATA AND FOR ESTAB FIRM POINTS IN TOOL DESIGN

2 CONTACT DESIGN REPRESENTATIVE IN EVENT OF CONFLICT BETWEEN DATA ON THIS DWG AND ENGINEERING INFORMATION PREVIOUSLY REL TO MFG ON DETAIL DWGS.

| TITLE | APPROVAL | DATE |
|---|---|---|
| P.E. | | |
| MFG | | |
| THERM | | |
| ORIN | | |
| MTL | | |
| STRUCT | | |
| LD DES | MATZA | |
| CHK BY | | |
| DRAWN BY | MATZA | |
| CUSTOMER | | |
| CONTRACT NO. | | |

VOUGHT MISSILES AND SPACE COMPANY
LTV AEROSPACE CORPORATION
P.O. BOX 6267 DALLAS, TEXAS 75265

L.E. ASSY COORDINATES
ENGINEERING & TOOL DESIGN DATA
RPP PHASE II - TASK I

SIZE 24 X 44 | IDENT NO. 11813 | T143E00003

SCALE NONE | REV LTR A | SHEET



FOLDOUT FRAME

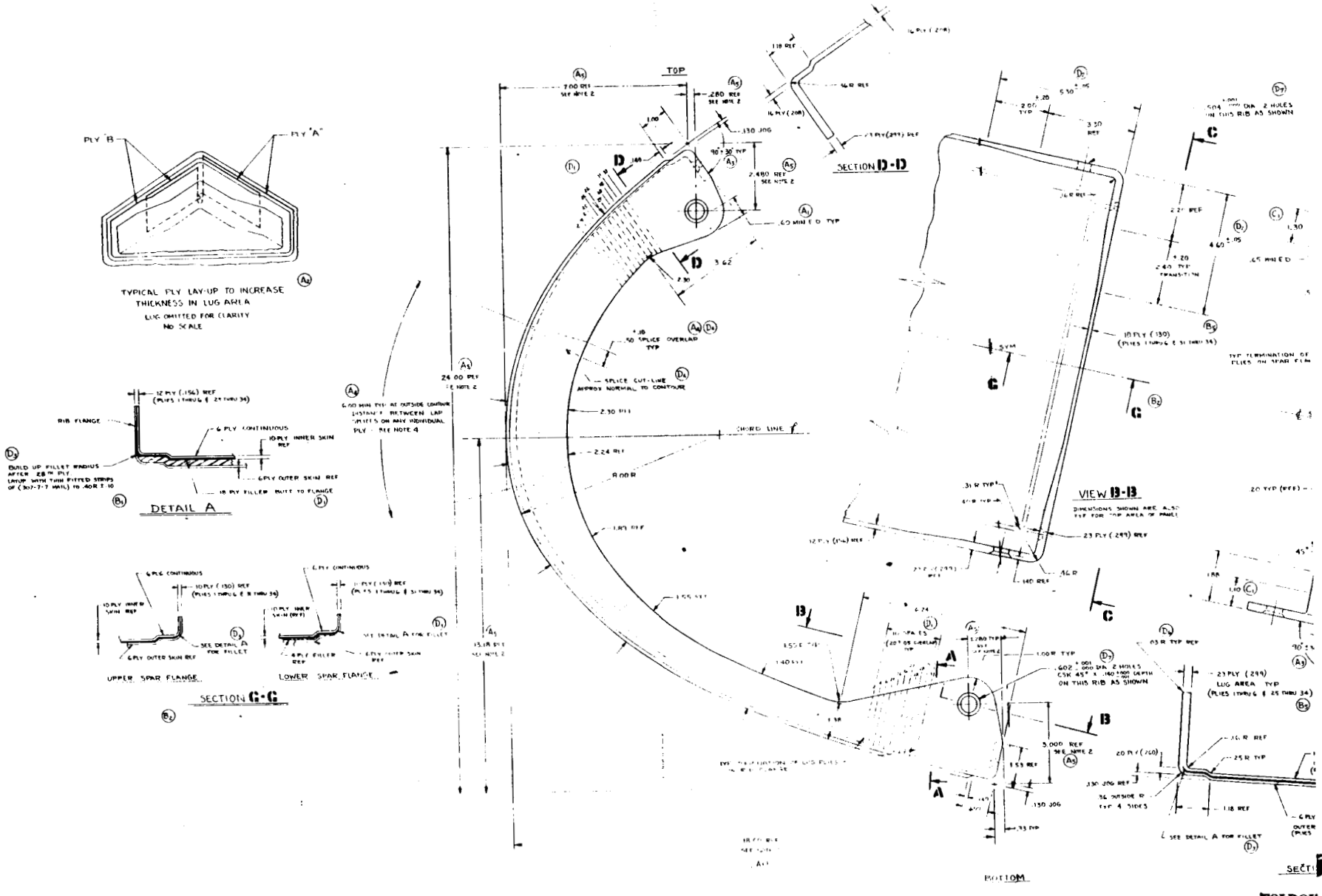


FOLDOUT FRAME

FOLDOUT FRAME

FOLDOU

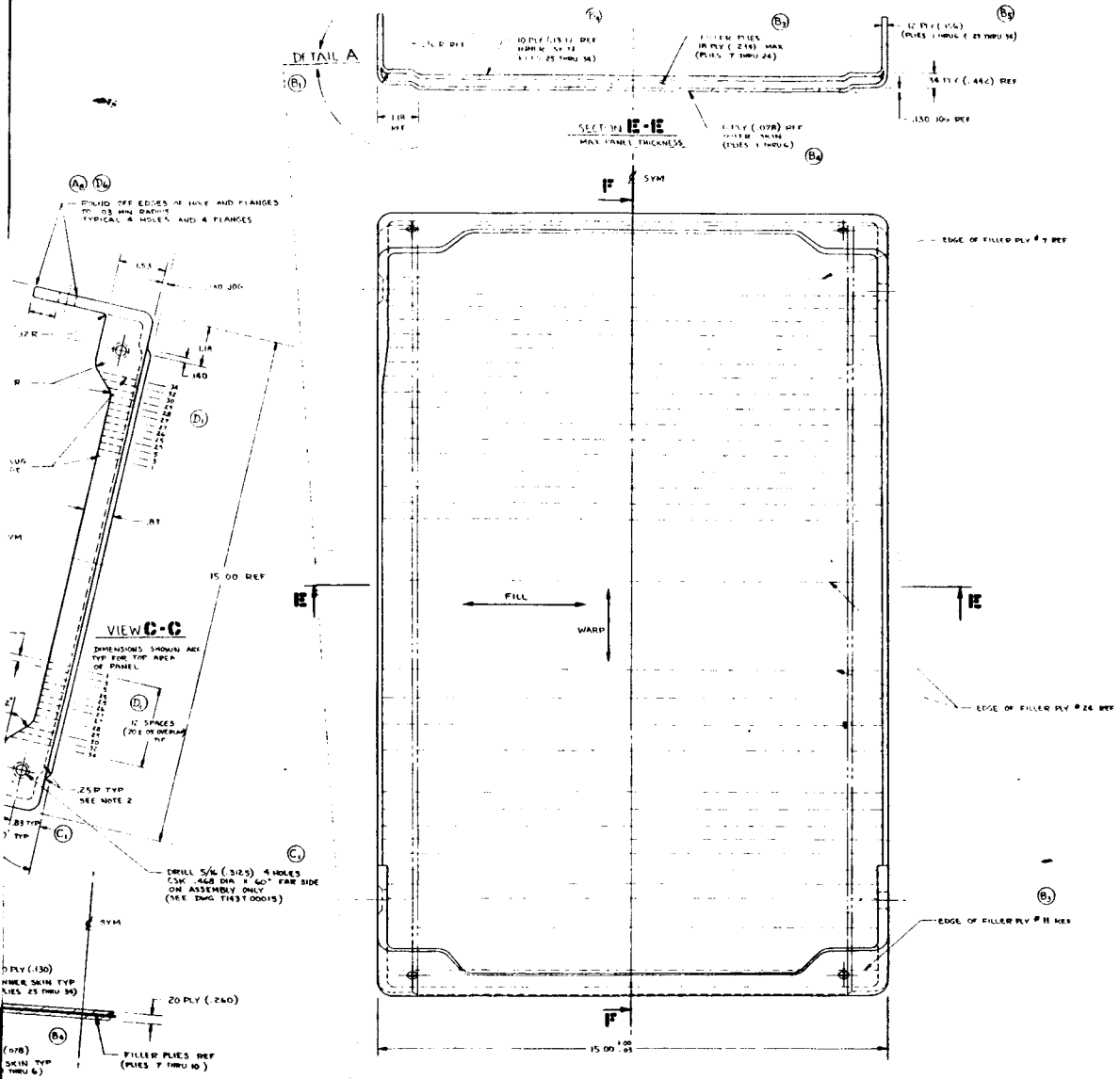


(-1) PANEL
LEADING EDGE FAIL-SAFE
LOOKING FWD - RH WING

| REVISIONS | | | |
|---|---|---|---|
| SYM | DESCRIPTION | DATE | APPROVED |
| A | 1. ADDED MIN ED CALLOUT<br>2. ADDED FINGER LAY-UP DETAIL<br>3. ADDED FLANGE ANGLE CALLOUT<br>4. ADDED NOTE 4 AND FIELD CALLOUT FOR LAP SPLICE ON RIB FLANGE<br>5. ADDED REF SEE NOTE 2 FOR PANEL AND HOLE DIMS - REMARKED NOTE 2<br>6. ADDED GEN NOTE 5<br>7. ADDED SHEET 2 RMD<br>8. ADDED HOLE RADIUS CALLOUT | | |
| B | 1. ADDED DETAIL A - RIB FLANGE LAYUP<br>2. ADDED SECTION G-G - UPPER & LWR STRR FLANGE LAYUP<br>3. REVISED FILLER PLY IDENT NUMBERS<br>4. ADDED SKIN PLY IDENT NUMBERS<br>5. ADDED PLY NUMBER CALLOUT FOR LUG & FLANGES. | | |
| C | 1. ADDED RIVET HOLE LOCATION<br>2. ADDED NOTES 6 THRU 9 | | |
| D | 1. ADDED PLY IDENT IN AREA OF LUGS FOR PLY TERMINATION & OVERLAP DIMS<br>2. REVISED DIMS & TOL FOR LENGTH OF TAPER OF PLIES IN AREA OF LUGS<br>3. ADDED CALLOUT FOR BUILD-UP OF FLANGE FILLET RADIUS.<br>4. ADDED TOL FOR SPLICE OVERLAP & DIRECTION OF CUT.<br>5. REVISED NOTE 4<br>6. REVISED CALLOUT TO ADD .03 W ON ALL FLANGE EDGES<br>7. REVISED HOLE CALLOUT SEE .75 DIA-4 HOLES<br>8. REVISED NOTE 7 TO ADD T143-EB-2002 | | |

## Notes

1. INITIAL RELEASE OF THIS DRAWING IS FOR EXTERNAL LINES CONFIGURATION USE ONLY.
2. THE FAIL-SAFE PANEL WILL BE FABRICATED USING PHASE II TOOLING (REF T143T00003) AND THE MASTER TEMPLATE.
3. DIMENSIONAL TOLERANCE EXCEPT AS NOTED:
   XX ± .03
   XXX ± .01
4. LAP SPLICES ON ADJACENT PLIES TO BE STAGGERED BY .50 ± .25, NO TWO SPLICES TO BE PERMITTED AT THE SAME POINT, EXCEPT THAT TWO OVERLAPS WILL BE PERMITTED ON THE RIB FLANGES ONLY, BUT NOT ON ADJACENT PLYS. NUMBER OF SPLICES OPTIONAL.
5. LOCATION OF TRIM FOR FILLER PLIES MAY VARY ± .25 FROM LOCATIONS SHOWN (SEE SHEET 2)
6. MATERIAL PER SPEC 307-7-7
7. CURE PARTS PER PROCESS SPEC 308-7-10A AND T143-EB-2002
8. RADIOGRAPHIC INSPECT PER S-40540/ZAVO-90, METHOD I.
9. ULTRASONIC INSPECT WITH THROUGH-TRANSMISSION, TECHNIQUE 1 OR 2 (S-40540/ZAVO-90)

NEXT ASSEMLY - T143T00015

| | | | |
|---|---|---|---|
| DR | | | LEADING EDGE PANEL SHUTTLE RPP FAIL-SAFE |
| MFG | | | |
| QUAL | | | |
| PROJ | | | |
| STRU | | | |
| SYS ENG | | | |
| CHIEF DESIGNER | | | |
| CHIEF ENGINEER | | | |
| CONTRACT NO NAS 9-14745 | | | SIZE D · CODE IDENT NO 11013 · T143T00007 · SCALE 1/4 · REV LTR D · SHEET 1 OF 2 |

A-3-10

FOLDOUT FRAME 4

FOLDOUT FRAME 3

are fabricated from Inconel 718, while the lower fittings are a combination of Inconel 718 and polyimide fiberglass.

A truss configured 6Al-4V titanium support structure bridges the gap between the RPP and the 6061-T6 aluminum web that simulates the wing front spar.

Upper and lower external panels simulate RSI panels and are composed of 6Al-4V titanium structure with 10 PCF Dynaquartz insulation bonded with RTV-560 through R-M RL1973 foam strain isolator.

Two steel lug fittings, one upper and one lower, bolt to the back of the aluminum spar, and provide a means of attaching the leading edge assembly to ground test support structure.

There are eight pieces of insulation per leading edge segment assembly. These consist of insulation to protect each Inconel support fitting, a removable canted heatshield, and "picture frame" insulation around the forward side of the canted heatshield. Each insulation assembly is comprised of Dynaquartz insulation, foam strain isolator, RTV-560 bond and a support structure of either titanium or polyimide fiberglass. The fiberglass is used for the canted heatshield, while titanium carrier panels are used for all other insulation assemblies. When two segments are brought together to form one assembly, additional insulation components are installed between adjacent upper and lower support fittings. In addition, Dynaflex flexible insulation is installed in cracks between adjacent assemblies. The support

fitting insulation employs 15 PCF Dynaquartz while all other components use 10 PCF Dynaquartz.

## 4.0 APPROACH

The ground test program is designed to impose the most critical design conditions (or those for which there is no prior data or exposure) to verify structural/thermal integrity of the leading edge assemblies. On this basis the following conditions will be simulated, although not necessarily in the order listed:

(1) Boost flight pressure loads - These design conditions generally produce the highest static stresses on the RPP and support structure.

(2) Boost acoustic noise at maximum dynamic pressure (max q) - This produces maximum dynamic loads on the leading edge, support structure, and insulation heatshield assemblies. (See discussion below on vibration environment).

(3) Orbital vacuum/low temperature - While element testing and comparative analysis do not indicate critical design conditions for either vacuum or low temperature, component testing has not been previously performed at these conditions and, therefore, has been included in this plan.

(4) Entry temperature - Thermoelastic analysis of the RPP shows that thermal stresses are lower than pressure load stresses except in one local region of the skin, where the margin is high (134%). However, it is necessary to prove by test, structural integrity under conditions producing maximum temperatures and maximum temperature gradients. The entry

profile is also the critical condition for sizing the various insulation assemblies and support fittings for thermal protection of metallic or fiberglass structure.

Those conditions that will not be simulated and the justification for their deletion are as follows:

(1) Boost acoustic noise at lift off - The noise level and spectrum are less severe than the noise level at max q.

(2) Boost vibration level - While the leading edge assembly was designed for a 32 g-rms limit dynamic load, the extreme and unbelievable magnitude of this load level, the uncertainties of the appropriateness of this environment level, and the fact that the vibration environment is produced predominantly by the acoustic environment (which is being simulated) led to the elimination of a separate vibration test. Acoustic noise application will therefore suffice for dynamic testing in this program phase.

(3) Boost heating - Both maximum temperature and total heat load during boost are considerably below entry values and are therefore not critical.

(4) Combined load/thermal stress during entry - Analysis of design conditions show that maximum pressure loads occur during boost at max q when there are insignificant thermal stresses. Likewise, maximum thermal stresses are experienced during the early stages of entry at high altitude when pressure loads are insignificant. Examination of intermediate entry

conditions indicates no rational combination of load and thermal stresses exist that could be as severe as the peak values of each of these individually. As a result, no combined loading test conditions are proposed.

(5) Cruise flight to landing - Analysis of maneuver flight loads reveals pressures and stresses less severe than those during boost. The proposed test program will require application of the more severe boost loading so that cruise maneuver loading is not critical.

(6) Entry plasma arc heating - While this type of testing may be the best representation of environmental conditions at maximum heating, there are a number of drawbacks for this type of testing for this phase of the program. Among these are: (a) unavailability of a fully characterized facility to handle components of the size involved, (b) inability of a plasma arc facility to follow the desired time-temperature profile and (c) cost of performing such a test on this technology program. For these reasons radiant heating to verify structural/thermal integrity is planned.

(7) Miscellaneous loads - Specific tests for handling, transportation or erection are considered insignificant for this phase of testing. Meteoroid impact, salt spray, humidity, rain erosion, ultraviolet radiation, and similar tests are best performed as element tests and are not planned for the Phase III assemblies.

Rain ingestion with subsequent freezing had been considered as a possible test for these assemblies. However, the insulation, which may be

most affected by this test, is only an interim selection and the results would not be conclusive. (However, free standing 10 PCF Dynaquartz has been exposed to water-freeze-thaw cycles in element test without apparent degradation.)

The order in which the tests are to be conducted is based on the following primary considerations:

(1) A structural loading, being most critical to structural components, should follow thermal exposure to ensure that any thermal degradation can influence structural test performance.

(2) Considering the low strength of the interim insulation, thermal tests should be conducted prior to acoustic loading to ensure that the insulation is intact for thermal testing without having to repair.

(3) Orbital environments are not expected to be critical and can be performed at any convenient time.

(4) Thermocouples will be destroyed during load testing and strain gages will be destroyed during thermal testing.

With these considerations in mind, the following test sequence will be employed:

(1) Entry temperature.

(2) Boost static pressure loads.

(3) Orbital vacuum/temperature.

(4) Boost acoustic.

(5) Ultimate load test.

Each of these tests are defined in the following section.

# 5.0 TESTS

## 5.1 ENTRY TEMPERATURE TESTS

### 5.1.1 Objectives

Simulated entry heating evaluations of the test article shall have the following objectives:

- Confirm predicted temperature distribution within the leading edge system.
- Confirm resistance of the RPP structure to induced thermal stresses.
- Evaluate effects or changes, if any, of multiple heating cycles.
- Assess adequacy of heatshield and support lug attachment designs to limit primary structure to 350°F maximum.
- Evaluate accuracy of thermal modeling techniques and identify areas for improvement.

### 5.1.2 Thermal Simulation Requirements

The test article shall be configured per T143T00017-2 and exposed to five (5) simulated entry heating cycles. Both the temperature distribution and the temperature-time profile for the external surfaces of the test article shall be simulated. The required heating may be supplied by a source such as radiant lamps or graphite heaters not in contact with the test article.

Temperature shall be controlled at eleven (11) points on the external surface of the test article. The required temperature-time profiles for these points are defined in Figures 5.1-1 and 5.1-2 and the locations of these control points are defined in Figures 5.1-4 through 5.1-7. The temperature distribution around the periphery of the test article is defined in Figure 5.1-3 for a spanwise location 12 inches from the end of the test article as shown in Figure 5.1-4. Heat in put to the test article in a spanwise direction shall be uniform within $\pm 7\%$. Tolerance on the control temperatures is $\pm 50^{\circ}F$.

5.1.3 Atmospheric Pressure Simulation Requirements

The required pressure around the test article is 10 torr ($\pm 20\%$) air or nitrogen for the first 2800 seconds of each heating cycle. The pressure shall then be brought up to atmospheric pressure in 1200 seconds or less and held there for the remainder of the cycle.

5.1.4 Thermal Isolation

Each end of the test article shall be insulated with 3.5 inches of 6.2 $lb/ft^3$ density graphite felt insulation to prevent either input heating to these ends or radiation from them.

5.1.5 Thermal Instrumentation

The test article shall be instrumented with 88 thermocouples as shown in Figures 5.1-4 through 5.1-7. Temperature requirements for these thermocouples are defined in Table 5.1-1. Thermocouples 1-10 and 80 are control point thermocouples to actively control the temperatures at these

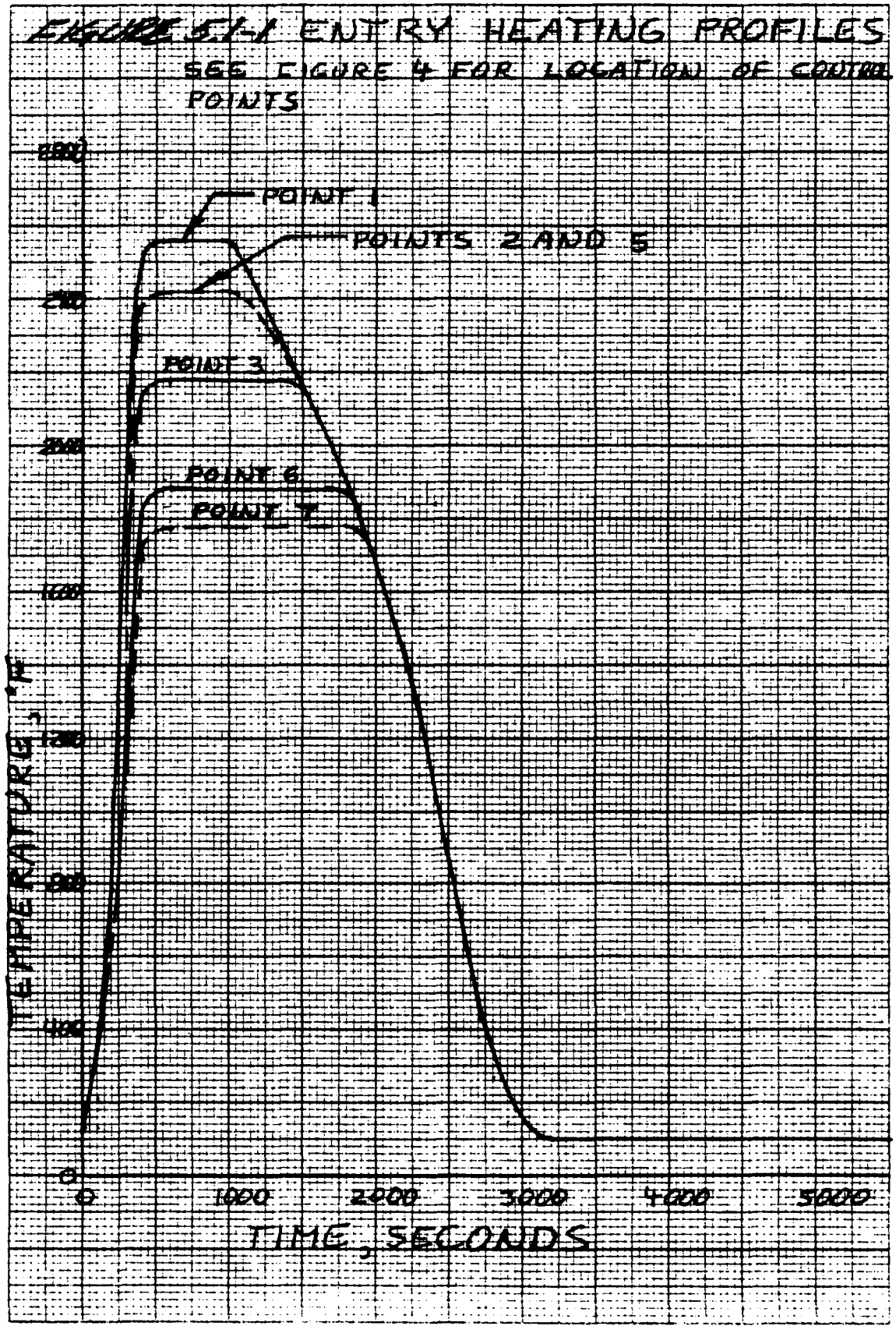
FIGURE 5.1-1 ENTRY HEATING PROFILES
SEE FIGURE 4 FOR LOCATION OF CONTROL POINTS
POINT 1
POINTS 2 AND 5
POINT 3
POINT 6
POINT 7
TEMPERATURE, °F
TIME, SECONDS
0
1000
2000
3000
4000
5000

FIGURE 5.4.2 ENTRY HEATING PROFILES

SEE FIGURES 5, 6 AND 7 FOR LOCATION OF CONTROL POINTS

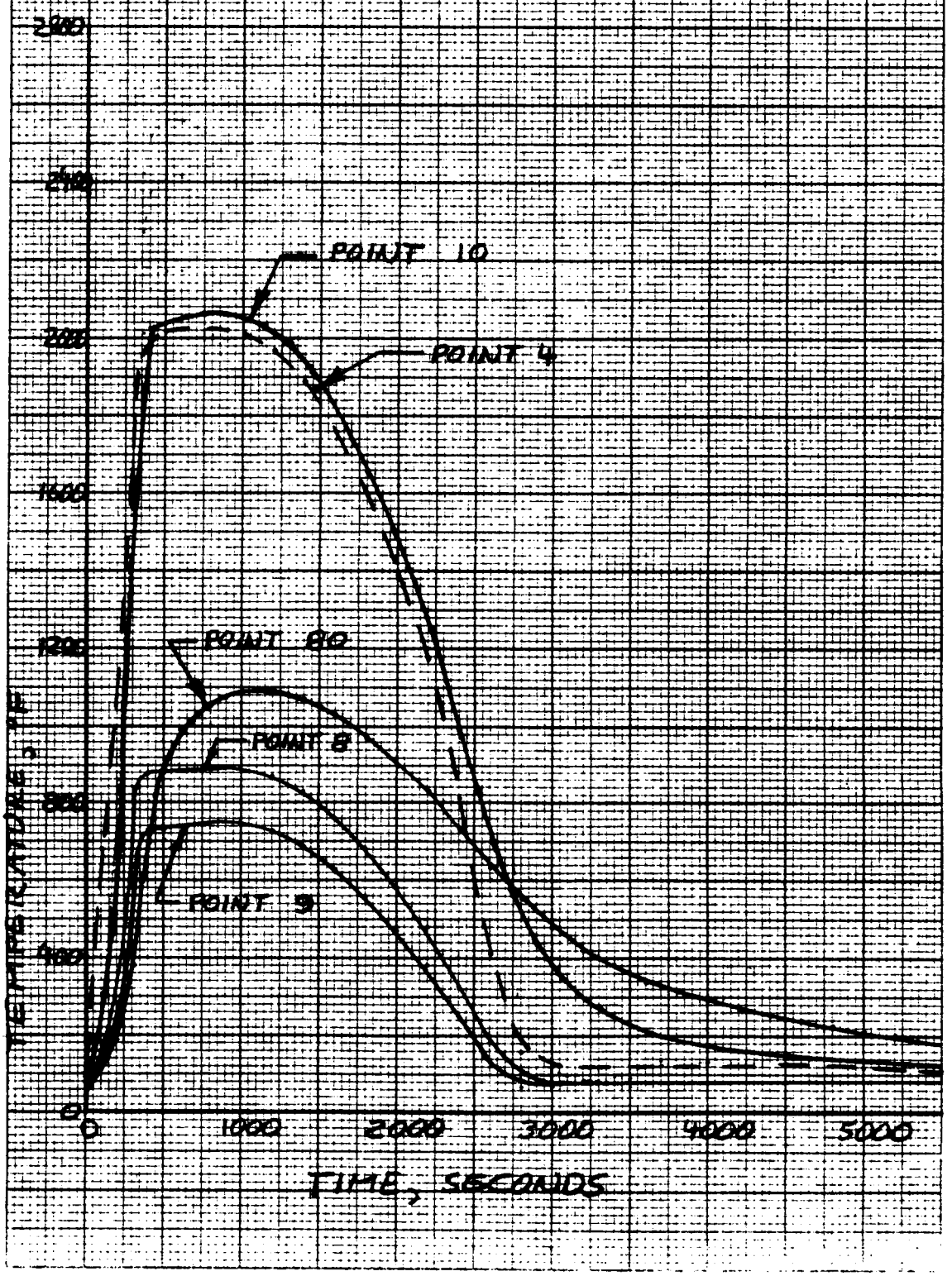

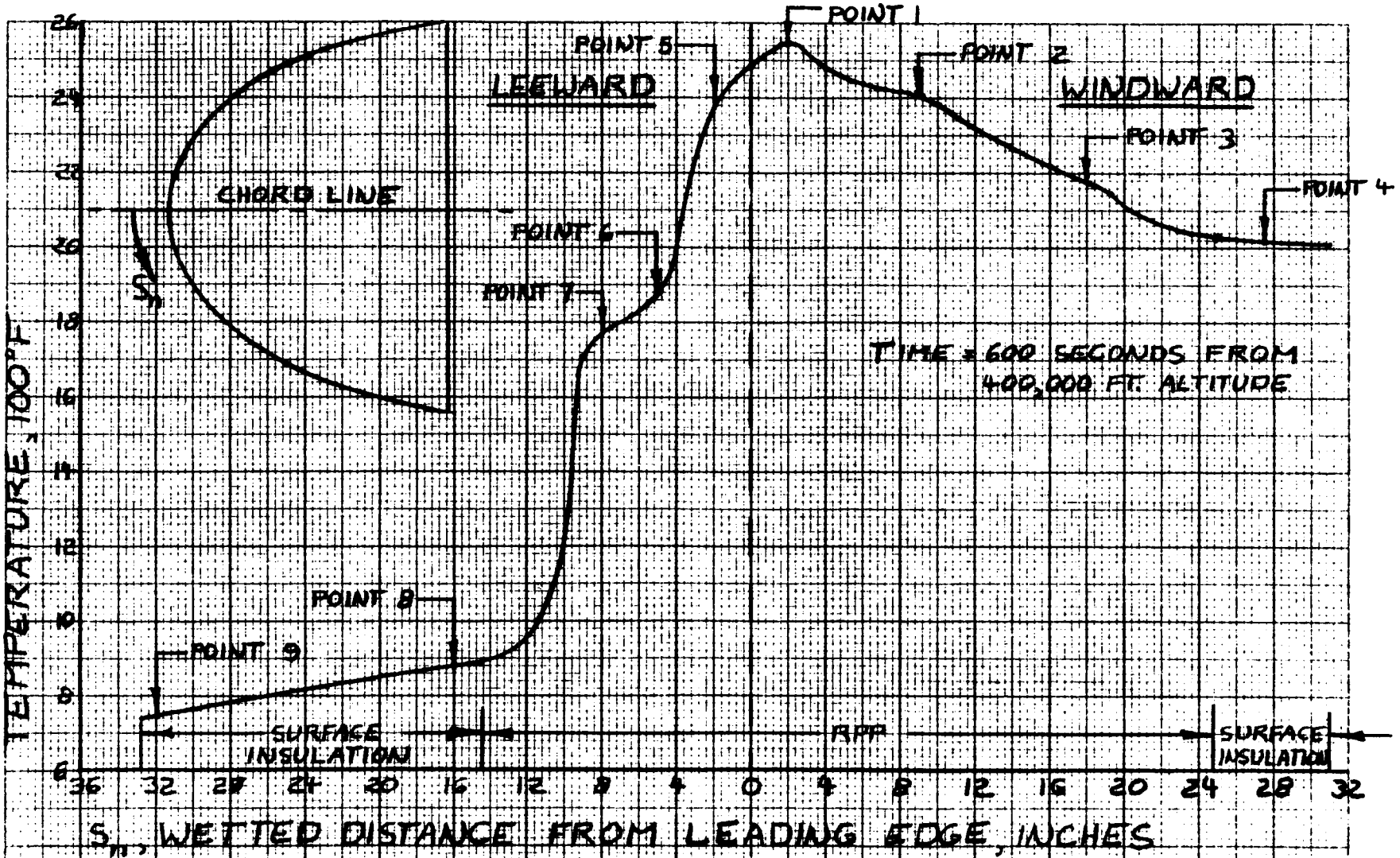


FIGURE 5.1-3 TEMPERATURE DISTRIBUTION AROUND LEADING EDGE

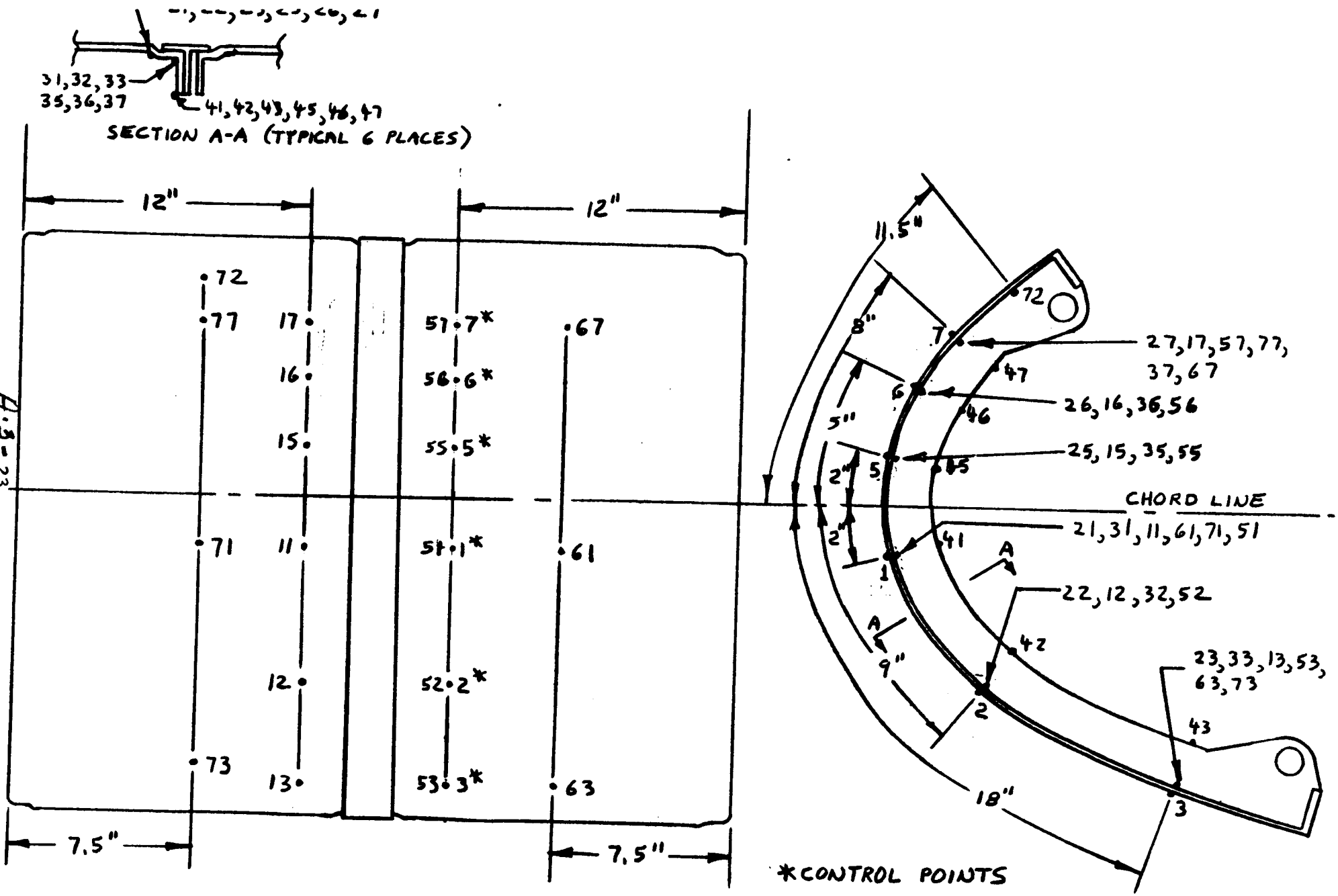


FIGURE 5.1-4, THERMOCOUPLE LOCATIONS, RPP SKIN AND RIBS

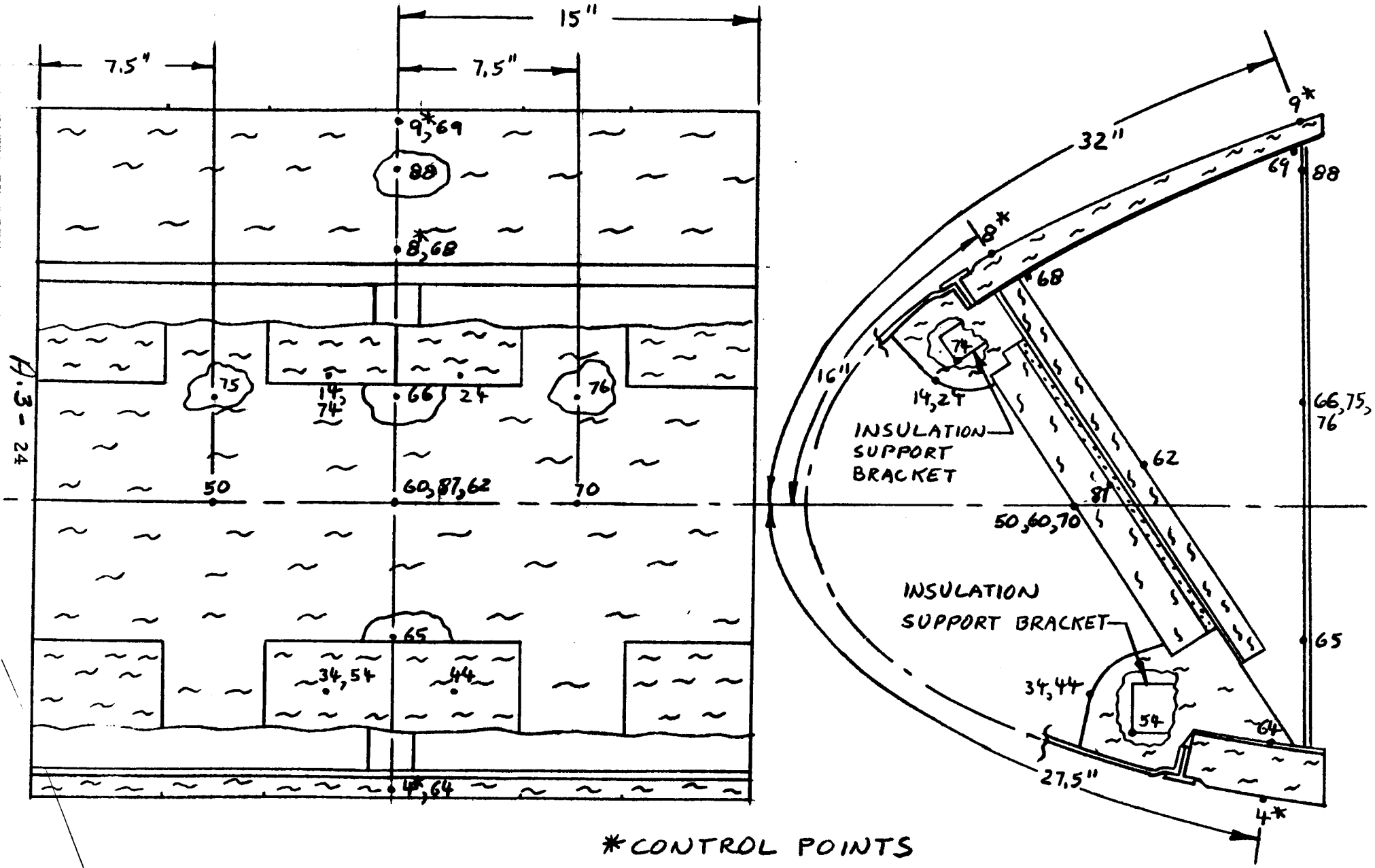


*CONTROL POINTS

FIGURE 5.1-5, THERMOCOUPLE LOCATIONS, INSULATION AND STRUCTURE

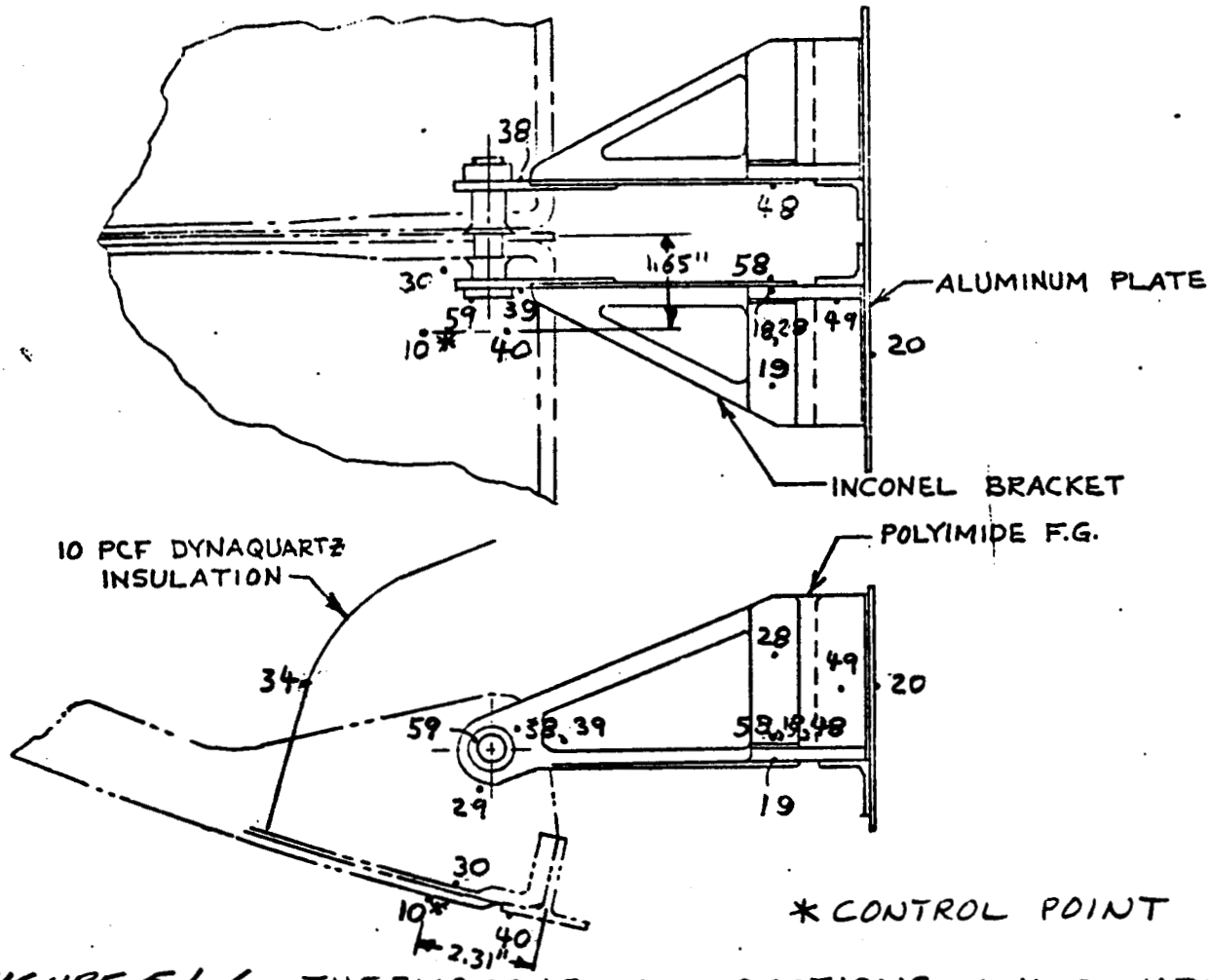


FIGURE 5.1-6, THERMOCOUPLE LOCATIONS, WINDWARD SUPPORT LUG

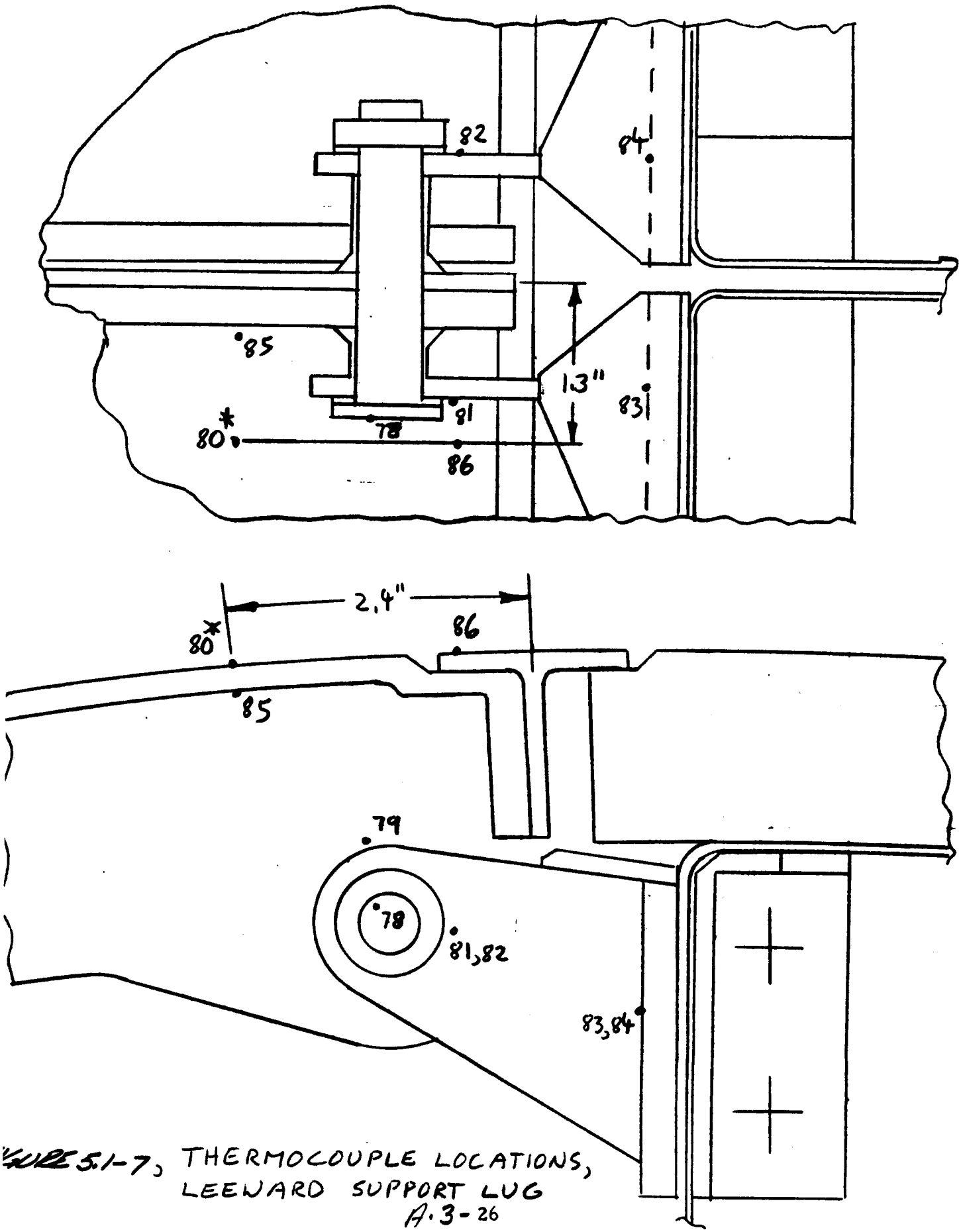


FIGURE 5.1-7, THERMOCOUPLE LOCATIONS, LEEWARD SUPPORT LUG

TABLE 5.1-1

THERMOCOUPLE MAXIMUM TEMPERATURE REQUIREMENTS

| THERMOCOUPLE NUMBER | MAXIMUM TEMPERATURE REQUIREMENT °F |
|---|---|
| 1, 11, 21, 31, 41, 51, 61, 71 | 2650 |
| 2, 12, 22, 32, 42, 52, 5, 15, 25, 35, 45, 55 | 2500 |
| 50, 60, 70, 34, 44, 14, 24 | 2400 |
| 3, 13, 23, 33, 43, 53, 67, 73 | 2300 |
| 4, 10, 30, 40 | 2200 |
| 6, 16, 26, 36, 46, 56 | 2000 |
| 7, 17, 27, 37, 47, 57, 67, 77 | 1900 |
| 72, 29 | 1800 |
| 38, 39, 59 | 1600 |
| 80, 85, 86, 79, 78, 81, 82 | 1200 |
| 8, 9 | 1000 |
| 18, 19, 28, 48, 58, 83, 84, 87, 54, 74, 64 | 800 |
| 20, 49, 62, 65, 66,68, 69, 75, 76, 88 | 500 |

Suggested Thermocouples:

(1) For coated surface up to 1750°F and for metallic parts less than 2100°F - P/N K-702-INC4-U-T3-18, Conax Corporation, 18 inch Chromel vs Alumel (Hoskins trade name) ISA Type K Thermocouple (wire size 36 gage) encased in .040 Inconel 718 sheath with magnesium oxide insulation and an ungrounded thermocouple junction.

TABLE 5.1-1 (Cont'd.)

(2) For coated surface in inert or chemically reducing atmosphere - 30 gage tungsten 5 percent Rhenium vs Tungsten 26 percent Rhenium thermocouple (W5RE/W26RE) with magnesium oxide insulators or aluminum oxide insulators. Thermocouple junction coated with thin coating of Astro-Ceram and overcoated with C34 graphite paste to provide electrical isolation. Attached to surface with Astroceram and covered with C34 graphite paste.

points to the temperature-time curves in Figures 5.1-1 and 5.1-2. There shall be back-up thermocouples at each of these eleven (11) control points. Provision shall be made for shifting control from a primary to a backup thermocouple in the event of failure of the primary thermocouple. All thermocouples shall be installed to permit replacement without disassembling the test article. Temperatures shall be recorded for all thermocouples from the start of heating until the last of the temperatures has peaked.

5.1.6 Test Procedure

Thermal Calibration - Calibration runs shall be performed to verify required temperature-time profiles in Figures 5.1-1 and 5.1-2. The two Phase II leading edges supplied to NASA-MSC shall be used for these runs. These articles, defined in VMSC drawing T143-T-00005, shall be bolted together for the calibration runs. The ends shall be insulated in the same manner as described previously for the test article. The support fixture (from the Phase II leading edge thermal test) for the calibration article can be supplied by VSC at the request of NASA-MSC. This fixture shall be insulated as defined in Figure 5.1-8. The calibration article shall be instrumented with eleven primary and eleven back-up thermocouples located identically to the eleven control thermocouples in Figures 5.1-4 through 5.1-7. Procedure for the calibration runs shall be identical to that defined below for the test runs. At least 5500 seconds of the heating cycle shall be included in these runs to establish that test article heat-up and cool-down rates can both be met.

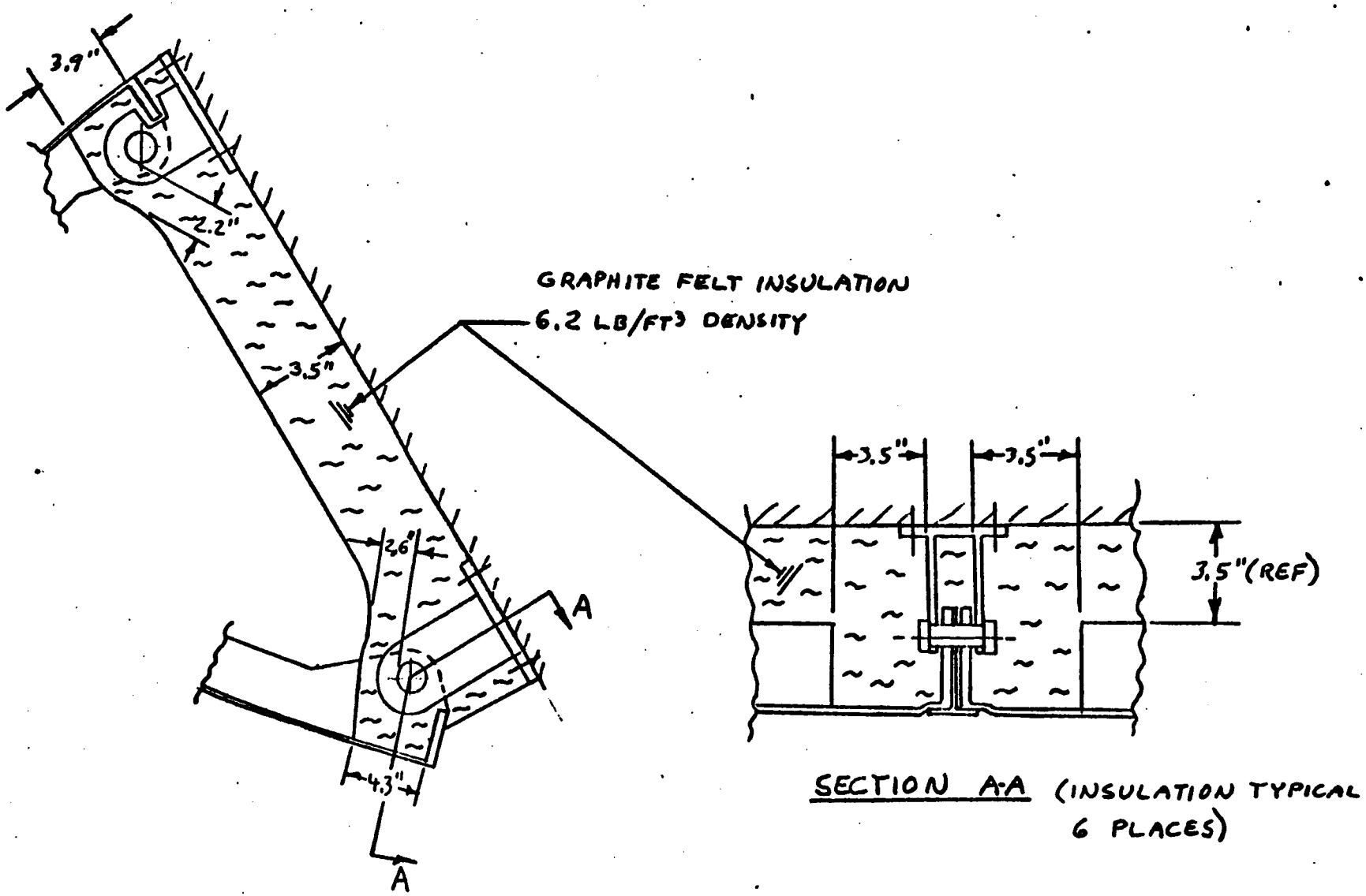


FIGURE 5.1-8
INSULATION INSTALLATION
CALIBRATION ARTICLE

Thermal Test - The pressure around the test article shall be reduced to 10 torr and maintained at this level for two hours to stabilize the pressure throughout the article. Heating and data recording shall then be initiated, and the required temperature-time profiles followed. The initial temperature of the test article shall be room temperature. At 2800 seconds the pressure shall be raised within 1200 seconds to atmospheric. When all temperatures have peaked, the test cycle shall be considered at an end, and data recording may be terminated. However, all temperatures shall be monitored periodically after the end of the test to determine when the test article has cooled sufficiently for inspection. The article shall not be actively cooled at any time.

After the test article has cooled to room temperature, the insulation on the ends of the article shall be removed and the article inspected for failures. If there are no failures the next heating cycle shall be initiated. The heating tests will be completed after five (5) heating cycles.

Test Instrumentation Failures - If during a heating cycle a control thermocouple fails, control shall be shifted to the backup thermocouple. If this thermocouple also fails, heating shall be terminated, the article allowed to cool to room temperature and all failed thermocouples (control or other) replaced prior to retest.

The following shall also be considered cause for aborting a heating cycle:

- Heating profiles cannot be followed.
- Ten (10) or more thermocouples (other than control) fail.

5.1.7 Data Reduction

All thermocouple output data shall be plotted ($^{o}F$) as a function of time (minutes). Each cycle of test for a given thermocouple shall be plotted on a common graph for ease of evaluation of repeatability.

5.1.8 Post Test Operations

Following completion of the five thermal cycles and inspection of the test article, the thermocouples shall be removed in preparation for the boost pressure test. See Section 6.0 for inspection instructions.

5.2 BOOST PRESSURE LOADS TESTS

5.2.1 Objectives

Boost pressure loads tests to be conducted on a leading edge assembly have the following objectives:

- Demonstrate the structural integrity of the leading edge system assembly and in particular the RPP leading edge itself under the application of the maximum design loads.
- Evaluate the accuracy of structural modeling techniques in predicting stresses and deflections.
- Uncover any problem areas that might exist so that corrective action can be taken for production design, analysis, and/or fabrication.

5.2.2 Simulation Requirements

One leading edge and support structure assembly shall be tested as a unit. All insulation shall be removed except the outside surface of the

upper access panel as it is a permanent installation. The installation and preparation of this assembly shall be in accordance with drawing T143T00017-1.

Boost phase pressures are the critical static design conditions for the leading edge assembly. The four limit load cases, Ref. (A), are shown in Figures 5.2-1 through 5.2-4. The four limit load cases are presented in tabular form in Tables 5.2-1 through 5.2-4. The loads are specified in 20% increments which represent discrete loading points (reference test procedure in Section 5.2.4). Load Case II produces the minimum margin of safety during boost and is specified as the ultimate load test condition, reference Table 5.2-5.

The suggested method of loading utilizes rubber air bags held in place by wooden blocks shaped to the contour of the test article as shown in Figure 5.2-5. Restraint of the internal blocks is not shown; however, they may be held by rigid external test structure or by being tied to the external wooden block through end plates. This method had been successfully used in the Phase II program. Clearance between the blocks and test article should be approximately 0.125 inch. The air bags are self-contained and bonded to the edges of the blocks and have individual fill valves running through the blocks. Phase II air bags were made from 0.10 inch thick silicone rubber per AMS 3302. The various inner and outer pressure cavities are identified in Figure 5.2-5. This test setup permits easy combination of pressures for the different load cases. The geometry of the pressure areas is defined in Figure 5.2-6.

# LIMIT LOAD CASE I

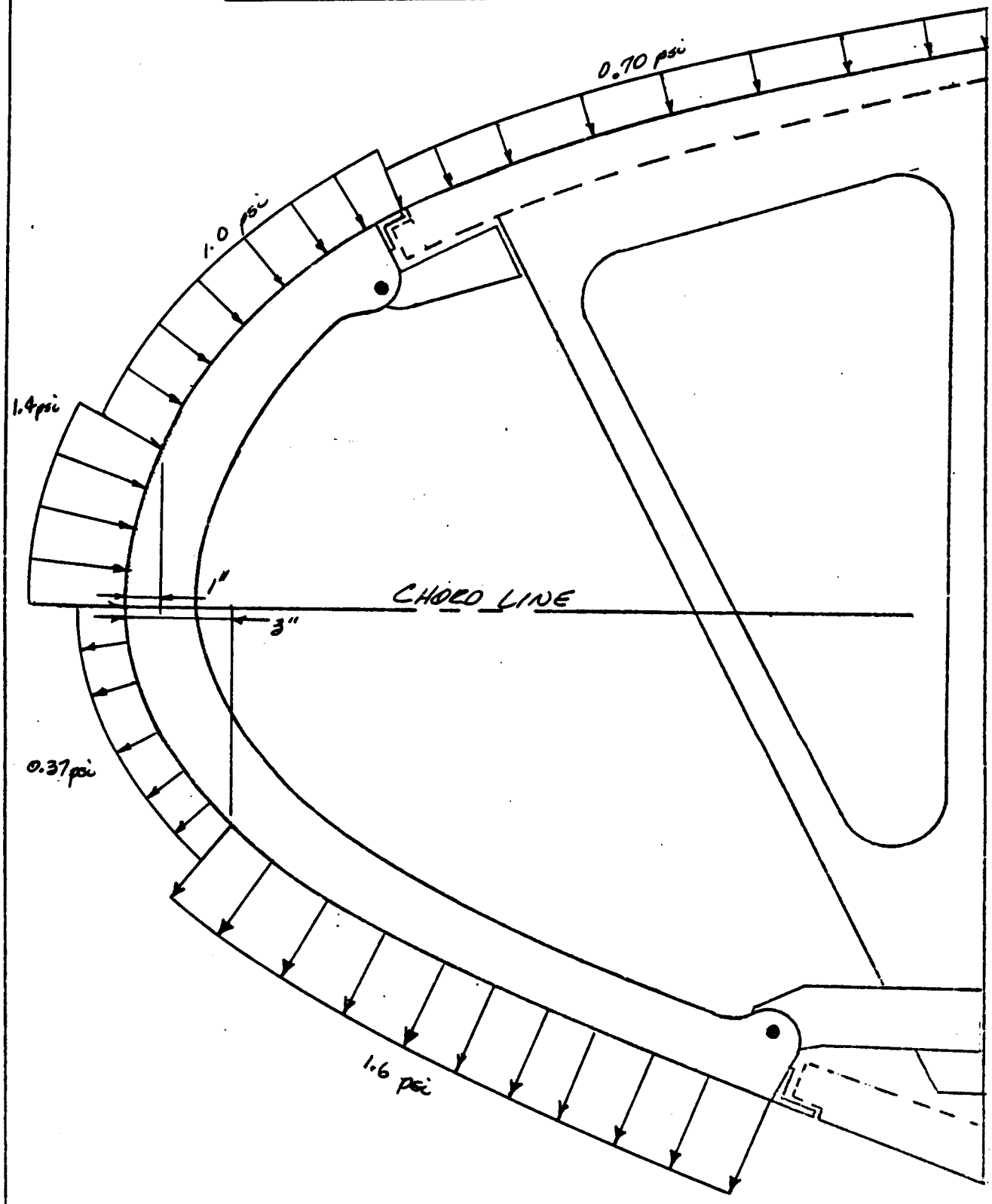


FIGURE 5.2-1

# LIMIT LOAD CASE II

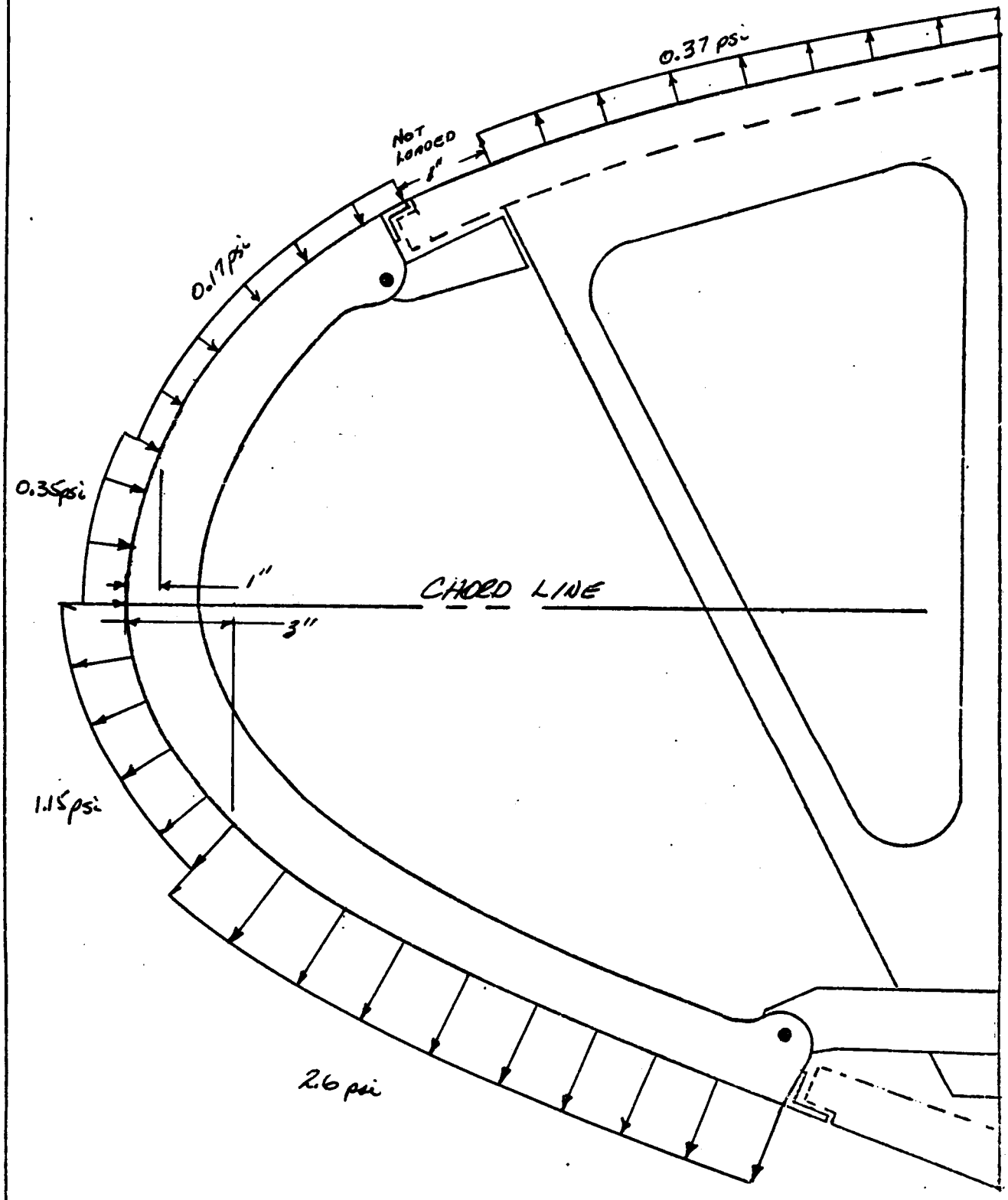


FIGURE 5.2-2

# LIMIT LOAD CASE III

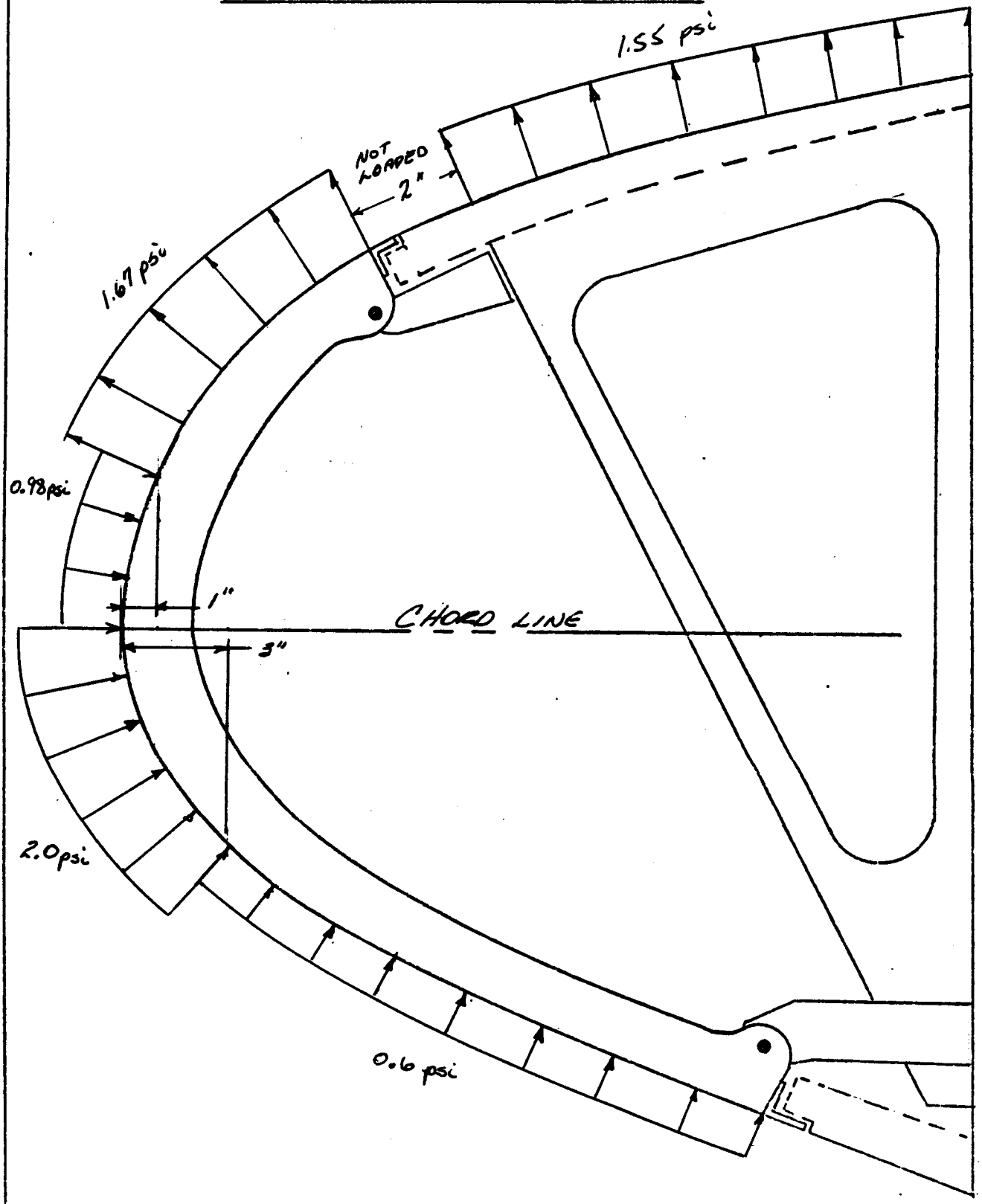


FIGURE 5.2-3

# LIMIT LOAD CASE IV

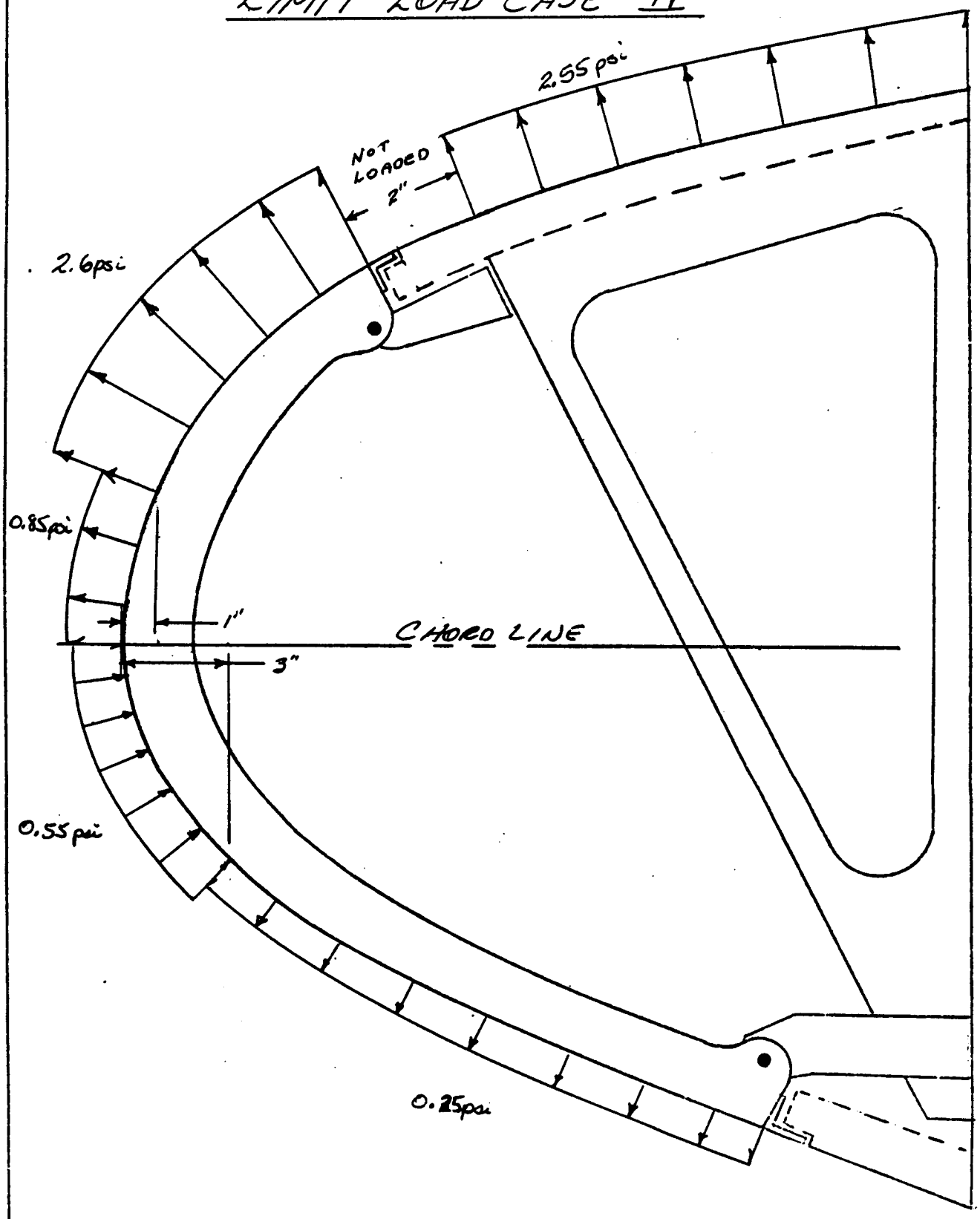


FIGURE 5.2-4

# TABLE 5.2-1

## LOAD CASE 1

| % LOAD | PO-1 | PI-1 | PO-2 | PI-2 | PO-3 | PI-3 | PO-4 | PI-4 | PO-5 | PI-5 |
|---|---|---|---|---|---|---|---|---|---|---|
| 0 | - | 0 | - | 0 | 0 | - | 0 | - | 0 | - |
| 20 | - | 0.32 | - | .074 | 0.28 | - | 0.20 | - | 0.14 | - |
| 40 | - | 0.64 | - | 0.148 | 0.56 | - | 0.40 | - | 0.28 | - |
| 60 | - | 0.96 | - | 0.222 | 0.84 | - | 0.60 | - | 0.42 | - |
| 80 | - | 1.28 | - | 0.296 | 1.12 | - | 0.80 | - | 0.56 | - |
| 100 | - | 1.60 | - | 0.37 | 1.4 | - | 1.0 | - | 0.70 | - |
| 20 | - | 0.32 | - | 0.074 | 0.28 | - | 0.20 | - | 0.14 | - |

TABLE 5.2-2

## LOAD CASE II

| % LOAD | PO-1 | PI-1 | PO-2 | PI-2 | PO-3 | PI-3 | PO-4 | PI-4 | PO-5 | PI-5 |
|---|---|---|---|---|---|---|---|---|---|---|
| 0 | - | 0 | - | 0 | 0 | - | 0 | - | - | 0 |
| 20 | - | 0.52 | - | 0.23 | 0.07 | - | 0.034 | - | - | 0.074 |
| 40 | - | 1.04 | - | 0.46 | 0.14 | - | 0.068 | - | - | 0.148 |
| 60 | - | 1.56 | - | 0.69 | 0.21 | - | 0.102 | - | - | 0.222 |
| 80 | - | 2.08 | - | 0.92 | 0.28 | - | 0.136 | - | - | 0.296 |
| 100 | - | 2.60 | - | 1.15 | 0.35 | - | 0.17 | - | - | 0.37 |
| 20 | - | 0.52 | - | 0.23 | 0.07 | - | 0.034 | - | - | 0.074 |

TABLE 5.2-3

## LOAD CASE III

| % LOAD | PO-1 | PI-1 | PO-2 | PI-2 | PO-3 | PI-3 | PO-4 | PI-4 | PO-5 | PI-5 |
|---|---|---|---|---|---|---|---|---|---|---|
| 0 | 0 | - | 0 | - | 0 | - | - | 0 | - | 0 |
| 20 | 0.12 | - | 0.4 | - | 0.196 | - | - | 0.334 | - | 0.31 |
| 40 | 0.24 | - | 0.8 | - | 0.392 | - | - | 0.668 | - | 0.62 |
| 60 | 0.36 | - | 1.2 | - | 0.588 | - | - | 1.0 | - | 0.93 |
| 80 | 0.48 | - | 1.6 | - | 0.784 | - | - | 1.33 | - | 1.24 |
| 100 | 0.6 | - | 2.0 | - | 0.98 | - | - | 1.67 | - | 1.55 |
| 20 | 0.12 | - | 0.4 | - | 0.196 | - | - | 0.334 | - | 0.31 |



J-57192 R2

# TABLE 5.2-4

## LOAD CASE IV

| % LOAD | PO-1 | PI-1 | PO-2 | PI-2 | PO-3 | PI-3 | PO-4 | PI-4 | PO-5 | PI-5 |
|---|---|---|---|---|---|---|---|---|---|---|
| 0 | - | 0 | 0 | - | - | 0 | - | 0 | - | 0 |
| 20 | - | 0.05 | 0.11 | - | - | 0.17 | - | 0.52 | - | 0.51 |
| 40 | - | 0.10 | 0.22 | - | - | 0.34 | - | 1.04 | - | 1.02 |
| 60 | - | 0.15 | 0.33 | - | - | 0.51 | - | 1.56 | - | 1.53 |
| 80 | - | 0.20 | 0.44 | - | - | 0.68 | - | 2.08 | - | 2.04 |
| 100 | - | 0.25 | 0.55 | - | - | 0.85 | - | 2.6 | - | 2.55 |
| 20 | - | 0.05 | 0.11 | - | - | 0.17 | - | 0.52 | - | 0.51 |

# TABLE 5.2-5

## LOAD CASE II - ULTIMATE

| % LOAD | PO-1 | PI-1 | PO-2 | PI-2 | PO-3 | PI-3 | PO-4 | PI-4 | PO-5 | PI-5 |
|---|---|---|---|---|---|---|---|---|---|---|
| 20 | - | 0.52 | - | 0.23 | 0.07 | - | 0.034 | - | - | 0.074 |
| 40 | - | 1.04 | - | 0.46 | 0.14 | - | 0.068 | - | - | 0.148 |
| 60 | - | 1.56 | - | 0.69 | 0.21 | - | 0.102 | - | - | 0.222 |
| 80 | - | 2.08 | - | 0.92 | 0.28 | - | 0.136 | - | - | 0.296 |
| 100 | - | 2.60 | - | 1.15 | 0.35 | - | 0.17 | - | - | 0.37 |
| 120 | - | 3.12 | - | 1.38 | 0.42 | - | 2.04 | - | - | 0.445 |
| 140 | - | 3.64 | - | 1.61 | 0.49 | - | 2.38 | - | - | 0.518 |

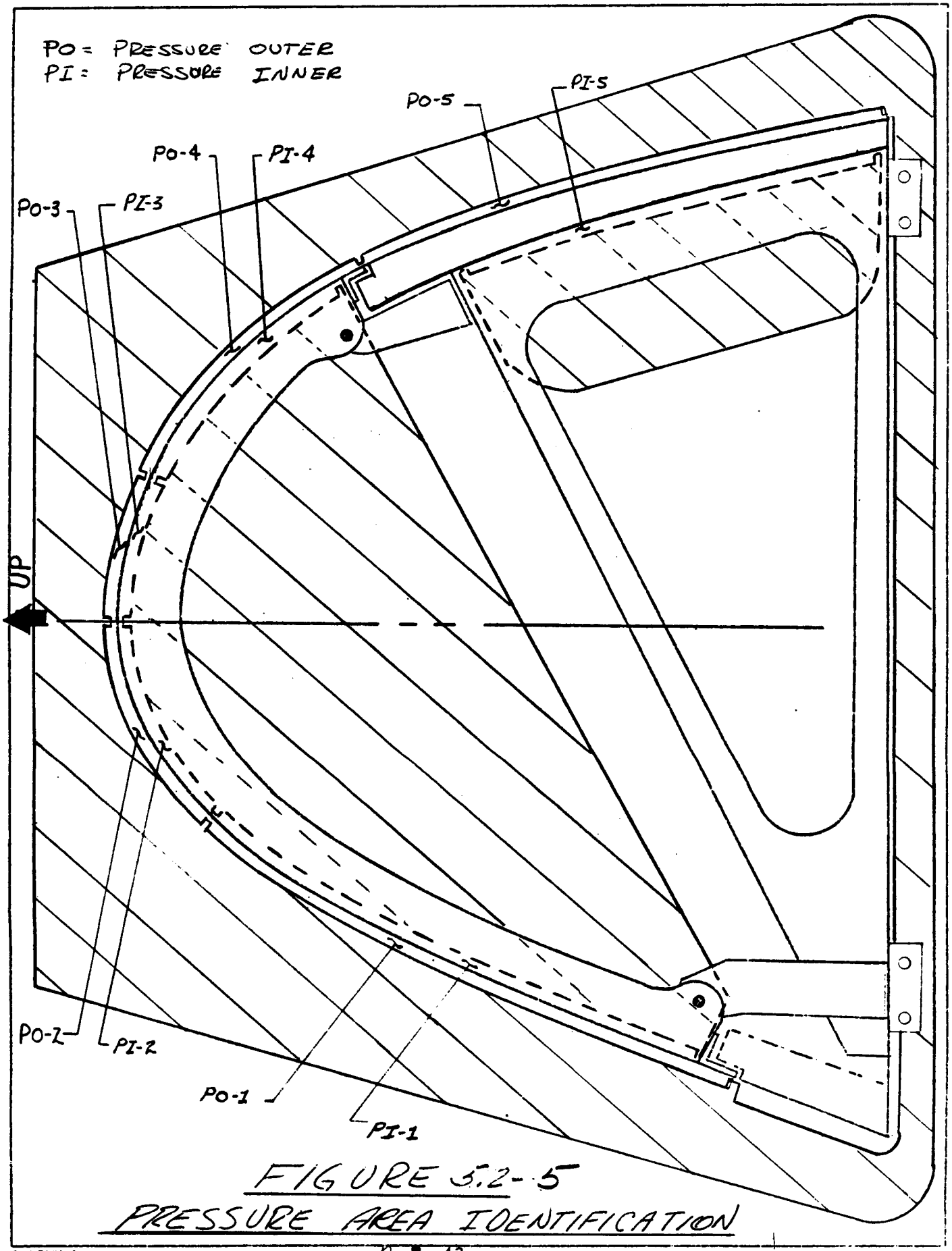


FIGURE 5.2-5
PRESSURE AREA IDENTIFICATION

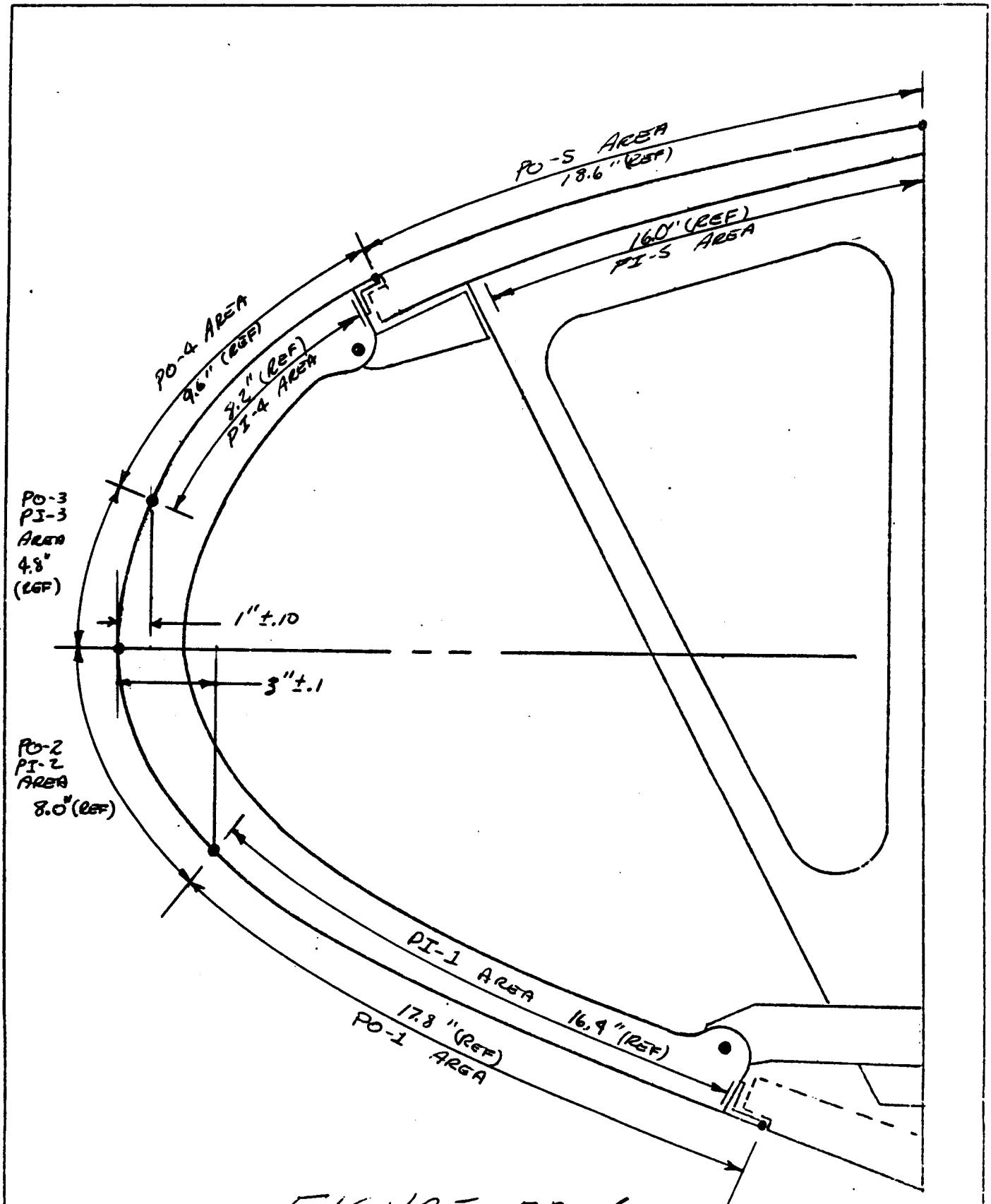


FIGURE 5.2-6

PRESSURE AREA GEOMETRY

5.2.3 Instrumentation

Strain gages and deflection transducers are identified and located in Figures 5.2-7 and 5.2-8 for the RPP leading edge and support structure, respectively. The suggested strain gages are the 120 ohm type from Micro Measurement. The specified strain gages have a 0.5 inch gage length, which reduces the sensitivity to surface crazing of the test specimen. Specifically, the gages are, Ref. (B):

| | |
|---|---|
| Axial | EA - OX - 500BH - 120 - W |
| Tee | WA - OX - 500WT - 120 |
| Rosette ($45^{o}$) | WA - OX - 500 WR - 120 |

OX = temperature compensation

03 for RPP leading edge

05 for sheet metal support structure

The position, location, and type of strain gages are summarized in Table 5.2-6. Nomenclature is specified in Figures 5.2-7 and 5.2-8; in addition, the gage positions may be scaled from these figures. Strain gages have been successfully installed on coated RPP by using the following procedure.

A. Surface Preparation

(1) Buff gage area lightly with 120 grit silicon carbide sand paper.

(2) Blow surface clean with dry $N_2$.

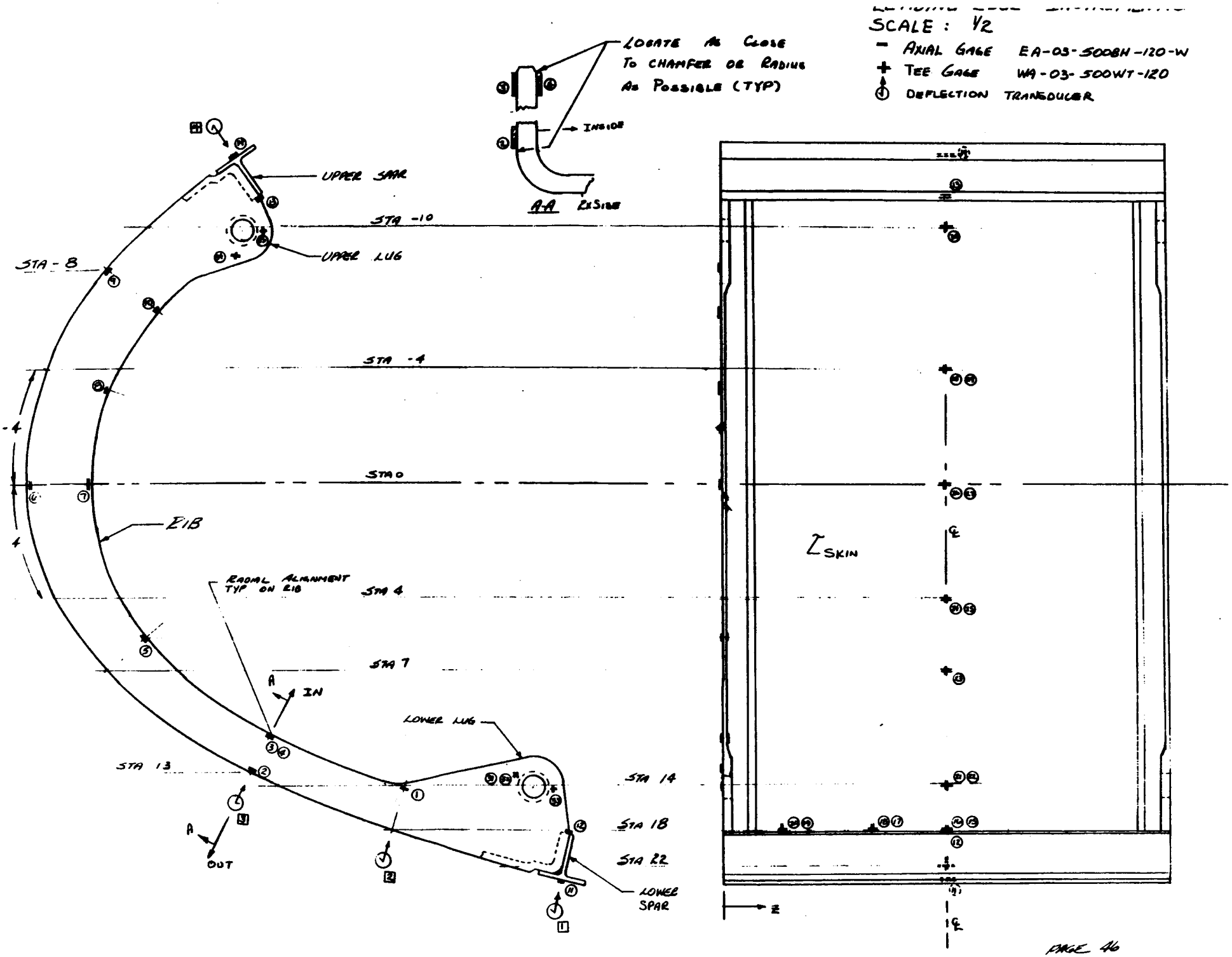
SCALE : 1/2
AXIAL GAGE EA-03-500BH-120-W
TEE GAGE WA-03-500WT-120
DEFLECTION TRANSDUCER
LOCATE AS CLOSE TO CHAMFER OR RADIUS AS POSSIBLE (TYP)
INSIDE
A-A
UPPER SPAR
UPPER LUG
STA -10
STA -8
STA -4
STA 0
STA 4
STA 7
STA 13
STA 14
STA 18
STA 22
RIB
RADIAL ALIGNMENT TYP ON RIB
IN
OUT
LOWER LUG
LOWER SPAR
SKIN

A.3-46

SUPPORT STRUCTURE INSTRUMENTATION

SCALE : 1/2

= AXIAL GAGE EA-05-500BH-120-W

↗ ROSETTE GAGE WA-05-500WR-120

⊙ DEFLECTION TRANSDUCER

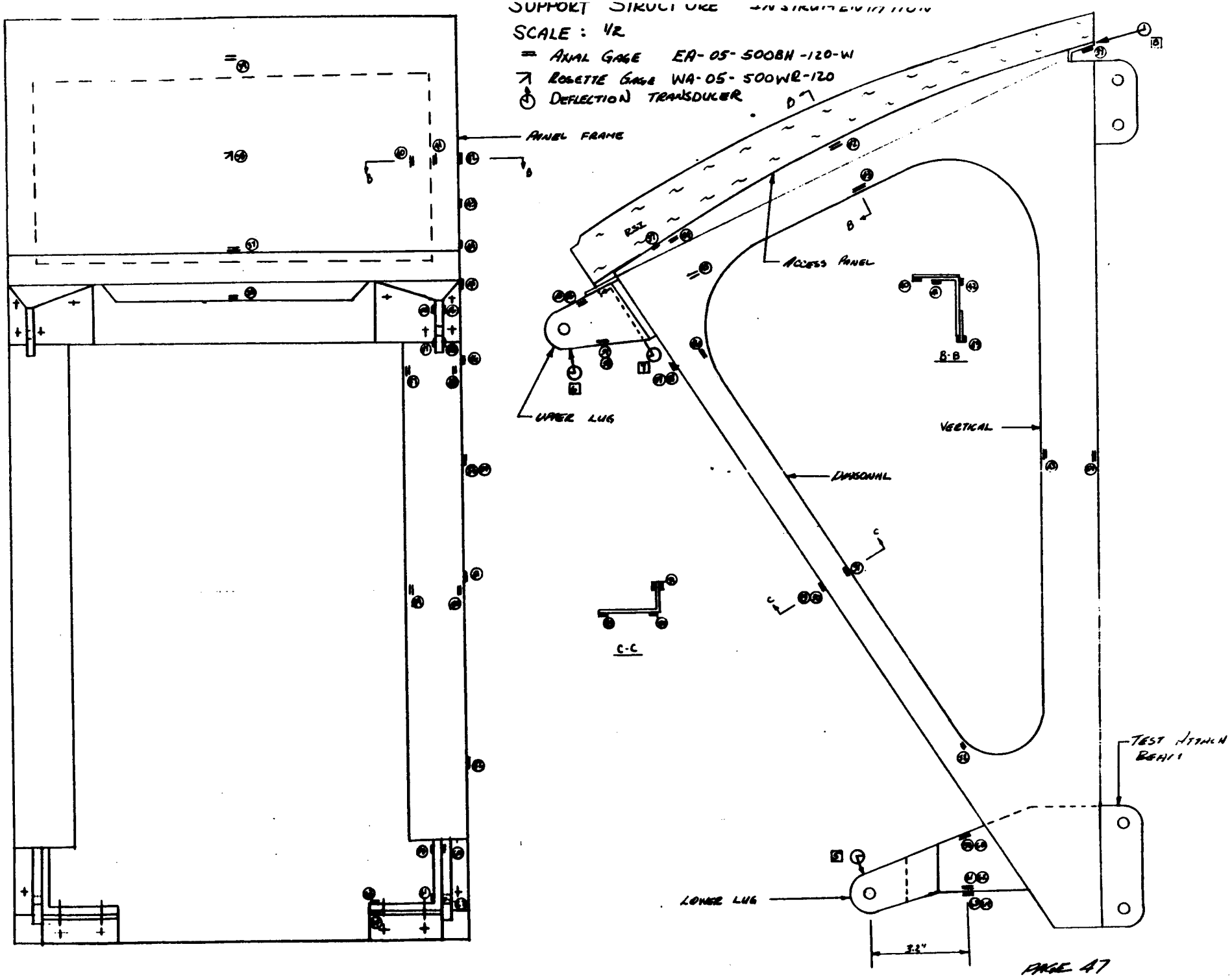


A.3-47

TABLE 5.2-6

SUMMARY - LEADING EDGE ASSEMBLY STRAIN GAGES

| Number | Position | Location | Type |
|---|---|---|---|
| 1 | Sta 18 | Rib-In | Axial |
| 2 | Sta 13 | Rib-Out | Axial |
| 3 | Sta 13 | Rib - In | Axial |
| 4 | Sta 13 | Rib-In (Inside) | Axial |
| 5 | Sta 7 | Rib-In | Axial |
| 6 | Sta 0 | Rib-Out | Axial |
| 7 | Sta 0 | Rib-In | Axial |
| 8 | Sta -4 | Rib-In | Axial |
| 9 | Sta -8 | Rib-Out | Axial |
| 10 | Sta -8 | Rib-In | Axial |
| 11 | ℄ | L. Spar-Out | Axial |
| 12 | ℄ | L. Spar-In | Axial |
| 13 | ℄ | U. Spar-In | Axial |
| 14 | ℄ | U. Spar-Out | Axial |
| 15 | ℄ - Sta 18 | Skin-In | Tee |
| 16 | ℄ - Sta 18 | Skin-Out | Tee |
| 17 | Z = 5.0 - Sta 18 | Skin-In | Tee |
| 18 | Z = 5.0 - Sta 18 | Skin-Out | Tee |
| 19 | Z = 2.0 - Sta 18 | Skin-In | Tee |
| 20 | Z = 2.0 - Sta 18 | Skin-Out | Tee |
| 21 | ℄ - Sta 14 | Skin-In | Tee |
| 22 | ℄ - Sta 14 | Skin-Out | Tee |
| 23 | ℄ - Sta 7 | Skin-In | Tee |
| 24 | ℄ - Sta 4 | Skin-In | Tee |

TABLE 5.2-6 (Continued)

SUMMARY - LEADING EDGE ASSEMBLY STRAIN GAGES

| Number | Position | Location | Type |
|---|---|---|---|
| 25 | ℄ - Sta 4 | Skin-Out | Tee |
| 26 | ℄ - Sta 0 | Skin-In | Tee |
| 27 | ℄ - Sta 0 | Skin-Out | Tee |
| 28 | ℄ - Sta -4 | Skin-In | Tee |
| 29 | ℄ - Sta -4 | Skin-Out | Tee |
| 30 | ℄ - Sta -10 | Skin-In | Tee |
| 31 | As Shown | L. Lug | Tee |
| 32 | As Shown | L. Lug (Inside) | Tee |
| 33 | As Shown | L. Lug | Tee |
| 34 | As Shown | U. Lug | Tee |
| 35 | As Shown | U. Lug | Tee |
| 36* | ℄ | Access Panel Flange | Axial |
| 37 | ℄ - Fwd | Access Panel (Fwd) | Axial |
| 38 | ℄ - Center | Access Panel (Center) | Rosette |
| 39 | ℄ - Aft | Access Panel Support Flange (Aft) | Axial |
| 40 | Left Side - ℄ | Access Panel | Axial |
| 41 | Left Side - ℄ | Panel Frame | Axial |
| 42 | Left Side - ℄ | Panel Frame | Axial |
| 43* | Left Side - ℄ | Panel Frame | Axial |
| 44 | Left Side - Fwd | Panel Frame | Axial |
| 45* | Left Side - Fwd | Panel Frame | Axial |
| 46* | Left Side - Upper | Diagonal | Axial |
| 47 | Left Side - Upper | Diagonal | Axial |
| 48 | Left Side - Upper | Diagonal | Axial |

TABLE 5.2-6 (Continued)

SUMMARY - LEADING EDGE ASSEMBLY STRAIN GAGES

| Number | Position | Location | Type |
|---|---|---|---|
| 49 | Left Side - ℄ | Diagonal | Axial |
| 50 | Left Side - ℄ | Diagonal | Axial |
| 51* | Left Side - ℄ | Diagonal | Axial |
| 52* | Left Side - Lower | Diagonal | Axial |
| 53* | Left Side - Middle | Vertical | Axial |
| 54 | Left Side - Middle | Vertical | Axial |
| 55 | Upper Side | Upper Lug | Axial |
| 56 | Upper Side | Upper Lug | Axial |
| 57 | Lower Side | Upper Lug | Axial |
| 58 | Lower Side | Upper Lug | Axial |
| 59 | Upper Side | Lower Lug | Axial |
| 60 | Upper Side | Lower Lug | Axial |
| 61 | Lower Side | Lower Lug | Axial |
| 62 | Lower Side | Lower Lug | Axial |
| 63 | Flange - Outer | Lower Lug | Axial |
| 64 | Flange - Outer | Lower Lug | Axial |

* Two axial gages back to back and averaged.

(3) Apply thin coat of Micro-Measurement (M-M) M-Bond AE-10 to gage area and cure, reference M-M bulletin A-137-2. The purpose of this step is to provide a smooth surface as shown:

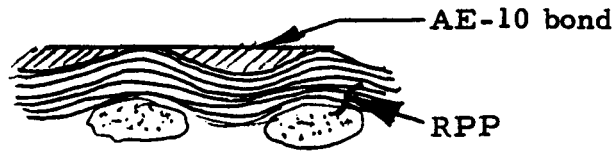


(4) Buff lightly with 120 grit silicon carbide sandpaper to knock off rough bumps and etch surface.

(5) Blow surface clean with dry $N_2$.

B. Gage Installation

(1) Install gages in standard fashion with M-M M-Bond AE-10 epoxy. Position gage axes as shown in Figure 5.2-7.

Normal preparation is required for the sheet metal support structure.

The deflection transducers are summarized in Table 5.2-7 and are shown in Figures 5.2-7 and 5.2-8. The maximum range of deflections should not exceed +0.12 to -0.05 at limit load.

TABLE 5.2-7

SUMMARY - LEADING EDGE ASSEMBLY DEFLECTION TRANSDUCERS

| No. | Position | Location |
|---|---|---|
| 1 | ℄ | Lower Spar |
| 2 | ℄ | Skin |
| 3 | Sta 13 | Rib |
| 4 | ℄ | Upper Spar |
| 5 | Over Bolt | Lower Lug |
| 6 | Over Bolt | Upper Lug |
| 7 | ℄ | Access Panel (Fwd) |
| 8 | ℄ | Access Panel (Aft) |

5.2.4 Test Procedure

Limit Load Tests - The leading edge and support structure will have to be disassembled to install the loading fixtures. Reassemble the fixtures and test article making sure that approximately 0.125 inch of clearance exists everywhere so the specimen will not deflect and touch the loading fixtures. Verify strain gage and deflection transducer installation. In order to stabilize and check out instrumentation, apply 0.15 psi to each pressure area independently. Subject the test article to Load Case I per Table 5.2-1. Apply the combination of loads as defined in 20% increments to 100% of limit, then return to 20%. At each increment record strain gage and deflection transducer

reading. Repeat the above procedure for Load Cases II, III and IV. Predicted deflections and stresses versus percent load are presented in Figures 5.2-9 through 5.2-14. These deflections and stresses shall be monitored during testing as a means of spot checking the progress of the test. Repeat load Case II to produce a total of five limit load cycles before proceeding with vacuum and acoustic tests.

Ultimate Load Test - The ultimate load test will be performed after all other testing (through vacuum and acoustic) has been completed. The leading edge assembly shall be prepared and checked out as in the limit load test. Strain gages, damaged in handling or testing, shall be replaced and checked before proceeding with this test.

Load Case II is the critical load condition and is defined in Table 5.2-5. Obtain hysteresis data by loading in 20% increments to 100% and returning to 0% in 20 increments. Cycle for a total of 3 times, recording stresses and deflections at each increment. Load in 20% increments to 140% and as before record the stresses and deflections at each increment during loading and unloading.

5.2.5 Data Reduction

The stress-strain relations for plane stress in the orthotropic RPP material are:

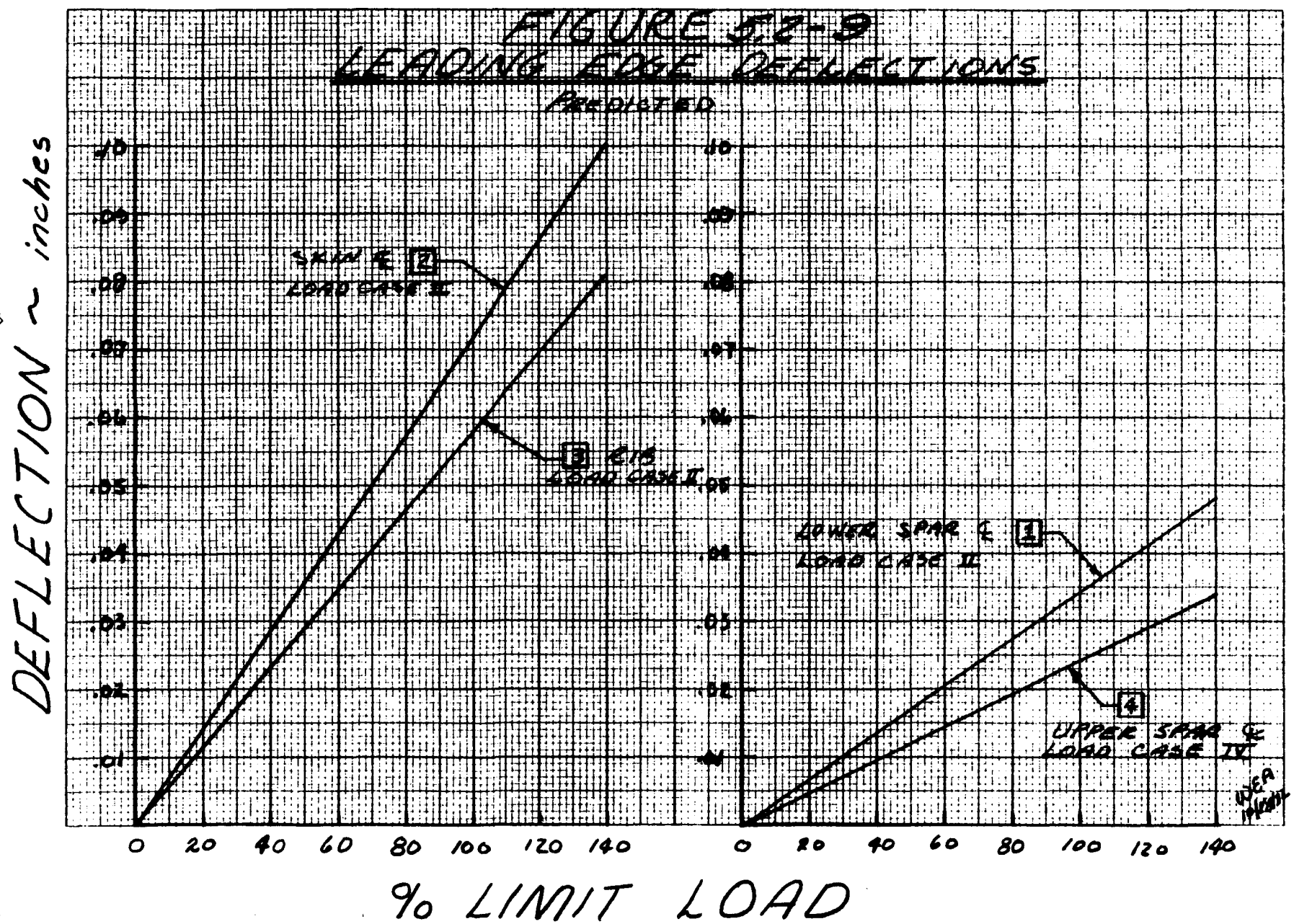
FIGURE 5.2-9
LEADING EDGE DEFLECTIONS
PREDICTED
SKIN ℄ 2
LOAD CASE II
3 ℄ RIB
LOAD CASE II
LOWER SPAR ℄ 1
LOAD CASE II
4
UPPER SPAR ℄
LOAD CASE IV
DEFLECTION ~ inches
% LIMIT LOAD
0 20 40 60 80 100 120 140
.01 .02 .03 .04 .05 .06 .07 .08 .09 .10

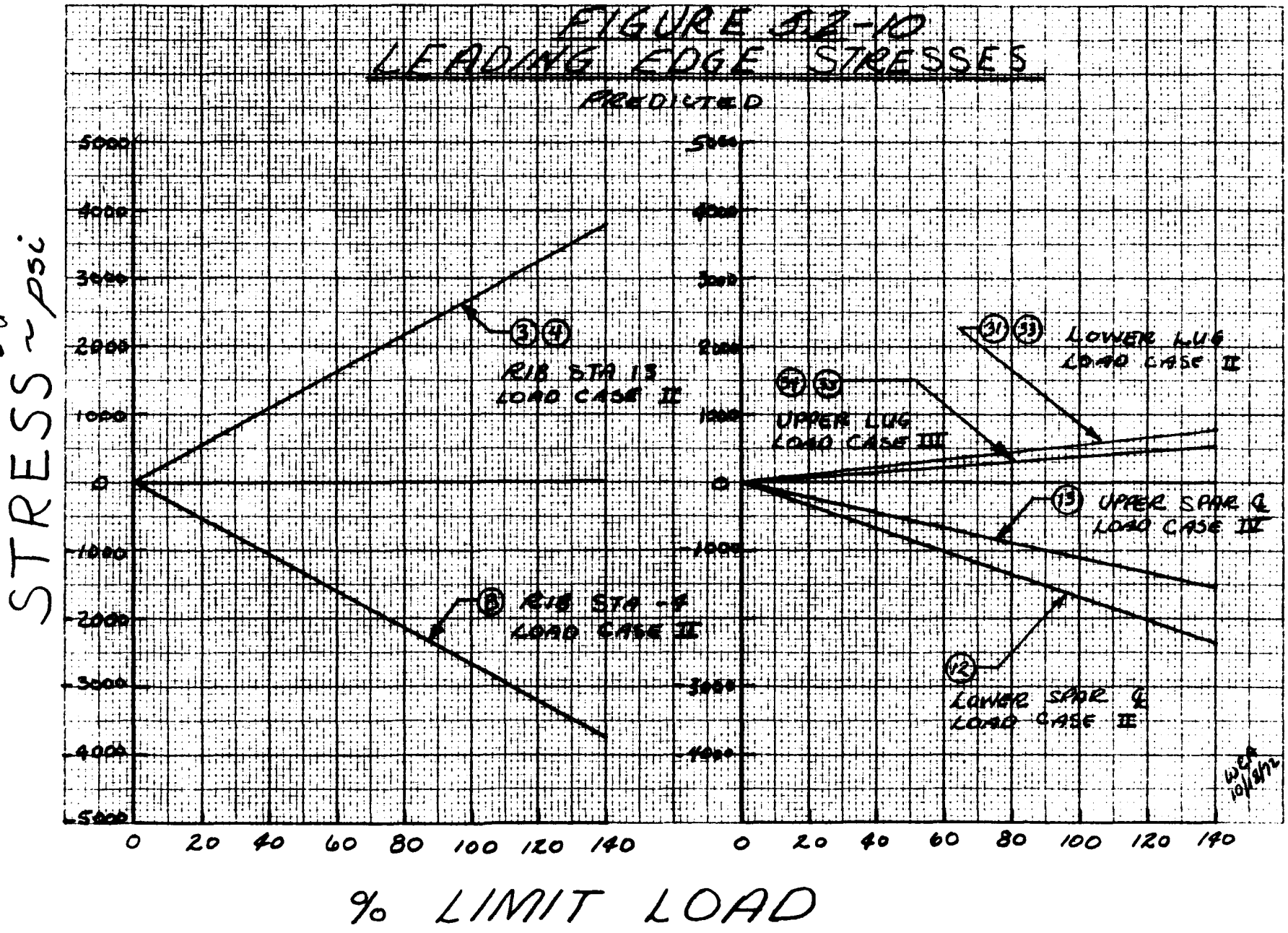
FIGURE A2-10
LEADING EDGE STRESSES
PREDICTED
STRESS ~ psi
5000
4000
3000
2000
1000
0
-1000
-2000
-3000
-4000
-5000
0 20 40 60 80 100 120 140
% LIMIT LOAD
3 4
RIB STA 13
LOAD CASE II
8
RIB STA -4
LOAD CASE II
31 33
LOWER LUG
LOAD CASE II
37 33
UPPER LUG
LOAD CASE III
13
UPPER SPAR ℄
LOAD CASE IV
12
LOWER SPAR ℄
LOAD CASE III
WCA
10/8/72

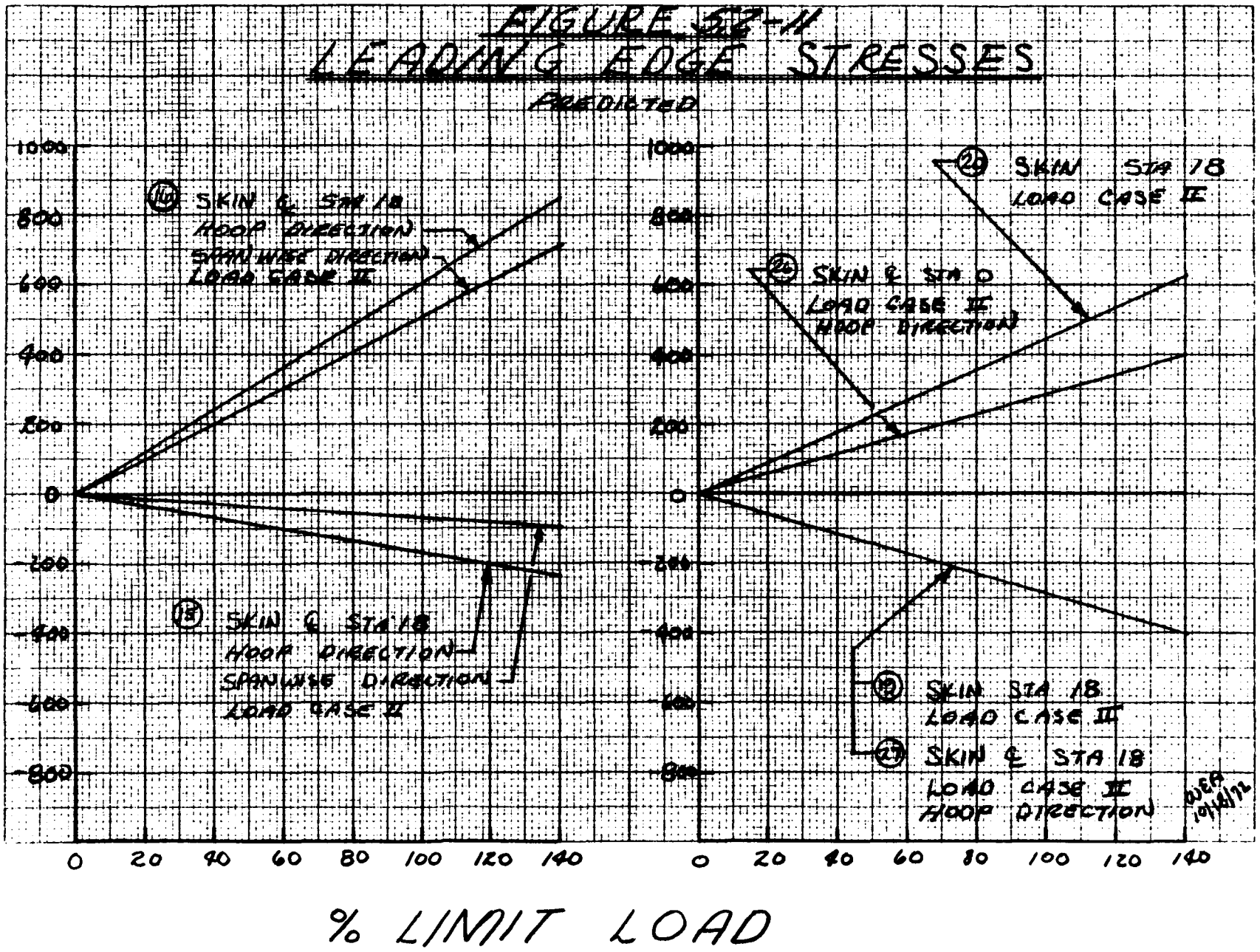
FIGURE 52-11
LEADING EDGE STRESSES
PREDICTED
STRESS ~ psi
% LIMIT LOAD
1000
800
600
400
200
0
-200
-400
-600
-800
0
20
40
60
80
100
120
140
16 SKIN ℄ STA 18
HOOP DIRECTION
SPANWISE DIRECTION
LOAD CASE II
15 SKIN ℄ STA 18
HOOP DIRECTION
SPANWISE DIRECTION
LOAD CASE II
20 SKIN STA 18
LOAD CASE II
26 SKIN ℄ STA 0
LOAD CASE II
HOOP DIRECTION
19 SKIN STA 18
LOAD CASE II
27 SKIN ℄ STA 18
LOAD CASE II
HOOP DIRECTION
WEA
10/18/72

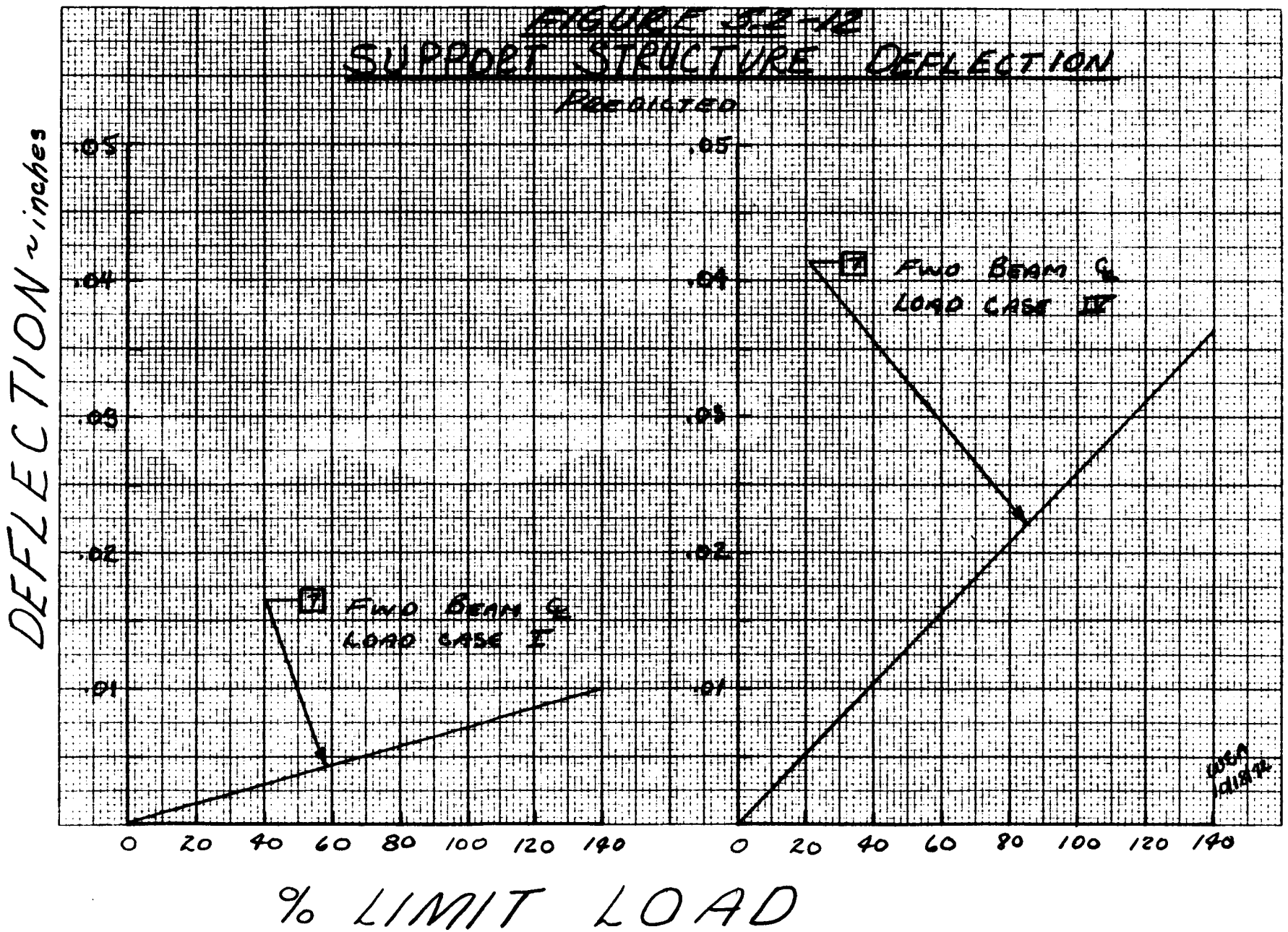
FIGURE 5.2-12
SUPPORT STRUCTURE DEFLECTION
PREDICTED
DEFLECTION ~ inches
.05
.04
.03
.02
.01
0
20
40
60
80
100
120
140
FWD BEAM ℄
LOAD CASE I
FWD BEAM ℄
LOAD CASE II
% LIMIT LOAD

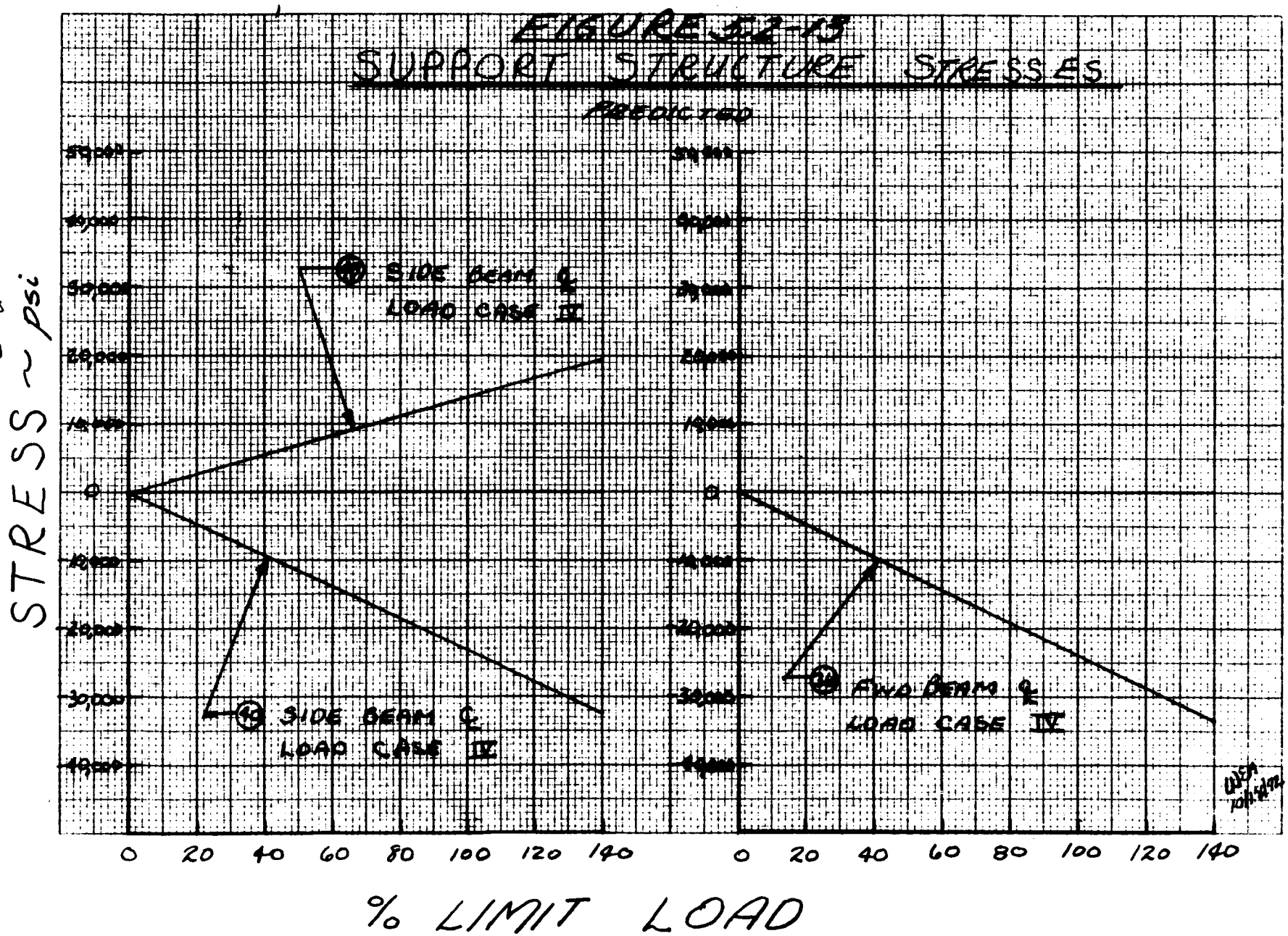
FIGURE 5.2-13
SUPPORT STRUCTURE STRESSES
PREDICTED
STRESS ~ psi
SIDE BEAM ℄
LOAD CASE IV
SIDE BEAM ℄
LOAD CASE IV
FWD BEAM ℄
LOAD CASE IV
0
20
40
60
80
100
120
140
% LIMIT LOAD

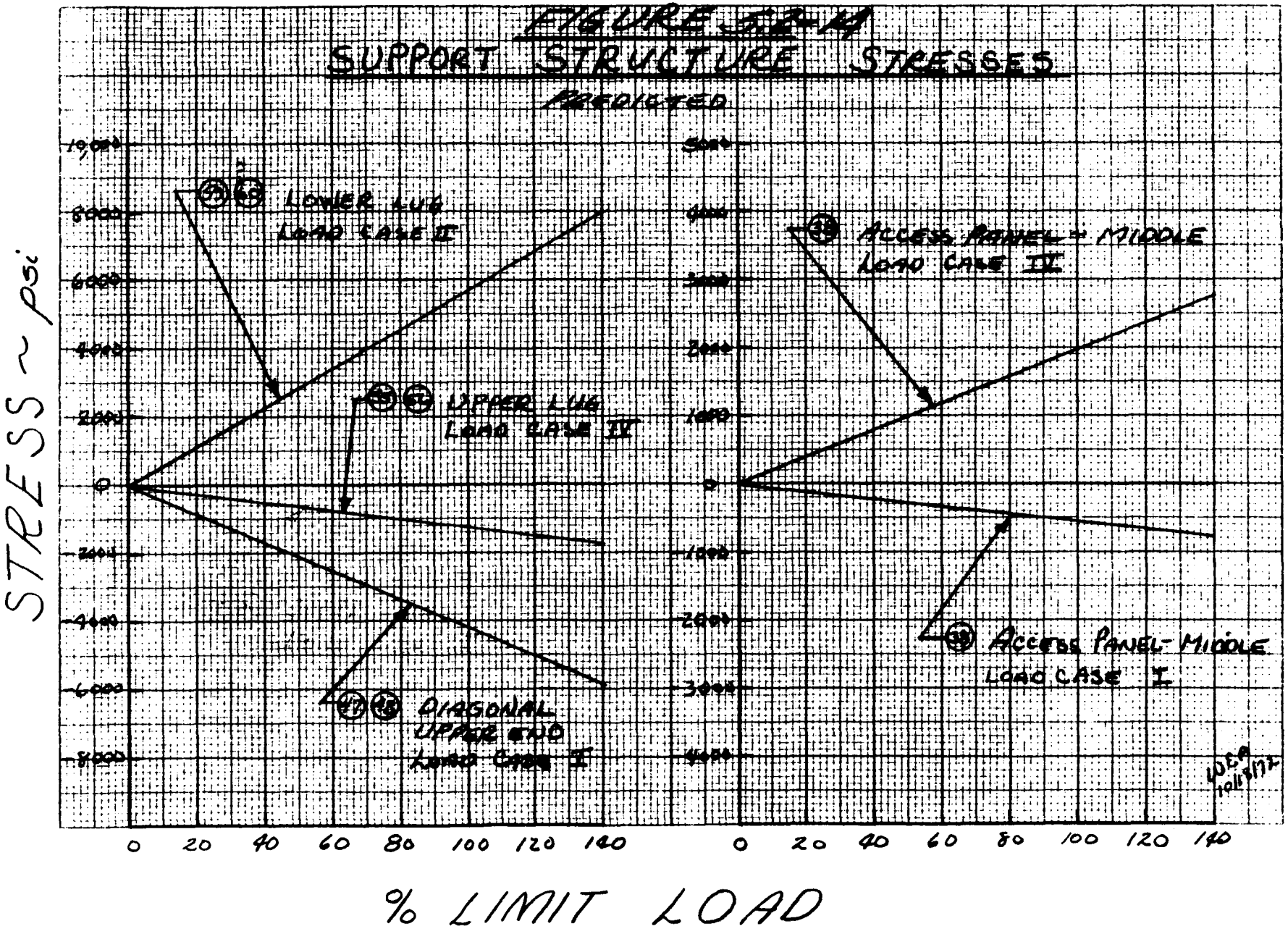
FIGURE A.3-4
SUPPORT STRUCTURE STRESSES
PREDICTED
LOWER LUG
LOAD CASE II
UPPER LUG
LOAD CASE IV
DIAGONAL
UPPER END
LOAD CASE II
ACCESS PANEL - MIDDLE
LOAD CASE IV
ACCESS PANEL - MIDDLE
LOAD CASE I
STRESS ~ psi
% LIMIT LOAD
0
20
40
60
80
100
120
140

$$\begin{Bmatrix} \sigma_1 \\ \sigma_2 \\ \tau_{12} \end{Bmatrix} = \begin{bmatrix} Q_{11} & Q_{12} & 0 \\ Q_{12} & Q_{22} & 0 \\ 0 & 0 & Q_{66} \end{bmatrix} \begin{Bmatrix} \epsilon_1 \\ \epsilon_2 \\ \gamma_{12} \end{Bmatrix}$$

where:

subscript 1 is the warp direction

subscript 2 is the fill direction

$$Q_{11} = \frac{E1}{(1 - \nu_{12}\,\nu_{21})}$$

$$Q_{12} = \frac{\nu_{12}\ E2}{(1 - \nu_{12}\,\nu_{21})}$$

$$Q_{22} = \frac{E2}{(1 - \nu_{12}\,\nu_{21})}$$

$$Q_{66} = G_{12}$$

E = Young's Modulus

G = Modulus of Rigidity

$\nu$ = Poisson's Ratio

The average engineering constants that were used in the RPP structural analysis and which should be used in the data reduction are listed below:

$$Q_{11} = 1.536 \times 10^6$$

$$Q_{12} = 0.2304 \times 10^6$$

$$Q_{22} = 1.152 \times 10^6$$

$$Q_{66} = 0.99 \times 10^6$$

Reduction of the strain data for the sheet metal support structure is accomplished by standard equations and properties.

All strain gage data shall be reduced and plotted.

5.2.6 Post Test Operations

Following the limit load tests and inspection (Section 6.0), the test article insulation shall be reassembled to form a complete T143T00017-1 assembly. Strain gage installation should be preserved, where practical, because it will be used in the ultimate load test following acoustic testing.

5.3 ORBITAL VACUUM/TEMPERATURE TEST

5.3.1 Objectives

Vacuum and orbital temperature testing on the leading edge assembly will have the following objective:

- Evaluate the structural integrity of the leading edge assembly and insulation installations under orbital conditions that could produce such effects as outgassing, strain isolator extension/compression, differential thermal expansion at cryogenic temperatures, or embrittlement at cryogenic temperatures.

5.3.2 Simulation Requirements

A leading edge assembly shall be tested, complete with RPP leading edge, support structure and insulation (heatshield) assemblies. The test assembly used in the boost pressure load test shall be configured per drawing T143T00017-1.

Pressure shall be maintained at $10^{-8}$ torr, while the temperature is cycled between -250°F and +180°F as measured on the outside surface of the RPP. Temperature shall be maintained at each maximum level for a period of four hours to ensure stabilization throughout the assembly. Transition between temperature extremes shall be at any convenient rate, but shall not be less than 1/2 hour. One cycle consists of starting at ambient temperature, reduce level to -250°F, hold for four hours, increase temperature to +180°F, hold for four hours, and return to ambient temperature. A total of five cycles shall be applied. Rate of pressure increase to ambient following completion of the test shall not be less than 20 minutes.

5.3.3 Instrumentation

Twenty-one thermocouples shall be installed on the RPP leading edge to monitor temperature response during test. Temperature control shall be maintained at three points noted on Figure 5.3.1, where thermocouple location is shown. Copper/constantan (36 gage) type thermocouples bonded to the surface with a material such as Narmco Resin 7343 and Curing Agent 7139 is recommended. If alternate bonds are used, they shall be of the non-filled type.

5.3.4 Test Procedure

The T143T00017-1 test assembly shall be supported at the assembly support lugs on a suitable stand or fixture. Orientation (i.e., vertical or horizontal) of the test article is unimportant. Four-inches of guard insulation of any low density, low temperature type shall be installed

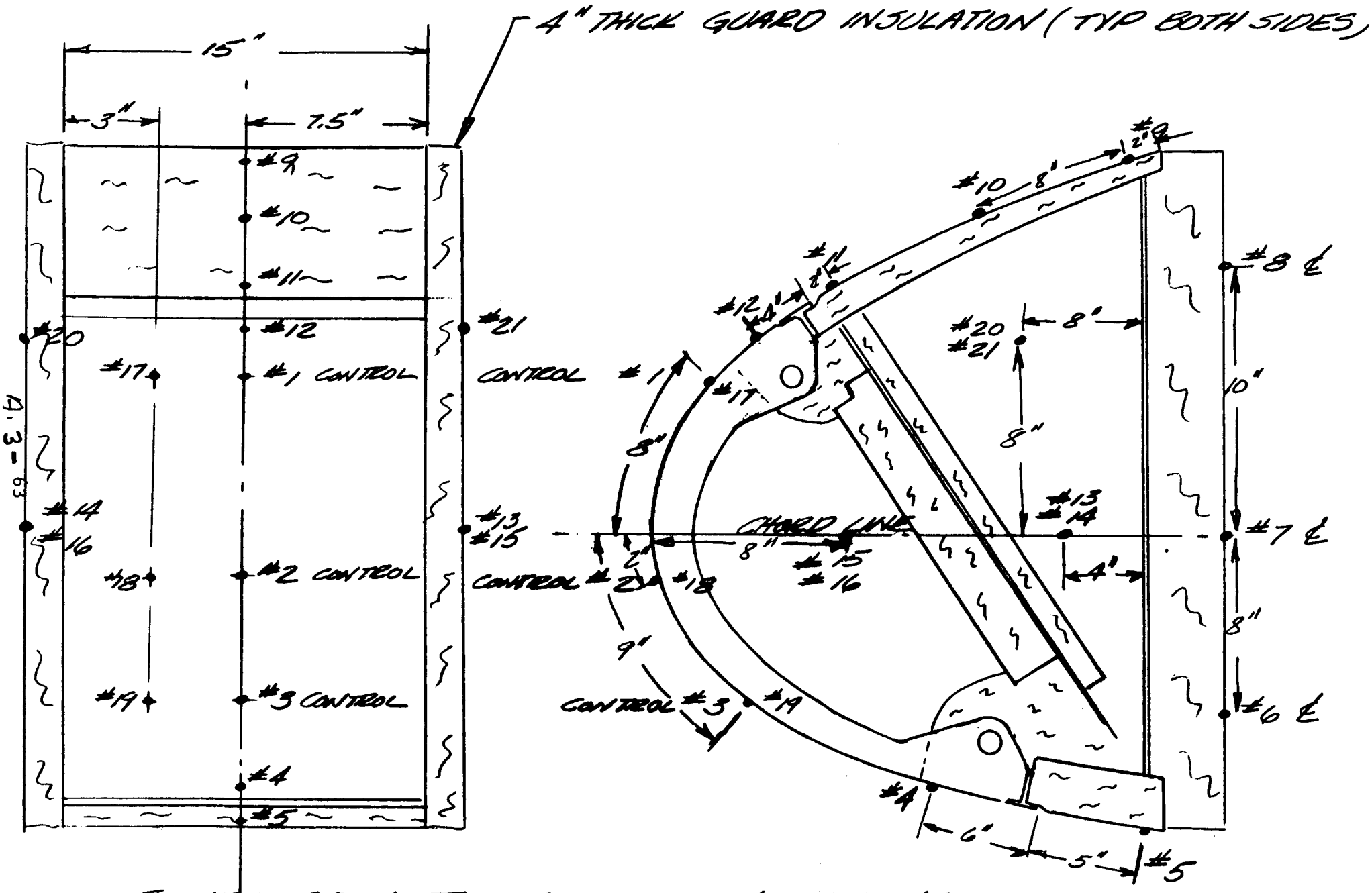


FIGURE 5.3-1 THERMOCOUPLE LOCATIONS
VACUUM/TEMPERATURE TEST

at each side of the leading edge to close the open cavity and to approximate a two-dimensional heat flow. Similarly, four inches of insulation shall be installed on the aft side of the aluminum simulated front spar to force heat flow primary through the RPP leading edge. In this way thermal gradients during temperature changes can be approximated.

With the test article installed the vacuum chamber shall be pumped down to the vacuum requirement and maintained at this condition for at least four hours before proceeding with the temperature cycling. Temperature cycling shall then proceed as outlined under "Simulation Requirements" above.

5.3.5 Data Reduction

Temperature histories of the three thermocouples shall be plotted.

5.3.6 Post Test Operations

The test article shall be thoroughly inspected for evidence of changes (e.g., color, crazing, etc.) and failures. Observations of changes shall be recorded and these areas photographed. See Section 6.0.

Thermocouples shall be removed and the test article prepared for the acoustic test to follow.

5.4 BOOST ACOUSTIC NOISE TEST

5.4.1 Objectives

The boost acoustic noise test has the following objectives:

(1) Demonstrate the overall structural integrity of the leading edge assembly.

(2) Verify that the RPP leading edge support points are not subject to coating chipping under the action of dynamic loads.

(3) Determine acoustic noise spectrum within the leading cavities, bounded by the RPP and the canted heatshield, and between the canted heatshield and front spar.

(4) Determine dynamic response of critical components to compare against design requirements.

Specifically excluded from evaluation for the flight article by this test is all of the insulation components. While these will be included in the test article, failure of these components may occur during test. The insulation employed in the Phase III test article is a substitute material of known low strength, and, depending upon the response of the structure to the imposed environment and the duration of test, could fail in fatigue.

5.4.2 Simulation Requirements

The test article for the acoustic test will be that leading edge segment of the T143T00017-1 configuration that had previously undergone boost static load and orbital vacuum tests. Testing will be conducted in an acoustic chamber.

The environment to be imposed externally to the test article is given in Figure 5.4-1. Tolerances will be -2 to +4 db of the sound pressures specified within each octave band. Six microphones will be used to measure the actual sound pressure field around the test article. The average of these

[redacted]

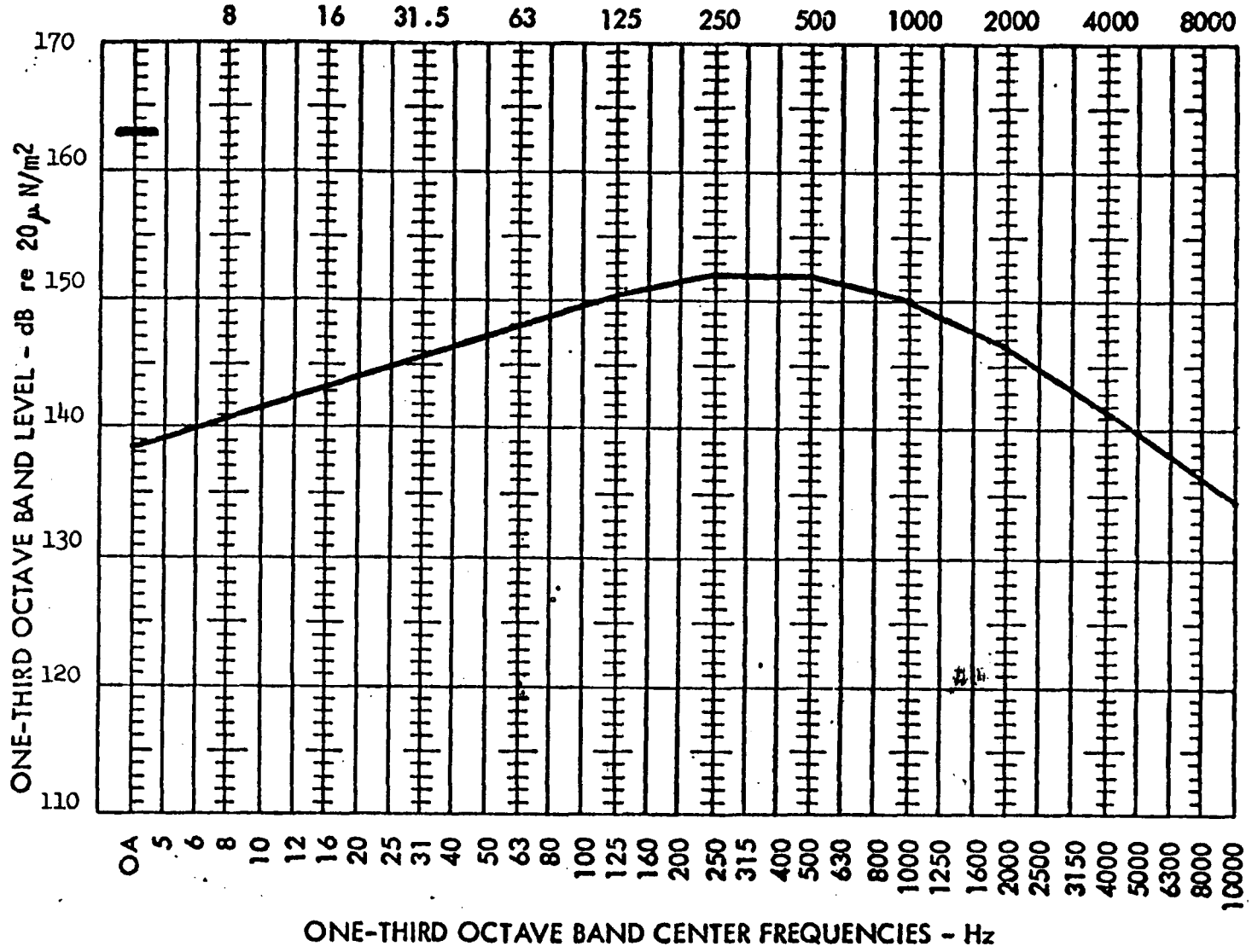


FIG 54-1 ACOUSTIC CRITERIA FOR SPACE SHUTTLE ORBITER WING LEADING EDGES (50 MIN.)

A.3-66

Page 8 of 1

six field measurements will be considered the nominal input to the test article. Testing will be conducted at ambient temperature.

5.4.3 Instrumentation Requirements

Eight microphones and eleven accelerometers (4 uni-axial and 7 tri-axial) will be used in the test. Six of the microphones shall be used to monitor and control the imposed environment, while the remaining two will monitor internal cavity noise fields. The accelerometers will be mounted on various areas of the structure to determine dynamic response. Locations of the various instrumentation are shown on Figure 5.4-2 and Drawing T143T00017, and tabulated in Table 5.4-1. The location of the two "far field" microphones will be established at the time of test, since their location is dependent upon the test facility used. Accelerometers having a $\pm$ 100 g output range and a frequency response of 2-10 KC shall be used.

Accelerometers mounted to the canted heatshield and to the upper lug insulation support bracket will require the removal of a core of insulation, strain isolator pad, and RTV-560 bond to permit installation of the accelerometers. The core removed shall be the minimum diameter required for cleaning the mounting surface and bonding the accelerometer in place. Extreme care shall be taken to avoid damage to the insulation and the insulation bond line, each of which have low strength and are readily subject to mishandling damage. Solvents shall not be used to clean the exposed surface unless approved by VSD.

# FIG 5.4-2 MICROPHONE LOCATIONS

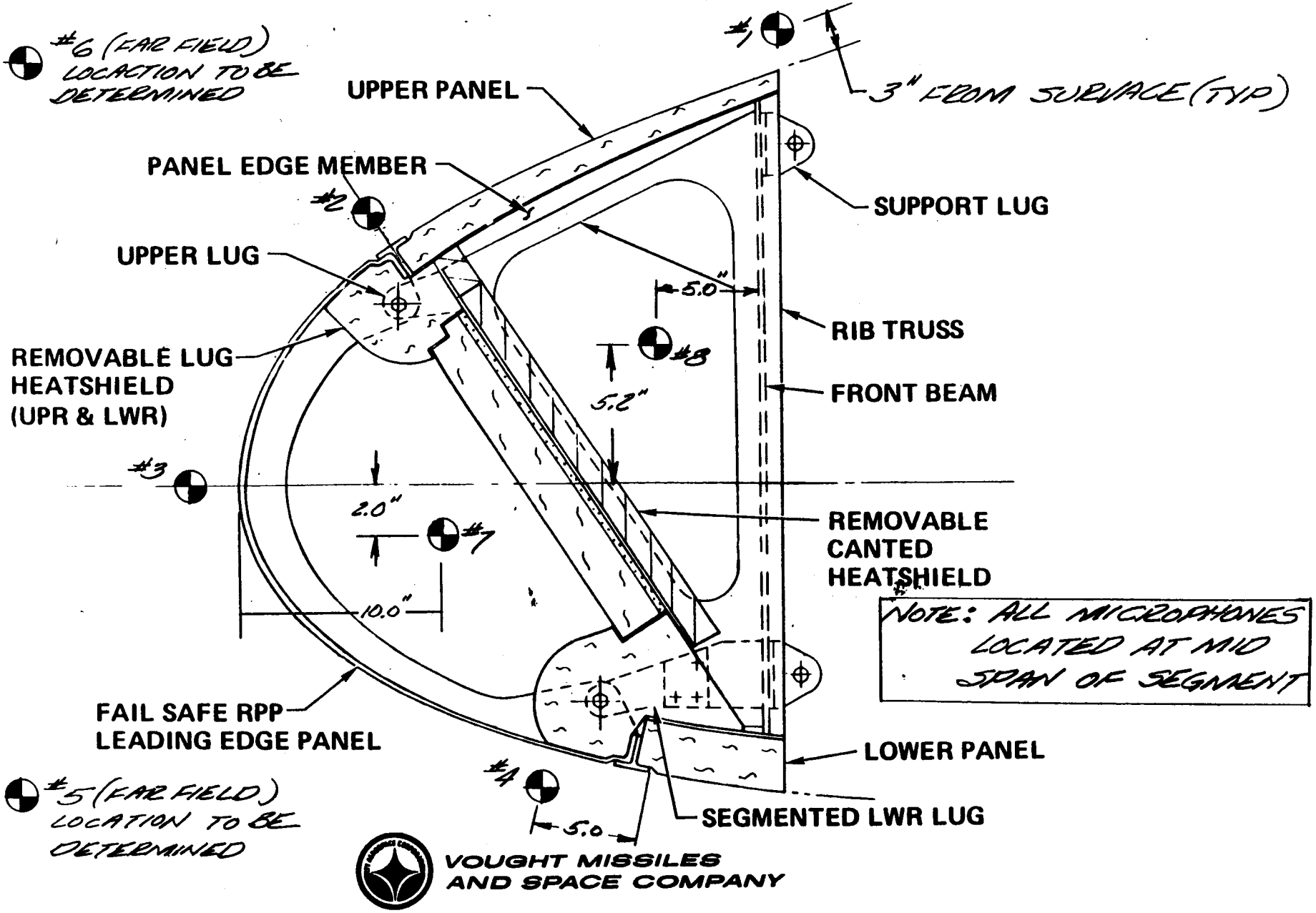

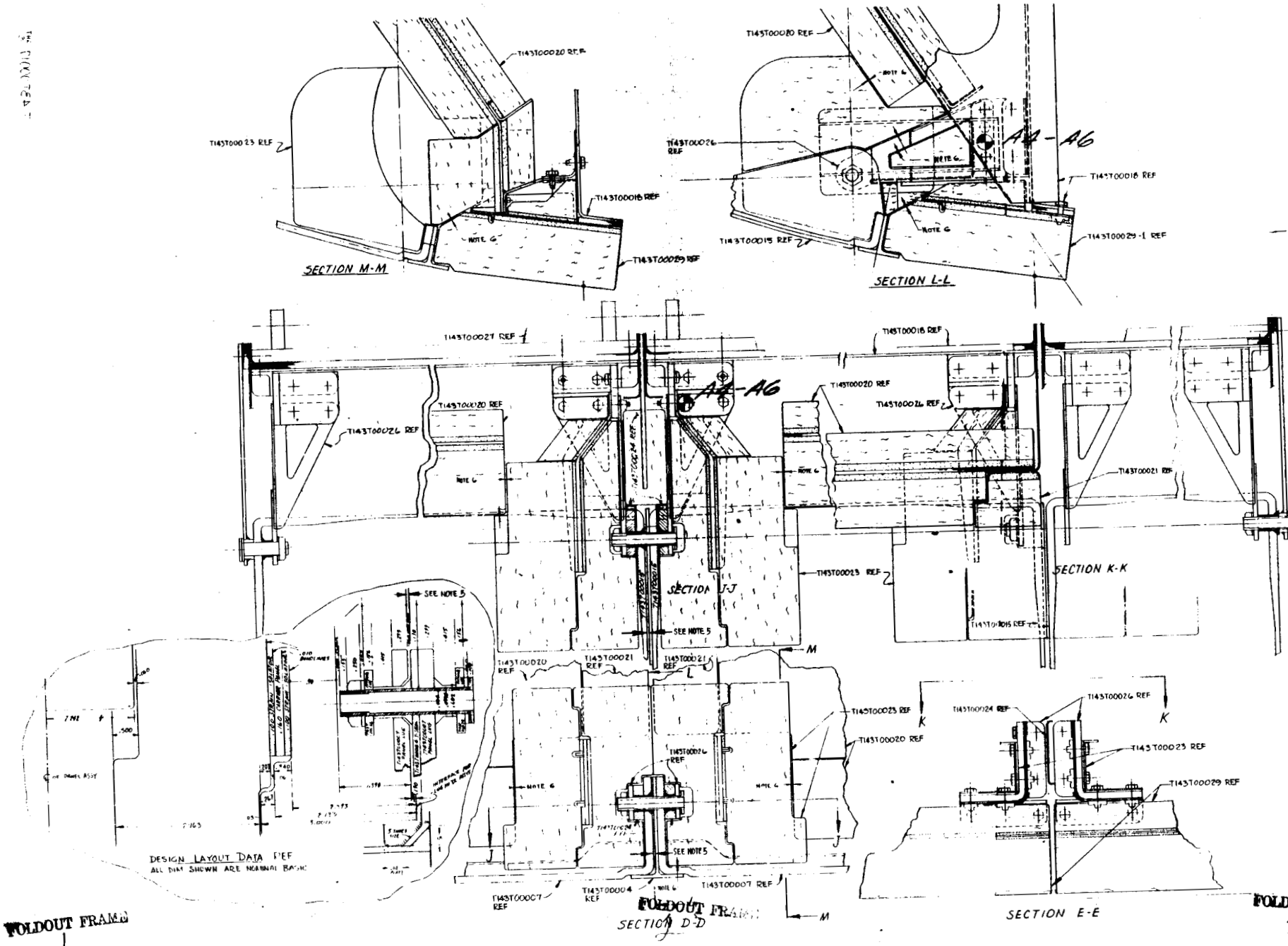


FOLDOUT FRAME 1

FOLDOUT FRAME 3

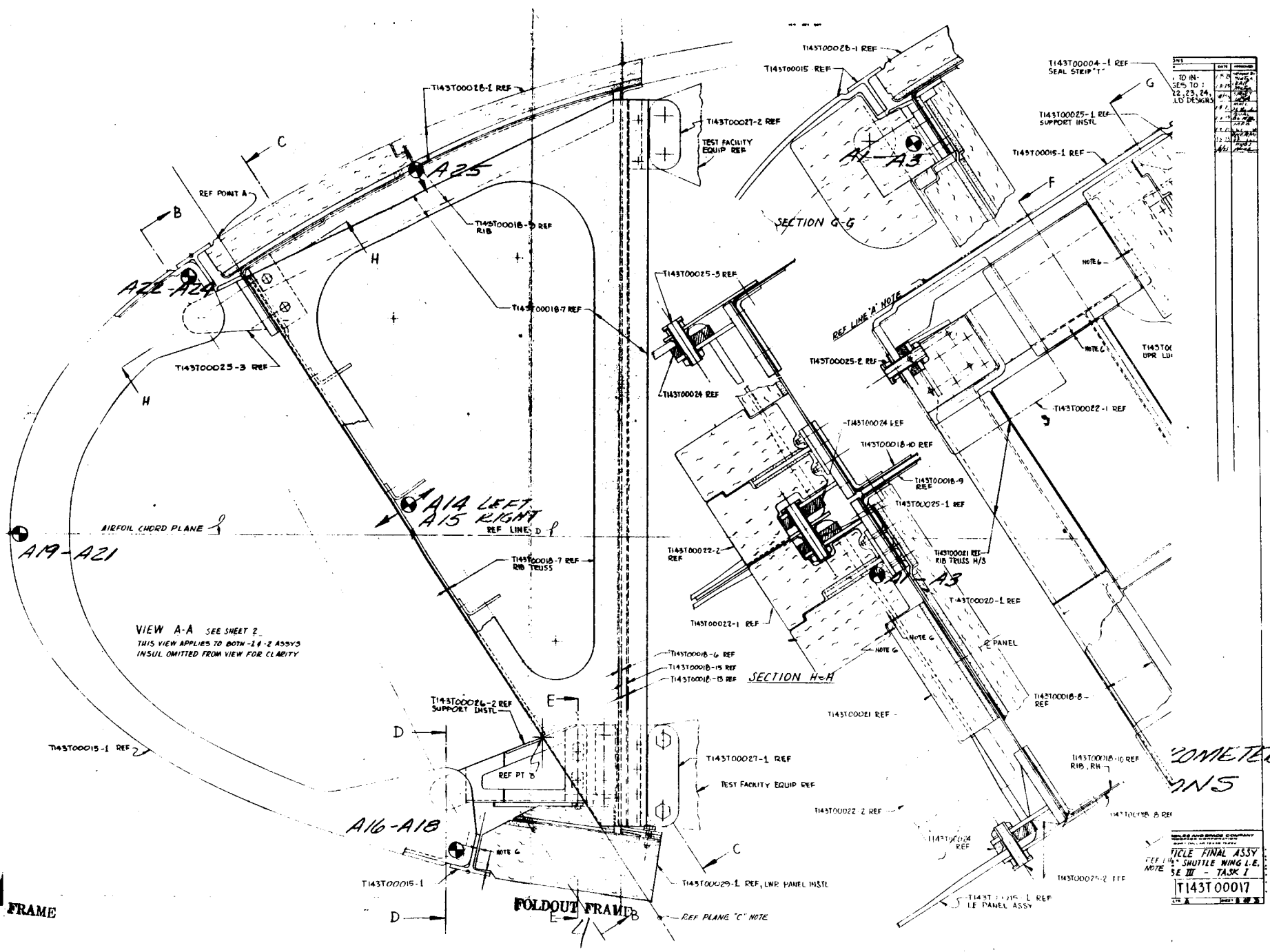
T143T00028-1 REF
T143T00027-2 REF
TEST FACILITY EQUIP REF
A25
REF POINT A
T143T00018-9 REF RIB
A22-A24
T143T00018-7 REF
T143T00025-3 REF
T143T00025-3 REF
T143T00024 REF
A14 LEFT
A15 RIGHT
AIRFOIL CHORD PLANE
REF LINE D
A19-A21
T143T00018-7 REF RIB TRUSS
VIEW A-A SEE SHEET 2
THIS VIEW APPLIES TO BOTH -1 & -2 ASSYS
INSUL OMITTED FROM VIEW FOR CLARITY
T143T00026-2 REF SUPPORT INSTL
T143T00015-1 REF
REF PT B
A16-A18
NOTE G
T143T00015-1
T143T00027-1 REF
TEST FACILITY EQUIP REF
T143T00029-1 REF, LWR PANEL INSTL
REF PLANE "C" NOTE
FOLDOUT FRAME
T143T00018-6 REF
T143T00018-15 REF
T143T00018-13 REF
SECTION H-H
T143T00025-5 REF
T143T00025-2 REF
T143T00024 REF
T143T00018-10 REF
T143T00018-9 REF
T143T00025-1 REF
T143T00022-2 REF
T143T00021 REF RIB TRUSS H/3
A3
T143T00020-1 REF
T143T00022-1 REF
NOTE G
LE PANEL
T143T00018-8 REF
T143T00021 REF
T143T00018-10 REF RIB, RH
T143T00022-2 REF
T143T00025-2 REF
T143T00015-1 REF LE PANEL ASSY
T143T00028-1 REF
T143T00015 REF
SECTION G-G
A3
REF LINE 'A' NOTE
T143T00004-1 REF SEAL STRIP "T"
T143T00025-1 REF SUPPORT INSTL
T143T00015-1 REF
NOTE 6
NOTE 6
T143T00022-1 REF
T143T00017
FOLDOUT FRAME

NOTE:
ACCELEROMETER LOCATIONS INDICATED BY ⊕ & NUMBER

| REVISIONS | | | |
|---|---|---|---|
| SYM | ZONE | DESCRIPTION | DATE / APPROVED |
| A | | REVISED ALL VIEWS TO INCORPORATE CHANGES TO: T143T00020, 21, 22, 23, 24, 28 & 29 HEAT SHIELD DESIGNS | |

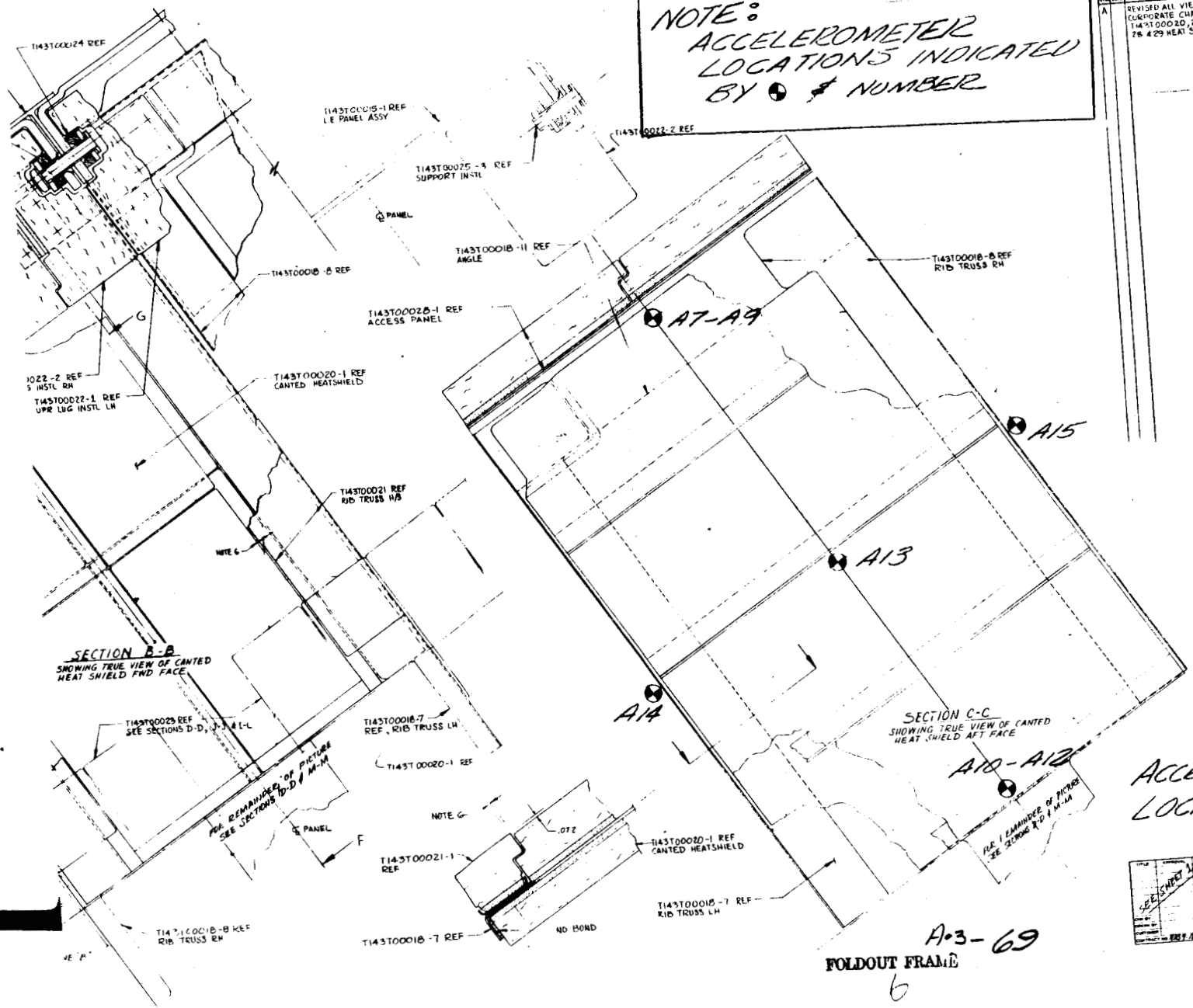

TABLE 5.4-1

ACCELEROMETER RECORDING REQUIREMENTS

| Measurement No. | Accelerometer Location | Type Measurement |
|---|---|---|
| A1 - A3 | Upper right support lug insulation | Tri-axial |
| A4 - A6 | Lower left support lug insulation | Tri-axial |
| A7 - A9 | Canted heatshield, upper center | Tri-axial |
| A10 - A12 | Canted heatshield, lower center | Tri-axial |
| A13 | Canted heatshield, center | Uni-axial |
| A14 | Canted support frame, left midpoint | Uni-axial |
| A15 | Canted support frame, right midpoint | Uni-axial |
| A16 - A18 | RPP segment, rib, lower left | Tri-axial |
| A19 - A21 | RPP segment, rib, centerline | Tri-axial |
| A22 - A24 | RPP segment, rib, upper left | Tri-axial |
| A25 | Upper panel, center | Uni-axial |

5.4.4 Test Procedure

The test article shall be visually inspected thoroughly to ensure that there is no evidence of failure from previous tests or handling. Suspected areas not confirmed shall be photographed to document the before-test condition. Accelerometers shall be installed as noted in the previous section. The leading edge assembly shall be mounted at the ground test support lugs to a suitable fixture (bolts torqued to 20-25 in-lb) and installed in the test chamber. Microphones shall be located as required by Section 5.4.3.

The open sides of the leading edge assembly and the aft side of the simulated front spar shall be acoustically insulated in an effort to limit the application of the environment only to the wing leading edge external surfaces.

Calibration - The leading edge test assembly will be used to calibrate the reverberant chamber prior to performing the full acoustic test. Test runs of minimum duration shall be performed to determine that the acoustic spectrum of Figure 5.4-1 is achieved. The octave band level tolerance, as noted previously, is -2 db to +4 db. The six external microphones used to measure the imposed environment will be averaged to determine conformance to the desired spectrum. The duration of each calibration run and the spectral distributions achieved shall be recorded.

Test - The test article shall be subjected to the test environment of Figure 5.4-1 as developed from the calibration runs. Total test time shall be 50 minutes, less the time accumulated during the chamber calibration runs.

This test time represents 100 missions.

At the beginning of the test, at each two-minute interval through the first 10 minutes, and at each five minutes thereafter during the test, 30-second recording of the output of all accelerometers and microphones shall be made on magnetic tape. This tape shall be retained until approval and release of the test report.

Should failure of any insulation component occur prior to completion of the test, the test shall be stopped and a substitute component installed. The substitute will be composed of the insulation structural support with a piece of aluminum bolted into place to produce a weight equivalent of the failed insulation. Testing will then continue. In the event failure occurs to either the upper or lower simulated RSI external panels (T143T00028 and T143T00029), the insulation shall be re-bonded and wired and/or taped into place to preserve a degree of acoustic attenuation capability of these panels, and the test continued.

5.4.5 Data Reduction

The primary results of the test will be a qualitative determination of the satisfactory performance (freedom from failure) of the various components making up the assembly. To determine this the test article will be disassembled for detail visual inspection and observations will be recorded by description and photograph.

Quantitative data required from the test is as follows:

(1) Time history of each accelerometer output (g-rms).

(2) Accelerometer spectral density plots for each accelerometer output at times corresponding to the beginning, middle, and end of the 50 minute test time.

(3) Plots of octave band external and internal (cavity) pressure levels. The plots shall contain:

(a) Average octave band sound pressure level.

(b) Maximum and minimum octave band sound pressure levels.

5.4.6 Post Test Operations

The leading edge assembly shall be disassembled and visually inspected per Section 6.0 for damage or failures. These shall be documented by verbal description and photographs.

Following disposition per Section 7.0, the leading edge assembly shall then be reassembled for the utlimate load boost pressure test defined in Section 5.2

## 6.0 INSPECTION

Before and after each test the test article shall be thoroughly inspected to ensure conformance to Engineering drawings and to ensure that test failures or observations are recorded at the proper test sequence.

Pre-test inspection shall verify that the test configuration is in compliance with the drawings and that gaps or clearances meet requirements. Instrumentation and leads shall not interfere with gaps or clearances.

Post-test inspection shall critically examine for differences observed in the test article during the test. This inspection shall include examination for such items as:

(1) Fractures

(2) Gap/clearance changes

(3) Cracks/delaminations

(4) Color changes

(5) Melting, warping, shrinking

(6) Spalling, flaking, chipping

(7) Seizing, binding

(8) Chemical reaction

(9) Debonding

Any changes noted in the test article shall be recorded photographed, and x-rayed where practical. Speculation as to the

cause of a failure, damage, or discoloration or the significance of these is discouraged until a thorough investigation is completed. Significant anomalies will be treated individually in subsequent investigations which should be performed in-depth.